

**Role of Substituents on the Reactivity of Mononuclear *cis*-  
Platinum(II) Complexes with 2-(phenylthiomethyl)pyridyl/quinolyl  
Non-leaving Ligands.**

By

**Wakhiwe M. Mthiyane**

BSc. (Hons.) (University of Kwa-Zulu Natal)



**UNIVERSITY OF  
KWAZULU-NATAL**

---

**INYUVESI  
YAKWAZULU-NATALI**

School of Chemistry and Physics

Pietermaritzburg

February 2017

**Role of Substituents on the Reactivity of Mononuclear *cis*-  
Platinum(II) Complexes with 2-(phenylthiomethyl)pyridyl/quinolyl  
Non-leaving Ligands.**

By

**Wakhiwe M. Mthiyane**

BSc. (Hons.) (University of Kwa-Zulu Natal)

*A thesis submitted in fulfilment of the requirements for the degree of*

**Master of Science**

**School of Chemistry and Physics**

**Pietermaritzburg**

**February 2017**

# Declaration

I hereby declare that this thesis reports results from original work investigated in the School of Chemistry and Physics, University of Kwa-Zulu Natal, Pietermaritzburg, and has not been submitted for the fulfilment of any degree at any University.

.....

**Wakhiwe Mthandi Mthiyane**

I hereby certify that this statement is correct.

.....

**Dr. Allen Mambanda**

**Supervisor**

.....

**Prof. Deogratius Jaganyi**

**Co-Supervisor**

School of Chemistry and Physics

University of Kwa-Zulu Natal

Pietermaritzburg

February 2017

*To my late grandparents Mr Mzochithiweyo Sibiya & Mrs Busisiwe Mdlalose-Sibiya. I cherish the childhood memories fondly and the wonderful times spent with you.*

## Abstract

Substitution reactions of aqua ligands from *cis*-Pt(II) square-planar complexes by thiourea nucleophiles were studied by stopped-flow and UV-vis spectrophotometric techniques at pH 2 as a function of concentration and temperature. Six mononuclear complexes bearing an N,S-bidentate core ligand containing either a pyridyl or quinolyl backbone linked *via* a flexible methylene linker to a thioether were synthesised and fully characterised by NMR ( $^1\text{H}$ ,  $^{13}\text{C}$  and  $^{195}\text{Pt}$ ), IR spectroscopy, mass spectrometry and elemental analysis. Substituents at the *para*-position of the phenyl group on the thioether differ in their electronic and steric properties. The solutions of the thiourea nucleophiles *viz.*, thiourea (**tu**), N,N'-dimethylthiourea (**dmtu**) and N,N,N',N'-tetramethylthiourea (**tmtu**) were provided in at least 10-fold excess to the complex concentration to ensure *pseudo*-first-order kinetics onto the reactions. Low energy chemical structures and related data were calculated by Density Functional Theory (DFT) and the data was used to explain trends in the experimental results.

The rate of substitution of the aqua co-ligands was found to be sensitive to the nature of the *para*-substituents on the phenyl group of the thioether moiety of the N,S-bidentate ligands. Both positive and negative  $\sigma$ -inductive substituents on the phenyl ring accelerated the rate of substitution compared to the unsubstituted complex albeit by different mechanisms. The positive  $\sigma$ -inductive effect of the *tert*-butyl group enhanced the  $\sigma$ -*trans*-labilizing effect of the thioether in the ground-state of the complexes. The negative  $\sigma$ -inductive effect of the fluoro group activated the  $\pi$ -acceptor property of the thioether which pulled electron density away from the metal centre making it more electrophilic. The effect of changing the donor group from pyridyl to a quinolyl led to reduced rates of substitution due to the poor  $\pi$ -acceptor properties of the latter.

The *pKa* results show that deprotonation of the aqua ligands is sensitive to the nature of the substituents on the phenyl group; lower *pKa* values were observed for  $\sigma$ -inductive electron-withdrawing groups.  $^{195}\text{Pt}$  NMR studies using **Pt(pyS<sup>PhF</sup>)Cl<sub>2</sub>** as an example, showed that upon reaction with thiourea nucleophiles, the N,S-bidentate ligand eventually underwent ring-opening at the N-end. The reactivity of the complexes is influenced by steric sizes of the nucleophiles; sterically bulk nucleophiles retarded the rate of substituting the aqua ligands. The low and positive enthalpy as well as the high and negative entropy values

supported an associative mode of activation associated with substitution reactions in square-planar Pt(II) complexes.

## Acknowledgements

I would like to give a huge thanks to my supervisor Dr A. Mambanda for the support and mentorship throughout the duration of this work. I commend his open-door policy and willingness to thoroughly review draft after draft of this work.

I would also like to thank my co-supervisor Prof. D. Jaganyi for overseeing this work and giving positive and constructive feedback.

I would like to thank my parents for being the pillars of strength throughout the years and especially for the past two years. I appreciate your faith and support in everything I do.

This work would not have been conducted timeously without the support from friends, colleagues and technical staff whom always ensured that they provide a good working environment. Therefore, I would like to give thanks to the following people:

- ✓ Colleagues from the Kinetics Research Group: Dr I. Wekesa, Dr R. Bellam, Mr B.B Khusi, Mr A. Panyako, Ms T. Papo, Mr M. Sitati, Mr M. Olegun, Mr G. Mutua, Mr X. Thikazi and Mr D. Onuga for the fruitful discussions and willingness to proof read drafts.
- ✓ Labmates from Room 22 for the love and wonderful times shared.
- ✓ SCP technical staff: Mr C. Grimmer for running NMR samples, Mrs C. J van Rensburg for running MS and CHN samples, Ms P. Lubanyana, Mrs I. Ngubane and Mr M. Makhathini for operational assistance in the laboratory.
- ✓ The glass-blowers: Messrs P. Forder, C. Mortlock and B. Sikwekwe for their service and fixing of broken glassware.
- ✓ The academic staff of the School of Chemistry and Physics are acknowledged for their continued support and advice.

The National Research Foundation of South Africa and the University of Kwa-Zulu Natal are hereby acknowledged for financial assistance.

## **Conference Contribution: Oral Presentation**

*Kinetic, Mechanistic and Thermodynamic Study of Novel Bifunctional, Mononuclear Pt(II) Complexes mixed N,S-Bidentate Chelates.* University of Kwa-Zulu Natal's College of Agriculture, Engineering and Science (CAES) Postgraduate Research and Innovation Day, Howard College Durban, South Africa, 29 November 2016. The talk was awarded Second Price and a prize token to the South African Chemical Society (SACI) Conference to be held in June 2017, Western Cape.



## Abbreviations

### Ligands

pyS <sup>Ph</sup>	2-(phenylthiomethyl)pyridine
pyS <sup>Ph(t-But)</sup>	2-(4- <i>tert</i> -butylphenylthiomethyl)pyridine
pyS <sup>PhF</sup>	2-(4-fluorophenylthiomethyl)pyridine
QnS <sup>Ph</sup>	2-(phenylthiomethyl)quinoline
QnS <sup>Ph(t-But)</sup>	2-(4- <i>tert</i> -butylphenylthiomethyl)quinoline
QnS <sup>PhF</sup>	2-(4-fluorophenylthiomethyl)quinoline

### Complexes

Pt(pyS <sup>Ph</sup> )	Pt{2-(phenylthiomethyl)pyridine}(H <sub>2</sub> O) <sub>2</sub> } <sup>2+</sup>
Pt(pyS <sup>Ph(t-But)</sup> )	Pt{2-(4- <i>tert</i> -butylphenylthiomethyl)pyridine}(H <sub>2</sub> O) <sub>2</sub> } <sup>2+</sup>
Pt(pyS <sup>PhF</sup> )	Pt{2-(4-fluorophenylthiomethyl)pyridine}(H <sub>2</sub> O) <sub>2</sub> } <sup>2+</sup>
Pt(QnS <sup>Ph</sup> )	Pt{2-(phenylthiomethyl)quinoline}(H <sub>2</sub> O) <sub>2</sub> } <sup>2+</sup>
Pt(QnS <sup>Ph(t-But)</sup> )	Pt{2-(4- <i>tert</i> -butylphenylthiomethyl)quinoline}(H <sub>2</sub> O) <sub>2</sub> } <sup>2+</sup>
Pt(QnS <sup>PhF</sup> )	Pt{2-(4-fluorophenylthiomethyl)quinoline}(H <sub>2</sub> O) <sub>2</sub> } <sup>2+</sup>

### Other chemicals

LiOTf	lithium trifluoromethanesulfonate, CF <sub>3</sub> SO <sub>3</sub> Li
HOTf	trifluoromethanesulfonic acid, CF <sub>3</sub> SO <sub>3</sub> H
AgOTf	silver trifluoromethanesulfonate, CF <sub>3</sub> SO <sub>3</sub> Ag
HCl	hydrochloric acid
tu	thiourea
dmtu	N,N-dimethylthiourea
tmtu	N,N,N',N'-tetramethylthiourea

EtOH ethanol

### Other abbreviations

A Absorbance

A Associative mechanism

Å Angstrom ( $10^{-10}$  m)

°C Celsius

CDC3-d deuterated chloroform

DMF-d7 deuterated dimethylformamide

DFT Density Functional Theory

D dissociative

DNA deoxyribonucleic acid

HOMO Highest Occupied Molecular Orbital

I Ionic strength

I Interchange

I<sub>a</sub> Associatively activated interchange

I<sub>d</sub> Dissociatively activated interchange

IR Infrared

LFER Linear Free Enery Relationship

LUMO Lowest Unoccupied Molecular Orbital

$k_{\text{obs}}$  averaged observed rate constants

$k_1, k_{-1}, k_2, k_{-2}$  rate constants

K Kelvin

$\Delta E$	Energy gap between the HOMO and LUMO
M	Molarity ( $\text{mol dm}^{-3}$ ) or metal
NBO	Natural Bond Orbital
NER	nucleotide excision repair
nm	nanometer
NMR	<u>N</u> uclear <u>M</u> agnetic <u>R</u> esonance
Nu	nucleophile
s, d, t	(NMR) <u>s</u> inglet, <u>d</u> ouble, <u>t</u> riplet
$\Delta H^\ddagger$	activation enthalpy
$\Delta S^\ddagger$	activation entropy
ppm	parts per million
py	pyridine
R	gas constant ( $8.3145 \text{ JK}^{-1} \text{ mol}^{-1}$ )
T	temperature
T.S.	<u>t</u> ransition <u>s</u> tate(s)
UV	ultraviolet
vis	visible

## List of Figures

**Figure 1.1:** Structures of cisplatin and its active analogues: (a) cisplatin, (b) carboplatin, (c) oxaliplatin, (d) nedaplatin, (e) heptaplatin, and (f) lobaplatin.

**Figure 1.2:** Biochemical equilibrium reactions of cisplatin and related compounds.

**Figure 1.3:** Structure of the cisplatin DNA adduct formed mainly through the N7 atom of guanosine. This causes axial instability with an axial twist of about 13%.

**Figure 1.4** Absorption and pre-binding interactions of cisplatin and its analogues with DNA. (i) Drug uptake; (ii) Activation by chloride metathesis; (iii) DNA adducts formation and (iv) DNA-helix instability that spirals into apoptosis.

**Figure 1.5:** Different structural cross-links formed by platinum complexes on DNA nucleobases.

**Figure 1.6:** Structure of DNA-intercalating  $[\text{PtCl}_2(\text{DIP})]$ , DIP = 4,7-diphenyl-1,10-phenanthroline.

**Figure 1.7:** Structures of inactive transplatin (g) together with active *trans*-Pt(II) complexes with various heterocyclic N-donor ligands.

**Figure 1.8:** Structure of *trans*-{bis[*trans*-diamminechloroplatinum(II)( $\mu$ -1,6-hexadiazine)]} diammineplatinum(II).

**Figure 1.9:** Structures of Pt(IV) complexes which have undergone clinical trials.

**Figure 1.10:** Hydrogen peroxide-assisted oxidation of cisplatin to its octahedral Pt(IV) derivative, which is subsequently reduced by a biological reductant.

**Figure 1.11:** Anticancer and anti-metastatic Ru(III) agents **NAMI-A** and **KP1019** which act by unique mechanisms to Pt(II) compounds.

**Figure 1.12:** Structures of the *cis*-Pt(II) complexes with N,N-bidentate chelates studied by Summa *et al.*

**Figure 1.13** Structures of the Pt(dach) analogues studied by Summa *et al.*

**Figure 1.14:** Structures of Pd(II)-imidazolin-2-imine complexes studied by Bogojeski *et al.*

**Figure 1.15:** Structures of mononuclear Pt(II) complexes studied by Hochreuther *et al.*

**Figure 1.16:** Structures of *cis*-Pt(II) complexes with N,S-bidentate ligands.

**Figure 2.1** Heterolytic bond-making and bond-breaking processes.

**Figure 2.2** Energy profile of the substitution mechanisms moving from D or I<sub>d</sub> to A or I<sub>a</sub>.

**Figure 2.3** Plot of  $k_{\text{obs}}$  vs [Nu] for the first aqua substitution in the complex *cis*-[Pt{2-(4-*tert*-butylphenylthiomethyl)pyridine}(H<sub>2</sub>O)<sub>2</sub>]<sup>2+</sup> in 0.1 M LiOTf/HOTf at 25 °C.

**Figure 2.4** Substitution in square-planar *d*<sup>8</sup> complexes showing (i) the slow formation of a five-coordinate solvent-complex intermediate **ML<sub>2</sub>ASX** prior to a rapid substitution by entering ligand Y and (ii) a direct substitution of the leaving group X by Y.

**Figure 2.5** Retention of the starting geometrical *cis* and *trans* configurations during associative nucleophilic substitution in square-planar complexes.

**Figure 2.6** Schematic energy profile and possible coordination changes during associative substitution in square-planar complexes of ligand X by Y. Energy maxima at **2**, **4**, **6**, and **8** represent the transition states and intermediates have energies **3**, **5**, and **7**.

**Figure 2.7** Charge distribution in induced dipoles by  $\sigma$ -fashion in the L-Pt-X coordinate. (i) The  $\sigma$ -bond strengths of L and X are identical (ii) The  $\sigma$ -bond strength of L is much greater than that of X.

**Figure 2.8** Schematic representation of the  $\pi$ -bonding mechanism for the *trans*-effect. (i)  $\pi$ -*trans*-director L forms only a  $\sigma$  bond, no  $\pi$ -bonding involved ; (ii) L forms both a  $\sigma$  bond for the donation of electron density from L onto filled *d*-orbitals of the metal ion and  $\pi$ -bonds for back-donation of this electron density from the metal onto the empty  $\pi^*$  orbitals of L.

**Figure 2.9** Schematic representation of the Molecular Orbital diagram of PtCl<sub>4</sub><sup>2-</sup>.

**Figure 2.10** The  $\sigma$ -*trans*-effect due to the stabilization of the trigonal bipyramidal intermediate. (i) The ground-state has only the  $p_x$  orbital available for  $\sigma$ -bonding of ligands A and X (ii)  $\sigma$ -bonding of ligands A, X and Y in the trigonal plane are accommodated on the  $p_x$  and  $p_z$  orbitals.

**Figure 2.11** Steric effects of a mesityl ligand in a square-planar complex showing the trigonal intermediate for the *cis* and *trans* isomers.

**Figure 3.1** Schematic diagram of a double beam UV-visible spectrophotometer.

**Figure 3.2** Schematic diagram of a stopped-flow mixing apparatus.

**Figure 4.1** Formulae of *cis*-Pt(II) complexes investigated.

**Figure 4.2** UV-visible spectra for the titration of 0.2 mM **Pt(pyS<sup>PhF</sup>)** with NaOH in the pH range 2-9 at *T* = 298 K. *Inset*: Absorbance versus pH data at 300 nm.

**Figure 4.3** <sup>195</sup>Pt NMR spectra recorded for the reaction of **Pt(pyS<sup>PhF</sup>)Cl<sub>2</sub>** and 2 equiv. of **tu**, indicating the unreacted *cis*-Pt(II) complex (**a**,  $\delta$  = -2796.4 ppm) before the reaction and the final ring-opened product (**d**,  $\delta$  = -3884.7 ppm) corresponding to **[Pt( $\kappa_1$ -S<sup>PhF</sup>N)S<sub>3</sub>]<sup>4+</sup>**. Intermediate products (**b** and **c** at  $\delta$  = -3414.5 and -3584.9 ppm) correspond to **[PtNS(tu)Cl]<sup>+</sup>** and **[Pt(NS(tu)<sub>2</sub>]<sup>2+</sup>**, respectively.

**Figure 4.4** Computer-simulated HOMO and LUMO frontier molecular orbitals of Pt(II) complexes.

**Figure 4.5** UV-visible spectra recorded for the reaction of 0.1 mM **Pt(pyS<sup>Ph</sup>)** with 7 mM **dmtu** at pH 2 (*I* = 0.1 M LiOTf/HOTf) and 25 °C.

**Figure 4.6** A typical time-resolved kinetic trace for a reaction of 0.1 mM **Pt(pyS<sup>Ph</sup>)** with 2 mM **tu** followed on the stopped-flow at wavelength 321 nm. pH 2 (*I* = 0.1 M LiOTf/HOTf) and 25 °C.

**Figure 4.7** Plots of *k*<sub>obs1</sub> vs [Nu] for the first substitution step of the reaction of 0.165 mM **Pt(pyS<sup>Ph(t-But)</sup>)** at pH 2 (*I* = 0.1 M LiOTf/HOTf) and 25 °C.

**Figure 4.8** Temperature dependence plots for the reaction of 0.046 mM **Pt(pyS<sup>Ph(t-But)</sup>)** with 2.75 mM (Nu = **tu**, **dmtu** and **tmtu**).

**Figure 4.9**: Thermal ellipsoid diagram (50% probability surfaces) of the molecular structure of **Pt(pyS<sup>PhF</sup>)Cl<sub>2</sub>**.

**Figure 5.1** Structures of the *cis*-Pt(II) complexes with 2-(phenylthiomethyl)quinolone moieties.

**Figure 5.2** UV-visible spectra for the titration of 0.2 mM **Pt(QnS<sup>Ph</sup>)** with NaOH in the pH range 2-7 at *T* = 298 K. *Inset*: Absorbance versus pH data at 284 nm.

**Figure 5.3** DFT geometry-optimized structures of the Pt(II) complexes.

**Figure 5.4** Preliminary UV-visible spectra prior to kinetics measurements on the stopped-flow recorded for the reaction of 0.05 mM **Pt(QnS<sup>Ph</sup>)** with 3 mM **dmtu** at pH 2.

**Figure 5.5** Plots of  $k_{\text{obs}1}$  vs [Nu] for the (a) first and (b) second substitutions steps of the reaction of 0.1 mM **Pt(QnS<sup>Ph</sup>)** at pH 2 ( $I = 0.1$  M LiOTf/HOTf) and 25 °C.

**Figure 5.6** A typical time-resolved kinetic trace at 293 nm for the first substitution step for the reaction of 0.115 mM **Pt(QnS<sup>Ph</sup>)** and 2.29 mM **tu** followed on the stopped-flow analyser.

**Figure 5.7** Eyring plots for (a) first and (b) second substitution reactions of 0.1 mM **Pt(QnS<sup>Ph</sup>)** and the thiourea nucleophiles. pH 2 ( $I = 0.1$  M LiOTf/HOTf) and 25 °C.

## List of Tables

**Table 2.1** Steric effects on the rates of substitution of *cis*- and *trans*-Pt(PEt<sub>3</sub>)<sub>2</sub>Cl by pyridine at various temperatures.

**Table 2.3** Solvent effects on chloride substitution reactions.

**Table 4.1** Summary of p*K*<sub>a</sub> values obtained for the sequential deprotonation of the aqua ligands from the *cis*-Pt(II) complexes.

**Table 4.2** Computer simulated data by DFT for *cis*-Pt(II) complexes.

**Table 4.3** Summary of the rate constants for the consecutive substitution steps of the Pt(II) complexes by **tu**, **dmtu** and **tmtu** (*I* = 0.1 M LiOTf/HOTf).

**Table 4.4** Summary of the activation parameters for the consecutive substitution steps of the investigated complexes by **tu**, **dmtu** and **tmtu**, (*I* = 0.1 M LiOTf/HOTf).

**Table 4.5** Comparison of the experimental and theoretical bond lengths (Å) and bond angles (°) for Pt(pyS<sup>PhF</sup>)Cl<sub>2</sub>.

**Table 4.6** Crystal data and structure refinement for Pt(pyS<sup>PhF</sup>)Cl<sub>2</sub>.

**Table 5.1** Summary of p*K*<sub>a</sub> values obtained for the consecutive deprotonation of aqua ligands coordinated to the Pt(II) complexes.

**Table 5.2** DFT calculated parameters for the *cis*-Pt(II).

**Table 5.3** Summary of the rate constants for the consecutive substitution steps.

**Table 5.4** Summary of the activation parameters for the consecutive substitution steps.



# Table of Content

Acknowledgements	i
Conference contribution: Oral Presentation	ii
Abbreviations	iii
List of Figures	vi
List of Tables	x

## Chapter 1: Metal-based compounds as anticancer therapeutics

1.0 Introduction	1
1.1.1 <i>Cancer Treatment by Metal-based Drugs</i>	1
1.2 Platinum(II) Complexes as Anti-tumour Agents	2
1.2.1 <i>Cisplatin Chemistry</i>	2
1.2.2 <i>Mechanism of Action and Resistance</i>	4
1.2.3 <i>Active cisplatin analogues</i>	8
1.3 Non-classical platinum complexes: A unique mechanism of activation to cisplatin	11
1.3.1 <i>trans-Pt complexes</i>	11
1.3.2 <i>Multinuclear Platinum complexes</i>	12
1.3.3 <i>Pt(IV) pro-drugs</i>	13
1.4 Non-platinum anticancer active complexes: ruthenium complexes as anticancer agents	16
1.5 Mechanistic studies of <i>cis</i> -Pt(II) and Pd(II) complexes with bidentate non-leaving ligands	18

1.6 Aims of the Study	22
1.7 References	25

## **Chapter 2: Theoretical considerations of the substitution reactions in square-planar complexes**

2.0 Introduction	30
2.1 Substitution reaction mechanisms	32
2.2 Substitution Reactions of Square-planar Complexes	33
2.2.1 <i>Mechanism of Substitution</i>	34
2.2.2 <i>Geometries of the intermediates</i>	37
2.3 Factors controlling the reactivity of square-planar complexes	38
2.3.1 <i>The trans-effect</i>	38
2.3.1.1 <i>The <math>\sigma</math>-trans-Effect</i>	39
2.3.1.2 <i>The <math>\pi</math>-trans-effect</i>	40
2.3.1.3 <i>The <math>\sigma</math> and <math>\pi</math>-trans-Effects</i>	41
2.3.2 <i>The cis-effect</i>	44
2.3.3 <i>The substituting nucleophile (Y)</i>	47
2.3.4 <i>The leaving ligand (X)</i>	47
2.3.5 <i>The role of the solvent</i>	48
2.4 References	50

## Chapter 3: Measurement of Kinetic reactions

3.1 Introduction	53
3.2 The rate law	55
3.2.1 <i>Measurement of the rate constants</i>	55
3.3 Integrated Rate Expressions	56
3.3.1 <i>First-Order Reactions</i>	56
3.3.2 <i>Reversible First-Order Reactions</i>	57
3.3.3 <i>Second-Order Reactions</i>	58
3.3.4 <i>Reversible Second-Order Reactions</i>	60
3.4 Measurement of activation parameters	62
3.4.1 <i>Measurement of enthalpy of activation (<math>\Delta H^\ddagger</math>) and entropy of activation (<math>\Delta S^\ddagger</math>)</i>	62
3.4.2 <i>Measurement of Volume of Activation (<math>\Delta V^\ddagger</math>)</i>	64
3.5 Instrumental techniques used for ligand substitution in Pt(II) complexes	65
3.5.1 <i>UV-visible spectrophotometer</i>	65
3.5.2 <i>Flow Methods</i>	67
3.6 References	69

## Chapter 4: Substitution of aqua ligands from *cis*-Pt(II) complexes bearing 2-(phenylthiomethyl)pyridine spectator ligands

4.0 Abstract	71
4.1 Introduction	72
4.2 Experimental	74

4.2.1 Procedures and Chemicals	74
4.2.2 Synthesis of the ligands	74
4.2.3 Synthesis of Pt(II) complexes	76
4.3 Preparation of the diaqua Pt(II) complexes	77
4.4 Instrumentation and physical measurements	78
4.4.1 pKa determination for the coordinated aqua ligand of the complexes	78
4.4.2 Kinetics measurements	79
4.4.3 Computer simulation studies	79
4.4.4 X-ray crystallography	79
4.5 Results	80
4.5.1 pKa determination of diaqua Pt(II) complexes	80
4.5.2 NMR studies	82
4.5.3 DFT-calculated optimised structures	85
4.5.4 Kinetic Measurements	89
4.5.5 Activation parameters	93
4.5.6 Crystal structure of Pt(pyS <sup>PhF</sup> )Cl <sub>2</sub>	94
4.6 Discussion	97
4.7 Conclusions	99
4.8 References	100
4.9 Supplementary Information	104

## Chapter 5: Role of extended $\pi$ -conjugation on the rate of substitution of aqua ligands in *cis*-Pt(II) complexes with 2-((4-substituted)phenylthiomethyl)quinoline non-leaving ligands

5.0 Abstract	117
5.1 Introduction	118
5.2 Experimental	120
5.2.1 <i>Materials</i>	120
5.2.2 <i>Synthesis of the N,S ligands</i>	121
5.2.3 <i>Synthesis of Pt(II) complexes</i>	122
5.3 <i>Preparation of the diaqua Pt(II) complexes</i>	124
5.4 <i>Instrumentation and physical measurements</i>	124
5.4.1 <i>pKa determination for the diaqua complexes</i>	124
5.4.2 <i>Kinetics measurements</i>	125
5.4.3 <i>Computer simulation studies</i>	125
5.5 Results	125
5.5.1 <i>Acidity of the diaqua Pt(II) complexes</i>	126
5.5.2 <i>DFT-calculated optimised structures</i>	128
5.5.3 <i>Kinetic Measurements</i>	132
5.6 Discussion	137
5.7 Conclusions	139
5.8 References	140
5.9 Supplementary Information	144

# Chapter 1

## Metal-based compounds as anticancer therapeutics

### 1.0 Introduction

#### 1.1 Cancer Treatment by Metal-based Drugs

Cancer is an abnormal growth of tissue resulting from a continuous proliferation of mutative cells that have the ability to invade and metastasise to other tissues.<sup>1</sup> Major causes of cancers in human are prolonged exposure to carcinogenic chemicals, ultra-violet (UV-B) radiation, prolonged dietary intakes of food contaminated with carcinogenic additives, smoking and in some cases hereditary defects.

Cancerous cells can grow into malignant tumours from connective and supportive tissue, such as bone, cartilage, nerve, blood vessels, muscle, and fat.<sup>2</sup> These tumours are called sarcomas. It can also originate from cells in the epithelial tissues *e.g.*, skin and the lining of the body cavities and organs, and glandular tissues.<sup>2</sup> These are called carcinomas. When cells in the blood and lymph fluids become cancerous, the results are leukaemias or lymphomas.<sup>2</sup>

Cancer tumours are mitigated from proliferation mainly through surgical removal, radiology and chemotherapy.<sup>2</sup> Nowadays, a combination of the therapies can be used to treat aggressive cancers. In most cases, chemotherapy is used as one of the methods in the combination therapies. The chemical drugs used in chemotherapy include: alkylating agents, antimetabolites, hormone antagonists and metallo-drugs.<sup>3,4</sup>

## 1.2 Platinum(II) Complexes as Anti-tumour Agents

### 1.2.1 Cisplatin Chemistry

For a long time, metal complexes have been known to treat cancer. Platinum(II) metal-based drugs were the first to be used to treat cancer. However, metal complexes of other metal ions such as Ru(II) and Ru(III); Os(II); Ir(I); Pt(IV); Au(I) and Au(III) can potentially treat cancer. The major underlying mechanism that kill cancer cells by metal-based antitumour drugs is DNA-complex formation *via* ligand exchange substitution reactions.<sup>5</sup> Due to the efficacy of cisplatin as a chemotherapeutic drug, numerous square-planar Pt(II) complexes have been prepared and used as model complexes for understanding the mechanisms and rates of substitution of labile ligands from the complexes.<sup>6</sup>

Cisplatin, *cis*-diamminedichloroplatinum(II) **Figure 1.1 (a)**, was the first metallo-drug to be used for combating aggressive cancer, usually in a combination with other therapeutic methods.<sup>5</sup> It was a revelation that this seemingly simple inorganic compound could in fact inhibit cell division, let alone suppressing tumour growth given that it had been known for more than a century.<sup>7</sup> The anticancer properties of cisplatin were discovered by chance by Rosenberg *et al.*<sup>8,9</sup> In an experiment designed to study the effect of an electric field on the growth of bacteria, cisplatin and its Pt(IV) analogue, *cis*-[Pt(NH<sub>3</sub>)<sub>2</sub>Cl<sub>4</sub>], were unexpectedly formed in electrochemical cells from a chemical reaction involving the Pt electrode and NH<sub>3</sub> electrolyte buffer. These two compounds caused *E. coli* to grow into filaments, prompting their investigation as possible inhibitors of DNA replication.<sup>10</sup>

Cisplatin was clinically approved by America's Food and Drug Administration (FDA) in 1978 and has since been routinely used as a cytostatic drug against epithelial malignancies of the lung, ovarian, bladder, testicular, breast, head and neck, oesophageal, gastric and pancreatic.<sup>11-13</sup> Although cisplatin is an effective anticancer drug, it is quite toxic, and this is caused by side reactions with non-targeted species such as sulphur-containing biomolecules, proteins, amino acids and enzymes. Side effects which include: nephrotoxicity, neurotoxicity, ototoxicity, myelosuppression, and emesis have been reported in patients undergoing cisplatin chemotherapy.<sup>12</sup> In addition, cisplatin is only sensitive to a limited range of tumours. In some cancer cells, it is intrinsically inactive. It can develop resistance in some cells after an initial response.<sup>14</sup> This meant that new metallo-drugs were required to address

the following challenges of cisplatin: (i) acute toxicity, (ii) cisplatin resistance, (iii) poor water solubility, (iv) increase the spectrum of anticancer activity, and (v) increase tumour selectivity.<sup>12</sup> **Figure 1.1** shows the structure of cisplatin and other related complexes which will be reviewed in this Chapter.

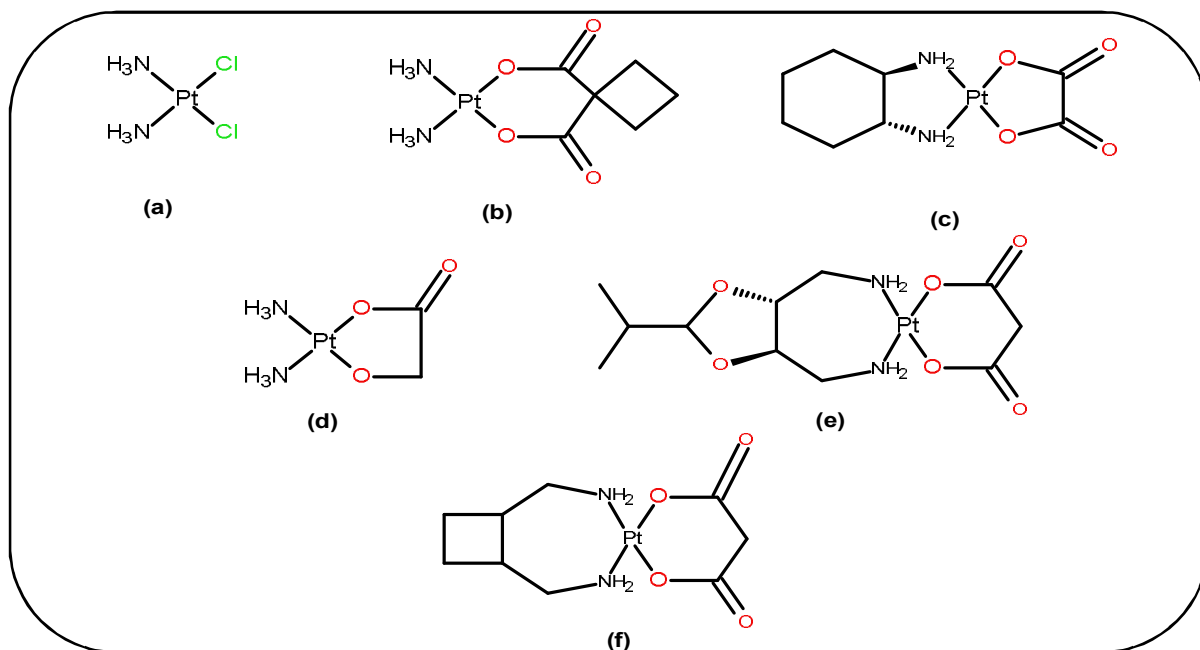


**Figure 1.1:** Structures of cisplatin and its active analogues: (a) cisplatin, (b) carboplatin, (c) oxaliplatin, (d) nedaplatin, (e) heptaplatin, and (f) lobaplatin.

The guiding rules to improving cisplatin's chemotherapeutic potency were pronounced as a structure-activity relationships (SARs) checklist.<sup>3,15-17</sup> The empirical structure-activity rules predicted the following structural features are crucial in the development of platinum-based anticancer drugs for effective activity:

- A *cis* configuration which on substitution forms a 1,2 DNA-metallocycle adduct.
- The complex must be neutral. Neutrality enhances efficient uptake of the drug due to ease of absorption.<sup>18</sup>
- The general formula should be  $cis-[Pt(Am)_2X_2]$ , in which Am = a non-leaving monodentate or chelating am(m)ine ligand and X = a monodentate anionic or ring-forming ligand (*e.g.* chloro, carboxylate, hydroxo etc.).
- The presence of at least one N-H group, important for hydrogen bonding interactions between the complex and DNA purine bases.<sup>19</sup>



Extensive research, guided by a strict adherence to the SAR rules was undertaken by many biochemists globally.<sup>20</sup> The impetus was to synthesise as well as conduct cytotoxicity tests on some of the potential anticancer compounds which would ameliorate cisplatin therapeutic shortcomings. It only yielded lead compounds, which were structurally similar to cisplatin and could only inhibit rapid cell growth by the same mechanism.<sup>21-23</sup> Later on, *trans*-square planar Pt(II) compounds (**Figure 1.7**) were also discovered to possess cytostatic activity comparable to cisplatin both *in vitro* and *in vivo* (vide infra).<sup>24</sup>

### 1.2.2 Mechanism of Action and Resistance

Most of what is known on the chemotherapeutic effect and development of resistance is based on the data of cisplatin.<sup>25</sup> Because cisplatin is toxic and has poor solubility, it is administered intravenously at an average dose of 100-200 mg d<sup>-1</sup> for up to 5 consecutive days for effective treatment.<sup>11,26</sup> The drug is predominantly excreted in the kidney and liver organs.<sup>27</sup> It is believed that cellular uptake of cisplatin and related metallo-drugs into the cells occurs by passive diffusion and in some cells by an active transport mechanism (a copper influx transporter through constitutive triple response 1 (CTR1) receptor, in mammalian cells).<sup>28,29</sup>

Prior to cellular absorption, the drug remains in its neutral form, *cis*-[Pt(NH<sub>3</sub>)<sub>2</sub>Cl<sub>2</sub>], due to the high concentration of chloride ions in the plasma, which suppress hydrolysis.<sup>12</sup> Inside the cell the concentration of the chloride ions is low (4 mM) and this facilitates a stepwise reversible hydrolysis to produce the charged mono- and diaqua species, *cis*-Pt(NH<sub>3</sub>)<sub>2</sub>(Cl)(H<sub>2</sub>O)<sup>+</sup> and *cis*-Pt(NH<sub>3</sub>)<sub>2</sub>(H<sub>2</sub>O)<sub>2</sub><sup>2+</sup>, respectively.<sup>30</sup> These active species of cisplatin are highly reactive towards DNA, are frequently deactivated by ubiquitous and nucleophilic compounds in the cytosol of the cell.<sup>31</sup> These reactive species cause the acute toxicity of cisplatin and in some cases development of drug resistance.<sup>24</sup>

Nucleophilic substitution reactions of active cisplatin species with DNA, in which the labile water ligands are displaced, lead to the covalent binding of the *cis*-Pt(NH<sub>3</sub>)<sub>2</sub><sup>2+</sup> unit to the purine heterogeneous bases.<sup>28</sup> It has been suggested that only 1% of the drug reaches its critical target DNA due to the ever-present detoxifying agents, particularly sulphur-containing species, that it can possibly interact with.<sup>32</sup> **Figure 1.2** depicts the equilibria of cisplatin and its active species in the cytosol.

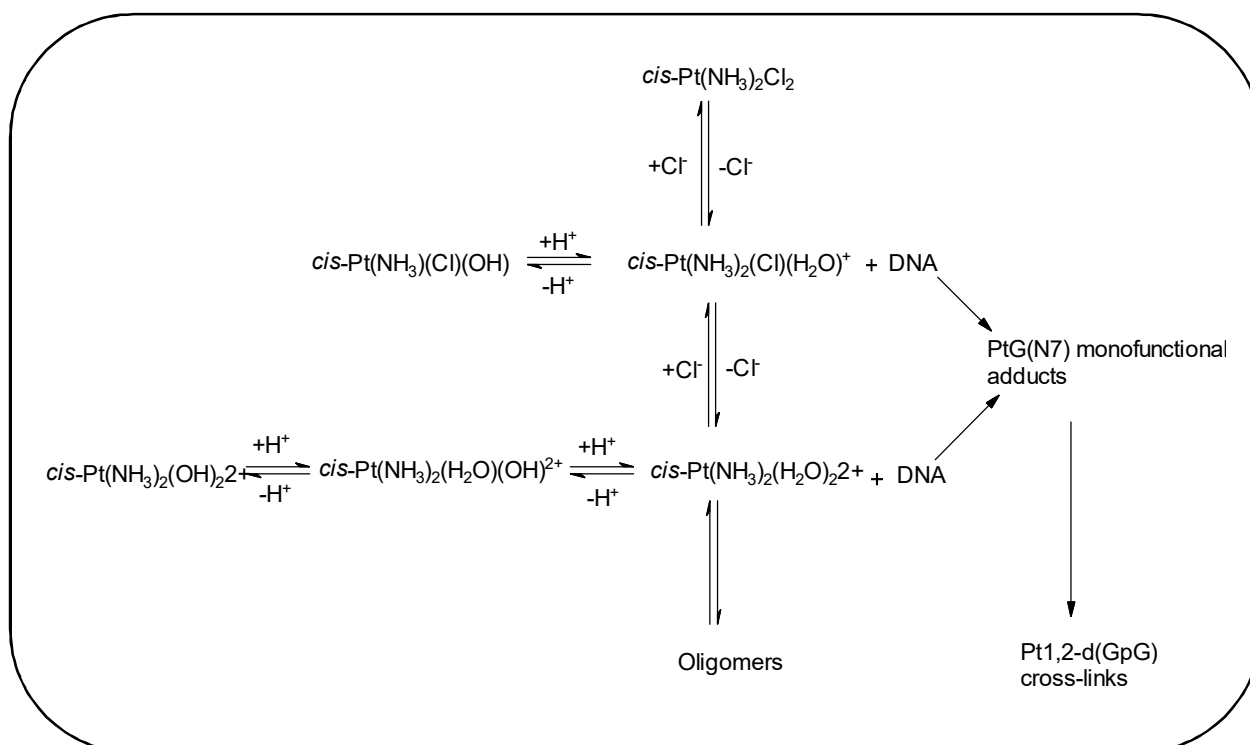


**Figure 1.2:** Biochemical equilibrium reactions of cisplatin and related compounds.<sup>13,33</sup>

The major bifunctional DNA adducts formed by cisplatin comprise:

- ca. 65% 1,2-intrastrand cross-links between adjacent bases, with *cis*-[Pt(NH<sub>3</sub>)<sub>2</sub><sup>2+</sup>] (*cis*-GG) as the major type;
- 25% *cis*-[Pt(NH<sub>3</sub>)<sub>2</sub>{d(ApG)}] (*cis*-AG);
- ca. 5-10% 1,3-intrastrand cross-links between non-adjacent guanines, 1,3-d(GpNpG) (*cis*-GNG); and
- 1-3% interstrand adducts, and mono-functional binding to guanine.<sup>34</sup>

The binding of the *cis*-Pt(NH<sub>3</sub>)<sub>2</sub><sup>2+</sup> unit of cisplatin induces a major groove bending of 30-35%, and a 13% local unwinding of the DNA double helix. Solution studies aimed at understanding the *in vivo* pharmacokinetics of cisplatin using nuclear magnetic resonance spectroscopy (NMR) (<sup>15</sup>N, <sup>195</sup>Pt)<sup>35,36</sup> and x-ray crystallographic<sup>37,38</sup> data, showed that the N7 atom of the purine bases is the preferred site for platinum binding.

**Figure 1.3** shows the possible binding products of cisplatin to DNA purine bases. Due to its *cis* configuration, it can form:<sup>12,39</sup>

- an interstrand adduct cross-linking two different strands of one DNA molecule,
- an intrastrand adduct cross-linking two neighbouring nucleobases of a single DNA strand,
- a simple complex formation through bonding with N- and O-atoms of one guanine,

- a DNA-protein cross-link.

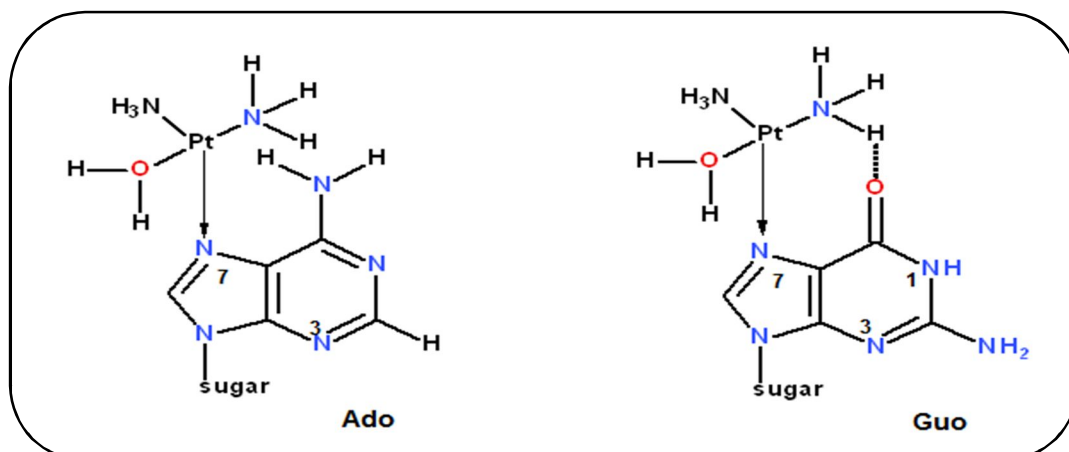


**Figure 1.3:** Structure of the cisplatin DNA adduct formed mainly through the N7 atom of guanosine. This causes axial instability with an axial twist of about 13%.<sup>19</sup>

The same alteration on the structure of the double helix of DNA is imparted by carboplatin and oxaliplatin, two analogues with carboxylate leaving groups. The pre-binding interactions that cisplatin undergoes prior to substitution of its labile ligands by DNA are shown in **Figure 1.4**.

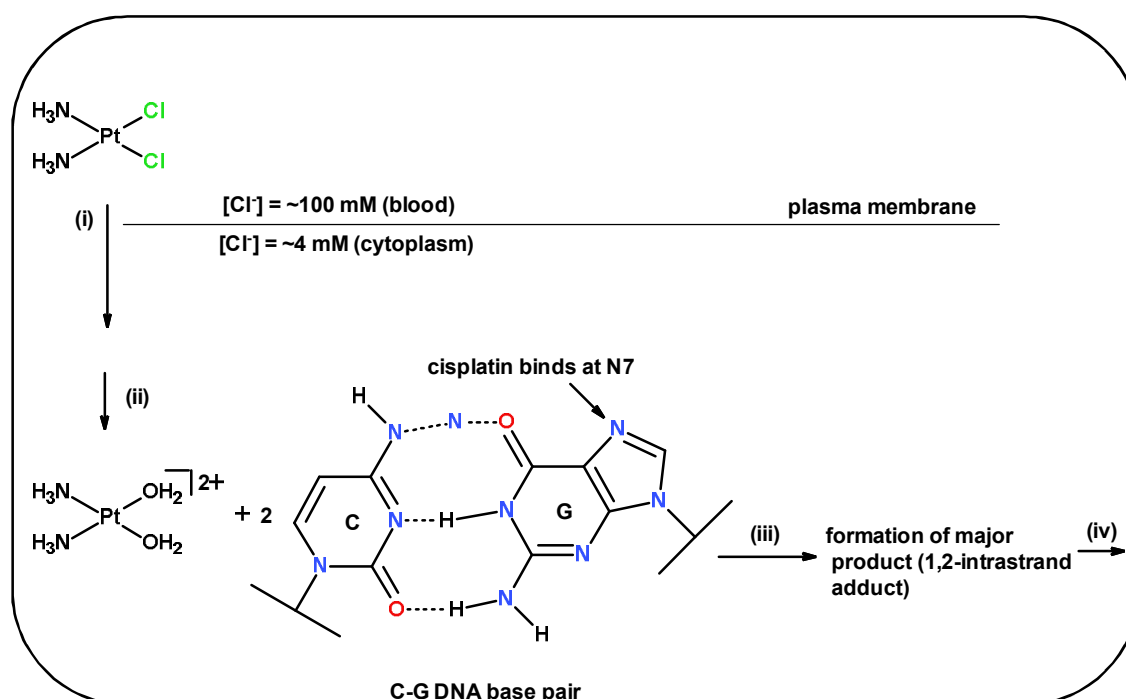


**Figure 1.4** Absorption and pre-binding interactions of cisplatin and its analogues with DNA.<sup>25,40</sup> (i) Drug uptake; (ii) Activation by chloride metathesis; (iii) DNA adducts formation and (iv) DNA-helix instability that spirals into apoptosis.

The covalent binding of cisplatin to the double-helical structure of DNA leads to the twisting and bending of helix and triggers obstruction of cellular pathways such as replication and transcription in fast growing cells.<sup>18</sup> Consequently, programmed cell death, or apoptosis, is executed. A group of proteins called the high mobility group box (HMGB1) are immobilised to the Pt-DNA damaged lesions and activate apoptosis leading to cell death.<sup>37,41</sup> These proteins can be systematically bypassed by another counteracting arsenal: the nucleotide excision repair (NER) machinery.<sup>42</sup> The nucleotide excision repair facilitates the restoration of platinum damaged DNA by the removal of such lesions. The easy recognition as well as removal by the NER machinery of these lesions accounts for one of the mechanisms of acquired or intrinsic resistance of platinum-based anticancer drugs. The possible platinum-DNA adducts formed during cisplatin activity are shown in **Figure 1.5** below.

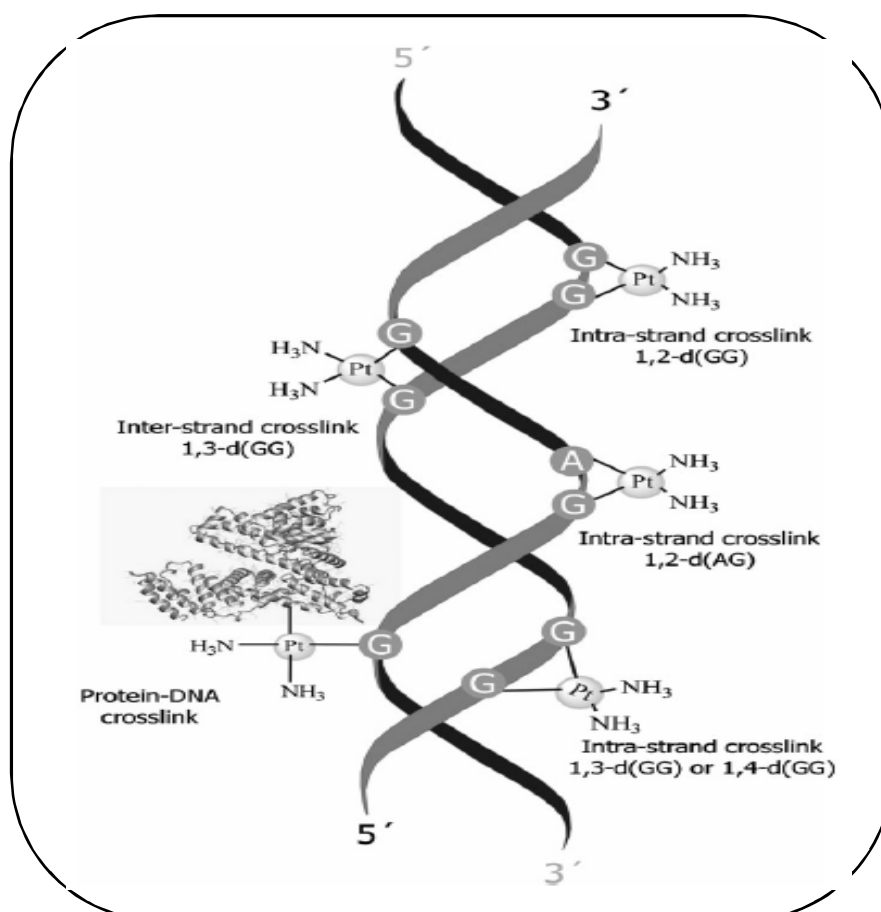


**Figure 1.5:** Different structural cross-links formed by platinum complexes on DNA nucleobases.<sup>43</sup>

The activity of cisplatin and related compounds can be reduced *in vivo* by platinum loving biomolecules. Since Pt(II) is a soft and easily polarizable ion, it has a great affinity to bind to other soft donors. Among these are nitrogen and sulphur-containing proteins and amino acids. This binding to biological substrates leads to the development of resistance of tumours to treatment. Acquired resistance of cisplatin as well as other active platinum complexes can also be a result of the following:<sup>39,44,45</sup>

- Inefficient absorption of the drug leading to reduced levels of uptake and/or increased efflux.
- Reactions with cellular sulphur-containing platinophiles, *e.g.* Glutathione (GSH) and Metallothionein (MT).
- Efficient DNA repair and/or increased damage tolerance, and
- Failure of cell-death pathways (apoptosis) due to repair of platinum-modified DNA lesions.

### 1.2.3 Active cisplatin analogues

Cisplatin chemotherapeutic index is unsurpassed and thus widely employed as a standalone or in combination with other non-metal anticancer drugs.<sup>33</sup> Despite impressive treatment rates of up to 45 to 95 % for testicular cancer, its clinical use is impeded by severe and unpleasant side-effects (cumulative nephrotoxicity being dose-limiting) which significantly lowers its pharmacological efficacy.<sup>46,47</sup> These drawbacks are promoting scientists to engage in platinum drug-development research. The fundamental goal of this study was to design (whilst adhering to the SAR rules) and synthesise potential drug candidates which would address cisplatin short-comings such as its selective cell-killing ability. Emphasis was for the future drugs to show minimum or no side effects for the benefit of patients.

Carboplatin (*cis*-diammine-[1,1-cyclobutanedicarboxylato]platinum(II) (CDBCA or JM8) (**Figure 1.1 (b)**), was developed in the UK and introduced into the clinics in 1989.<sup>26,48</sup> It retains the similar structural attributes as cisplatin with two inert (ammine groups) as well as the bidentate labile (cyclobutane-1,1-dicarboxylato unit) ligand in a square-planar geometry associated with compounds designed from a 'classical' SARs viewpoint. The six-membered cyclobutane-1,1-dicarboxylato sub-unit introduces enhanced kinetic stability against

hydrolysis and good aqueous solubility.<sup>18,39</sup> This ensures slow associatively-activated ligand substitution reactions of the drug *in vivo*.<sup>31</sup> As a result, carboplatin is less toxic (diminished kidney toxicity and neurotoxicity) when compared to cisplatin despite having both drugs exhibit a similar spectrum of activity to tumours. Lower toxicity of carboplatin allows for a higher average dose of 400 mg/m<sup>2</sup> when compared to the 100 mg/m<sup>2</sup> for cisplatin.<sup>11,23,31</sup>

Just like cisplatin, carboplatin is also administered intravenously; oral administration has been shown to cause gastrointestinal toxicity and poor absorption in patients.<sup>5</sup> Myelosuppression, particularly thrombocytopenia, is dose-limiting for this drug.<sup>26,31,47</sup> However, the use of combination of carboplatin with other active drugs, notably paclitaxel and gemcitabine *in vitro*,<sup>49</sup> results in better cytotoxicity and reduced toxicity.<sup>13</sup> Combination therapy is effective on ovarian, head and neck and bladder cancers as well as on non-small cell lung cancer.<sup>49</sup>

Another 'second generation' drug resembling carboplatin, *cis*-diammine-glycolato-O,O'-platinum(II) (nedaplatin or 254-S (**Figure 1.1 (d)**)), (granted permission in 1995 only in Japan) showed encouraging results at Phase II trials for treating head and neck, testicular, lung, oesophageal, bladder, ovarian, and cervical cancers.<sup>22,48</sup> The *cis* ammine non-leaving groups in nedaplatin are retained as in cisplatin and carboplatin. Due to the thermodynamic "chelate effect" the complex has additional stability when compared to its non-chelated analogues.<sup>50</sup> The ring-forming glycolate, improves the water solubility (10 mg/mL) of the complex when compared to the mono-dentate chloride ligands of cisplatin (2.5 mg/mL).<sup>25</sup> Nedaplatin shows reduced nephrotoxicity, neurotoxicity, and gastrointestinal toxicity when compared to cisplatin.<sup>49</sup> However, further tests have since been abandoned due to severe myelosuppression being dose-limiting as well as for not showing any significantly better potency toward cisplatin-sensitive and resistant tumours.<sup>31</sup>

Although carboplatin and nedaplatin are less toxic than cisplatin, they are only sensitive in the same regime of cells as cisplatin. Kidani and co-workers synthesised *trans*-L-diaminocyclohexane)oxalatoplatinum(II) (oxaliplatin or L-OHP (**Figure 1.1 (c)**)), a complex which was later discovered to have enhanced efficacy and lower resistance and toxicity when compared to cisplatin.<sup>51,52</sup> This drug is not cross-resistant with either cisplatin nor carboplatin in sensitive cells. It is mainly used for the treatment of secondary metastatic colorectal

cancer.<sup>13</sup> Cisplatin and carboplatin are inactive against this cancer. It also does not exhibit neurotoxicity; myelosuppression nor ototoxicity.

By introducing the bulky 1,2-diaminocyclohexane (DACH) carrier ligand, this complex showed a lack of cross-cellular resistance in cisplatin-resistant cell lines.<sup>51</sup> The difference in activity of this drug is linked to the formation of the  $\{cis\text{-Pt}(\text{DACH})\}_4$  adducts, which are different to those formed by cisplatin, carboplatin and nedaplatin. It is also used as a combination drug. For instance, a combination of oxaliplatin and 5-fluorouracil (5FU)/folic acid (FA), gemcitabine, cisplatin, carboplatin, topoisomerase I inhibitors, and taxanes enhances the treatment rates compared to when the drug is used as a single agent.<sup>4,49</sup> Oxaliplatin, however, has limited approval for clinical use in China, Europe and, for colorectal cancer, in USA.<sup>24</sup>

Heptaplatin (**Figure 1.1 (e)**) developed under the name SKI 2053R) was approved by the Korean Food and Drug Administration in 1999 for the treatment of gastric cancer.<sup>25</sup> The two R stereo centres in the seven-membered chelating carrier ligand are presumed vital for the anti-tumour activity of this drug. The leaving dianionic ring-forming group, malonate, can be hypothesised to introduce slow ligand aquation due to enhanced stability as well as conferring good saline solubility similar to carboplatin (vide supra). This is significant since the drug has a lower toxicity profile when compared to cisplatin.

Lobaplatin (1,2-diaminocyclobutanelactatoplatinum(II) (D-19466) (**Figure 1.1 (f)**), has clinical approval only in China, received in 2010.<sup>20</sup> It is clinically utilized for the treatment of chronic myelogenous leukemia (CML), small cell lung cancer (SCLC), and metastatic breast cancer.<sup>49</sup> Patients undergoing lobaplatin treatment experience gastrointestinal side-effects with hematologic toxicity being dose-limiting.<sup>20</sup>

The investigations that have been made to date, prove that a careful study on the effect of changing the structure for both the non-leaving and leaving groups around the square-planar geometry, remains a promising approach into unlocking new drugs of improved potency.<sup>41,53</sup> A recent study by Liu *et al.*<sup>54</sup> on oxaliplatin derivatives has demonstrated that altering the structure of carboplatin by introducing a dichloroacetate group in the 1,1-dicarboxylate moiety produces derivatives that induce marked activity on human (A549) and ovarian (SK-OV-3, SK-OV-3/DDP) cancer cell lines.

Recently, Shahabadi *et al.*<sup>55</sup> reported the synthesis of a *cis*-Pt(II) complex which adheres to the benchmark 'classical' SAR rules (**Figure 1.6**). The structure has been altered from the *cis*-ammines of carboplatin to bear a 4,7-diphenyl-1,10-phenanthroline bidentate chelate.<sup>55</sup> Such alterations in structure are anticipated to have reduced toxicity of the compound as was found for carboplatin. The complex was used for DNA studies using calf thymus DNA.<sup>55</sup> The mode of DNA binding was found to be the formation of adducts though DNA-intercalation.<sup>55</sup> The binding of the complex causes a kink in the double-helical structure of DNA which was confirmed by use of various physicochemical methods.<sup>55</sup>

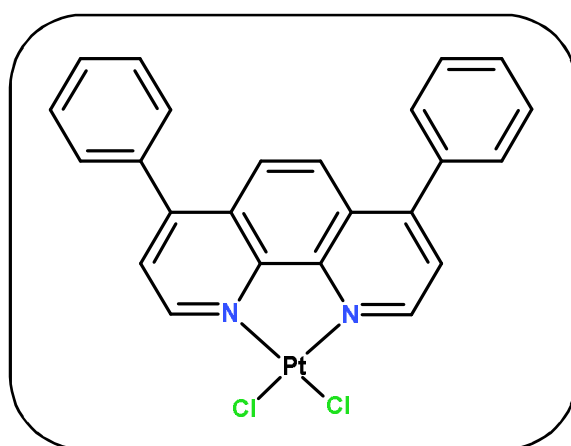


**Figure 1.6:** Structure of DNA-intercalating  $[PtCl_2(DIP)]$ , DIP = 4,7-diphenyl-1,10-phenanthroline.<sup>55</sup>

### 1.3 Non-classical platinum complexes: A unique mechanism of activation to cisplatin

#### 1.3.1 *trans*-Pt complexes

A group of *trans* square-planar Pt(II) complexes emerged that disobeyed the initially-proven structure-activity relationships blueprint for active metallo-drugs.<sup>56,57</sup> It had been established initially that the geometric isomer of cisplatin, *trans*-diamminedichloroplatinum(II), *trans*-DDP (**Figure 1.7 (g)**), had no cancer killing properties.<sup>57</sup> This was attributed to its kinetic instability caused by rapid hydrolysis *in vivo*.<sup>39</sup> Additionally, *trans*-DDP was incapable of forming the important 1,2-intrastrand DNA crosslinks known for the cytotoxic effect of cisplatin.<sup>39</sup> The kinetically preferred 1,3-intrastrand crosslinks formed



by *trans*-DDP on DNA bases were easily recognised and repaired by the nucleotide excision repair (NER) machinery rendering it inactive.<sup>58</sup>

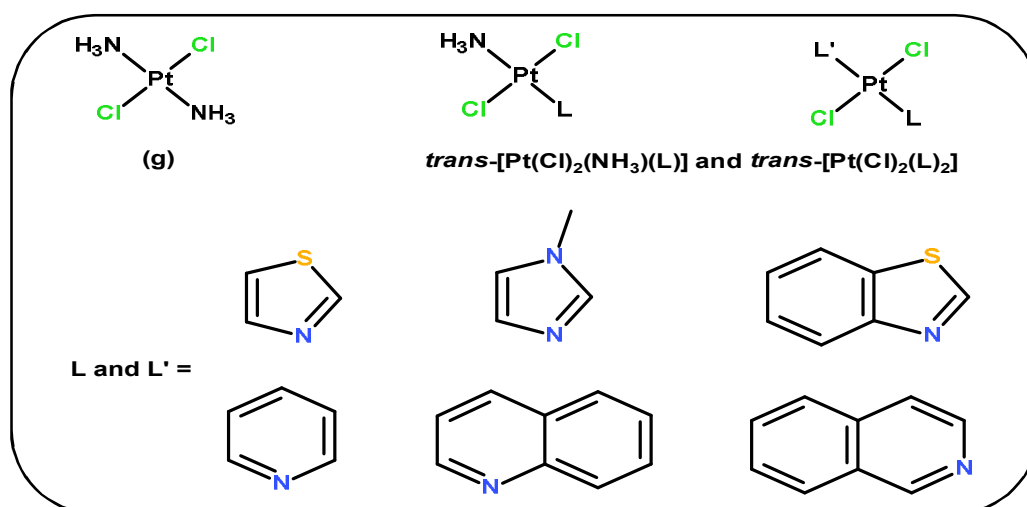


**Figure 1.7:** Structures of inactive transplatin (**g**) together with active *trans*-Pt(II) complexes with various heterocyclic N-donor ligands.<sup>56</sup>

Altering the structure of transplatin by introducing sterically hindered or planar heterocyclic nitrogen spectator ligands afforded therapeutic drugs with a different spectrum of activity from cisplatin. The active *trans*-Pt(II) complexes generally have the formula *trans*-[PtCl<sub>2</sub>(NH<sub>3</sub>)(L)] and *trans*-[PtCl<sub>2</sub>(L)(L')] comprising:

- i. L = N-donor aromatic heterocycle and L' = ammine, sulphoxide or a second aromatic N-donor ligand;<sup>56</sup>
- ii. L = iminoethers and ketimines and L' = ammine or iminoether; and
- iii. L = aliphatic amines and L' = a secondary aliphatic amine.

The mode of activity of these groups of *trans*-Pt(II) compounds is different from that of their *cis* counterparts: the former characterised by the formation of mono-functional adducts and interstrand cross-links with DNA.

### 1.3.2 Multinuclear Platinum complexes

One of the promising approaches of circumventing platinum acquired or natural resistance in tumours was to develop polynuclear (*i.e.* bi-, tri, or tetranuclear) platinum complexes.<sup>45,59</sup> Failure by many cisplatin analogues to overcome resistance is primarily due to the formation of similar Pt-DNA adducts as the prototype drug. The many possibilities in

which multinuclear Pt compounds can bind to DNA meant that unique adducts could be formed with DNA purine bases. The unique adducts would induce distinct anticancer activity in cells that are insensitive to cisplatin.

Because these compounds possess two or more platinum metals tethered by a flexible or rigid linker, they are able to bind covalently with DNA at more than one side forming long range intra- or interstrand cross-links which are immune to repair by proteins.<sup>25</sup> Multinuclear complexes induce different conformational changes on the helix of DNA. Thus, cytotoxicity profiles were found to be different from those of cisplatin whilst also being active against cisplatin-resistant tumours.<sup>25</sup>

The lead compound in this class of complexes is a tri-nuclear compound BBR3464 (**Figure 1.8**).<sup>45</sup> The structure consists of two *trans*-[PtCl(NH<sub>3</sub>)<sub>2</sub>] units joined by a tetra-amine [*trans*-Pt(NH<sub>3</sub>)<sub>2</sub>{H<sub>2</sub>N(CH<sub>2</sub>)<sub>6</sub>NH<sub>2</sub>}<sub>2</sub>]<sup>2+</sup> unit. BBR3464 has a high formal charge of +4 which confers the compound with enhanced molecular binding to DNA when compared to neutral cisplatin and related drugs. Since it possesses two platinum binding sites, BBR3464 can form long-range intra- and interstrand cross-links unique and different to cisplatin and related compounds. The major DNA adduct formed by this compound is the 1,4-interstrand cross-link.<sup>25</sup>

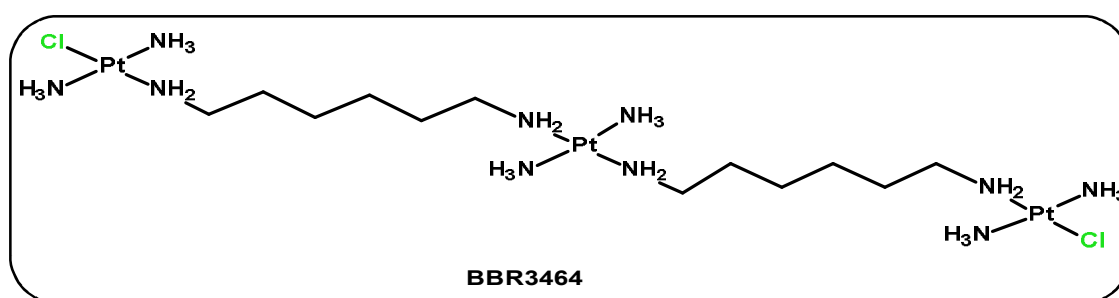


**Figure 1.8:** Structure of *trans*-{bis[*trans*-diamminechloroplatinum(II)( $\mu$ -1,6-hexadiazine)]} diammineplatinum(II).<sup>45</sup>

### 1.3.3 Platinum(IV) pro-drugs

A great deal of research has focused on Pt(II) complexes at the expense of Pt(IV) despite a Pt(IV) compound being identified as one of the two compounds that had led to the inhibition of bacterial DNA replication in early experiments by Rosenberg.<sup>60</sup> The ligand

substitution reactions of Pt(IV) compounds are slower when compared to their Pt(II) counterparts due to their octahedral structure. Thus, they have a greater pharmacological chance to survive inactivation. They are orally administered due to a higher formal charge.<sup>61,62</sup> Most importantly Pt(IV) drugs can be used in sophisticated 'synchronous' targeting and delivery systems.<sup>25,63,64</sup> Activation of Pt(IV) drugs occurs *via* an irreversible redox-reduction step *in vivo*, resulting in loss of the two axial ligands, to yield their active *cis*-Pt(II) complexes which react with the target DNA.<sup>61,65</sup> The biochemical intra- and/or extracellular components are known to aid in this process. Glutathione and ascorbic acid are intracellular reducing agents that have been reported to facilitate the two-electron reduction process of Pt(IV) compounds through reaction steps compared to other related thiols.<sup>65,66</sup> For this reason, active Pt(IV) compounds are pro-drugs and the structures of some active complexes are shown below in **Figure 1.9**.

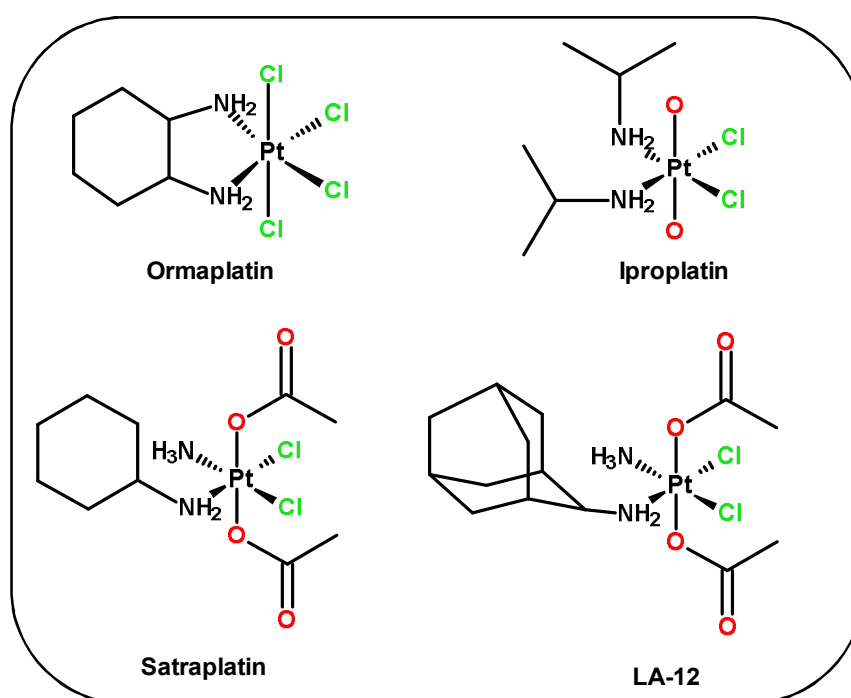


**Figure 1.9:** Structures of Pt(IV) complexes which have undergone clinical trials.

The kinetics of the reduction of several Pt(IV) complexes containing various carrier groups have been studied with reductants such as GHS<sup>66</sup>, ascorbate<sup>52</sup>, 5'-GMP.<sup>67,68</sup> The axial ligand bonds confer varying kinetic stabilities which affect both the rate of substitution and reduction. The steric hindrance and electronic factors in the axial and carrier ligands were observed to greatly influence the reduction potentials of these Pt(IV) complexes.<sup>39</sup> This in turn affected the DNA-binding ability: higher reduction rates correlate to enhanced DNA-binding.

**Figure 1.10** shows a schematic reaction of the reduction process of a Pt(IV) analogue of cisplatin.

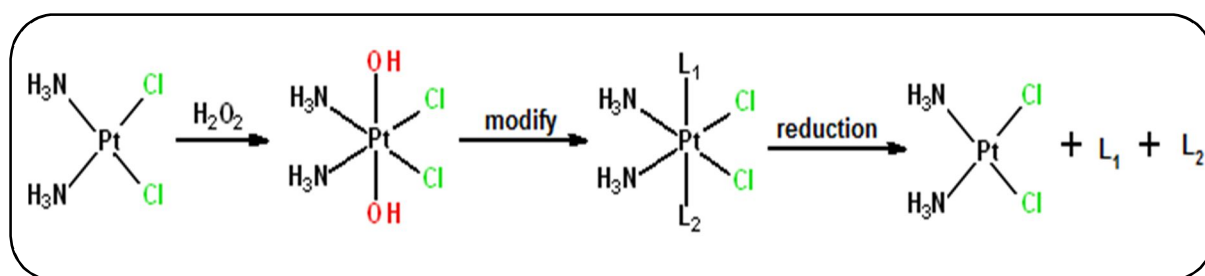


**Figure 1.10:** Hydrogen peroxide-assisted oxidation of cisplatin to its octahedral Pt(IV) derivative, which is subsequently reduced by a biological reductant.<sup>63</sup>

Ormaplatin (also known as tetraplatin) is a Pt(IV) pro-drug for oxaliplatin comprising of a DACH ligand as a *trans*-R,R- and *trans*-S,S racemic mixture. Ormaplatin has marked cytotoxic effects against cisplatin-resistant cell lines as well as showing diminished nephrotoxicity when compared to cisplatin.<sup>49</sup> However, ormaplatin failed Phase I of clinical trials due to its acute brain toxicity encountered by patients. The cyclohexane-1,2-diamine motif in this drug is proposed to confer this neurotoxic effect similar to its Pt(II) congener oxaliplatin.<sup>32</sup> Iproplatin (*cis,trans,cis*-dichlorodihydroxobis(isopropylamine)platinum(IV), JM9) is another drug that went to clinical trials as a potential anticancer active compound.<sup>25</sup> It is cytotoxic to cancers of the lung, ovary, breast, head and neck, as well as showing no cross-resistance with cisplatin and carboplatin. However, it does not readily undergo reduction by bio-related reductants.<sup>25</sup> This is proposed to aid in a prolonged bio-distribution of the drug in the biological system. Nevertheless, it has not met the crucial requirements to permit its use as an anti-proliferative cancer agent.<sup>25</sup>

Satraplatin, (bis(acetato)ammine-dichloro(cyclohexylamine)platinum(IV), JM216) is an orally administered Pt(IV) lipophilic cytotoxic, active in hormone-refractory prostate cancer.<sup>49</sup> It comprises of a cisplatin-like fragment (*cis* ammine and aminocyclohexane non-leaving ligands) and two axial acetate ligands. The drug undergoes an *in vivo* reduction elimination reaction with a loss of the axial acetate ligands. This biotransformation produces several products, the most prominent being JM118 (*cis*-amminedichloro-cyclohexylamineplatinum(II)).<sup>26</sup> The drug interacts with DNA bases by most likely forming the adducts having the {Pt(NH<sub>3</sub>)(NH<sub>2</sub>C<sub>6</sub>H<sub>11</sub>)} fragments. Combination therapy of satraplatin

together with an anti-inflammatory agent, prednisone, for the treatment of hormone-refractory prostate cancer looks promising with survival rates of 14.9 months in patients compared to 11.9 months for prednisone alone.<sup>26,69</sup>

LA-12 (*OC-6-43*)-bis(acetato)(1-adamantylamine)amminedichloroplatinum(IV) is a novel Pt(IV) drug that has recently entered Phase I clinical trials. It bears a 1-adamantylamine non-leaving group which differs from the cyclohexylamine ligand contained in its derivative satraplatin. LA-12 shows superior cytotoxic effects than cisplatin and satraplatin, as well as reduced acute toxicity *in vivo*.<sup>20</sup>

#### **1.4 Non-platinum anticancer active complexes: ruthenium complexes as anticancer agents**

The slow ligand exchange kinetics of ruthenium, particularly Ru(II) and Ru(III) ions, are comparable to that of Pt(II), making this transition metal ion a favourable candidate for anticancer and anti-metastatic investigations.<sup>69</sup> Ru(III) is transported as a complex by serum proteins called transferrins.<sup>44</sup> This is because ruthenium has the ability to imitate iron species, a property which suits it well for medicinal purposes such as tumour targeting.<sup>70</sup> However, there is not much research that has been conducted on ruthenium complexes as potential anticancer agents. This presents a need for Ru-focused research as anticancer agents. The scope can include the development of homonuclear (Ru-Ru) and heteronuclear (Ru-Pt, Ru-Pd) complexes. A change of the metal ion to Ru may give complexes with better and low toxicological profile, good aqueous solubility for oral administration, improved spectrum of anticancer activity and more vitally compounds showing minimum or no resistance to tumours. The structures of the two most promising Ru(III) compounds that have entered human clinical trials are shown in **Figure 1.11**.

The first ruthenium compound to enter clinical trials for cancer treatment was the low-spin  $d^5$  octahedral ruthenium(III) complex, NAMI-A, imidazolium *trans*-[tetrachloro(dimethylsulfoxide)(imidazole)ruthenate(III)].<sup>71</sup> The activity of NAMI-A is dissimilar to that of cisplatin where covalent bifunctional adducts with DNA are formed. NAMI-A is transported by a vesicle transferrin receptor-mediated endocytosis mechanism to the site of cancerous cells where it gets localised unhindered as a Ru(III) species. It induces its activity by suppressing tumours.<sup>69</sup> At the site of action and under conditions of low pH, the inert Ru(III)

complexes undergo an activation-by-reduction reaction to their active Ru(II) congeners.<sup>70</sup> Therefore, in this manner they act as pro-drugs. The metal-metal bond formation of the Ru-transferrin complex is reversible.<sup>44</sup> NAMI-A is active against secondary metastatic tumours. A formation of severe blisters on the hands and feet of patients undergoing NAMI-A therapy was shown to be a dose-limiting side effect.<sup>70</sup>

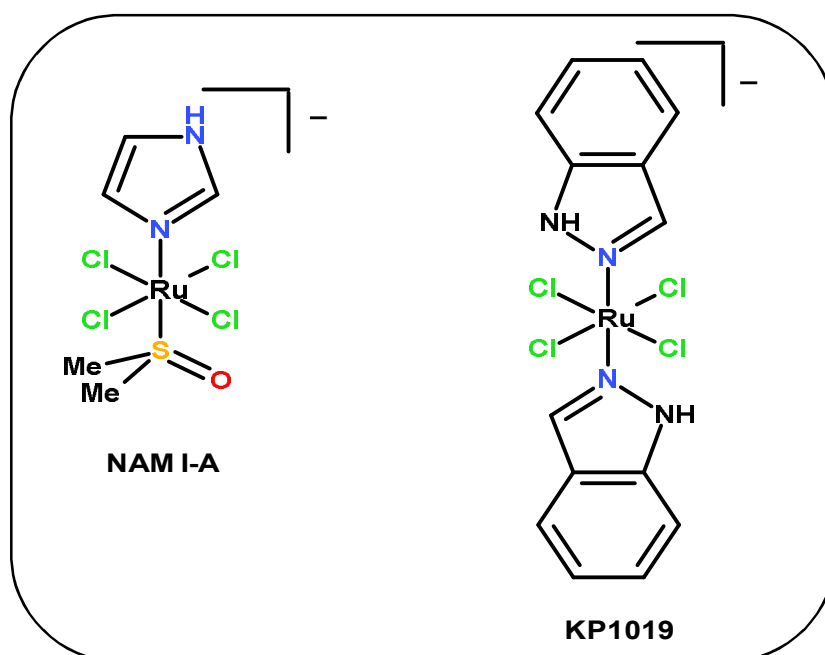


**Figure 1.11:** Anticancer and anti-metastatic Ru(III) agents **NAMI-A**<sup>71</sup> and **KP1019**<sup>70</sup> which act by unique mechanisms to Pt(II) compounds.

Indazolium Ru(III) complex *trans*-[tetrachloro-bis(1H-indazole)ruthenate(III)] (KP1019 or FFC14A) is an anticancer agent with comparable rates of hydrolysis as cisplatin.<sup>44</sup> Unique to NAMI-A, KP1019 does have cytotoxic effects against primary tumours such as colorectal cancer, for which clinical trials are still undergoing.<sup>69</sup> A similar mechanism of transport to that of NAMI-A is proposed for this cytotoxic in which two ligands of the KP1019 complex bind to transferrin. The exact mechanism for the cytotoxicity it is not fully known. When delivery of KP1019 to the cancerous cells occurs, the drug can either bind to biomolecules such as DNA, preferentially to guanine and adenine residues,<sup>69</sup> forming Ru-DNA strands which cause a kink in the double-helical structure. Alternatively, the drug may interact with histidine protein residues,<sup>69</sup> although this latter mechanism has no substantial backing. Between these two ruthenium-based antineoplastic drugs, only KP1019 has been proposed to enter Phase II of human trials for colorectal cancer.<sup>70</sup>

## 1.5 Mechanistic studies of *cis*-Pt(II) and Pd(II) complexes with bidentate non-leaving ligands

The realisation that antitumour activity could still be maintained when mono-dentate ammine (NH<sub>3</sub>) groups of cisplatin are substituted by bidentate ligands as found in the structures of carboplatin, oxaliplatin and other complexes raised the hope that a future cisplatin analogue can be possible through careful choice or adjusting of the peripheral groups on existing bidentate ligands.<sup>29</sup> An example of such design attempts is the DNA intercalator and covalent binder **PtCl<sub>2</sub>(DIP)**, presented in **Figure 1.6** in Section 1.2.3 of this Chapter. Kineticists are curious to understand the reactivity and mechanism of such candidate complexes.

Summa *et al.*<sup>72</sup> synthesised a series of *cis*-Pt(II) complexes with **en** (ethylenediamine), **dach** (*cis*-1,2-diaminocyclohexane), **amp** (2-aminomethylpyridine) and **bipy** (N,N'-bipyridine) N,N-bidentate chelates (**Figure 1.12**) and studied their substitution reactions with bio-relevant nucleophiles *viz.*, (thiourea (tu), *L*-methionine (*L*-Met) and guanosine-5'-monophosphate (5'-GMP). The rate of aqua substitution from the complexes was studied under *pseudo*-first order conditions. The rate increased with increasing number of pyridines due to back donation of electrons from the metal orbitals into the π\* -acceptor orbitals of the pyridines.

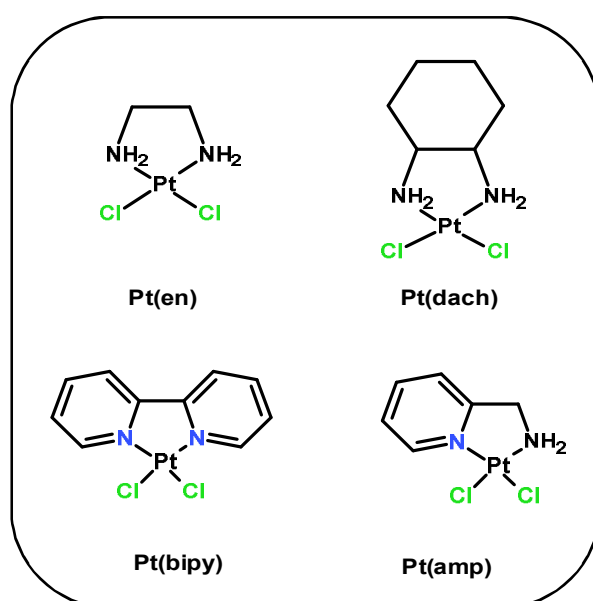


**Figure 1.12:** Structures of the *cis*-Pt(II) complexes with N,N-bidentate chelates studied by Summa *et al.*<sup>72</sup>

In the case of **dach**, the rate was influenced by the positive inductive donation toward the Pt metal centre as well as steric bulk effects, both of which decreased the rate. The ratio for the magnitude of retardation from **en** to **bipy** was observed to be: tu (1:149); <sub>L</sub>-Met (1:31); and 5'-GMP(1:6).

In another study, Summa *et al.*<sup>73</sup> reported the aqua substitution from Pt(dach) derivatives differing in the bidentate groups O-O (CBDCA; *O,O*-cyclobutane-1,1-dicarboxylate); N-O (gly, glycine), and N-S (<sub>L</sub>-Met, methionine) (**Figure 1.13** below) using thiourea (tu), <sub>L</sub>-methionine (<sub>L</sub>-Met), glutathione (GSH) and guanosine-5'-monophosphate (5'-GMP) as nucleophiles. Substitution of bidentates proceeded consecutively *via* a direct nucleophilic attack of one end (ring-opening) of the coordinated O-O (CBDCA; *O,O*-cyclobutane-1,1-dicarboxylate ); N-O (gly, glycine), and N-S (<sub>L</sub>-Met, methionine) followed by an attack on the coordinated end or ring-closure (in case of <sub>L</sub>-Met as a nucleophile).

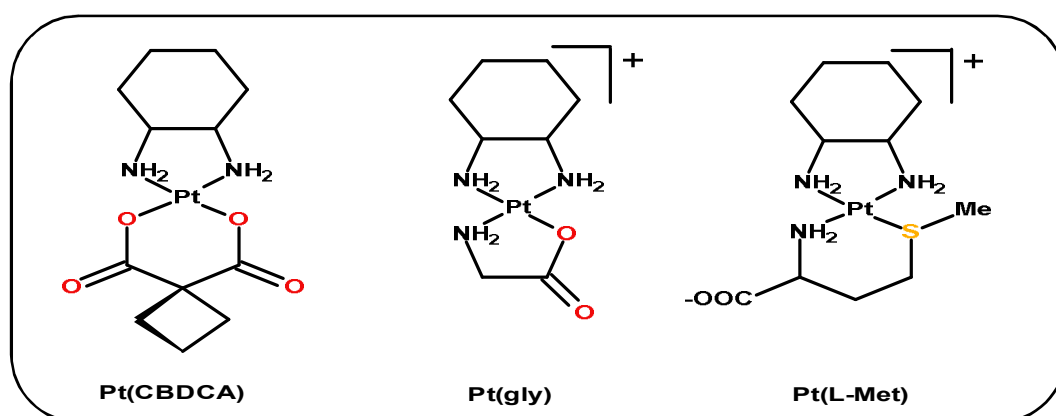


**Figure 1.13** Structures of the Pt(dach) analogues studied by Summa *et al.*<sup>73</sup>

The reactivity of the complexes increased in the following order: Pt(dach)(CBDCA) < Pt(dach)(L-Met) < Pt(dach)(gly). The trend in the reactivity of the nucleophiles was: thiourea > GSH > L-Met > 5'-GMP. The soft S-donor biomolecules have a high affinity for platinum which may exacerbate the *in vivo* toxicity of Pt(II) drugs in addition to deactivating them before reaching the nucleus of the cell. Thus, the *in vitro* kinetic data as well as the proposed mechanisms of substitution affords a better understanding of the possible modes of interactions of such complexes with platinumophiles prior to DNA binding.

Recently, Ray *et al.*<sup>74</sup> compared the reactivity of **Pt(dach)(oxalate)** and **Pt(bipy)(oxalate)** towards thiourea, 2-thiouracil, diethyldithiocarbamate, <sub>DL</sub>-penicillamine



and thiosemicarbazide. The **Pt(dach)(oxalate)** complex was used to model the *in vivo* reactivity of oxaliplatin. They observed the same order of reactivity reported by Summa *et al.*<sup>73</sup> **Pt(bipy)(oxalate)** was found to be more reactive when compared to **Pt(dach)(oxalate)** towards all the nucleophiles. The bipy ligand of **Pt(bipy)(oxalate)** disperses electron density from the metal *via* the  $\pi$ -acceptor effect. This makes the Pt(II) metal centre more electrophilic and better at stabilising the transition state during the formation of a new bond with the incoming nucleophile. The rate of substitution is thereby increased.

Bogojeski *et al.*<sup>75</sup> examined the chloride ligand substitution reactions of four *cis*-Pt(II) complexes bearing N,N-carrier groups. Two of the complexes that were studied, [Pt(dach)Cl<sub>2</sub>] and [Pt(en)Cl<sub>2</sub>], were similar to those studied by Summa *et al.*<sup>76</sup> However, Summa's complexes were aqua derivatives which by comparison, were more reactive towards N-donor nucleophiles namely 5'-GMP, L-histidine and 1,2,4-triazole. Since the aqua ligand is weaker when compared to the chloride ligand and it is easily substituted.<sup>77</sup> Similarly, the [Pt(dach)Cl<sub>2</sub>] complex is more labile than [Pt(dach)(CBDCA)] or [Pt(dach)(gly)] towards substitution.<sup>73</sup> Put together, the rate of substitution from the *cis*-Pt(II) complexes with N,N-bidentate non-leaving ligand could be controlled either by varying the inert spectator ligands or the labile leaving groups and this can be a gateway to optimise their potential cytotoxicity.

Kinetic data of Pd(II) complexes is relevant to the search of antitumour metallo-drugs even though their reactivity are 10<sup>4</sup>-10<sup>5</sup> times more than those of Pt(II) complexes which are considered reference cytostatic complexes due to their moderate and comparable rate of ligand exchange to that of replication in cancerous cells. Bogojeski *et al.*<sup>78</sup> investigated the rate of chloride substitution in a set of *cis*-Pd(II) complexes. Imidazolin-2-imine spectator ligands (2-[(1,3-diisopropyl-4,5-dimethyl-imidazol-2-ylidene)amino]ethanamine, **EAlm**<sup>iPr</sup>; 2-[(1,3-diisopropyl-4,5-dimethyl-imidazol-2-ylidene)amino]-N,N-dimethyl-ethanamine, **DMEAlm**<sup>iPr</sup>; (1S,2S)-2-[(1,3-diisopropyl-4,5-dimethyl-imidazol-2-ylidene)amino]-1,2-diphenyl-ethanamine, **DPENIm**<sup>iPr</sup>; N-[2-[(1,3-diisopropyl-4,5-dimethyl-imidazol-2-ylidene)amino]ethyl]-1,3-diisopropyl-4,5-dimethyl-imidazol-2-imine, **BL**<sup>iPr</sup>; N-[(1R,2R)-2-[(1,3-diisopropyl-4,5-dimethyl-imidazol-2-ylidene)amino]cyclohexyl]-1,3-diisopropyl-4,5-dimethyl-imidazol-2-imine, **DACH(Im**<sup>iPr</sup>)<sub>2</sub>) of varying steric and electronic properties were coordinated to the Pd(II) metal centre (**Figure 1.14**). The complex [Pd(en)Cl<sub>2</sub>] was used as a model reference to the reactivity of cisplatin. The reactivity trend for the step-wise

substitution of the chloride ligands by all bio-relevant nucleophiles thiourea (tu), *L*-methionine (*L*-met), *L*-histidine (*L*-his) and glycine (gly) decreased in the order: **[Pd(en)Cl<sub>2</sub>] > [Pd(EAlm<sup>iPr</sup>)Cl<sub>2</sub>] > [Pd(DMEAlm<sup>iPr</sup>)Cl<sub>2</sub>] > [Pd(DPENIm<sup>iPr</sup>)Cl<sub>2</sub>] > [Pd(BL<sup>iPr</sup>)Cl<sub>2</sub>] > [Pd(DACH(Im<sup>iPr</sup>)<sub>2</sub>)Cl<sub>2</sub>]**.

The rate constants,  $k_1$  and  $k_2$  for the first and second substitution steps decreased by factors of 4238: 762: 41: 31: 1 and 215: 12: 6: 4: 3: 1 for **[Pd(en)Cl<sub>2</sub>]: [Pd(EAlm<sup>iPr</sup>)Cl<sub>2</sub>]: [Pd(DMEAlm<sup>iPr</sup>)Cl<sub>2</sub>]: [Pd(DPENIm<sup>iPr</sup>)Cl<sub>2</sub>]: [Pd(BL<sup>iPr</sup>)Cl<sub>2</sub>]: [Pd(DACH(Im<sup>iPr</sup>)<sub>2</sub>)Cl<sub>2</sub>]**, respectively, when thiourea (tu) was the entering nucleophile.<sup>78</sup> The reactivity trend was attributed to both steric bulkiness and  $\sigma$ -donation properties of the substituents on the imidazolin-2-imine non-leaving ligands.<sup>78</sup> Donation of electron density onto the Pd(II) centre leads to a decrease in electrophilicity of Pd and slowing of the approach of the entering ligand, leading to lower rates of substitution. Through careful design of the steric hindrance/bulk of non-leaving and leaving groups the highly reactive and anti-tumour inactive Pd complexes can be kinetically moderated into less reactive species which may be anti-tumour active and have good potential to avoid deactivation by ubiquitous sulphur containing bio-nucleophiles.

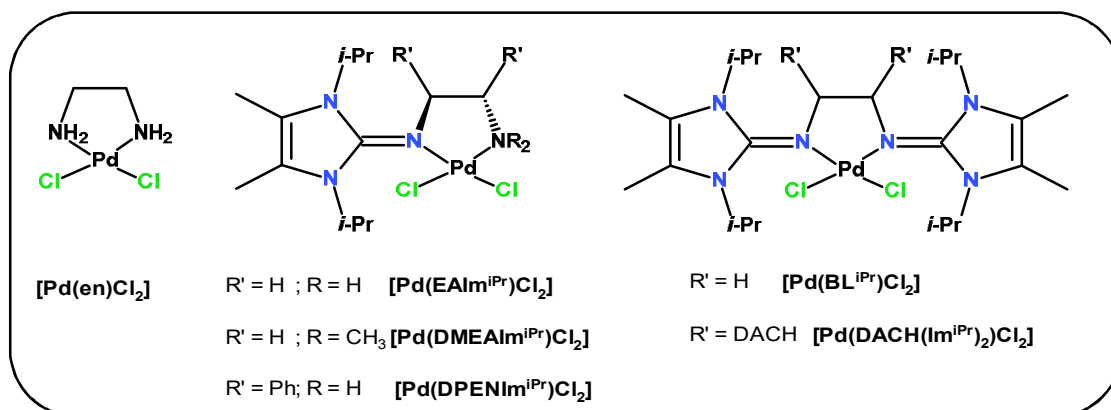


**Figure 1.14:** Structures of Pd(II)-imidazolin-2-imine complexes studied by Bogojeski *et al.*<sup>78</sup>

Hochreuther *et al.*<sup>79-81</sup> investigated the  $\sigma$ -donor and  $\pi$ -acceptor effects on the rate of substitution from two diaqua *cis*-Pt(II) complexes namely, **Pt(mtp)** (mtp = 2-methylthiomethylpyridine) and **Pt(amp)** shown in (Figure 1.15). The complexes bear a thioether (-SCH<sub>3</sub>) and pyridine ring or amine (-NH<sub>2</sub>) in their bidentate ligands. The thioether and primary amine units have different effects on the rate of substitution of the leaving groups. The first aqua ligand to be substituted is the one *trans* to the S-thioether due to the

strong *trans* labilizing effect of sulphur in the **Pt(mtp)** complex. However, in **Pt(amp)**, the aqua ligand *trans* to pyridine is substituted first as was also noted by Samanta *et al.*<sup>82</sup> on the same complex. The pyridine ring accepts electron density from the metal centre rendering it more electrophilic and increasing the rate of aqua ligand substitution. Between the two complexes, **Pt(mtp)** is more reactive than **Pt(amp)**. Similar results were reported for the dinuclear Pt analogues of the complexes with N,N-bidentates.<sup>79,80</sup>

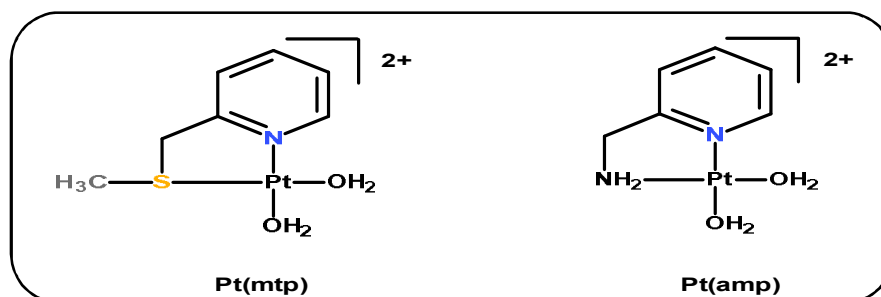


**Figure 1.15:** Structures of mononuclear Pt(II) complexes studied by Hochreuther *et al.*<sup>79-81</sup>

## 1.6 Aims of the Study

For more than 40 years since its discovery and clinical use, cisplatin has proven to be the only superior platinum-based drug.<sup>29</sup> Several structurally related ‘classical’ derivatives as well as structurally unrelated ‘non-classical’ compounds were subsequently produced but with less efficacy when compared to cisplatin. The need to find novel platinum complexes with better anti-mutative properties but diminished natural or acquired resistance to cancer proliferation still exists. Rational design of platinum complexes with carefully chosen carrier ligands to facilitate their stability may be one of the many approaches in the search of new lead Pt-compounds for clinical trials. In general, chelation of a non-leaving group stabilises the square-planar Pt(II) geometry, and where the ligand is planar, the complex may intercalate between the base pairs of DNA in addition to covalent binding to it, both of which induces helical instability and downstream apoptotic-related cellular pathways. Imperative to this search of lead compounds is the kinetics and thermodynamics data. Such data is fundamental in understanding mechanisms of drug toxicity in general and specifically the mode of alleviating sulphur deactivation through chemo-protection and reducing the intrinsic reactivity of platinum(II) complexes.<sup>62,77</sup> Square-planar platinum complexes can be systematically modified through electronic push-and-pull factors as well as steric effects.

In the current study, six mononuclear *cis*-Pt(II) complexes with mixed N,S-bidentates comprising of either a 2-(phenylthiomethyl)pyridine or 2-(phenylthiomethyl)quinoline core chelates were synthesised and characterised. The thioether was incorporated into the non-leaving group to stabilise the complexes against aqueous hydrolysis (**Figure 1.16** below). The difference in the structures of the N,S-bidentate enables one to infer on the effect on the rate of substitution of changing the N-donor (pyridyl/quinolyl), and also the role of the substituents on the phenyl ring of the thioether S-donor end of the bidentate chelates. Their substitution kinetics was done using bio-relevant thiourea nucleophiles under *pseudo*-first-order conditions.

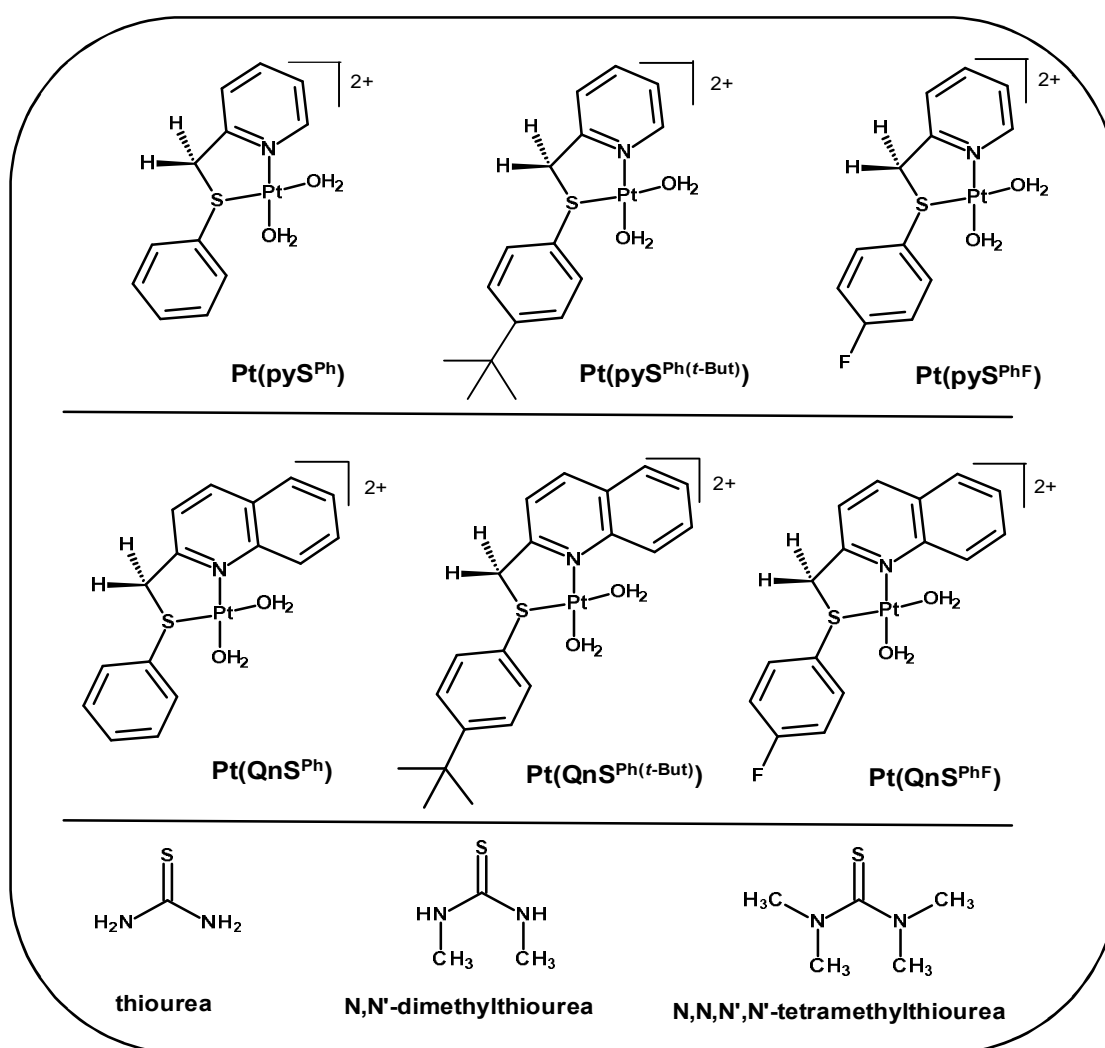


**Figure 1.16:** Structures of *cis*-Pt(II) complexes with N,S-bidentate ligands.

As already pointed out, there are few reports on the reactivity of *cis*-Pt(N,S)(H<sub>2</sub>O)<sub>2</sub>.<sup>81</sup> The bidentate ligands were chosen on motivation from two recent reports by Khushi *et al.*<sup>83 84</sup>

on the rates of aqua substitution from a structurally related set of *cis*-Pt(N,N)(H<sub>2</sub>O)<sub>2</sub> where N,N is a flexible (pyrazolylmethyl)pyridine or (pyrazolylmethyl)quinoline bidentate ligand. An interesting anomalous trend was that the analogues complex with a quinoline in the N,N-bidentate was less reactive when compared to its pyridine counterpart. This was attributed to the accumulation of electron density on the metal centre due to the relative poor  $\pi$ -acceptor ability of quinoline despite its conjugated benzopyridine rings. This anomalous observation was first reported in the work of Ongoma and Jaganyi.<sup>85</sup> Kinunda and Jaganyi<sup>86</sup> and Wekesa and Jaganyi<sup>87</sup> also confirmed a slow rate of substitution of the leaving group for tridentate Pt(II) complexes, where the quinoline formed part of the chelate in a *cis* position. Also noted was that one of the pyridine coordinated-complex studied by Khushi *et al.*<sup>83</sup> had been shown by Segapelo *et al.*<sup>53</sup> to have remarkable cytotoxicity against a model of human HeLa cell lines.

The nucleophiles *viz.*, thiourea (tu), N,N'-dimethylthiourea (dm tu) and N,N,N',N'-tetramethylthiourea (tmtu) were carefully chosen because of their biological relevance. These S-containing nucleophiles have an interesting biphilic character in that they can either act as  $\sigma$ -donors (thioether) or  $\pi$ -acceptors (thiolates), a property which is also known for some biomolecular species. Therefore, it is vital to understand the reactivity of these model *cis*-Pt(II) complexes with such nucleophiles to elucidate their possible mechanism of action with the hope of advancing the medicinal use of metal-based drugs.

For convenience of reporting, the six complexes were grouped into sub-groups *i.e.* those that have pyridine and quinoline at the donor end of the N,S-bidentate. Through a comparative analysis of the second order rate constants,  $k_1$  and  $k_2$ , in each sub-category of the complexes, the effect of the substituent on the phenyl ring of the thioether on the reactivity of the Pt complexes was assessed. A comparison of the rates of substitution for paired analogues of the pyridine/quinoline in each set was used to confirm the effect of quinoline on the rate *i.e.* whether it retarded the rate as already reported in literature.<sup>83-87</sup>

## 1.7 References

1. M.-H. Pan and C.-T. Ho, *Chemical Society Reviews*, 2008, **37**, 2558-2574.
2. B. A. J. Ponder and M. J. Waring, *The Science of cancer treatment*, Kluwer Academic Publishers, Dordrecht; Boston, 1990.
3. M. J. Cleare, *Coordination Chemistry Reviews*, 1974, **12**, 349-405.
4. M. Galanski, M. A. Jakupec and B. K. Keppler, *Current Medicinal Chemistry*, 2005, **12**, 2075-2094.
5. M. Fanelli, M. Formica, V. Fusi, L. Giorgi, M. Micheloni and P. Paoli, *Coordination Chemistry Reviews*, 2016, **310**, 41-79.
6. J. Reedijk, *Proceedings of the National Academy of Sciences*, 2003, **100**, 3611-3616.
7. M. Peyrone, *Justus Liebigs Annalen der Chemie*, 1844, **51**, 1-29.
8. B. Rosenberg and L. Vancamp, *Nature*, 1969, **222**, 385-386.
9. B. Rosenberg, *Naturwissenschaften*, 1973, **60**, 399-406.
10. B. Rosenberg, E. Renshaw, L. Vancamp, J. Hartwick and J. Drobnik, *Journal of Bacteriology*, 1967, **93**, 716-721.
11. J. Reedijk, *Chemical Communications*, 1996, 801-806.
12. E. R. Jamieson and S. J. Lippard, *Chemical Reviews*, 1999, **99**, 2467-2498.
13. L. M. Pasetto, M. R. D'Andrea, A. A. Brandes, E. Rossi and S. Monfardini, *Critical Reviews in Oncology/Hematology*, 2006, **60**, 59-75.
14. T. A. Connors, *Platinum Metals Review*, 1973, **17**, 98-101.
15. M. J. Cleare, P. C. Hydes, B. W. Malerbi and D. M. Watkins, *Biochimie*, 1978, **60**, 835-850.
16. M. J. Cleare and J. D. Hoeschele, *Platinum Metals Review*, 1973, **17**, 2-13.
17. M. J. Cleare and J. D. Hoeschele, *Bioinorganic Chemistry*, 1973, **2**, 187-210.
18. R. C. Todd and S. J. Lippard, *Metallomics*, 2009, **1**, 280-291.
19. J. Reedijk, *Platinum Metals Review*, 2008, **52**, 2-11.
20. P. Bouchal, J. Jarkovsky, K. Hrazdilova, M. Dvorakova, I. Struharova, L. Hernychova, J. Damborsky, P. Sova and B. Vojtesek, *Proteome Science*, 2011, **9**, 1-9.
21. A. J. Thomson, *Platinum Metals Review*, 1977, **21**, 2-15.
22. A. Bakalova, *Journal of the University of Chemical Technology and Metallurgy*, 2006, **41**, 119-124.

23. K. Irena, *Recent Patents on Anti-Cancer Drug Discovery*, 2006, **1**, 1-22.
24. A. G. Quiroga, *Current Topics in Medicinal Chemistry*, 2011, **11**, 2613-2622.
25. T. C. Johnstone, K. Suntharalingam and S. J. Lippard, *Chemical Reviews*, 2016, **116**, 3436-3486.
26. L. Kelland, *Nat Rev Cancer*, 2007, **7**, 573-584.
27. P. Joanna, J. Dagmara, W. Dariusz and C. n. Lech, *Current Pharmaceutical Analysis*, 2014, **10**, 2-9.
28. D. Wang and S. J. Lippard, *Nat Rev Drug Discov*, 2005, **4**, 307-320.
29. F. Muggia, A. Bonetti, J. Hoeschele, M. Rozenzweig and S. Howell, *Journal of clinical oncology: official journal of the American Society of Clinical Oncology*, 2015, **33**, 4219-4226.
30. N. Nagai, R. Okuda, M. Kinoshita and H. Ogata, *Journal of Pharmacy and Pharmacology*, 1996, **48**, 918-924.
31. B. Desoize and C. Madoulet, *Critical Reviews in Oncology/Hematology*, 2002, **42**, 317-325.
32. G. Markus, A. J. Michael and K. K. Bernhard, *Current Medicinal Chemistry*, 2005, **12**, 2075-2094.
33. C. J. Jones and J. Thornback, *Medicinal applications of coordination chemistry*, Royal Society of Chemistry, 2007.
34. S. Ahmad, *Verlag Helvetica Chimica Acta AG*, 2010, **7**, 543-566.
35. D. P. Bancroft, C. A. Lepre and S. J. Lippard, *Journal of the American Chemical Society*, 1990, **112**, 6860-6871.
36. M. K. Brière, R. Goel, H. F. Shirazi, J. D. Stewart and P. I. C. Smith, *Cancer Chemotherapy and Pharmacology*, 1996, **37**, 518-524.
37. P. M. Takahara, A. C. Rosenzweig, C. A. Frederick and S. J. Lippard, *Nature*, 1995, **377**, 649-652.
38. P. M. Takahara, C. A. Frederick and S. J. Lippard, *Journal of the American Chemical Society*, 1996, **118**, 12309-12321.
39. E. Wong and C. M. Giandomenico, *Chemical Reviews*, 1999, **99**, 2451-2466.
40. T. C. Johnstone, K. Suntharalingam and S. J. Lippard, *Philosophical Transactions of the Royal Society of London A: Mathematical, Physical and Engineering Sciences*, 2015, **373**.

41. K. S. Lovejoy and S. J. Lippard, *Dalton Transactions*, 2009, DOI: 10.1039/B913896J, 10651-10659.
42. C. X. Zhang and S. J. Lippard, *Current Opinion in Chemical Biology*, 2003, **7**, 481-489.
43. D. Esteban-Fernandez, E. Moreno-Gordaliza, B. Canas, M. Antonia Palacios and M. Milagros Gomez-Gomez, *Metallomics*, 2010, **2**, 19-38.
44. P. J. Sadler and Z. Guo, *Pure and Applied Chemistry*, 1998, **70**, 863-871.
45. N. J. Wheate and J. G. Collins, *Coordination Chemistry Reviews*, 2003, **241**, 133-145.
46. K. R. Harrap, *Cancer Treatment Reviews*, 1985, **12**, 21-33.
47. C. F. J. Barnard, *Platinum Metals Review*, 1989, **33**, 162-167.
48. D. Lebwohl and R. Canetta, *European Journal of Cancer*, 1998, **34**, 1522-1534.
49. T. Boulikas, A. Pantos, E. Bellis and P. Christofis, *Cancer Ther*, 2007, **5**, 537-583.
50. P. W. Atkins, *Shriver & Atkins' inorganic chemistry*, Oxford University Press, Oxford; New York, 2010, 202, 218.
51. Y. Kidani, R. Kizu, M. Miyazaki, M. Noji, A. Matsuzawa, Y. Takeda, N. Akiyama and M. Eriguchi, in *Platinum and Other Metal Coordination Compounds in Cancer Chemotherapy 2*, eds. H. M. Pinedo and J. H. Schornagel, Springer US, Boston, MA, 1996, DOI: 10.1007/978-1-4899-0218-4\_5, pp. 43-51.
52. R. Kizu, T. Nakanishi, K. Hayakawa, A. Matsuzawa, M. Eriguchi, Y. Takeda, N. Akiyama, T. Tashiro and Y. Kidani, *Cancer Chemotherapy and Pharmacology*, 1999, **43**, 97-105.
53. T. V. Segapelo, I. A. Guzei, L. C. Spencer, W. E. V. Zyl and J. Darkwa, *Inorganica Chimica Acta*, 2009, **362**, 3314-3324.
54. W. Liu, J. Jiang, Y. Xu, S. Hou, L. Sun, Q. Ye and L. Lou, *Journal of Inorganic Biochemistry*, 2015, **146**, 14-18.
55. N. Shahabadi, S. Kashanian and A. Fatahi, *Bioinorganic Chemistry and Applications*, 2011, **2011**, 687571.
56. M. Van Beusichem and N. Farrell, *Inorganic Chemistry*, 1992, **31**, 634-639.
57. U. Kalinowska-Lis, J. Ochocki and K. Matlawska-Wasowska, *Coordination Chemistry Reviews*, 2008, **252**, 1328-1345.
58. D. Gibson, *Dalton Transactions*, 2009, DOI: 10.1039/B918871C, 10681-10689.
59. V. Brabec, P. Christofis, M. Slámová, H. Kostrhunová, O. Nováková, Y. Najajreh, D. Gibson and J. Kašpárková, *Biochemical Pharmacology*, 2007, **73**, 1887-1900.



60. B. Rosenberg, *Interdisciplinary Science Reviews*, 1978, **3**, 134-147.
61. K. Lemma, T. Shi and L. I. Elding, *Inorganic Chemistry*, 2000, **39**, 1728-1734.
62. K. Lemma, S. K. C. Elmroth and L. I. Elding, *Journal of the Chemical Society, Dalton Transactions*, 2002, 1281-1286.
63. D. Gibson, *Dalton Transactions*, 2016.
64. Y.-R. Zheng, K. Suntharalingam, T. C. Johnstone and S. J. Lippard, *Chemical Science*, 2015, **6**, 1189-1193.
65. K. Lemma, D. A. House, N. Retta and L. I. Elding, *Inorganica Chimica Acta*, 2002, **331**, 98-108.
66. K. Lemma, J. Berglund, N. Farrell and L. I. Elding, *Journal of Biological Inorganic Chemistry*, 2000, **5**, 300-306.
67. P. D. J., *Cancer chemotherapy reports. Part 1*, 1975, **59**, 287.
68. S. Choi, L. Vastag, C.-H. Leung, A. M. Beard, D. E. Knowles and J. A. Larrabee, *Inorganic Chemistry*, 2006, **45**, 10108-10114.
69. M. J. Hannon, *Pure and Applied Chemistry*, 2007, **79**, 2243-2261.
70. E. S. Antonarakis and A. Emadi, *Cancer chemotherapy and pharmacology*, 2010, **66**, 1-9.
71. L. Messori, F. Kratz and E. Alessio, *Metal-Based Drugs*, 1996, **3**, 1-9.
72. N. Summa, W. Schiessl, R. Puchta, N. van Elkema Hommes and R. van Eldik, *Inorganic Chemistry*, 2006, **45**, 2948-2959.
73. N. Summa, T. Soldatović, L. Dahlenburg, Ž. D. Bugarčić and R. van Eldik, *JBIC Journal of Biological Inorganic Chemistry*, 2007, **12**, 461-475.
74. S. Ray, P. Karmakar, A. Chattopadhyay, D. Nandi, R. Sarkar and A. K. Ghosh, *International Journal of Chemical Kinetics*, 2016, **48**, 347-357.
75. J. Bogojeski, Ž. D. Bugarčić, R. Puchta and R. van Eldik, *European Journal of Inorganic Chemistry*, 2010, **2010**, 5439-5445.
76. W. S. N. Summa, R. Puchta, N. van Elkema Hommes and R. van Eldik, *Inorg. Chem.*, 2006, **45**, 2948-2959.
77. Ž. D. Bugarčić, J. Bogojeski and R. van Eldik, *Coordination Chemistry Reviews*, 2015, **292**, 91-106.
78. J. Bogojeski, J. Volbeda, M. Freytag, M. Tamm and Ž. D. Bugarčić, *Dalton Transactions*, 2015, **44**, 17346-17359.

79. S. Hochreuther, R. Puchta and R. van Eldik, *Inorganic Chemistry*, 2011, **50**, 8984-8996.
80. S. Hochreuther, R. Puchta and R. van Eldik, *Inorganic Chemistry*, 2011, **50**, 12747-12761.
81. S. Hochreuther, S. T. Nandibewoor, R. Puchta and R. van Eldik, *Dalton Transactions*, 2012, **41**, 512-522.
82. A. Samanta, G. K. Ghosh, I. Mitra, S. Mukherjee, J. C. Bose, S. Mukhopadhyay, W. Linert and S. C. Moi, *RSC Adv.*, 2014, **4**, 43516-43524.
83. B. B. Khusi, A. Mambanda and D. Jaganyi, *Transition Metal Chemistry*, 2016, **41**, 191-203.
84. B. B. Khusi, A. Mambanda and D. Jaganyi, *Journal of Coordination Chemistry*, 2016, **69**, 2121-2135.
85. P. Ongoma and D. Jaganyi, *Dalton Transactions*, 2012, **41**, 10724-10730.
86. G. Kinunda and D. Jaganyi, *Transition Metal Chemistry*, 2014, **39**, 451-459.
87. I. M. Wekesa and D. Jaganyi, *Journal of Coordination Chemistry*, 2016, **69**, 389-403.

# Chapter 2

## Theoretical considerations of the substitution reactions in square-planar complexes

### 2.0 Introduction

Extensive research has been carried out on the substitution of Pt(II) square-planar complexes since the discovery of the antitumour properties of cisplatin by Rosenberg and co-workers.<sup>1</sup> The mechanism by which cisplatin imparts its cytotoxicity involves, in part, nucleophilic substitution reactions with DNA nucleobases.<sup>2</sup> Data on the substitution kinetics of Pt(II) complexes cement the understanding of the interactions of the complexes in terms of maximising efficacy and minimising toxicity of potential new anticancer compounds and the development of resistance from cytoplasmic nucleophiles.<sup>3</sup>

A ligand substitution reaction entails replacement of a labile ligand in the coordination shell by another usually with stereochemical retention.<sup>4</sup> In an act of a simple substitution, there is no change in the oxidation state of the reaction centre. However, since bond-making and bond-breaking processes are involved, there is a temporary change in the coordination number in moving reactants to the transition state.

Substitution at the metal centre of coordination complex is similar to one at the carbon atom for organic reactions. In inorganic reactions, substitution reactions are classified per the way bonds are formed or broken. An electron pair in a chemical bond can be broken by having both electrons being shared between the reaction centre and the process is referred to as a homolysis reaction.<sup>5</sup> If an electron pair is added to the new bond with the reaction centre the process is called electrolytic.<sup>5</sup> If the leaving group departs with its pair of electrons, the bond between the electrophile and the nucleophile is said to have dissociated heterolytically. The aforementioned reactions can be described according to *Equations 2.1 - 2.3*, in which M and X represent the metal centre and the leaving group, respectively.<sup>6</sup>





Electrophilic and nucleophilic heterolysis processes correspond to the organic-type Lewis acid-base reactions. An electrophilic process presents the metal centre (M) as a Lewis base whilst a nucleophilic process presents it as a Lewis acid. In the latter case, the oxidation state of the reaction centre is insensitive to the change in number of the coordinated ligands and has no effect upon the number of bonding electrons.<sup>4, 5</sup> However, the electrophilic process is sensitive to the bonding of the previously non-bonding electrons, which correspond to a two-electron oxidation. Departure of the ligand as a Lewis acid completes the electrophilic substitution, whilst the attachment of a Lewis base (+L:) from the medium leads to a stabilization of the higher oxidation state. The electrophilic bonding and non-bonding processes are summarized in **Figure 2.1** below.

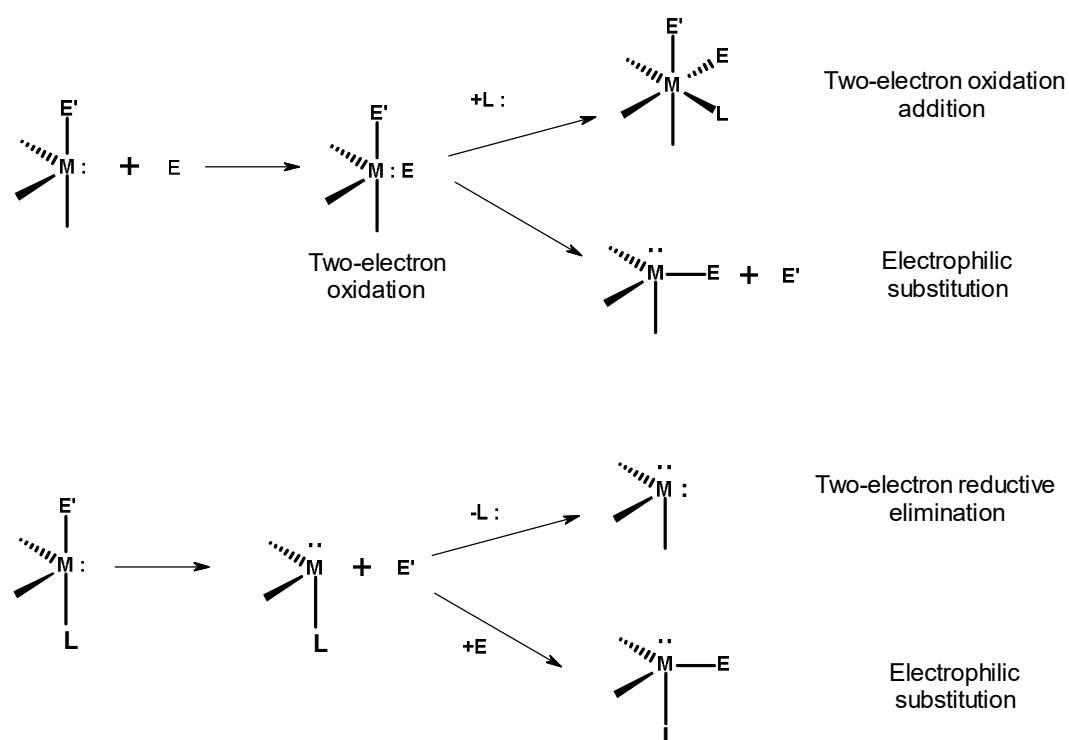


**Figure 2.1** Heterolytic bond-making and bond-breaking processes.<sup>4,5</sup>

## 2.1 Substitution reaction mechanisms

The concepts of *stoichiometric* and *intimate* mechanisms, were coined by Langford and Gray to describe the modes of substitution of inorganic reactions particularly those of transition metals (**Figure 2.2**).<sup>7</sup> The stoichiometric mechanism is classified according to three categories depending on the nature of the intermediate species:<sup>4,5,8</sup>

- I. **An associative (A) process** – the reaction coordinate has an identifiable intermediate of higher coordination number formed by an attack of the entering ligand onto the coordination sphere. The formation of the new bond is the rate-determining step, and hence the rate of the reaction is sensitive to the entering ligand. The first transition state (T.S.1) has a maximum of higher energy when compared to that of the second (T.S.2).
- II. **A dissociative (D) process** – is characterized by an intermediate of lower coordination number in which a bond on the reactant is broken first. The rate of reaction is dependent upon the strength of the bond between the metal and the leaving group making it the rate-determining step. The second transition state (T.S.2) has a maximum of higher energy when compared to that of the first (T.S.1).
- III. **An interchange (I) process** – has an act of bond-breaking and bond-making occurring at the same time or within a pre-formed aggregate.

The stoichiometric interchange mechanism can be further classified per its intimate character, which is an indication of its mode of activation.

- I. **Associative Interchange (I<sub>a</sub>)** – the rate-determining step and hence the transition state is the formation of the bond between the metal (M) and the oncoming ligand (Y).
- II. **Dissociative Interchange (I<sub>d</sub>)** – the rate-determining step and transition state is the breaking of the bond between the metal (M) and the leaving ligand (X).

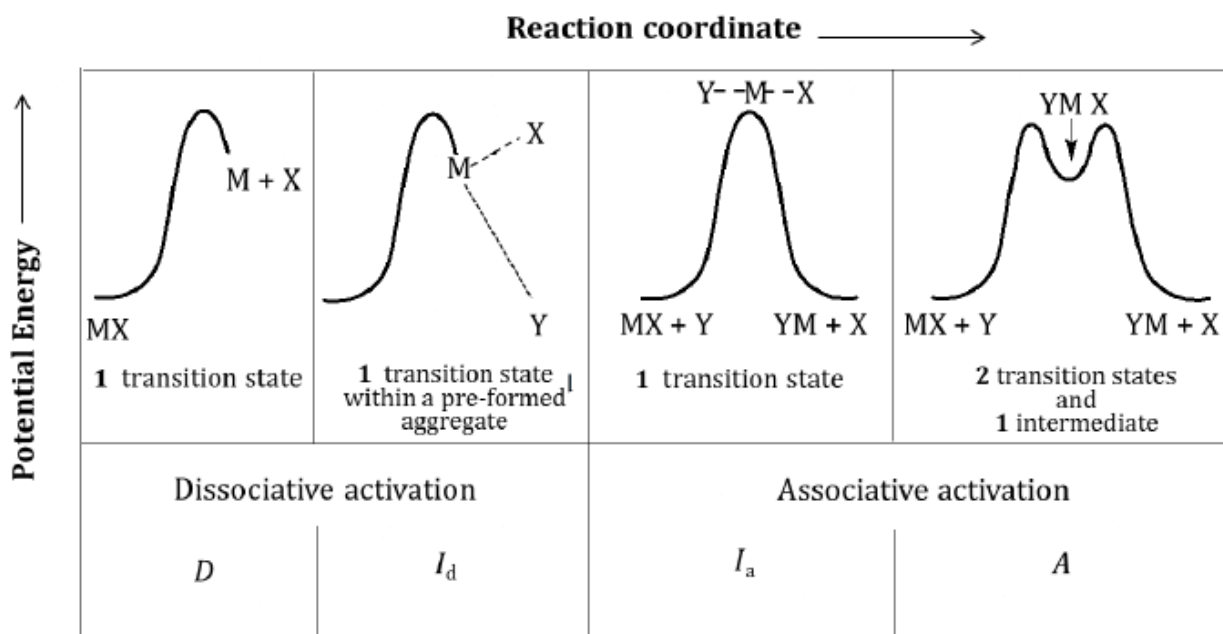


**Figure 2.2** Energy profile of the substitution mechanisms moving from D or  $I_d$  to A or  $I_a$ .

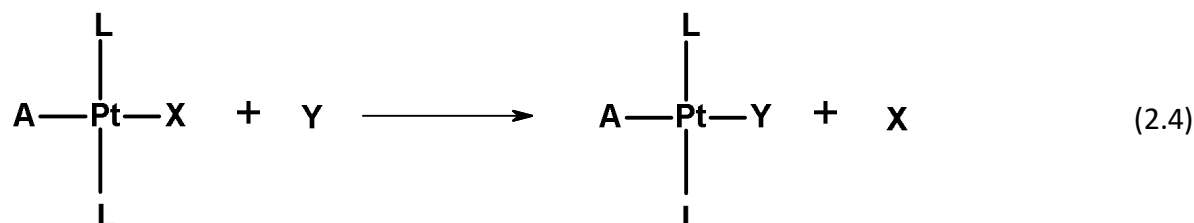
## 2.2 Substitution Reactions of Square-planar Complexes

The mechanism of ligand exchange in square-planar, particularly of Pt complexes has been studied extensively. This is due to the ease with which reactions can be monitored because of their time-scale.<sup>9-11</sup> Square-planar complexes are formed from coordination of four ligand sites around a  $d^8$  metal ion such as Pt(II), Pd(II), Au(III), Ni(II), Rh(I) and Ir(I) to form 16-electron species which are coordinatively unsaturated. They can easily undergo oxidative addition to attain an 18-electron octahedral coordination geometry.<sup>12</sup> This can be viewed as the mechanism that is prevalent if their substitution is associative. However, when the mechanism involves the loss of electrons from a 16-electron square-planar to form a 14-electron three-coordinate (T-shaped) transition state, substitution is described as being dissociative.<sup>13</sup> These cases are rare and require that the non-leaving ligand is sterically bulk so that the approach of the oncoming ligands is well shielded.<sup>14</sup>

Alkyl and aryl groups with positive  $\sigma$ -inductive effects coordinated directly onto the metal ion aid the accumulation of electron density onto the metal centre, making it electronegative. This results in the repulsion of charge from the oncoming ligands. Romeo and co-workers<sup>15</sup> studied the thioether ligand substitution by nucleophiles in complexes of the type *cis*-[PtR<sub>2</sub>S<sub>2</sub>] (R = Me or Ph; S = thioethers or Me<sub>2</sub>SO). The mode of substitution was dissociatively activated.

### 2.2.1 Mechanism of Substitution

The mechanism of substitution in square-planar complexes usually involves a direct attack of the leaving group (X) by the entering nucleophile (Y).



Represented by reaction 2.4 is a bimolecular substitution of the leaving group (X) containing a two-term rate law. The first term is first-order with respect to the complex ( $\text{PtL}_2\text{AX}$ ) while the second is first-order with respect to both the metal complex ( $\text{PtL}_2\text{AX}$ ) and the entering nucleophile (Y)

$$\text{Rate} = -\frac{d[\text{PtL}_2\text{AX}]}{dt} = k_1[\text{PtL}_2\text{AX}] + k_2[\text{PtL}_2\text{AX}][\text{Y}] = (k_1 + k_2[\text{Y}])[\text{PtL}_2\text{AX}] \quad (2.5)$$

If the concentration of the entering ligand, [Y], is at least 10-fold greater than the concentration of the complex,  $[\text{PtL}_2\text{AX}]$ , then *Equation 2.5* simplifies to *Equation 2.6*, where the observed *pseudo*-first-order rate constant,  $k_{\text{obs}}$ , is related to individual rate constants by *Equation 2.7*:

$$\text{Rate} = k_{\text{obs}}[\text{PtL}_2\text{AX}] \quad (2.6)$$

$$\text{Rate} = k_1 + k_2[\text{Y}] \quad (2.7)$$

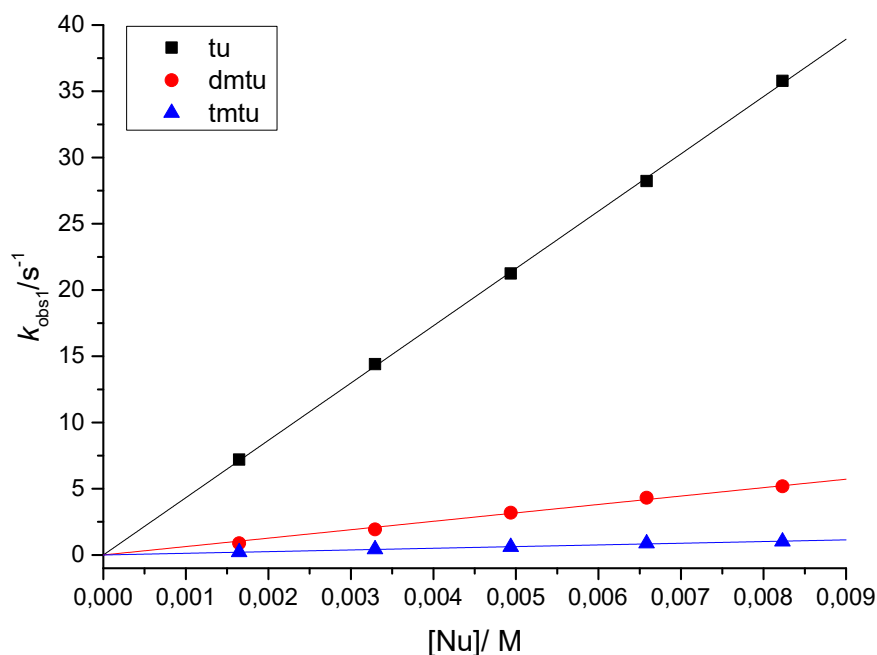


**Figure 2.3** Plot of  $k_{\text{obs}}$  vs  $[\text{Nu}]$  for the first aqua substitution in the complex  $\text{cis-}[\text{Pt}\{2\text{-}(4\text{-tert-butylphenylthiomethyl})\text{pyridine}\}(\text{H}_2\text{O})_2\}^{2+}$  in 0.1 M LiOTf/HOTf at 25 °C (Chapter 4, **Figure 4.7**).

Under such conditions a plot of  $k_{\text{obs}}$  vs  $[\text{Y}]$  yields a linear regression for which the y-intercept equals to  $k_1$  while the slope gives  $k_2$ , the second-order rate constant for the direct substitution of the leaving group (X).<sup>7,16</sup> The reaction in **Figure 2.3** has plots passing through the origin indicating the absence of the  $k_1$  term. The value of  $k_1$  is independent of the nature and concentration of the entering ligand while  $k_2$  is sensitive to the nature of the entering nucleophile.<sup>16,17</sup>

For coordinating solvents, such as water and methanol a rate constant  $k_1$  represents the rate of solvent participation in the substitution process.<sup>18,19</sup> Solvent participation in the substitution process is presented in the first pathway in **Figure 2.4**. For this mechanistic pathway, the leaving group (X) is first substituted slowly by the solvent (S) followed by a fast substitution of S by the entering nucleophile (Y).<sup>18,19</sup>



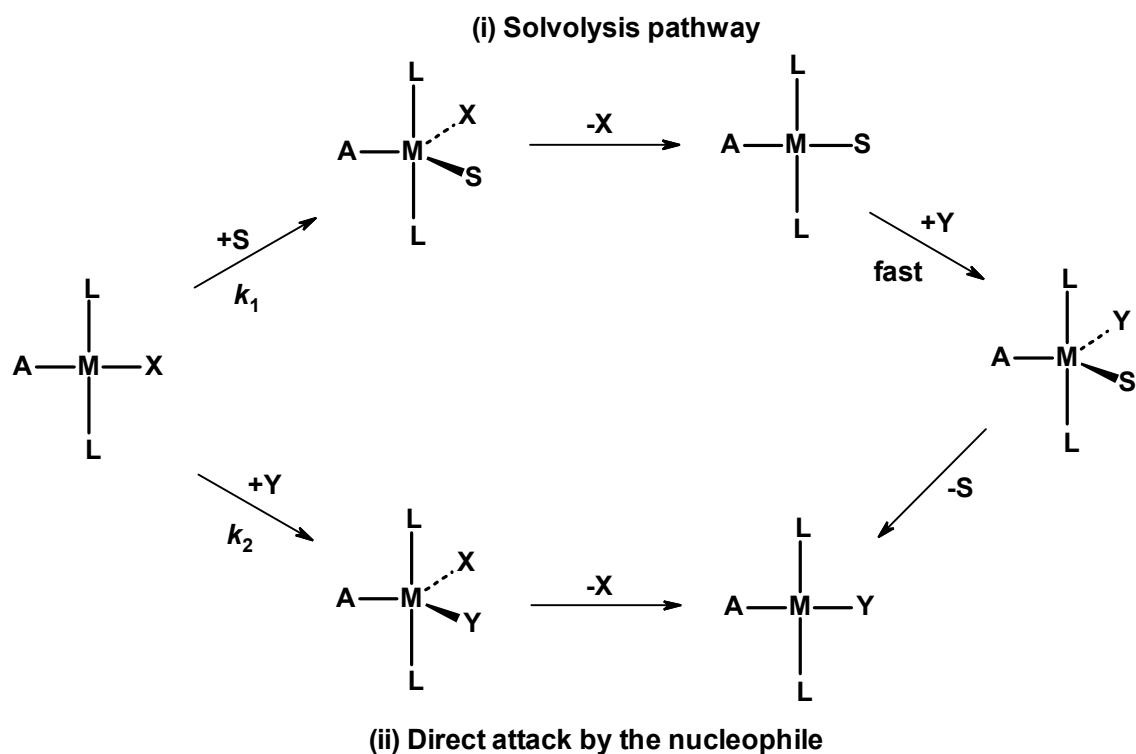


**Figure 2.4** Substitution in square-planar  $d^8$  complexes showing (i) the slow formation of a five-coordinate solvent-complex intermediate  $ML_2ASX$  prior to a rapid substitution by entering ligand Y and (ii) a direct substitution of the leaving group X by Y.

In a square-planar geometry the low energy  $p_z$  orbital of Pt(II) complexes can readily accept a lone pair of electrons from an oncoming ligand in the transition state. This leads to the formation of an energetically favoured 18-electron five-coordinate transition state during the substitution process. Thus in the majority of cases the substitution is characteristically limiting associative.<sup>4</sup> Evidence of a rapid formation of a long-lived, stable distorted square pyramidal five-coordinate intermediate has been isolated and characterized by X-ray crystallography for the complex  $[Pt(bpy)_2\{PPh(PhSO_3)_2\}]\cdot 5.5H_2O$  where  $bpy = 2,2'$ -bipyridine and  $PPh(PhSO_3)_2^{2-} = bis(p\text{-sulfonatophenyl})\text{-phenylphosphine}$ .<sup>20</sup> Retention of the starting geometrical configuration of the *cis* and *trans* species during substitution provides further proof of an associative mode of substitution in square-planar complexes as shown in **Figure 2.5**.

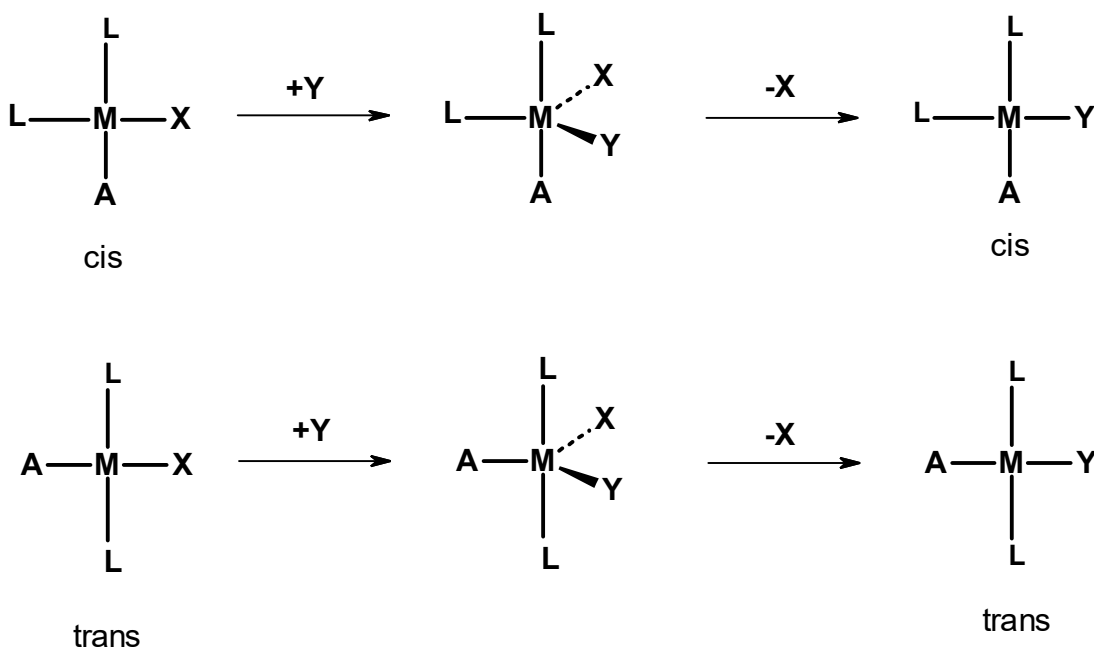


**Figure 2.5** Retention of the starting geometrical *cis* and *trans* configurations during associative nucleophilic substitution in square-planar complexes.

### 2.2.2 Geometries of the intermediates

The dominant associatively activated substitution pathway in square-planar complexes has a five-coordinate transition state(s) and an intermediate of higher coordination number between the two transition states.<sup>5,21</sup> As illustrated in **Figure 2.5**, the substitution process occurs with a complete retention of the *cis* or *trans* configurations as shown by complexes **1** and **9** in **Figure 2.6**. During substitution, the *cis* ligands occupy the axial positions while the entering ligand is positioned on the equatorial site and the process takes place with retention of the trigonal bipyramid symmetry for both the transition states and the intermediate species.

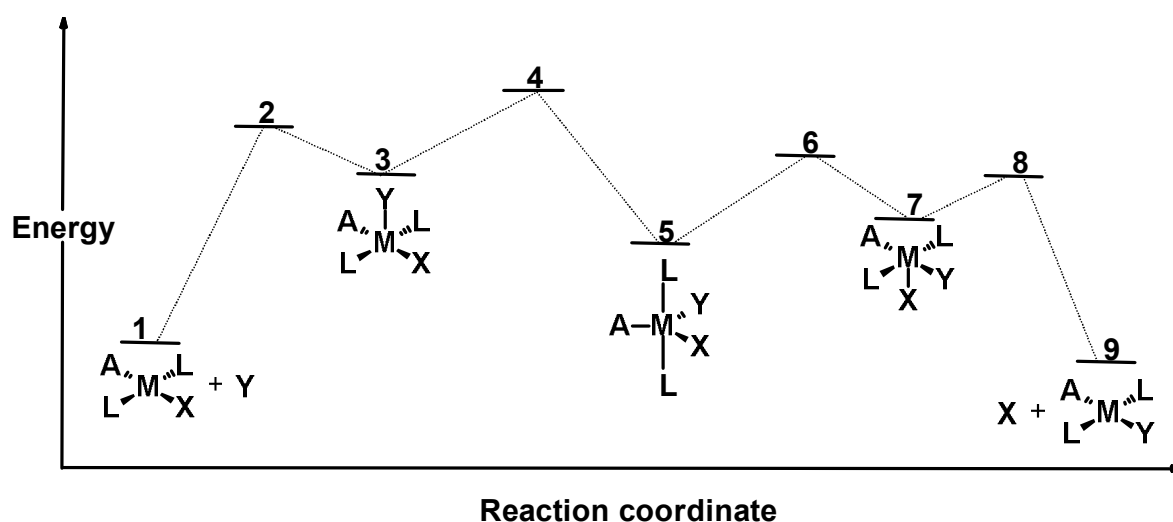


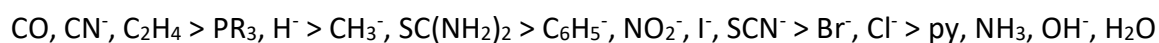
**Figure 2.6** Schematic energy profile and possible coordination changes during associative substitution in square-planar complexes of ligand X by Y. Energy maxima at **2, 4, 6, and 8** represent the transition states and intermediates have energies **3, 5, and 7**.<sup>17</sup>

### 2.3 Factors controlling the reactivity of square-planar complexes

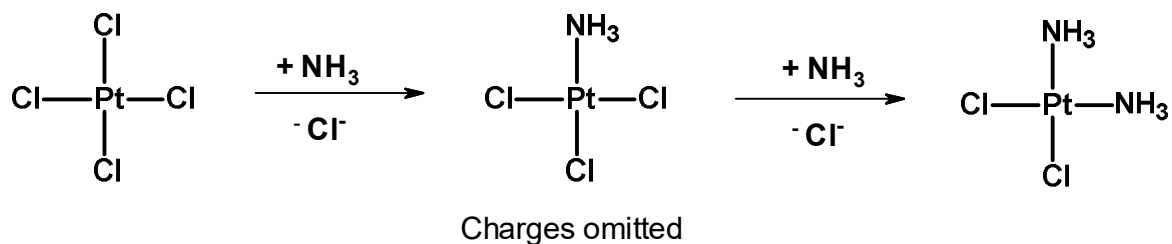
The substitution behaviour of the leaving group (X) by the oncoming ligand (Y) in square-planar complexes is affected by various factors described in the following sections:

#### 2.3.1 The *trans*-effect

The most important role of a non-leaving ligand on the rate of substitution in Pt square-planar complexes has been its *trans*-effect.<sup>5,7,8,17,22,23</sup> The leaving group *trans* to the non-leaving ligand can be labilised depending on the strength of its *trans*-effect. This effect can be through  $\sigma$ -inductive or  $\pi$ -acceptor properties of the ligand. This was demonstrated in the classical experiment of Werner<sup>24</sup> for the synthesis of cisplatin and transplatin *via* a careful choice of the reactants and order of substituting the ligands. The complex order covering the strong  $\sigma$ -donor/ $\pi$ -acceptor ligand to the least *trans*-labiliser follows the order:

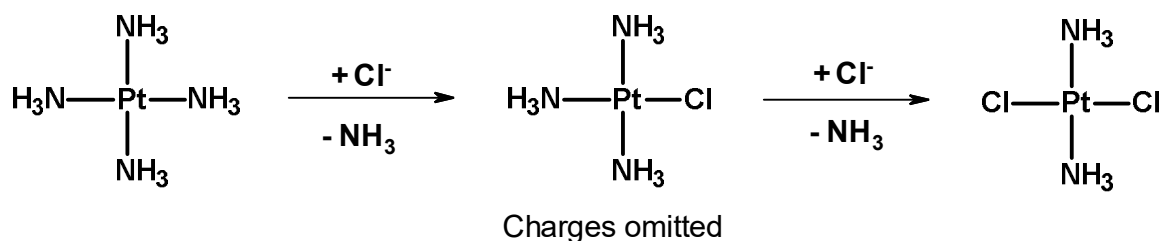


The *trans*-effect is mostly utilized in the synthesis of desired Pt(II) complexes of differing *cis* and *trans* geometries. A prime example demonstrating the *trans*-directing ability of non-leaving ligands is presented in Schemes 2.1 and 2.2 for the synthesis of the isomeric *cis*- and *trans*-Pt(NH<sub>3</sub>)<sub>2</sub>Cl<sub>2</sub> complexes.<sup>14</sup>



**Scheme 2.1** Preparation of cisplatin from  $\text{PtCl}_4^{2-}$  as a starting reactant.

The first ammonia ( $\text{NH}_3$ ) ligand can enter at any of the coordination sites of the  $\text{PtCl}_4^{2-}$  complex. The chloro group *trans* to ammonia in  $\text{PtNH}_3\text{Cl}_3^-$  is inert to substitution by the second  $\text{NH}_3$  ligand due to its greater *trans* labilizing effect when compared to  $\text{NH}_3$ .<sup>14</sup> Therefore, the second  $\text{NH}_3$  group enters the *cis* position resulting in the formation of *cis*- $\text{Pt}(\text{NH}_3)_2\text{Cl}_2$ .



**Scheme 2.2** Preparation of transplatin from  $\text{Pt}(\text{NH}_3)_4^{2+}$  as a starting reactant.

The *trans* isomer is synthesised from  $\text{Pt}(\text{NH}_3)_4^{2+}$ , in which the already coordinated chloride ion in  $\text{Pt}(\text{NH}_3)_3\text{Cl}^+$  substitutes the  $\text{NH}_3$  group *trans* to itself for the formation of *trans*- $\text{Pt}(\text{NH}_3)_2\text{Cl}_2$ . The *trans*-effect originates from two theories: the  $\sigma$ -bonding and  $\pi$ -bonding theories which are considered in the next section. Both effects contribute to the overall influence of a *trans*-directing ligand on the properties of the *trans* metal-leaving group bond in square-planar complexes.

### 2.3.1.1 The $\sigma$ -*trans*-Effect

The  $\sigma$ -*trans*-effect which can be partially explained by the Grinberg's polarization theory<sup>25</sup> which presumes the electrostatic dipolar interactions between the  $L_\sigma$ -Pt-X axis, ( $L_\sigma = \sigma$ -donor ligand, X = leaving group) as the drivers for labilising X.<sup>26</sup> The dipoles on the  $L_\sigma$ -Pt bond induce a dipole on the Pt-X bond *trans* to it, which is of opposite polarity. This weakens the Pt-X bond characterised by a longer bond length.<sup>4,14</sup> This is also called the *trans*-influence of  $L_\sigma$ .<sup>7,27</sup> It affects the thermodynamics of the complex *via* destabilising the energies of the bond *trans* to the affector ligand which also renders it labile. A true  $\sigma$ -*trans*-effect will be observed if  $L_\sigma$

has a greater share of the empty  $6p_{\sigma}$  orbital of the metal in the ground-state when compared to the transition state. This would lead to a lesser change in the energy difference between the ground and transition states.<sup>26</sup> The overlap of the valence orbitals of the  $\sigma$ -*trans*-directing ligands with that of the metal ion  $6p_{\sigma}$  orbitals determines the strength of the  $\sigma$ -*trans*-effect of that particular ligand. **Figure 2.7** illustrates the charge distribution between the *trans*-directing ligand (L) and the *trans*-leaving group (X) on labilizing this bond due to electrostatic repulsion of its negative charge and the induced dipole of the Pt(II) metal ion.



**Figure 2.7** Charge distribution in induced dipoles by  $\sigma$ -fashion in the L-Pt-X coordinate. (i) The  $\sigma$ -bond strengths of L and X are identical (ii) The  $\sigma$ -bond strength of L is much greater than that of X.

The order of the  $\sigma$ -*trans*-effect decreases in the following order:



The ligands CO and  $\text{CN}^-$  lie lower in the  $\sigma$ -*trans*-effect series when compared to the overall *trans*-effect which reflects their influence as  $\pi$ -acceptors which has little effect on this series. Effects of  $\pi$ -acceptor ligands on the rate of substitution are considered below.

### 2.3.1.2 The $\pi$ -*trans*-effect

The  $\pi$ -*trans*-effect for square-planar complexes accounts for the change in reaction rate induced by a  $\pi$ -acceptor ligand ( $L_{\pi}$ ) which utilizing empty orbitals of  $\pi$ -symmetry, accommodates electron density from the filled metal  $d_{xz}$  orbital making it electropositive.<sup>14,22,26,28,29</sup> The ground-state of the complex is not affected by  $\pi$ -acceptor property of  $L_{\pi}$ .<sup>18,19,30</sup> Therefore, when a group with a high  $\pi$ -*trans*-effect is coordinated *trans* to the leaving group (X) two things will happen during a substitution process:

- I. The oncoming ligand (Y) will be nucleophilically coordinated on the metal ion at the site of the leaving group (X), due to its lower electron density. This would lead to its subsequent substitution via a five-coordinate activated complex.

- II. The five-coordinate 18-electron trigonal bipyramidal transition state, where  $L_{\pi}$ , X and the oncoming ligand (Y) are coordinated to the metal, is stabilised by the back donation of electron density into the empty  $\pi^*$  orbitals of the  $\pi$ -acceptor ligand  $L_{\pi}$ .<sup>26,28,31</sup> This increases the electrophilicity of the metal ion leading to high rates of substituting the leaving group X from the complex.

Likewise, the overlap of the valence orbitals of the  $\pi$ -*trans*-directing ligand with the  $6p_{\pi}$  orbitals (**Figure 2.8**) of the metal ion account for the observed high *trans*-effect of some ligands as follows:



Because the  $\pi$ -*trans*-effect involves a five-coordinate transition state, it is applicable only in associatively activated mechanisms (A or  $I_a$ ) such as in substitution reactions in square-planar complexes.

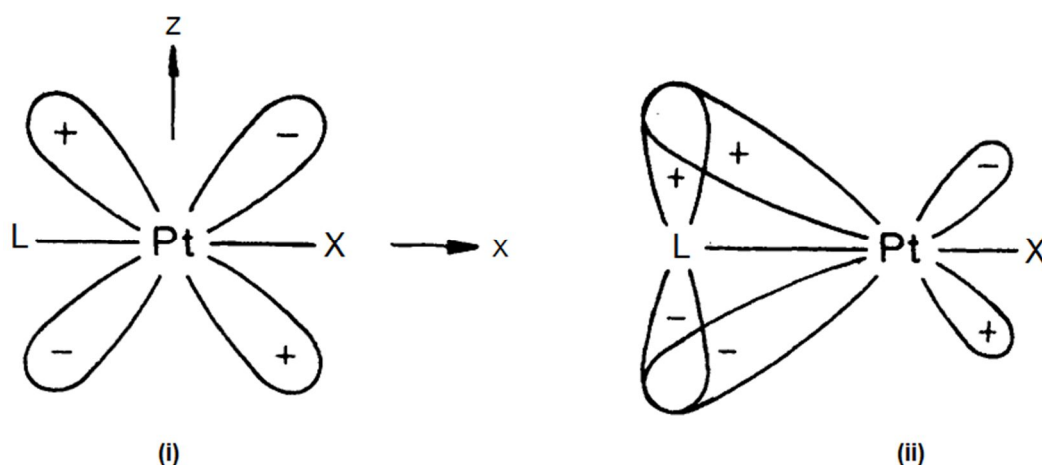


**Figure 2.8** Schematic representation of the  $\pi$ -bonding mechanism for the *trans*-effect.<sup>26</sup> (i)  $\pi$ -*trans*-director L forms only a  $\sigma$  bond, no  $\pi$ -bonding involved ; (ii) L forms both a  $\sigma$  bond for the donation of electron density from L onto filled  $d$ -orbitals of the metal ion and  $\pi$ -bonds for back-donation of this electron density from the metal onto the empty  $\pi^*$  orbitals of L.<sup>14</sup>

### 2.3.1.3 The $\sigma$ and $\pi$ -*trans*-Effects

The  $\sigma$ - and  $\pi$ -*trans*-effects for square-planar complexes discussed in the preceding sections 2.3.1.1 and 2.3.1.2, respectively, can be alternatively explained using Molecular Orbital (MO) theory. **Figure 2.9** depicts the MO diagram of  $\text{PtCl}_4^{2-}$  which shall be used to sum up the phenomena of the *trans* effect.

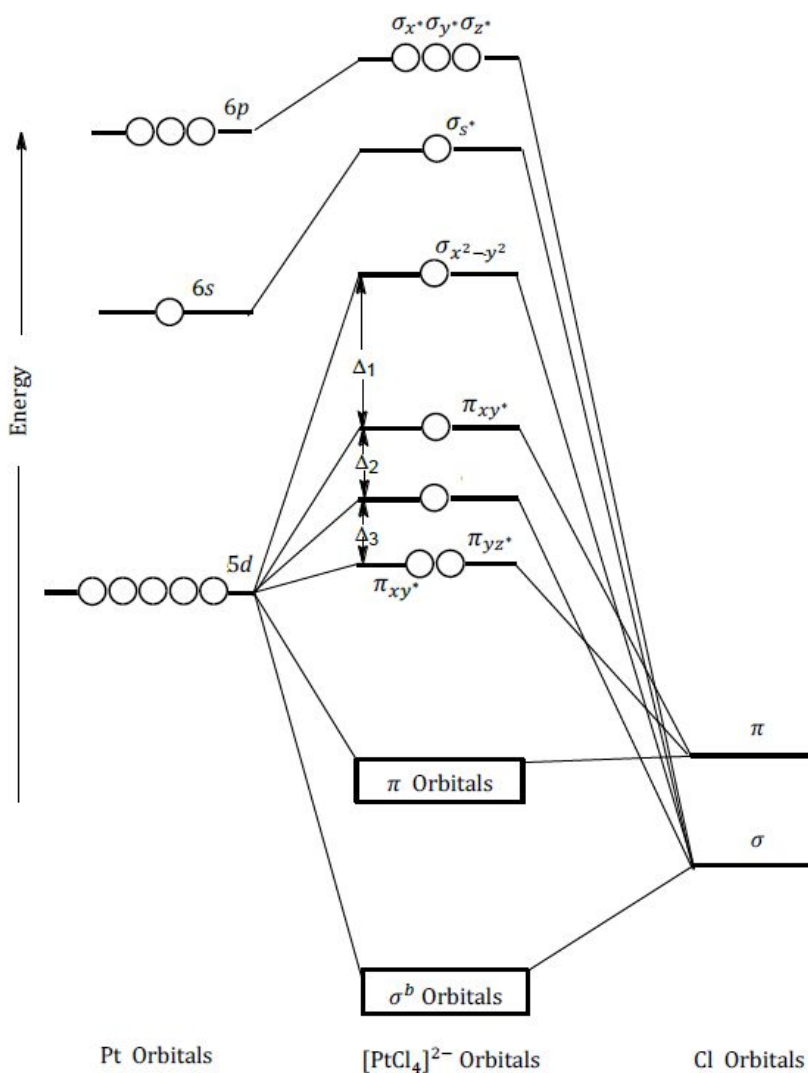


**Figure 2.9** Schematic representation of the Molecular Orbital diagram of  $PtCl_4^{2-}$ .

The  $\sigma$ - and  $\pi$ -bonding orbitals positioned on the four chloride ligands are the first and second most stable, respectively.<sup>14</sup> Derived from the  $5d$  atomic orbitals of Pt(II) are the  $\sigma$ - and  $\pi$ -antibonding MO orbitals with the symmetries  $\pi_{xz}^*$ ,  $\pi_{yz}^*$ ,  $\sigma_z^{2*}$  and  $\pi_{xy}^*$  which follow in terms of stability. The highest in energy is the non-bonding  $\sigma p_z$  valence orbital containing antibonding orbitals with symmetries  $\sigma_s^*$ ,  $\sigma_x^*$ , and  $\sigma_y^*$ .<sup>4, 14</sup>

The four  $\sigma$ -bonding atomic orbitals which can be used for square-planar complex formation are  $d_{x^2-y^2}$ ,  $s$ ,  $p_x$ , and  $p_y$ .<sup>14</sup> The  $p$  orbitals have the *trans* directing properties useful for overlap in the L-Pt-X x-axis of *trans*-PtA<sub>2</sub>LX. Both the *trans* ligand (L) and the leaving group (X) share the same  $\sigma_x$  orbital in the overall MO arrangements. The strong  $\sigma$ -donor *trans*-ligand ( $L_\sigma$ ) receives the greater share of this  $\sigma_x$  orbital when compared to X. Thus, the Pt-X bond is

lengthened in the ground-state, leading to it being weakened which enhances the substitution of X by the entering nucleophile (Y) (**Figure 2.7**). Langford and Gray elaborated further on the influence of the reaction rate based on the stabilization of the trigonal bipyramidal intermediate.<sup>7</sup> The ground-state has a singular  $p$  orbital,  $p_x$ , for bonding of the *trans* ligands L-Pt-X on the x-axis of the square-planar complex. Availability of additional orbitals during associative substitution in the transition state for  $\sigma$  bonding when compared to the ground-state square-planar complex, means that the addition of the oncoming ligand (Y) from above the xy plane leads to X moving down out of the plane, resulting in a trigonal plane containing Pt, L, X, and Y (**Figure 2.10**). Two  $p$  orbitals,  $p_x$  and  $p_z$ , are contained in this newly formed intermediate for bonding of three ligands (66.6 % statistical electron charge distribution) when compared to one orbital shared between two ligands in the ground state (50 %). Consequently, the high *trans*-effect of a good  $\sigma$ -donor ligand such as  $\text{H}^-$  and  $\text{CH}_3^-$  referred to as the  $\sigma$ -*trans*-effect is due to this additional strength of Pt-L $\sigma$   $p$  bond character in its molecular orbital with this metal centre.

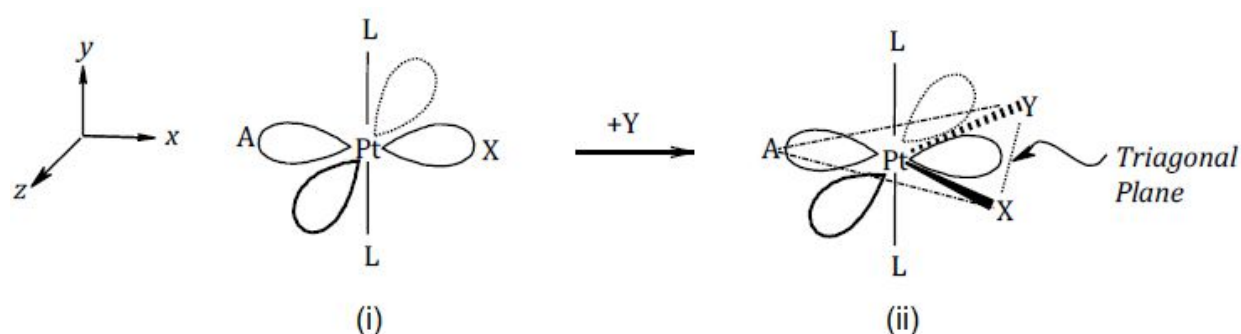


**Figure 2.10** The  $\sigma$ -*trans*-effect due to the stabilization of the trigonal bipyramidal intermediate.

(i) The ground-state has only the  $p_x$  orbital available for  $\sigma$ -bonding of ligands A and X (ii)  $\sigma$ -bonding of ligands A, X and Y in the trigonal plane are accommodated on the  $p_x$  and  $p_z$  orbitals.

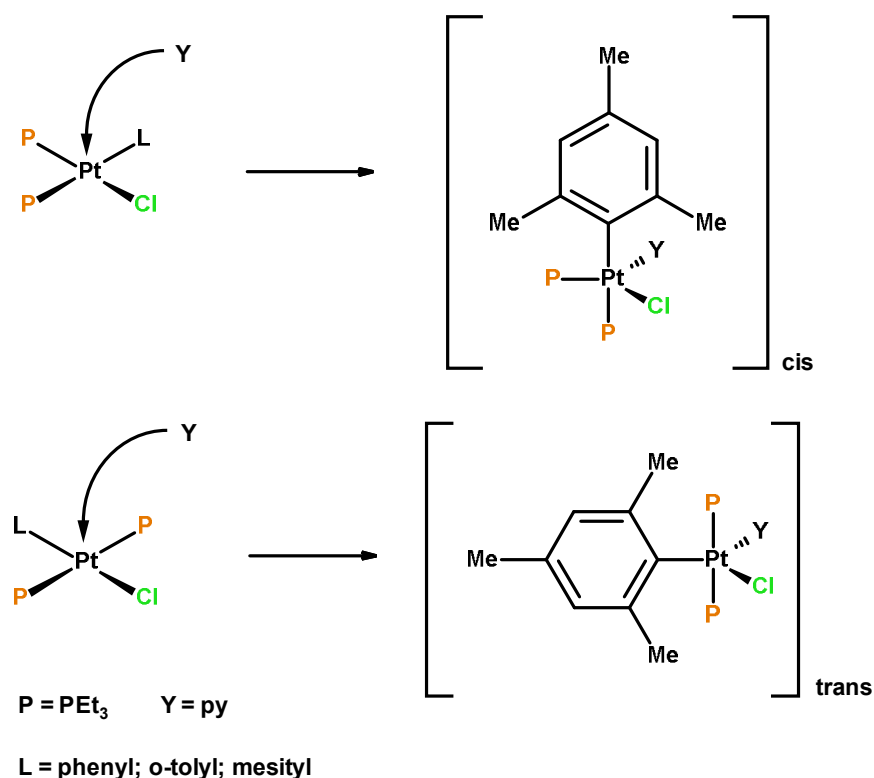
The MO theory places only three molecular orbitals namely  $\pi_{xz}^*$ ,  $\pi_{yz}^*$ , and  $\pi_{xy}^*$ , to have suitable  $\pi$ -bonding symmetry to  $\pi$ -metal centred  $d_\pi$  orbitals in square-planar complexes.<sup>14</sup> These can participate in the back donation of electron density from the metal ion, thereby stabilising the formation of the trigonal bipyramidal transition state.<sup>14</sup> Effectively, the strong  $\pi$ -acceptor ligand A (**Figure 2.10**) delocalizes electronic charge to the ligands X and Y and lowers the activation energy in the transition state leading to its stabilization.<sup>14</sup>



### 2.3.2 The *cis*-effect

The influence of the *cis*-positioned ligand (L) (**Figure 2.11**) on the reaction rate in square-planar complexes is generally weak when compared to the ligand positioned *trans* to the leaving group (X = Cl<sup>-</sup>). An exception, however, is when the *cis* ligand is sterically bulky which leads to a slower associative rate of substitution of the leaving group (X).<sup>12,32</sup> Steric hindrance of the *cis* ligand affects the stability of the five-coordinate intermediate formed during the attack of the oncoming ligand (Y = py). The *trans* ligand (L = phenyl, *o*-tolyl and mesityl) in the trigonal bipyramidal intermediate occupies the equatorial position in the trigonal plane and is away from the oncoming ligand and leaving group by an angle of 120°. <sup>12</sup> Conversely, when these ligands are positioned *cis*, they occupy axial sites in the activated complex and interact more effectively with the oncoming and leaving groups which are only 90° away *via* electron-electron repulsion.<sup>12</sup> Such modification of square-planar complexes through steric effects is vital when designing novel Pt(II) complexes of improved chemotherapeutic activity.<sup>33-35</sup>

A decrease in the rate of substitution of the leaving ligand(s) in a square-planar complex is usually accompanied by an increased inertness of the drug toward deactivation.<sup>36</sup> This is observed in carboplatin (as discussed in Chapter 1, section 1.2.3 **Figure 1.1(b)**) which has a chelating and sterically bulk cyclobutane-1,2-diammine spectator ligand, properties which account for less toxicity of the drug due to inertness.<sup>37,38</sup> The use of sterically bulk ligands with carbon donor ligands has been reported to cause a mechanistic changeover from associative to dissociative in square-planar Pt(II) complexes.<sup>39,40</sup> For a dissociative mechanism, steric hindrance increases the rate of substitution due to the relief of steric strain in the ground-state which facilitates a rapid approach of the oncoming ligand.<sup>15,41,42</sup>

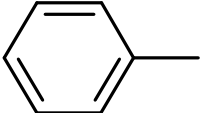
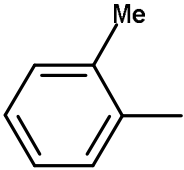
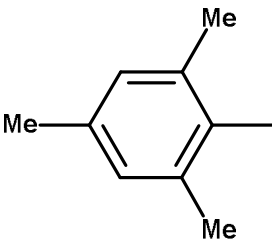


**Figure 2.11** Steric effects of a mesityl ligand in a square-planar complex showing the trigonal intermediate for the *cis* and *trans* isomers.<sup>16</sup>

For an associative mechanism of substitution where there is an increase in the coordination number of the trigonal bipyramidal intermediate due to an oncoming ligand, increase in steric bulk of the ligands in the *cis* position shields the approach of the oncoming ligand ( $Y = py$ ). This steric crowding of the equatorial position of the leaving group destabilizes the trigonal bipyramidal transition state and retards the rate of substitution. These observations are supported experimentally for the substitution reactions of the chloride ligand by pyridine ( $py$ ) in the square-planar complexes *cis*- and *trans*- $Pt(Et_3)_2LCl$  where  $L =$  phenyl, *o*-tolyl and mesityl. Increase in steric size of the aryl ligands from phenyl to mesityl positioned perpendicular to the square plane blocks the attack by an oncoming  $py$  nucleophile. The steric hindrance to attack is higher for the mesityl ligand which has two ortho methyl substituents shielding the approach on both sides of the square plane. The *cis*-steric ratios on the reactivity was reported to be 80 000: 200: 1. In sharp contrast, the ratio of only 35: 5: 1 was reported when the *trans*- $Pt(Et_3)_2LCl$  replaced its *cis* isomer for phenyl: *o*-tolyl: mesityl, respectively, when  $py$  is the oncoming ligand.<sup>16</sup> **Table 2.1** indicates that even though

both the *cis* and *trans* forms of Pt(Et<sub>3</sub>)<sub>2</sub>Cl are affected by increase in the steric size of L, the *cis* steric effect is more pronounced when compared to the *trans*-steric-effect.

**Table 2.1** Steric effects on the rates of substitution of *cis*- and *trans*-Pt(PEt<sub>3</sub>)<sub>2</sub>Cl by pyridine at various temperatures.<sup>16</sup>

	Ligand	<i>k</i> <sub>obs</sub> (s <sup>-1</sup> )	
		<i>cis</i> (0 °C)	<i>trans</i> (25 °C)
L = phenyl		8.0 x 10 <sup>-2</sup>	1.2 x 10 <sup>-4</sup>
L = <i>o</i> -tolyl		2.0 x 10 <sup>-4</sup>	1.7 x 10 <sup>-5</sup>
L = mesityl		1 x 10 <sup>-6</sup> (25 °C)	3.4 x 10 <sup>-6</sup>

For unsubstituted terpy Pt(II) complexes where steric crowding or hindrance is absent, replacement of a pyridine with a strong  $\sigma$ -donor deprotonated phenyl ring in the *trans* position retards the rate of substitution by a factor of 454 when thiourea is used as a nucleophile compared to when the strong  $\sigma$ -donor is positioned *cis* to the chloro leaving group.<sup>43</sup> These results on the *cis*-effect of the Pt-C bond to retard the rate of substitution when thioureas and azoles are oncoming nucleophiles, were corroborated by Jaganyi *et al.*<sup>44,45</sup> when the *cis*-positioned Pt-N pyridine bond of terpy was replaced by the Pt-C phenyl bond. The reactivity of the complexes for these reactions are purely electronic in nature. Electron density from Pt-C bond accumulates on the metal centre making it less electrophilic. This repels the approach of the oncoming nucleophiles and destabilizes the transition state.

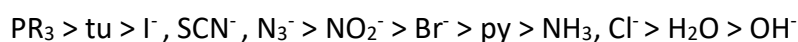
Even though it is generalised that the  $\sigma$ -*trans*-effect is greater than the  $\sigma$ -*cis*-effect, a study conducted by Hofmann *et al.*<sup>46</sup> indicated that the  $\pi$ -*cis*-effect is greater than the  $\pi$ -*trans*-effect. The  $\pi$ -acceptor pyridine positioned *cis* in [Pt(N-(pyridyl-2-methyl)-1,2-diaminoethane)OH<sub>2</sub>]<sup>2+</sup> (**aap**) reacts slightly faster ( $k_1 = 110 \text{ M}^{-1} \text{ s}^{-1}$ ) compared to when it is positioned *trans* in [Pt(2,6-bis-aminoethylpyridine)OH<sub>2</sub>]<sup>2+</sup> (**apa**) ( $k_1 = 101 \text{ M}^{-1} \text{ s}^{-1}$ ) when thiourea is considered as an oncoming nucleophile. The slower reactivity of **apa** was attributed to the ground-state accumulation of electron density on Pt(II) making it less electrophilic and thus retarding the rate of substitution. Despite this, the *cis*-effect is generally smaller when compared to the *trans*-effect.<sup>46</sup>

### 2.3.3 The substituting nucleophile (Y)

The rate of substitution for an associatively activated mechanism is sensitive to the nature and concentration of the oncoming ligand (Y). Nucleophilicity, which measures the strength of the nucleophile on substitution reactions in square-planar complexes, is affected by various factors such as:<sup>16</sup>

- i. Basicity: highly basic nucleophiles have a lone pair that can be used to form a bond at the metal centre leading to high rates of substituting the leaving group by nucleophile.<sup>47</sup>
- ii. Polarizability: This is explained by Pearson's Hard Soft Acid Base (HSAB) theory which states that a more polarizable ligand should be a better electron donor and therefore a better nucleophile.

The nucleophilicity of some ligands towards substitution decreases in the following order:



### 2.3.4 The leaving ligand (X)

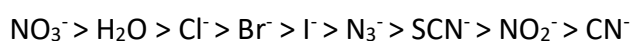
The effect of the leaving group on the reaction rate depends on the strength of the Pt-X bonds in the complex. For example, the Pt-OH<sub>2</sub> bond is more labile than Pt-Cl. This in turn depends on the nucleophilicity of the leaving ligand. The chloride ligand is a better nucleophile towards substitution when compared to water. Also, the bulkiness of the leaving ligand affects the reaction rate. Sterically bulk ligands are weakly bonded and thus easier to substitute. Catallini *et al.*<sup>48</sup> found that for the reactions of the type [Pt(bipy)(RSR')]<sup>+</sup> by halide ligands depended

on the substitution of the leaving thioether groups (RSR') for which the bond breaking transition state was the maxima with the highest energy. The high energy maxima for bond breaking indicated that this was the rate determining step for the reaction.<sup>14</sup>

To investigate the effect of the leaving group (X) on the rate of substitution in square-planar complexes, both the *cis* and *trans* groups must be kept constant. To provide information on the leaving group effects, substitution reactions of various leaving groups by pyridine as the oncoming nucleophile in the inert mononuclear complex [Pt(dien)X]<sup>+</sup> have been systematically studied (*Equation 2.8*).<sup>4,12</sup>



The rate of substitution of the leaving groups by pyridine decreased in the following order:



In this order of reactivity, the harder ligands NO<sub>3</sub><sup>-</sup> and Cl<sup>-</sup> are substituted more rapidly while the soft ligands NO<sub>2</sub><sup>-</sup> and CN<sup>-</sup> with π-bonding properties are substituted slowly. This is supported by the σ- and π-*trans*-effect theories, which suggest that good *trans*-labilizing groups form strong bonds to the metal centre. The reactivity factor between the most reactive H<sub>2</sub>O and the least reactive CN<sup>-</sup> is greater by six orders magnitude. This is indicative of the sensitivity of rate of substitution on the energy of bond breaking in the transition state albeit the reaction follows an associative mode of substitution.

### 2.3.5 The role of the solvent

Substitution reactions in square-planar complexes are accompanied by a two-term rate law as indicated above in *Equation 2.3*. The *k*<sub>1</sub> rate constant (independent of the nature and concentration of the entering ligand (Y)) in the first-term is attributed to the solvolysis pathway in which the solvent participates in the overall substitution reaction (**Figure 2.3**). The values of *k*<sub>1</sub> are also not affected by changes in charge of the complex. However, they are sensitive to steric hindrance as they are inversely related.<sup>22</sup>

The data in **Table 2.3** shows that the magnitude of the solvent rate constants, *k*<sub>1</sub>, correlate positively with the coordinating ability of the solvent. For example, in a chloride substitution reaction in DMSO, molecules competed favourably for coordinating to Pt(II) on the basis of the softness of S donor atom.<sup>12</sup> For these reactions there are larger values of *k*<sub>1</sub>

when compared to  $k_2$  values. On the other hand, for weakly coordinating solvents *e.g.* acetone, the reactions proceed by a direct attack of the oncoming  $\text{Cl}^-$  nucleophile and are thus sensitive to concentration of  $\text{Cl}^-$ .

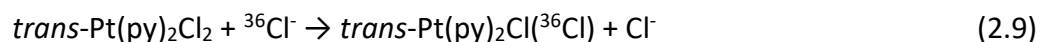


**Table 2.3** Solvent effects on chloride substitution reactions.<sup>49</sup>

Coordinating ability	Solvent	$k/10^{-5} \text{ s}^{-1}$
<b>Strong</b>	DMSO	380
	H <sub>2</sub> O	3.5
	EtOH	1.4
	<i>n</i> -PrOH	0.4
Coordinating ability	Solvent	$k/\text{M}^{-1} \text{ s}^{-1}$
<b>Weak</b>	CCl <sub>4</sub>	10 <sup>4</sup>
	C <sub>6</sub> H <sub>6</sub>	10 <sup>2</sup>
	<i>i</i> -BuOH	10 <sup>-1</sup>
	Acetone	10 <sup>-2</sup>
	DMF	10 <sup>-3</sup>

Because the effects of the solvents are purely based on their coordinating properties and not on dielectric constants, it is particularly interesting to note that nitromethane ( $\text{CH}_3\text{NO}_2$ ), generally not a good coordinating solvent, provides an effective path for chloride substitution. This is attributed to its  $\pi$ -bonding ability which allows *d*-orbital electrons on the platinum to delocalize into a vacant *p*-orbital on the nitrogen.<sup>22</sup>

Weak coordinating solvents have the propensity to occupy axial positions in the ground-state of square-planar complexes. This axial solvation diminishes during associative substitution wherein the intermediate of high coordination number is formed. Complexes containing strong  $\sigma$ -donor and  $\pi$ -acceptor properties have comparable discriminating capacities when interacting with various solvents. This is an indication that the metal-solvent interactions have no significance on the substitution kinetics. Thus, Linear Free Energy Relationships (LFER) are observed and there is no nucleophilicity order on changing the solvent.

## 2.4 References

1. B. Rosenberg and L. Vancamp, *Nature*, 1969, **222**, 385-386.
2. T. A. Connors, *Platinum Metals Review*, 1973, **17**, 98-101.
3. Ž. D. Bugarčić, J. Bogojeski and R. van Eldik, *Coordination Chemistry Reviews*, 2015, **292**, 91-106.
4. M. L. Tobe and J. Burgess, *Inorganic reaction mechanisms*, Longman, Harlow, Essex, England; New York, 1999, 30-43, 70-112.
5. M. L. Tobe, *Inorganic reaction mechanisms*, Nelson, London, 1972.
6. S. Asperger, *Chemical kinetics and inorganic reaction mechanisms*, Springer Science & Business Media, 2003, 34-40, 105-106.
7. C. H. Langford and H. B. Gray, *Ligand substitution processes*, W.A. Benjamin, Reading, Mass., 1974.
8. M. L. Tobe, *Reaction mechanisms in inorganic chemistry*, Butterworths; University Park Press, London; Baltimore, 1974.
9. S. Schindler, C. D. Hubbard and R. van Eldik, *Chemical Society Reviews*, 1998, **27**, 387-393.
10. A. Mambanda, D. Jaganyi, S. Hochreuther and R. van Eldik, *Dalton Transactions*, 2010, **39**, 3595-3608.
11. B. Petrović, Ž. D. Bugarčić, A. Dees, I. Ivanović-Burmazović, F. W. Heinemann, R. Puchta, S. N. Steinmann, C. Corminboeuf and R. van Eldik, *Inorganic Chemistry*, 2012, **51**, 1516-1529.
12. J. D. Atwood, *Inorganic and organometallic reaction mechanisms*, Wiley-VCH, New York, 1997.
13. R. Romeo, *Comments on Inorganic Chemistry*, 1990, **11**, 21-57.
14. F. Basolo and R. G. Pearson, *Mechanisms of inorganic reactions: a study of metal complexes in solution*, Wiley, 1967, 351-404.
15. R. Romeo, A. Grassi and L. Monsu Scolaro, *Inorganic Chemistry*, 1992, **31**, 4383-4390.
16. R. B. Jordan, *Reaction mechanisms of inorganic and organometallic systems*, Oxford University Press, New York, 1991, 29-40.
17. S. Asperger, *Chemical kinetics and inorganic reaction mechanisms*, Kluwer Academic/Plenum Publishers, New York, 2003, 34-40, 105-106.

18. T. R. Papo and D. Jaganyi, *Transition Metal Chemistry*, 2015, **40**, 53-60.
19. T. R. Papo and D. Jaganyi, *Journal of Coordination Chemistry*, 2015, **68**, 794-807.
20. W. K. C. Lo, G. Cavigliasso, R. Stranger, J. D. Crowley and A. G. Blackman, *Inorganic Chemistry*, 2014, **53**, 3595-3605.
21. J. C. Bailar and A. F. Trotman-Dickenson, *Comprehensive inorganic chemistry*, Pergamon Press; distributed by Compendium Publishers [Elmsford, N.Y.], [Oxford, 1973.
22. R. Summer Symposium on Mechanisms of Inorganic, R. K. Murmann, K. University of, S. American Chemical and C. Division of Inorganic, Washington, 81-105.
23. P. W. Atkins, *Shriver & Atkins' inorganic chemistry*, Oxford University Press, Oxford; New York, 2010, 202, 218.
24. A. Werner, *Zeitschrift für anorganische Chemie*, 1893, **3**, 267-330.
25. A. Grinberg, A. Grinberg, Y. Syrkin and H. C. Ann, *Acta physicochim. USSR*, 1935, **3**, 573.
26. F. R. Hartley, *Chemical Society Reviews*, 1973, **2**, 163-179.
27. R. G. Wilkins, *Kinetics and mechanism of reactions of transition metal complexes*, VCH, Weinheim; New York, 1991, 199-201.
28. J. Chatt, L. A. Duncanson and L. M. Venanzi, *Journal of the Chemical Society (Resumed)*, 1955, 4461-4469.
29. J. Chatt, L. A. Duncanson and L. M. Venanzi, *Journal of the Chemical Society (Resumed)*, 1955, DOI: 10.1039/JR9550004456, 4456-4460.
30. A. Shaira, D. Reddy and D. Jaganyi, *Dalton Transactions*, 2013, **42**, 8426-8436.
31. L. E. Orgel, *Journal of Inorganic and Nuclear Chemistry*, 1956, **2**, 137-140.
32. H. Kruger and R. van Eldik, *Journal of the Chemical Society, Chemical Communications*, 1990, DOI: 10.1039/C39900000330, 330-331.
33. M. Schmulling, A. D. Ryabov and R. van Eldik, *Journal of the Chemical Society, Chemical Communications*, 1992, DOI: 10.1039/C39920001609, 1609-1611.
34. J. Bogojeski, J. Volbeda, Ž. D. Bugarčić, M. Freytag and M. Tamm, *New Journal of Chemistry*, 2016, **40**, 4818-4825.
35. J. Bogojeski, J. Volbeda, M. Freytag, M. Tamm and Ž. D. Bugarčić, *Dalton Transactions*, 2015, **44**, 17346-17359.
36. S. Ahmad, *Chemistry & biodiversity*, 2010, **7**, 543-566.



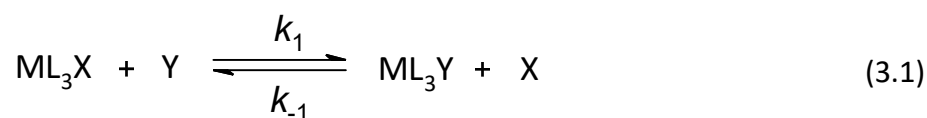
37. M. Fanelli, M. Formica, V. Fusi, L. Giorgi, M. Micheloni and P. Paoli, *Coordination Chemistry Reviews*, 2016, **310**, 41-79.
38. T. Boulikas, A. Pantos, E. Bellis and P. Christofis, *Cancer Ther*, 2007, **5**, 537-583.
39. M. R. Plutino, L. Monsù Scolaro, R. Romeo and A. Grassi, *Inorganic Chemistry*, 2000, **39**, 2712-2720.
40. R. Romeo, M. R. Plutino, L. Monsù Scolaro, S. Stoccoro and G. Minghetti, *Inorganic Chemistry*, 2000, **39**, 4749-4755.
41. S. Lanza, D. Minniti, P. Moore, J. Sachinidis, R. Romeo and M. L. Tobe, *Inorganic Chemistry*, 1984, **23**, 4428-4433.
42. D. Minniti, G. Alibrandi, M. L. Tobe and R. Romeo, *Inorganic Chemistry*, 1987, **26**, 3956-3958.
43. A. Hofmann, L. Dahlenburg and R. van Eldik, *Inorganic Chemistry*, 2003, **42**, 6528-6538.
44. D. Jaganyi, D. Reddy, J. A. Gertenbach, A. Hofmann and R. van Eldik, *Dalton Transactions*, 2004, DOI: 10.1039/B311595J, 299-304.
45. D. Reddy, K. J. Akerman, M. P. Akerman and D. Jaganyi, *Transition Metal Chemistry*, 2011, **36**, 593-602.
46. A. Hofmann, D. Jaganyi, O. Q. Munro, G. Liehr and R. van Eldik, *Inorganic Chemistry*, 2003, **42**, 1688-1700.
47. H. Erturk, A. Hofmann, R. Puchta and R. van Eldik, *Dalton Transactions*, 2007, DOI: 10.1039/B700770C, 2295-2301.
48. L. Cattalini, G. Marangoni, S. Degetto and M. Brunelli, *Inorganic Chemistry*, 1971, **10**, 1545-1546.
49. R. G. Pearson, H. B. Gray and F. Basolo, *Journal of the American Chemical Society*, 1960, **82**, 787-792.

# Chapter 3

## Measurement of kinetic reactions.

### 3.1 Introduction.

Chemical kineticists study the rates of chemical reactions (how fast or slow these reactions occur) to determine their mechanism.<sup>1-3</sup> For kinetics measurements, the molecularity of a chemical reaction which is defined as the number of molecules undergoing covalency changes, is important when assigning the mechanism of a chemical reaction. In this respect, a chemical process is broken down into *elementary reactions* characterized into a sequence of one or more single-step processes.<sup>4</sup> Chemical reactions in square-planar complexes are intrinsically bimolecular and can be represented by *Equations 3.1* and *3.2* below. In *Equation 3.2*, *A* represents the metal complex,  $ML_3X$ , whilst *B* represents the entering ligand, *Y*.



or



The forward elementary reaction is second-order, whilst the reverse reaction is first-order. Thus, the kinetics of the reaction is characterised by mixed-order behaviour. To minimize the complexity of the reaction, the forward substitution step is studied under *pseudo-first-order* reaction conditions. Experimentally, this is met by providing at least a 10-fold excess of *B* (nucleophile) over that of *A* (metal complex), such that  $[B]_0 \gg [A]_0$ . The derivation of the rate law representing a bimolecular reaction of this nature is dealt with below in Section 3.3.4 of this chapter.

The molecularity of a reaction allows for the assessment of the composition of the transition state which represents an energy barrier for a reaction to occur.<sup>4,5</sup> Entailed in the

barrier is the *activation energy* of the reaction which can give an indication of the rate of reaction. A low barrier indicates the ease with which the reactants can overcome the barrier to form the products due to having a high thermal energy. Thus, the rate of reaction will be fast. A high barrier means the rate of reaction will be slow due to insufficient energy leading to fewer reactants capable of overcoming the barrier. The energy barrier to reaction provides a source for temperature dependence studies of chemical reactions (Section 3.4.1).

Several variables influence the rate of a chemical reaction such as: concentration of the reactants, temperature and pressure, photophysical properties, ionic strength, pH and solvent participation:<sup>6</sup>

- The reactants in a chemical reaction have a directly proportional relationship to the **concentrations** of the species involved *i.e.* the rate of reaction is accelerated when the concentration is increased. A catalyst may also influence the rate of a reaction.
- Physical conditions such as **temperature** and **pressure** should be maintained constant throughout kinetic measurements. Temperature dependence studies allow, from the Gibbs free energy of activation  $G^\ddagger$ , the determination of the enthalpy and entropy of activation parameters,  $\Delta H^\ddagger$  and  $\Delta S^\ddagger$ , respectively. The energy of activation,  $E_a$ , can also be determined from the temperature dependence studies. Pressure dependence studies give the volume of activation,  $\Delta V^\ddagger$ . These parameters are paramount in assigning the mechanism of the reactions.
- **Photosensitive** chemical reactions may be affected by sunlight or lights in the room, changing the rate of a reaction.
- **Ionic strength** of the solution should be maintained constant to ensure uniform concentration of ions and charge in the solution throughout the course of a chemical reaction.
- $pK_a$  determination of the complex solution used for kinetic measurements is also crucial and should be accounted for. The  $pK_a$  values below those of the investigated complex solution ensure that it remains aquated.<sup>7,8</sup> Above their  $pK_a$ , deprotonation occurs which affects the rate of reaction in these different **pH** forms of the solution.
- **Solvent** participation in a chemical reaction that also influence the rate of reaction. Solvent molecules can act as a reactant or form a solvent cage which alters the kinetics

of a reaction. Thus, the preceding variables need to be controlled and their effect on the reaction quantified when investigating the kinetics of a chemical reaction.

### 3.2 The rate law.

#### 3.2.1 Measurement of the rate constants.

The rate of a chemical reaction gives an indication of the amount of consumption of reactants and the conversion of these into products. For a chemical reaction given below:



the capital letters indicate the chemical compounds while the small letters represent their stoichiometry. The rate of a reaction is presented in a manner which is independent of the amount of sample used and for which the units are given as molarity per second ( $M s^{-1}$ ).<sup>1,5</sup>

$$\text{Rate} = -\frac{d[\text{Reactant}]}{dt} = \frac{d[\text{Product}]}{dt} \quad (3.4)$$

The negative sign indicates that the reactants are being consumed as the reaction proceeds and hence the concentration is reduced.

The *rate law* is referred to as the study of the dependence of the reaction rates and rates constants on the concentrations of the various reactants in a reaction.<sup>6</sup> Considering the concentration of all the components, the rate can be expressed as:

$$\text{Rate} = -\frac{1}{a} \cdot \frac{d[A]}{dt} = -\frac{1}{b} \cdot \frac{d[B]}{dt} = \frac{1}{c} \cdot \frac{d[C]}{dt} = \frac{1}{d} \cdot \frac{d[D]}{dt} \quad (3.5)$$

Therefore, the rate law is generally represented as:

$$\text{Rate} = -k \prod_i [A_i]^{\alpha_i} [X_j]^{\beta_j} \quad (3.6)$$

where  $A_i$  represents the reactants,  $k$  the rate constant,  $X_j$  any other species (*i.e.* catalyst) that may influence the rate while  $\alpha$  and  $\beta$  indicate the order of the reactions.

The order of the reaction is defined as:

$$\text{Order of reaction} = \sum_i \alpha_i \quad (3.7)$$

### 3.3 Integrated Rate Expressions.

For an arbitrary chemical reaction given by *Equation 3.5*, the left-hand side of the rate law expression will involve the first derivative of concentration with respect to time. It follows that to process data acquired experimentally, an integration is necessary to obtain an expression which links the reactant concentration and time.

#### 3.3.1 First-Order Reactions.

First-order reactions are simple to interpret as they involve less complicated expressions. Most reactions follow first-order kinetics or are simplified to approximate first-order.<sup>9</sup> A first-order reaction of the type:



The rate for the above reaction is given as:

$$\text{Rate} = k[A] = -\frac{d[A]}{dt} \quad (3.9)$$

which rearranges to give:

$$-\frac{d[A]}{[A]} = k_1 dt \quad (3.10)$$

Integrating from  $t = 0$  to  $t = t$ ,  $[A]_t$  gives

$$\int_{[A]_0}^{[A]_t} \frac{d[A]}{[A]} = -k_1 \int_0^t dt \quad (3.11)$$

$$\ln \frac{[A]_t}{[A]_0} = -k_1 t \quad (3.12)$$

$$\ln[A]_t = -k_1 t + \ln[A]_0 \quad (3.13)$$

where  $[A] = [A]_0$  at time  $t = 0$  and  $[A] = [A]_t$  at time  $t = t$ .

From *Equation 3.13* a linear equation in the form ( $y = mx + c$ ) with  $y = \ln[A]_t$ ,  $x = t$  and  $c = \ln[A]_0$  can be deduced. Thus, a plot of  $\ln[A]_t$  versus  $t$  yields a linear regression for which the rate constant,  $k$ , can be determined from the slope.<sup>1,9</sup> *Equation 3.13* can be expressed as:

$$\frac{[A]_t}{[A]_0} = e^{-k_1 t} \quad (3.14)$$

and simplified to:

$$[A]_t = [A]_0 e^{-k_1 t} \quad (3.15)$$

Furthermore, *Equation 3.15* shows that a plot of  $[A]_t$  versus  $t$  varies exponentially.

### 3.3.2 Reversible First-Order Reactions

Chemical reactions composed of reversible or opposing reactions do not go to completion but form an equilibrium between the reactant and product species under certain reaction conditions. Considering the elementary reaction:



The rate law for the reaction represented by *Equation 3.16* is

$$\text{Rate} = -\frac{d[B]}{dt} = -\frac{d[A]}{dt} = -k_1[A]_t - k_{-1}[B]_t \quad (3.17)$$

At  $t = 0$ ,  $B = 0$ , and  $[A]_t = [A]_0$ , at any time

$$[B]_t = [A]_0 - [A]_t \quad (3.18)$$

Substituting *Equation 3.18* into *Equation 3.17* gives:

$$-\frac{d[A]}{dt} = k_1[A]_t - k_{-1}([A]_0 - [A]_t) \quad (3.19)$$

At equilibrium, no overall reaction occurs. Thus,

$$-\frac{d[A]}{dt} = 0 \quad (3.20)$$

Applying *Equation 3.20* to *Equation 3.17* gives

$$k_1[A]_{eq} = k_{-1}[B]_{eq} = k_{-1}([A]_0 - [A]_{eq}) \quad (3.21)$$

Which can be simplified to:

$$[A]_0 = \frac{k_1 + k_{-1}}{k_{-1}} [A]_{eq} \quad (3.22)$$

Substitution of *Equation 3.20* into *Equation 3.17* gives

$$-\frac{d[A]}{dt} = (k_1 + k_{-1})[A] - (k_1 + k_{-1})[A]_{eq} \quad (3.23)$$

Separating the variables and integrating eventually leads to

$$\int_{[A]_0}^{[A]_t} \frac{d[A]}{([A]_t - [A]_{eq})} = -(k_1 + k_{-1}) \int_0^t dt \quad (3.24)$$

solving the limits produces

$$\ln\left(\frac{[A]_0 - [A]_{eq}}{[A]_t - [A]_{eq}}\right) = (k_1 + k_{-1})t \quad (3.25)$$

Rearrangement of *Equation 3.25* gives

$$\ln([A]_t - [A]_{eq}) = -(k_1 + k_{-1})t + \ln([A]_0 - [A]_{eq}) \quad (3.26)$$

A plot of  $\ln([A]_t - [A]_{eq})$  versus  $t$  gives a linear regression with a slope of  $-(k_1 + k_{-1})$ . To determine each individual rate constant,  $k_1$  or  $k_{-1}$ , it is important to evaluate the thermodynamic equilibrium constant,  $K_{eq}$ .

The equilibrium constant is a ratio of the concentration of the remaining reactant and the formed product which can be correlated to the distinctive rate constant as follows:

$$K_{eq} = \frac{[B]_{eq}}{[A]_{eq}} = \frac{k_1}{k_{-1}} \quad (3.27)$$

Two equations with two unknowns can be difficult to treat and may lead to inaccurate measurement of  $[A]_{eq}$ . Furthermore, the observed rate constant,  $k_{obs}$ , is equal to the sum of the rate constant for the forward and reverse reactions, *i.e.*

$$k_{obs} = k_1 + k_{-1} \quad (3.28)$$

### 3.3.3 Second-Order Reactions

Second-order reactions generally represent those that use up an equivalent amount of two reactants at a rate that converts them to products in a proportional manner.<sup>10,11</sup> For a reaction:



The rate law can be given as:

$$\text{Rate} = k[A][B] \quad (3.30)$$

$$\text{Rate} = \frac{d[C]}{dt} = -\frac{d[A]}{dt} = -\frac{d[B]}{dt} = k_2[A]_t[B]_t \quad (3.31)$$

If at  $t = 0$ , the initial concentration of A and B are  $[A]_0$  and  $[B]_0$ , and at a particular time  $t$ , the concentration of A is reduced to  $[A]_0 - x$ , and concentration of B would be reduced to  $[B]_0 - x$ , where  $x$  is the amount of reactants that has reacted to form the product C. Therefore, the rate equation can be written as:<sup>6</sup>

$$-\frac{d[A]}{dt} = k_2([A]_0 - x)([B]_0 - x) \quad (3.32)$$

Since  $[A]_t = [A]_0 - x$ , hence  $\frac{dx}{dt} = -\frac{d[A]}{dt} = -\frac{d[B]}{dt}$  and thus the rate law shown in *Equation 3.32* can be written as:

$$\frac{dx}{dt} = k_2([A]_0 - x)([B]_0 - x) \quad (3.33)$$

Separation of the variables gives:

$$\frac{dx}{([A]_0 - x)([B]_0 - x)} = k_2 dt \quad (3.34)$$

Integrating *Equation 3.34* between the limits  $x = 0$  to  $x = x$  and  $t = 0$  to  $t = t$  produces an expression:

$$\int_0^x \frac{dx}{([A]_0 - x)([B]_0 - x)} = k_2 \int_0^t dt \quad (3.35)$$

Giving the following expression (provided  $[A]_0 \neq [B]_0$ ):

$$\frac{1}{[A]_0 - [B]_0} \ln \frac{[B]_0([A]_0 - x)}{[A]_0([B]_0 - x)} = k_2 t \quad (3.36)$$

This expression can be simplified to give:

$$\frac{1}{[A]_0 - [B]_0} \ln \frac{[B]_0[A]_t}{[A]_0[B]_t} = k_2 t \quad (3.37)$$

By using *Equation 3.37*, the second-order rate constant can only be determined when the values of  $[A]_0$ ,  $[B]_0$ ,  $[A]_t$  and  $[B]_t$  are known. This means kinetic measurements become complex and tedious.<sup>2,12,13</sup> To simplify the process, second-order reactions are usually studied under *pseudo*-first-order conditions. As previously highlighted, the concentration of one of the reagents (typically the nucleophile) is provided in excess. When  $[B]_0 \gg [A]_0$ , the



concentration of  $B$  remains unchanged during the reaction. Supposing that the reaction order with respect to  $A$  is one, then the rate law in *Equation 3.31* can be written as:

$$\begin{aligned} -\frac{d[A]}{dt} &= k_2[A]_t[B]_t \\ &= (k_2[B]_0)[A]_t \\ &= k_{obs}[A]_t \end{aligned} \quad (3.38)$$

where  $k_{obs}$  is the observed rate constant with unit of  $s^{-1}$  and is equal to  $k_2[B]_0$ .

A plot of  $\ln[A]_t$  versus time gives a linear regression with the observed rate constant,  $k_{obs}$ , as the slope. To determine the second-order rate constant,  $k_2$ , a series of  $k_{obs}$  values must be obtained by varying the concentration of  $B$  in excess. This generates several  $[B]_0$  values.

$$k_{obs} = k_2[B]_0 \quad (3.39)$$

A plot of  $k_{obs}$  vs  $t$  produces the second-order rate constant,  $k_2$ , with units  $M^{-1} s^{-1}$ .

### 3.3.4 Reversible Second-Order Reactions

Usually, ligand substitution reactions in square-planar complexes do not go to completion, but have a propensity to attain a state of equilibrium. Consider a reaction:



By applying *pseudo*-first-order conditions, the rate law can be expressed as:

$$-\frac{d[A]}{dt} = -\frac{d[B]}{dt} = -\frac{d[C]}{dt} = k_2[A]_t[B]_t - k_{-2}[C]_t \quad (3.41)$$

$$[A]_t = [A]_0 - [C]_t$$

and  $[B]_t = [B]_0 - [C]_t \quad (3.42)$

At equilibrium

$$[A]_{eq} = [A]_0 - [C]_{eq}$$

And

$$[B]_{eq} = [A]_0 - [C]_{eq} \quad (3.43)$$

At equilibrium, the rate of the forward reaction is equivalent to the rate of the reverse, as indicated by *Equation 3.44*.

$$-\frac{d[A]}{dt} = k_2[A]_{eq}[B]_{eq} - k_{-2}[C]_{eq} = 0 \quad (3.44)$$

Hence,

$$k_2[A]_{eq}[B]_{eq} = k_{-2}[C]_{eq} \quad (3.45)$$

By substituting for  $[C]_{eq}$  in *Equation 3.45*, using the value from *Equation 3.41* and rearranging gives:

$$k_{-2}[A]_0 = k_2[A]_{eq}[B]_{eq} + k_{-2}[A]_{eq} \quad (3.46)$$

Substitution of  $[C]_t$  from *Equation 3.42* with the term  $[A]_0 - [A]_t$ , and substituting into *Equation 3.41* gives the rate as:

$$\begin{aligned} -\frac{d[A]}{dt} &= k_2[A]_t[B]_t - k_{-2}([A]_0 - [A]_t) \\ &= k_2[A]_t[B]_t - k_{-2}[A]_0 = k_2[A]_t \end{aligned} \quad (3.47)$$

Combining *Equations 3.46* and *3.47* gives:

$$-\frac{d[A]}{dt} = k_2[A]_t[B]_t - k_{-2}[A]_{eq}[B]_{eq} - k_{-2}[A]_{eq} + k_{-2}[A]_t \quad (3.48)$$

Applying *pseudo*-first-order conditions where  $[B]_0 \gg [A]_0$  *Equation 3.48* becomes:

$$\begin{aligned} -\frac{d[A]}{dt} &= k_2[A]_t[B]_0 - k_{-2}[A]_{eq}[B]_0 - k_{-2}[A]_{eq} + k_{-2}[A]_t \\ &= (k_2[B]_0 + k_{-2})([A]_t - [A]_{eq}) \end{aligned} \quad (3.49)$$

Separating the variables and integrating *Equation 3.49* gives:

$$\begin{aligned} \int_{[A]_0}^{[A]_t} \frac{d[A]}{([A]_t - [A]_{eq})} &= -(k_2[B]_0 + k_{-2}) \int_0^t dt \\ \ln \left( \frac{[A]_t - [A]_{eq}}{[A]_0 - [A]_{eq}} \right) &= -(k_2[B]_0 + k_{-2})t \\ &= -k_{obs}t \end{aligned}$$

where  $k_{obs} = k_2[B]_0 + k_{-2} \quad (3.50)$

A plot of  $k_{obs}$  vs  $[B]_0$  gives a linear regression with  $k_2$  as the slope and  $k_{-2}$  as the intercept. Pseudo-first-order conditions of this kind are mostly used in kinetic studies of square-planar Pt(II) complexes.

The equilibrium constant,  $K$ , can be determined by calculating the ratio:<sup>14</sup>

$$K_{eq} = \frac{k_2}{k_{-2}} \quad (3.51)$$

Furthermore, this rate law applies to cases in which the reaction proceeds in two parallel pathways where the first is independent of  $[B]_0$  and the second is a solvolysis pathway.<sup>9</sup>

### 3.4 Measurement of activation parameters.

#### 3.4.1 Measurement of enthalpy of activation ( $\Delta H^\ddagger$ ) and entropy of activation ( $\Delta S^\ddagger$ ).

The rate of reaction in square-planar complexes have a directly proportional relationship to temperature.<sup>14,15</sup> Fundamental to assigning the mechanism of a reaction is the rate law.<sup>16</sup> However, determining the thermal activation parameters allows for the interpretation of the rate constants when the temperature is systematically varied. The experimental data obtained for the various terms that contribute to the rate law is analysed using the Arrhenius equation or by the Transition-State Theory (TST).<sup>9</sup> For the former, the pre-exponential factor,  $A$ , and activation energy,  $E_a$ , are determined. The enthalpy and entropy of activation parameters,  $\Delta H^\ddagger$  and  $\Delta S^\ddagger$ , are determined from the latter, respectively.

The Arrhenius equation expresses the rate constant as a function of temperature:

$$k = Ae^{\left(\frac{-E_a}{RT}\right)} \quad (3.52)$$

where:  $k$  is the rate constant for the reaction

$A$  is the Arrhenius pre-exponential factor ( $M^{-1} s^{-1}$ ),

$E_a$  is the Arrhenius activation energy ( $J mol^{-1}$ ),

$R$  is the gas constant (equal to  $8.315 J K^{-1} mol^{-1}$ ) and

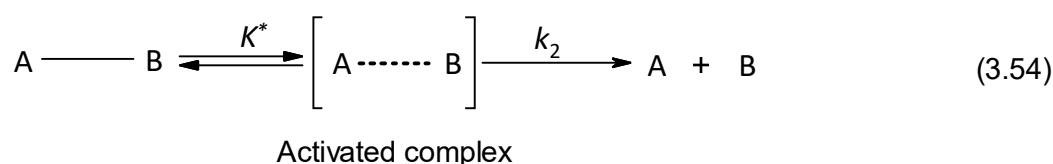
$T$  is the absolute temperature in K.

Taking the logarithms of Equation 3.52 gives Equation 3.53 in which  $\ln k$  varies linearly with  $\frac{1}{T}$ . The temperature-independent parameters,  $A$  and  $E_a$ , can be determined confidently over the temperature range 10-50 °C from the intercept and slope, respectively.

$$\ln k = \ln A - \frac{E_a}{R} \left(\frac{1}{T}\right) \quad (3.53)$$

The Arrhenius equation finds less use nowadays except in complex systems where there is uncertainty about where the measured rate constant is a composite of specific rate constants.<sup>1,2</sup>

The transition state or activated complex theory developed by H. Eyring, M. Evans and M. Polanyi in 1935 concedes that many reactions take place *via* a pre-equilibrium mechanism.<sup>1,17</sup> This theory works best in processing thermal activation parameters for ligand substitution reactions in square-planar Pt(II) complexes. For a bimolecular reaction such as this one:



The reaction rate can be represented as:

$$\frac{d[A]}{dt} = k_2 \{A \text{ --- } B\}^\ddagger = \frac{k_b T}{h} K^\ddagger [A][B] \quad (3.55)$$

where:  $k_b$  is the Boltzmann's constant ( $1.38 \times 10^{-23} \text{ J K}^{-1}$ ),

$T$  is the temperature in Kelvin (K),

$h$  is the Planck's constant ( $6.626 \times 10^{-34} \text{ J s}^{-1}$ ),

$K^\ddagger$  is the equilibrium constant.

The experimental second-order rate constant,  $k_{expt}$ , is expressed as:

$$k_{expt} = \frac{k_b T}{h} K^\ddagger \quad (3.56)$$

The Gibbs free energy of activation,  $\Delta G^\ddagger$ , is expressed as:

$$\begin{aligned} \Delta G^\ddagger &= -RT \ln K^\ddagger \\ &= \Delta H^\ddagger - T \Delta S^\ddagger \end{aligned} \quad (3.57)$$

where:  $\Delta H^\ddagger$  is the enthalpy of activation ( $\text{J mol}^{-1}$ ) and

$\Delta S^\ddagger$  is the entropy of activation ( $\text{J K}^{-1} \text{mol}^{-1}$ ).

Substituting *Equation 3.57* into *Equation 3.56* affords the following expression:

$$k_{\text{expt}} = \frac{k_b T}{h} e^{(-\frac{\Delta G^\ddagger}{RT})} = e^{(-\frac{\Delta H^\ddagger}{RT})} e^{(\frac{\Delta S^\ddagger}{R})} \quad (3.58)$$

Applying the natural logarithm on *Equation 3.58* affords:

$$\ln\left(\frac{k_{\text{expt}}}{T}\right) = \ln\left(\frac{k_b}{h}\right) - \frac{\Delta H^\ddagger}{RT} + \frac{\Delta S^\ddagger}{R} \quad (3.59)$$

*Equation 3.59* can be simplified and expressed in a linear form as:

$$\ln\left(\frac{k_{\text{expt}}}{T}\right) = -\frac{\Delta H^\ddagger}{R} \cdot \frac{1}{T} + \left(\ln\frac{k_b}{h} + \frac{\Delta S^\ddagger}{R}\right) \quad (3.60)$$

where

$$\ln\frac{k_b}{h} = 23.8 \quad (3.61)$$

Thus, from a plot, referred to as the Eyring Plot, of  $\ln\left(\frac{k_{\text{expt}}}{T}\right)$  vs  $\frac{1}{T}$ , the enthalpy of activation,  $\Delta H^\ddagger$ , is determined from the slope and the entropy of activation,  $\Delta S^\ddagger$ , is extrapolated at  $T = 0$  from the y-intercept of the graph.<sup>1,16,18</sup>

The thermal activation parameters are useful aids in assigning the mechanism of ligand substitution reactions in square-planar Pt(II) complexes. Low and positive enthalpy of activation values indicate the ease with which a new bond is formed due to the electrophilicity of the metal centre. High and negative entropy of activation values indicate a transition state that is highly ordered and more compact than either the reactant or product species.<sup>1,19</sup> Thus, the mechanism of substitution is said to undergo *via* an associative pathway.

### 3.4.2 Measurement of Volume of Activation, $\Delta V^\ddagger$ .

A more powerful and reliable parameter for identifying reaction mechanisms is the volume of activation,  $\Delta V^\ddagger$ . It is determined from kinetic experiments in which the observed rate constants,  $k_{\text{obs}}$ , are measured as the applied pressure is systematically varied.<sup>20</sup> Pressure-dependence of the rate constant is given by the equation:

$$\left(\frac{d \ln k_2}{dP}\right) = -\frac{\Delta V^\ddagger}{RT} \quad (3.62)$$

where,  $\Delta V^\ddagger$  is volume of activation and is equivalent to the difference in the partial molar volumes between the transition state and the reactants.<sup>10</sup>

Taking integrals of both sides of Equation 3.62 gives:

$$\ln k = -\left(\frac{\Delta V^\ddagger}{RT}\right)P \quad (3.63)$$

As a result, the plot of  $\ln k$  versus applied pressure produces a linear regression with a slope equal to  $-\frac{\Delta V^\ddagger}{RT}$ , from which the activation volume,  $\Delta V^\ddagger$ , can be directly evaluated. An increase in the applied pressure is accompanied by an acceleration of the rate constant for an associatively activated mechanism.<sup>20</sup> Negative volume of activation values imply a mechanism that occurs *via* a compacted transition state involving a greater degree of bond making. Conversely, positive volume of activation values corresponds to a dissociatively activated pathway in which bond breaking occurs in the transition state.

### 3.5 Instrumental techniques used for ligand substitution in Pt(II) complexes.

In the study of the rate of chemical reactions, it is important to have an accurate recording of the concentration of either reactants or products as a function of time. Most the reactions are monitored in aqueous solutions. The use of a suitable experimental method to monitor ligand substitution reactions in square-planar Pt(II) complexes is determined by the time scale of the reaction. For slow reactions, conventional spectroscopic techniques such as nuclear magnetic resonance (NMR), UV-visible, and infrared spectroscopy are used for data acquisition. For very fast reactions (which take 60 seconds to  $10^{-14}$  seconds) for completion, automated methods are required for data acquisition such as flow-through and pulse methods.<sup>1</sup> The spectroscopic techniques to be considered and described in detail are UV-visible spectroscopy (suitable for slow kinetic reactions) and stopped-flow (suitable for fast reactions).

#### 3.5.1 UV-visible spectrophotometer

UV-visible spectrophotometry is a slow but sensitive technique capable of detecting sample concentrations in the range of  $10^{-4}$  to  $10^{-6}$  M. It is used in the characterisation of electronic

transitions in a compound in which  $\pi$ -electrons are transferred from its highest occupied molecular orbital (HOMO) to the lowest unoccupied molecular orbital (LUMO) upon absorption of light in the ultraviolet (UV) and visible regions. **Figure 3.1** illustrates the skeleton diagram of a UV-visible spectrophotometer.

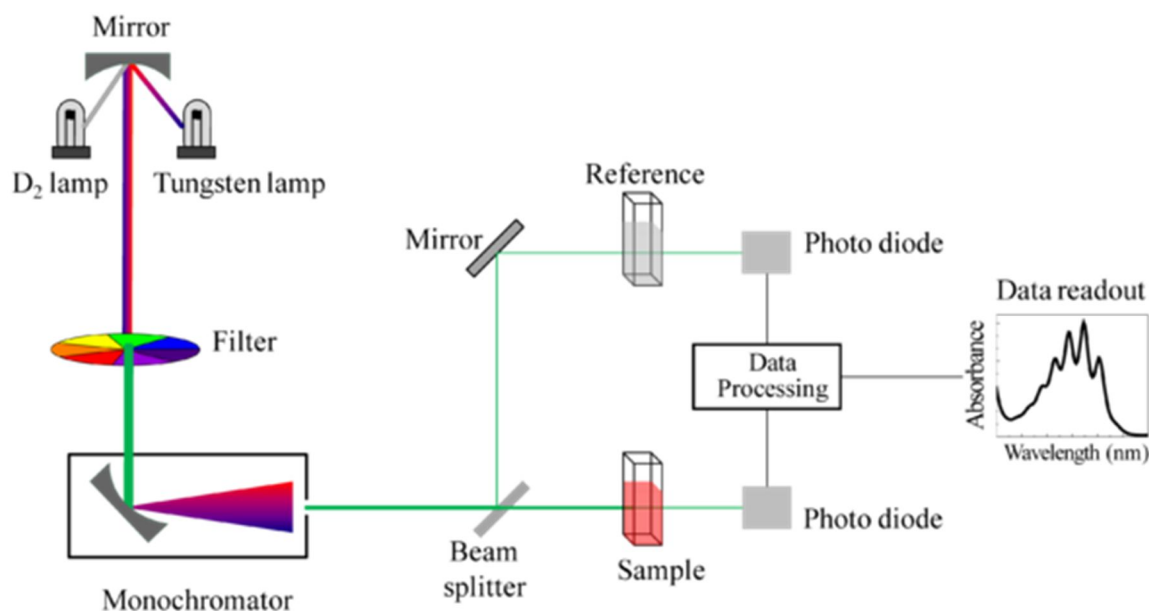


**Figure 3.1** Schematic diagram of a double beam UV-visible spectrophotometer.<sup>21</sup>

The spectrophotometer measures the amount of light transmitted,  $T$ , after irradiating a beam of light through a sample column. Transmittance is described as:

$$T = \frac{I}{I_0} \quad (3.64)$$

where:  $I$  is the intensity of the transmitted light (*sample intensity*) and

$I_0$  is the intensity of the incidence light (*reference intensity*).

The absorbance,  $A$ , is calculated from the logarithms of the intensities as follows:

$$A = \log\left(\frac{I_0}{I}\right) = -\log T \quad (3.65)$$

The optical transmittance,  $T$ , is related to the concentration of the species under study by the Beer's law:

$$A = \epsilon cl \quad (3.66)$$

where:  $A$  is the absorbance,

$\epsilon$  is the molar absorptivity or extinction coefficient ( $M^{-1}cm^{-1}$ ),

$c$  is the concentration ( $mol\ dm^{-3}$ ) of the sample and

$l$  is the path length ( $cm$ ).

For a first-order reaction, represented by *Equation 3.6*, at any time  $t$ , the absorbance is

$$A_t = \epsilon_X[X]_t + \epsilon_Y[Y]_t \quad (3.67)$$

where:  $A_t$  is the absorption at any time and

$\epsilon_X, \epsilon_Y$  is the molar absorptivity of X and Y, respectively.

Once the reaction has reached completion, the absorbance becomes

$$A_t = \epsilon_X[X]_0 + \epsilon_Y[Y]_0 \quad (3.68)$$

For kinetic measurements, the following expression is obtained from the absorbance:

$$\ln \frac{[X]_0}{[X]_t} = \ln \left( \frac{A_0 - A_\infty}{A_t - A_\infty} \right) = k_1 t \quad (3.69)$$

For experimental determination of rate constants, absorbance-time resolved data is acquired at a pre-determined wavelength at which a significant change in absorbance occurs with time. Therefore, the observed rate constant for the reaction (taken over a duplet runs) is obtained by a least squares fit of an absorbance-time plot at a specified wavelength. A concentration dependence study at different concentrations of the reactants allows for the determination of the rate constant for the reaction at a specified temperature.

### 3.5.2 Flow Methods

Flow techniques are designed to achieve rapid and efficient mixing of two solutions (metal complex and nucleophiles), ensuring that the ensuing reaction is promptly monitored as it commences a few milli-seconds after mixing has occurred.<sup>11</sup> In these techniques, reagent solutions are mixed together by flowing them through a mixer from which the reaction solution emerges to be analysed.<sup>3</sup>

As depicted in **Figure 3.2**, the reaction analyser consists of drive syringes filled with their respective (metal complex and nucleophile) solutions, thermostated to the required temperature through a water bath compartment. The reaction starts as the solutions are



charged out of their syringes by a compressed gas-driven piston (800 kPa) on the plunges, through the mixing chamber, and along the observation tube to the collector syringe. When the plunger of the latter reaches its stop, this both arrests the flow of the mixing solutions and triggers the recorder.<sup>3</sup> The amount of light, of the wavelength setting of the monochromator, transmitted through the mixed solution undergoes changes as the reaction proceeds in the now static mixed solution. A photomultiplier unit converts this transmitted light into an electric current, a grid resistor generates a voltage proportional to the light intensity and, using an analogue-to-digital (A/D) converter, this signal is fed to the computer, which samples at pre-determined intervals over an appropriate time interval.<sup>3</sup>

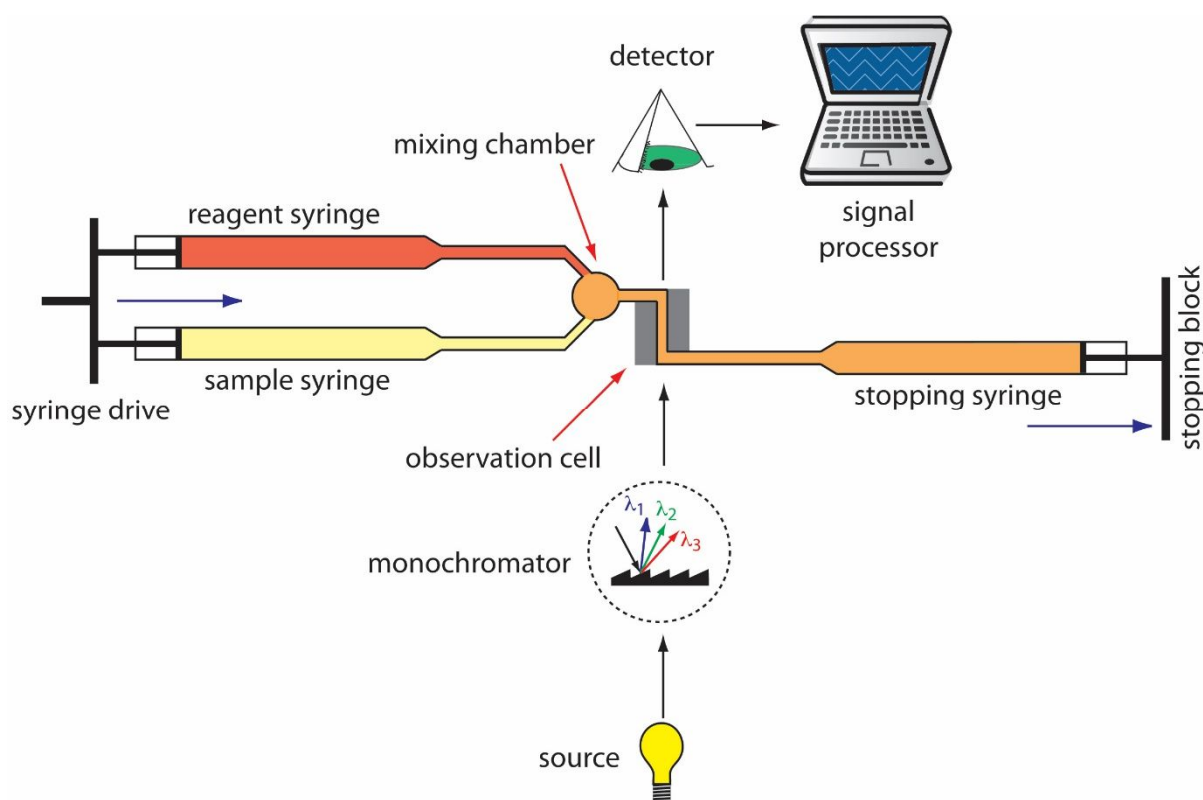


**Figure 3.2** Schematic diagram of a stopped-flow mixing apparatus.<sup>3</sup>

### 3.6 References

1. R. B. Jordan, *Reaction mechanisms of inorganic and organometallic systems*, Oxford University Press, New York, 1991, 29-40.
2. S. Asperger, *Chemical kinetics and inorganic reaction mechanisms*, Kluwer Academic/Plenum Publishers, New York, 2003, 34-40, 105-106.
3. S. R. Logan, *Fundamentals of chemical kinetics*, Longman, Essex, England, 1996, 1-30.
4. M. L. Tobe, *Inorganic reaction mechanisms*, Nelson, London, 1972.
5. M. L. Tobe and J. Burgess, *Inorganic reaction mechanisms*, Longman, Harlow, Essex, England; New York, 1999, 30-43, 70-112.
6. J. H. Espenson, *Chemical kinetics and reaction mechanisms*, McGraw-Hill, New York, 1995.
7. P. O. Ongoma and D. Jaganyi, *Dalton Transactions*, 2013, **42**, 2724-2734.
8. H. Erturk, A. Hofmann, R. Puchta and R. van Eldik, *Dalton Transactions*, 2007, DOI: 10.1039/B700770C, 2295-2301.
9. J. D. Atwood, *Inorganic and organometallic reaction mechanisms*, Wiley-VCH, New York, 1997.
10. D. Katakis and G. Gordon, *Mechanisms of inorganic reactions*, Wiley, New York, 1987.
11. R. G. Wilkins, *Kinetics and mechanism of reactions of transition metal complexes*, VCH, Weinheim; New York, 1991, 199-201.
12. C. H. Langford and H. B. Gray, *Ligand substitution processes*, W.A. Benjamin, Reading, Mass., 1974.
13. P. W. Atkins, *Shriver & Atkins' inorganic chemistry*, Oxford University Press, Oxford; New York, 2010, 202, 218.
14. F. Basolo and R. G. Pearson, *Mechanisms of inorganic reactions: a study of metal complexes in solution*, Wiley, 1967, 351-404.
15. A. G. Sykes, *Kinetics of inorganic reactions*, Pergamon, Oxford; New York, 1966.
16. D. Benson, *Mechanisms of inorganic reactions in solution: an introduction*, McGraw-Hill, London; New York, 1968.
17. M. G. Evans and M. Polanyi, *Transactions of the Faraday Society*, 1935, **31**, 875-894.

18. J. H. Espenson, *Chemical kinetics and reaction mechanisms*, McGraw-Hill, New York, 1981.
19. D. Jaganyi, K.-L. D. Boer, J. Gertenbach and J. Perils, *International Journal of Chemical Kinetics*, 2008, **40**, 808-818.
20. M. Kotowski, D. A. Palmer and H. Kelm, *Inorganic Chemistry*, 1979, **18**, 2555-2560.
21. D. A. Skoog, D. M. West and F. J. Holler, *Fundamentals of analytical chemistry*, Saunders College Pub., Fort Worth, 1996.

# Chapter 4

## Substitution of aqua ligands from *cis*-Pt(II) complexes bearing 2-(phenylthiomethyl)pyridine spectator ligands.

### 4.0 Abstract

Three mononuclear *cis*-Pt(II) complexes comprising pyridine moieties namely, [Pt{2-(phenylthiomethyl)pyridine}(H<sub>2</sub>O)<sub>2</sub>]<sup>2+</sup> **Pt(pyS<sup>Ph</sup>)**, [Pt{2-(4-*tert*-butylphenylthiomethyl)pyridine}(H<sub>2</sub>O)<sub>2</sub>]<sup>2+</sup> **Pt(pyS<sup>Ph(t-But)</sup>)** and [Pt{2-(4-fluorophenylthiomethyl)pyridine}(H<sub>2</sub>O)<sub>2</sub>]<sup>2+</sup> **Pt(pyS<sup>PhF</sup>)**, were synthesized. Acid-base titrations, as well as temperature and concentration dependent kinetics measurements of the reactions with three sulphur-donor nucleophiles were studied at pH 2. The reactions were monitored under *pseudo*-first-order conditions using stopped-flow and UV-visible spectrophotometric techniques in a 0.1 M LiOTf/HOTf aqueous medium.

The mechanism of substitution of the aqua ligands from the complexes is limiting associative, characterised by the dependence on the concentration of the incoming ligand, low enthalpy of activation ( $\Delta H^\ddagger$ ) and negative entropy of activation ( $\Delta S^\ddagger$ ) values. The sequential substitution of the first and second aqua ligands is described by the rate law:  $k_{\text{obs}(1/2)} = k_{(1/2)}[\text{Nu}]$ . The rate constant,  $k_1$ , relates to the substitution *trans* to the sulphur donor atom, which occurs first due to the strong  $\sigma$ -*trans* influence of sulphur while  $k_2$  is the rate constant for the subsequent substitution of the aqua ligand *trans* to the pyridine moiety. The rate of substitution of the first aqua leaving ligand decreases in the order: **Pt(pyS<sup>Ph(t-But)</sup>)** > **Pt(pyS<sup>PhF</sup>)** > **Pt(pyS<sup>Ph</sup>)** while that of the second ligand decreases in the order: **Pt(pyS<sup>Ph(t-But)</sup>)** > **Pt(pyS<sup>Ph</sup>)** > **Pt(pyS<sup>PhF</sup>)**. The order of reactivity of the nucleophiles: **tu** > **dmtu** > **tmtu** is in accordance with their steric bulk. The reactivity of the complexes is sensitive to the nature of the substituents on the *para*-position of the phenyl ring of the thioether. The positive  $\sigma$ -inductive electron-donating *tert*-butyl increases the rate of substitution by enhancing the *trans*-directing ability of the thioether. The negative  $\sigma$ -inductive electron-withdrawing fluoro substituent activates the thioether to have  $\pi$ -acceptor properties which also increases slightly

the rate of substitution. Interestingly, the complex with an unsubstituted phenyl **Pt(pyS<sup>Ph</sup>)** retards the rate of substitution due to weak  $\sigma$ -donor capacity. Arrayed <sup>195</sup>Pt spectra of aged solutions of complexes with the thiourea nucleophiles suggest a rapid nucleophile concentration-independent ring-opening of the N,S-bidentate ligand from the Pt complexes. A peak is observed at -3884 ppm at the end of the reaction and this is due to a Pt species coordinated to four S atoms (PtS<sub>4</sub>). Density functional theory (B3LYP(CPCM)/LANL2DZp//B3LYP/-LAN2DZp) calculations were computed to help explain the experimental data.

#### 4.1 Introduction

The *cis* geometry of cisplatin is key to cytotoxic activity of current Pt-based drugs.<sup>1,2</sup> The labile ligands are substituted to form covalent linked platino-purine/pyrimidine cycles with DNA.<sup>3,4</sup> Similar reactions also occur with other nucleophilic species in cells, most of which bring toxicity or development of resistance.<sup>5-7</sup> A careful choice of the non-leaving and leaving groups is therefore important in regulating the pharmaco-kinetic properties of Pt-drugs. The good examples credited for lower toxicity and propensity to avoid cisplatin resistance are carboplatin and oxaliplatin.<sup>8,9</sup> Recently, a cisplatin-derived Pt(II) complex with an ammine and 1-methyl-7-azaindole ligand was shown to have remarkable activity against cisplatin-sensitive A2780 but not against cisplatin-resistant A2780cisR cell lines.<sup>10</sup> Bidentate 2-(aminomethyl)pyridine and 2-(pyrazolylmethyl)pyridine ligands coordinated in a *cis* geometry to platinum have been shown to have encouraging signs of anticancer activity on human HeLa cancer cell lines.<sup>11,12</sup>

The activity at low and less toxic concentration levels, selectivity to target cancerous cells, enhanced lipophilicity of the drug and stability in aqueous biological system, remain the drivers in the design of new Pt drugs of improved potency.<sup>13,14</sup> A *cis*-Pd(II) complex containing 1,4-bis(2-hydroxyethyl)piperazine was designed to ensure some favourable non-bonding interactions such as hydrogen bonding of its hydroxyethyl with DNA nucleic bases.<sup>15</sup> In another study, the ammine ligands of cisplatin were replaced with a chelating 4,7-diphenyl-1,10-phenanthroline ligand to form a *cis*-Pt(II) complex which can intercalate into DNA in addition to forming covalent cross-links.<sup>16</sup> Other notable non-leaving ligands whose *cis*-Pt(II) complexes have shown good potential as anticancer agents are 3-hydroxymethylpyridine,<sup>17</sup>

1,2-diaminophenylalkane,<sup>18</sup> and 2-aminobenzothiazole.<sup>19</sup> The potential antitumour activity displayed by these complexes demonstrates that a careful design on the structure for both the non-leaving and leaving ligands around the square-planar *cis* geometry has genesis in the substitutional reactivity.

Often square-planar Pt(II) complexes are used as model complexes for understanding the mechanisms of substitution due to their moderate rates of ligand exchange kinetics.<sup>20,21</sup> The mechanistic studies of *cis*-Pt(II) and *cis*-Pd(II) complexes with N,N- and N,S-bidentate or monodentate non-leaving and/or leaving ligands have been reported in literature.<sup>22-30</sup> They all share a similar geometry to cisplatin. As a result, it can be hypothesised that they can form 1,2-intrastrand adducts with potential to induce cytotoxicity to cancer cells as does cisplatin.<sup>31</sup> In keeping with the idea of altering the non-leaving ligands yet keeping the cytostatic geometry of cisplatin, three mononuclear *cis*-Pt(II) complexes with a 2-(phenylthiomethyl)pyridine (N,S-chelate) non-leaving ligands were synthesized (**Figure 4.1**). The rate of substitution of the aqua ligands, from the complexes, by thiourea nucleophiles was measured under *pseudo*-first order conditions. The nature of the entering nucleophiles is important in that they model the possible interactions between the complexes with biological species such as sulphur-containing proteins and peptides which are known to have a strong affinity for platinum.<sup>32</sup>

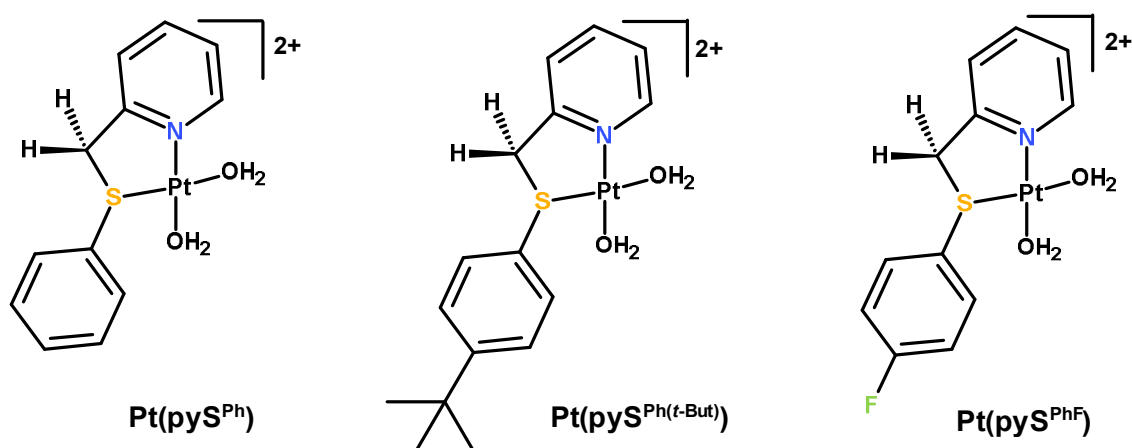


**Figure 4.1** Formulae of *cis*-Pt(II) complexes investigated.

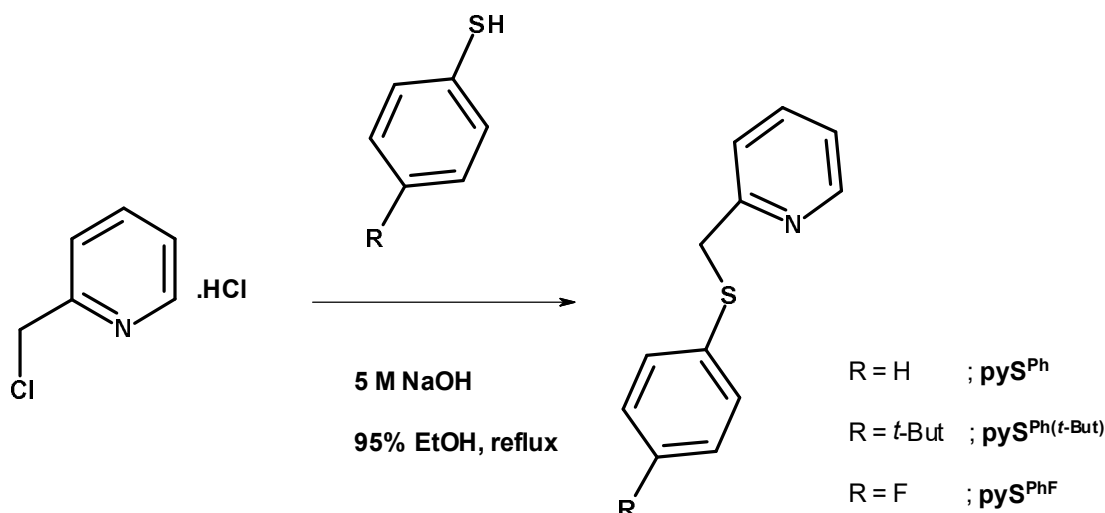
## 4.2 Experimental

### 4.2.1 Procedures and Chemicals

The ligands and the Pt complexes were synthesised from 2-(chloromethyl)pyridine hydrochloride (98%), thiophenol (97%), 4-*tert*-butylthiophenol (97%), 4-fluorothiophenol (98%), potassium tetrachloroplatinate (K<sub>2</sub>PtCl<sub>4</sub>, 99%), silver trifluoromethanesulfonate (CF<sub>3</sub>SO<sub>3</sub>Ag, 99%, Aldrich), lithium trifluoromethanesulfonate (CF<sub>3</sub>SO<sub>3</sub>Li, 99+%, Aldrich) and hydrochloric acid (HCl, 32%, Saarchem). All chemicals and reagents were used without further purification and stored according to material data sheet specifications. The nucleophiles *viz.*, thiourea (**tu**, 99%), N,N-dimethylthiourea (**dmtu**, 99%), and N,N,N',N'-tetramethylthiourea (**tmtu**, 99%) were likewise purchased from Aldrich and used without further purification. Ultrapure water (MODULAB purification system) was used for all aqueous reactions. All other chemicals and solvents were of reagent grade and used as received.

### 4.2.2 Synthesis of the ligands

The ligands, namely 2-(phenylthiomethyl)pyridine **pyS<sup>Ph</sup>**, 2-(4-*tert*-butylphenylthiomethyl)pyridine **pyS<sup>Ph(t-But)</sup>**, and 2-(4-fluorophenylthiomethyl)pyridine **pyS<sup>PhF</sup>** were prepared *via* a nucleophilic S-alkylation reaction of either thiophenol, 4-*tert*-butylthiophenol, or 4-fluorothiophenol with 2-(chloromethyl)pyridine hydrochloride in dry ethanol (**Scheme 4.1**) as reported by Malachowski *et al.*<sup>33,34</sup> The three ligands were synthesised to yield (57-89 %) yellow or brown oils of adequate purity for subsequent coordination on platinum. The purity of the ligands was confirmed by <sup>1</sup>H and <sup>13</sup>C NMR, TOF-MS-ESI<sup>+</sup> and elemental analysis (CHNS) techniques. The IR spectra of the ligands gave the following characteristic frequencies cm<sup>-1</sup>: 3100-3000 (broad, medium, Csp<sup>3</sup>-H stretch); 1583 (sharp and strong, Csp<sup>2</sup>=N stretch, pyridyl rings).



**Scheme 4.1** Synthesis of the (phenylthiomethyl)pyridine ligands

### 2-(phenylthiomethyl)pyridine (**pyS<sup>Ph</sup>**)

A mass (1.598 g, 9.74 mmol) of 2-(chloromethyl)pyridine hydrochloride was dissolved in 3 mL ultrapure water. A solution of 5 M NaOH was added drop-wise until a pink emulsion appeared. A solution of thiophenol (1.073 g, 9.74 mmol) in 20 mL ethanol (EtOH, 95%) was slowly added to the reaction flask. The mixture was stirred under reflux for 24 hours. The solution was allowed to cool to room temperature and extracted four times with 10 mL chloroform (CHCl<sub>3</sub>). The crude extract was concentrated and further purified in a short-column of aluminium oxide (Al<sub>2</sub>O<sub>3</sub>) using a mixture of CH<sub>2</sub>Cl<sub>2</sub> and CHCl<sub>3</sub>. The combined organic phase was back-washed with 2 x 10 mL deionised water and dried with 2-3 g of anhydrous MgSO<sub>4</sub>. Filtration and removal of the solvent *in vacuo* gave a bright yellow oil of **pyS<sup>Ph</sup>**.

The yield of 1.528 g (78 %) for **pyS<sup>Ph</sup>** was obtained. Proton-1 NMR (400 MHz: CDCl<sub>3</sub>): δ<sub>H</sub> (ppm) referenced to TMS; 4.30 (s, 2H, -CH<sub>2</sub>-), 7.16 (t, 1H, Ph), 7.27 (t, 2H, Ph), 7.37 (d, 2H, Ph), 7.33 (t, 1H, py), 7.52-7.54 (d, 1H, py), 7.60-7.64 (t, 1H, py), 8.56 (d, 1H, py). Carbon-13 NMR (100 MHz: CDCl<sub>3</sub>): δ<sub>C</sub> (ppm); 40.5; 122.1; 123.0; 126.4; 127.6; 128.9; 129.1; 129.7; 136.7; 149.3. Infrared (KBr, 4000-650 cm<sup>-1</sup>)  $\bar{\nu}$ : 3055 (C=C-H Asymmetric stretch), 1583 (C=N, pyridyl). Time-of-flight MS-ESI<sup>+</sup> *m/z*: 223.0930, 100 (M+Na)<sup>+</sup>. *Anal. Calc. for* C<sub>12</sub>H<sub>11</sub>NS: C: 71.60, H: 5.51, N: 6.96, S: 15.93 %. *Found*: C: 71.21, H: 5.58, N: 6.24, S: 16.09 %.



The ligands **pyS<sup>Ph(t-But)</sup>** and **pyS<sup>PhF</sup>** were synthesised using a similar procedure as for **pyS<sup>Ph</sup>**, with 2-(4-*tert*-butylthiophenol) and 2-(4-fluorothiophenol) replacing the thiophenol, respectively. The synthesised oils were stored in Schlenk tubes until their coordination to platinum.

#### **2-(4-*tert*-butylthiophenol)pyridine (pyS<sup>Ph(t-But)</sup>)**

The yield of 1.457 g (57 %, light-brown) for **pyS<sup>Ph(t-But)</sup>** was obtained. Proton-1 NMR (400 MHz: CDCl<sub>3</sub>):  $\delta_{\text{H}}$  (ppm) referenced to TMS; 1.30 (s, 9H, -C(CH<sub>3</sub>)<sub>3</sub>), 4.27 (s, 2H, -CH<sub>2</sub>-), 7.17-7.18 (t, 1H, py), 7.28 (d, 4H, Ph), 7.36 (d, 1H, py), 7.62-7.65 (t, 1H, py), 8.55 (d, 1H, py). Infrared (KBr, 4000-650 cm<sup>-1</sup>)  $\bar{\nu}$ : 3059 (C=C-H Asymmetric stretch), 1598 (C=N, pyridyl). Time-of-flight MS-ESI<sup>+</sup>  $m/z$ : 258.1181, 100 (M+1). *Anal. Calc. for* C<sub>16</sub>H<sub>19</sub>NS: C: 74.66, H: 7.44, N: 5.44, S: 12.46 %. *Found*: C: 74.47, H: 7.50, N: 5.58, S: 12.28 %.

#### **2-(4-fluorothiophenol)pyridine (pyS<sup>PhF</sup>)**

The yield of 1.698 g (74 %, light-orange) for **pyS<sup>PhF</sup>** was obtained. Proton-1 NMR (400 MHz: CDCl<sub>3</sub>):  $\delta_{\text{H}}$  (ppm) referenced to TMS; 4.19 (s, 2H, -CH<sub>2</sub>-), 6.91-7.00 (d, 2H, Ph), 7.12-7.15 (t, 1H, py), 7.23 (d, 1H, py), 7.32(d, 2H, Ph), 7.57-7.60 (t, 1H, py), 8.51-8.52 (d, 1H, py). Carbon-13 NMR (100 MHz: CDCl<sub>3</sub>):  $\delta_{\text{C}}$  (ppm); 41.8; 115.8; 116.1; 122.1; 123.1; 133.1; 136.6; 149.3; 157.6. Infrared (KBr, 4000-650 cm<sup>-1</sup>)  $\bar{\nu}$ : 3066 (C=C-H Asymmetric stretch), 1588 (C=N, pyridyl). Time-of-flight MS-ESI<sup>+</sup>  $m/z$ : 220.0488, 100 (M+1). *Anal. Calc. for* C<sub>12</sub>H<sub>10</sub>FNS: C: 65.73, H: 4.60, N: 6.39, S: 14.62 %. *Found*: C: 65.29, H: 4.31, N: 6.35, S: 14.43 %.

### **4.2.3 Synthesis of Pt(II) complexes**

[Pt{2-(phenylthiomethyl)pyridine}Cl<sub>2</sub>], **Pt(pyS<sup>Ph</sup>)Cl<sub>2</sub>**, [Pt{2-((4-*tert*-butylthiophenol)pyridine)Cl<sub>2</sub>], **Pt(pyS<sup>Ph(t-But)</sup>)Cl<sub>2</sub>**, and [Pt{2-((4-fluorothiophenol)pyridine)Cl<sub>2</sub>], **Pt(pyS<sup>PhF</sup>)Cl<sub>2</sub>**, were synthesised from their respective ligands according to a literature method with minor modifications.<sup>35</sup> K<sub>2</sub>PtCl<sub>4</sub> (0.47 g, 1.1 mol) was dissolved in ultrapure water (25 mL) and stirred for 10-15 minutes and filtered thereafter. A CHCl<sub>3</sub> solution of the N,S chelate ligand (0.23 g, 1.1 mmol) was added drop-wise into the reaction flask. The reaction mixture was left to stir under reflux for 24 h (in a light-free environment). A bright yellow solid precipitate which formed was collected *via* a Millipore micro filter paper after cooling the reaction mixture to room temperature. The precipitate was washed with water, ethanol and diethyl ether. It was dried under vacuum to give a fine yellow powder. The complexes **Pt(pyS<sup>Ph</sup>)Cl<sub>2</sub>**,

**Pt(pyS<sup>Ph(t-But)</sup>)Cl<sub>2</sub>** and **Pt(pyS<sup>PhF</sup>)Cl<sub>2</sub>** were characterised by NMR (<sup>1</sup>H, <sup>13</sup>C, and <sup>195</sup>Pt), CHN elemental analyser, TOF MS-ESI<sup>+</sup> and IR spectroscopy.

Single crystals suitable for X-ray diffraction analysis of **Pt(pyS<sup>PhF</sup>)Cl<sub>2</sub>** were obtained by vapour diffusion of ether into the nitromethane solution of its powder.

The yield of 0.4058 g (77 %, yellow) for **Pt(pyS<sup>Ph</sup>)Cl<sub>2</sub>** was obtained. Proton-1 NMR (400 MHz: DMF-d<sub>7</sub>): δ<sub>H</sub> (ppm) referenced to TMS; 4.30 (d, 2H, -CH<sub>2</sub>-, AB-spin system), 7.16 (t, 1H, Ph), 7.27 (t, 2H, Ph), 7.37 (d, 2H, Ph), 7.33 (t, 1H, py), 7.52-7.54 (d, 1H, py), 7.60-7.64 (t, 1H, py), 8.56 (d, 1H, py). Platinum-195 NMR (400 MHz: DMF-d<sub>7</sub>): δ<sub>Pt</sub> (ppm); -2778. Infrared (KBr, 4000-650 cm<sup>-1</sup>)  $\bar{\nu}$ : 3055 (C=C-H Asymmetric stretch), 1583 (C=N, pyridyl). *Anal. Calc. for* C<sub>12</sub>H<sub>11</sub>Cl<sub>2</sub>NPtS: C: 30.84, H: 2.37, N: 3.00, S: 6.68 %. *Found*: C: 30.60, H: 2.24, N: 2.91, S: 6.49 %.

The yield of 0.3257 g (57 %, light-brown) for **Pt(pyS<sup>Ph(t-But)</sup>)Cl<sub>2</sub>**. Proton-1 NMR (400 MHz: CDCl<sub>3</sub>): δ<sub>H</sub> (ppm) referenced to TMS; 1.30 (s, 9H, -C(CH<sub>3</sub>)<sub>3</sub>), 4.27 (d, 2H, -CH<sub>2</sub>-, AB-spin system), 7.17-7.18 (t, 1H, py), 7.28 (d, 4H, Ph), 7.36 (d, 1H, py), 7.62-7.65 (t, 1H, py), 8.55 (d, 1H, py). Platinum-195 NMR (400 MHz: DMF-d<sub>7</sub>): δ<sub>Pt</sub> (ppm); -2786. Infrared (KBr, 4000-650 cm<sup>-1</sup>)  $\bar{\nu}$ : 3059 (C=C-H Asymmetric stretch), 1598 (C=N, pyridyl). *Anal. Calc. for* C<sub>16</sub>H<sub>19</sub>Cl<sub>2</sub>NPtS: C: 36.72, H: 3.66, N: 2.68, S: 6.13 %. *Found*: C: 36.85, H: 3.53, N: 2.53, S: 7.06 %.

The yield of 0.698 g (74 %, off-orange) for **Pt(pyS<sup>PhF</sup>)Cl<sub>2</sub>**. Proton-1 NMR (400 MHz: CDCl<sub>3</sub>): δ<sub>H</sub> (ppm) referenced to TMS; 4.19 (s, 2H, -CH<sub>2</sub>-, AB-spin system), 6.91-7.00 (d, 2H, Ph), 7.12-7.15 (t, 1H, py), 7.23 (d, 1H, py), 7.32 (d, 2H, Ph), 7.57-7.60 (t, 1H, py), 8.51-8.52 (d, 1H, py). Platinum-195 NMR (400 MHz: DMF-d<sub>7</sub>): δ<sub>Pt</sub> (ppm); -2796. Infrared (KBr, 4000-650 cm<sup>-1</sup>)  $\bar{\nu}$ : 3066 (C=C-H Asymmetric stretch), 1588 (C=N, pyridyl). *Anal. Calc. for* C<sub>12</sub>H<sub>10</sub>Cl<sub>2</sub>FNPtS: C: 29.70, H: 2.08, N: 2.89, S: 6.60 %. *Found*: C: 30.14, H: 2.05, N: 2.52, S: 6.20 %.

### 4.3 Preparation of the diaqua Pt(II) complexes

Solutions of diaqua Pt(II) complexes of **Pt(pyS<sup>Ph</sup>)Cl<sub>2</sub>**, **Pt(pyS<sup>Ph(t-But)</sup>)Cl<sub>2</sub>**, and **Pt(pyS<sup>PhF</sup>)Cl<sub>2</sub>** were prepared following a method described in literature.<sup>36</sup> A known amount of Pt(II) dichloro complex and adding a stoichiometric excess (with respect to chloride) of CF<sub>3</sub>SO<sub>3</sub>Ag (1.98 molar ratio) were dissolved in 0.01 M trifluoromethanesulfonic (triflic) acid. The mixture was vigorously stirred at 50 °C for 24 hours in the dark. The white precipitate of silver chloride

(AgCl) was filtered off through 0.45  $\mu\text{m}$  nylon membrane using a Millipore filtration apparatus. The clear and colourless filtrate was acidified with 0.01 M ( $\text{CF}_3\text{SO}_3\text{H}$ ) (triflic) acid in a volumetric flask to make the required concentration of the complex in solution. An acidic medium ( $\text{pH} = 2$ ) was necessary to ensure that only diaqua complexes and not the mixture of the aqua/hydroxo species, were present in solution once the chloride metathesis reaction was complete. The adjustment of  $I = 0.10$  M with  $\text{CF}_3\text{SO}_3\text{Li}$  was undertaken to ensure a constant ionic strength throughout the kinetic measurements.

#### 4.4 Instrumentation and physical measurements

A Bruker NMR spectrometer (Bruker Avance DRX 400 or DRX 500) and a FLASH 2000 CHN analyser were used for the characterization and chemical analysis of the synthesized ligands and complexes, respectively. Low-resolution electron-spray ionization ( $\text{ESI}^+$ ) mass spectra of the ligands and complexes were recorded on a time-of-flight (TOF) micromass spectrometer. A Perkin Elmer Spectrum One FTIR spectrometer was used to obtain Infrared (IR) spectra of the ligands and complexes diluted with KBr. Rapid kinetic measurements were followed using an Applied Photophysics SX 18MV stopped-flow spectrophotometer coupled to an online data acquisition system. The temperature of the reaction was controlled to within  $\pm 0.1$   $^\circ\text{C}$  for all measurements. A Cary 100 BIO UV-visible spectrophotometer equipped with a Varian Peltier temperature controller with an accuracy of  $\pm 0.05$   $^\circ\text{C}$  was used for the determination of the  $\text{pK}_a$  values of the diaqua complexes. The pH measurements were determined on a Jenway 4330 pH meter equipped with a 4.5  $\mu\text{m}$  glass electrode. The micro-electrode was calibrated at 25  $^\circ\text{C}$  using standard buffer solutions (Merck) at pH 4.0, 7.0, and 10.0.  $\text{pK}_a$  titration curves and time-resolved kinetic traces were graphically analysed using Origin 7.5<sup>®</sup> software package.<sup>37</sup>

##### 4.4.1 $\text{pK}_a$ determination for the coordinated aqua ligand of the complexes

Acid-base titrations were undertaken to determine the  $\text{pK}_a$  values of the diaqua complexes. The complexes were titrated with NaOH and the pH (in the range 2-9) and the absorption spectrum of the solution was recorded. Initially, the base was added in small portions of crushed pellets and subsequently as its dilute solutions. After each addition of NaOH, ca 0.5 mL of solution was sampled for the pH measurement. The portion was discarded to avoid chloride contamination of the solution from leached ions coming from the electrode.

The spectral data was analysed with Origin7.5<sup>®</sup> for which a plot of the  $pK_a$  values were generated from the sigmoidal curve fitting using Boltmann distribution parameters.

#### 4.4.2 Kinetics studies

The substitution of the coordinated aqua ligands from all complexes by thiourea nucleophiles was studied as a function of concentration and temperature. The concentration of the nucleophiles was at least 10-fold greater than the Pt(II) complexes to simplify the reaction kinetics to first order. The ionic strength was maintained at 0.1 M with a mixture of a 0.09 M lithium trifluoromethanesulfonate (LiOTf) and 0.01 M HOTf. The low basicity of the triflate ion precludes its coordination to the Pt(II) metal centre. A pH of 2 ensured that the substitution reactions being monitored were that of the coordinated aqua ligands. The reactions were monitored on a stopped-flow analyser equipped with a pressure-driven cross-plugging technique to ensure efficient mixing of the complex and nucleophile solutions. Prior to kinetics measurements on the stopped-flow, a preliminary reaction for the change in absorbance of the mixture of the Pt(II) metal complex with nucleophile as a function of time was undertaken on the UV-visible spectrophotometer. This was done to determine suitable wavelengths at which kinetic traces could be followed. All the reported rate constants were averages of six to eight independent kinetic runs. The temperature of the medium was varied within the range of 15-35 °C to determine the activation parameters  $\Delta H^\ddagger$  and  $\Delta S^\ddagger$  from the Eyring equation.

#### 4.4.3 Computer simulation studies

The geometry optimized molecular structures of the complexes **Pt(pyS<sup>Ph</sup>)**, **Pt(pyS<sup>Ph(t-But)</sup>)** and **Pt(pyS<sup>PhF</sup>)** were computed at the DFT level of theory following the (B3LYP(CPCM)/LANL2DZp//B3LYP/-LAN2DZp) method<sup>38-40</sup> powered by the Gaussian 09 software suite.<sup>41</sup> The geometry optimized structures were conducted in the gaseous phase and the calculated structural parameters are presented in the results section. A charge of +2 was maintained for the cationic diaqua complexes.

#### 4.4.4 X-ray crystallography

Single crystal diffraction data of **Pt(pyS<sup>PhF</sup>)Cl<sub>2</sub>** was collected on a Bruker Apex II Duo equipped with an Oxford Instrument Cryojet operating at 100 K and an Incoatec microsource

operating at 30 W power. A Mo K $\alpha$  ( $\lambda = 0.71073 \text{ \AA}$ ) beam irradiated at a crystal-to-detector distance of 50 mm was used to collect the diffraction data. The Bruker instrument was calibrated to have the following optimum conditions: omega and phi scans with exposures taken at 30 W X-ray power and  $0.50^\circ$  frame widths using APEX2.<sup>42</sup> Data reduction was performed by the SAINT<sup>42</sup> suite of programmes using outlier rejection, scan speed scaling, and standard Lorentz and polarisation correction factors. The structure was solved by direct methods using SHELXS-97<sup>43</sup> and refined using SHELXL-97.<sup>43</sup> The **Pt(pyS<sup>PhF</sup>)Cl<sub>2</sub>** crystallized in the monoclinic space group, P21/c and contained one molecule with  $Z = 4$ . The crystal structure and a summary of the crystal data and structure refinement details are shown in the results section.

## 4.5 Results

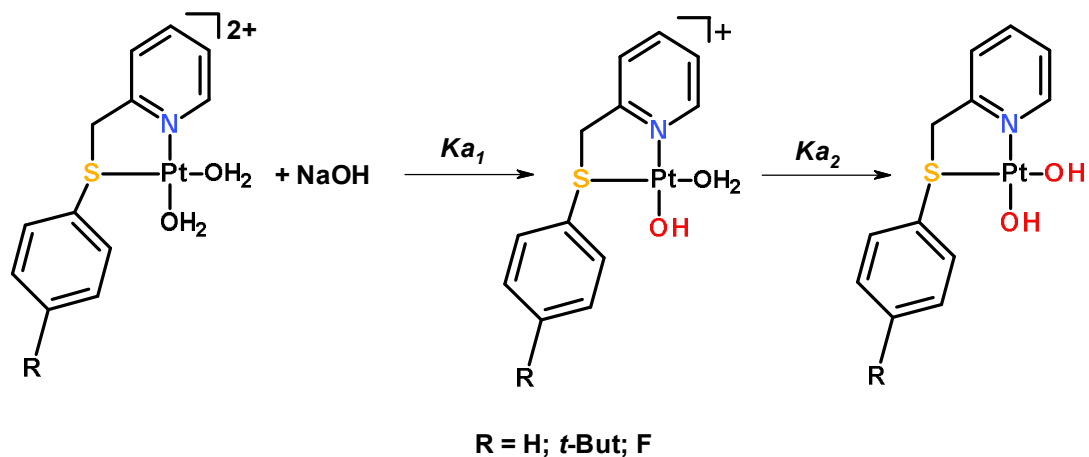
### 4.5.1 p*K*<sub>a</sub> determination of diaqua Pt(II) complexes

Previous studies have shown that high or low thermodynamic p*K*<sub>a</sub> values are an indication of the electrophilicity of the metal ion.<sup>44,45</sup> The neutralisation of the coordinated aqua ligands from the three complexes by NaOH was accompanied by spectral changes in the absorption spectrum of the complex **Pt(pyS<sup>PhF</sup>)** as shown in **Figure 4.2**. The plot of the absorbance at 300 nm *versus* pH was fitted to two sigmoidal (Boltzmann) functions. An inset is given as an example in **Figure 4.2**.

The hardness and  $\pi$ -acidity of the pyridyl nitrogen as compared to the soft and polarisable sulphur of the thioether will contribute differently in the observed p*K*<sub>a</sub> values.<sup>46</sup> A better  $\pi$ -acceptor stabilizes the electro-rich hydroxo species which forms from the coordinated aqua ligands upon neutralization with NaOH. Since pyridine is a strong electron  $\pi$ -acceptor, the first deprotonation should be on the aqua ligand *trans* to this moiety.<sup>25</sup> The p*K*<sub>a1</sub> values for the formation of the aqua/hydroxo complex are: **Pt(pyS<sup>Ph</sup>)** (3.58), **Pt(pyS<sup>Ph(t-But)</sup>)** (3.87), and **Pt(pyS<sup>PhF</sup>)** (3.06). The higher p*K*<sub>a1</sub> values for the complex indicate a reduction in charge from +2 (diaqua) to +1 (aqua/hydroxo).

The second aqua ligand is much weaker than the first due to the strong *trans*-influence of the thioether and thus deprotonates at higher p*K*<sub>a2</sub> values<sup>47</sup> of **Pt(pyS<sup>Ph</sup>)** (5.36), **Pt(pyS<sup>Ph(t-But)</sup>)** (5.60), and **Pt(pyS<sup>PhF</sup>)** (5.05). The observed higher p*K*<sub>a2</sub> values are in accordance

with the reduction of the overall charge of the complexes from +1 (aqua/hydroxo) to 0 (hydroxo/hydroxo) following the deprotonation of the second aqua ligand.<sup>48</sup>



**Scheme 4.2** Sequential deprotonation of the diaqua Pt(II) complexes.

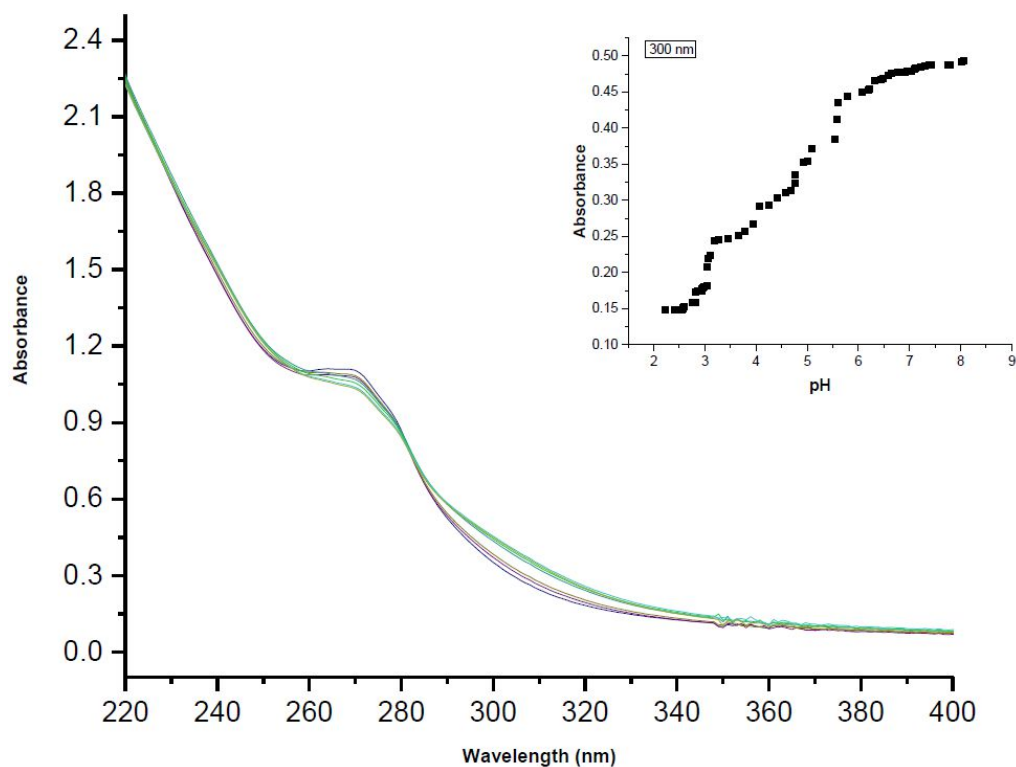


**Figure 4.2** UV-visible spectra for the titration of 0.2 mM **Pt(pyS<sup>PhF</sup>)** with NaOH in the pH range 2-9 at  $T = 298$  K. *Inset: Absorbance versus pH data at 300 nm.*

**Table 4.1** Summary of  $pK_a$  values obtained for the sequential deprotonation of the aqua ligands from the *cis*-Pt(II) complexes.

	<b>Pt(pyS<sup>Ph</sup>)</b>	<b>Pt(pyS<sup>Ph(t-But)</sup>)</b>	<b>Pt(pyS<sup>PhF</sup>)</b>
<b><math>pK_{a1}</math></b>	$3.58 \pm 0.02$	$3.87 \pm 0.04$	$3.06 \pm 0.02$
<b><math>pK_{a2}</math></b>	$5.36 \pm 0.07$	$5.60 \pm 0.06$	$5.05 \pm 0.04$

#### 4.5.2 NMR studies

The substitution reaction of the dichloro complex **Pt(pyS<sup>PhF</sup>)Cl<sub>2</sub>** by the nucleophile thiourea (**tu**) was confirmed by NMR spectroscopy to detect the possible intermediates and final products formed during the substitution process. This data is applicable to the mechanism of substitution reactions for diaqua complexes which were used in this kinetic study. The substitution reaction of **Pt(pyS<sup>PhF</sup>)Cl<sub>2</sub>** and **tu** was first confirmed using <sup>1</sup>H NMR spectroscopy (SI **Figure 4.1**). The solution of **Pt(pyS<sup>PhF</sup>)Cl<sub>2</sub>** dissolved in DMF-d<sub>7</sub> was reacted with two equivalents of **tu** at 303 K.

To further confirm the proposed sequential substitution of the leaving chloro ligands, the reaction of **Pt(pyS<sup>PhF</sup>)Cl<sub>2</sub>** and two equivalents of **tu** was followed using the <sup>195</sup>Pt NMR spectroscopic technique. <sup>195</sup>Pt NMR is a useful tool that can be used to identify and follow the evolution of species formed during a substitution reaction. **Figure 4.3** shows the spectra of the <sup>195</sup>Pt NMR peaks for the reaction of **Pt(pyS<sup>PhF</sup>)Cl<sub>2</sub>** and **tu**. The peak labelled as **a** at -2796 ppm represents the unreacted **Pt(pyS<sup>PhF</sup>)Cl<sub>2</sub>** complex. During the substitution process, new peaks appear at -3414 (**b**) and -3584 ppm (**c**), respectively. These peaks are indicative of the formation of two new species in solution. These peaks are likely to be due to the intermediate products **Pt(κ<sub>1</sub>-SN)tuCl** and **Pt(κ<sub>1</sub>-SN)S<sub>3</sub>** for the substitution of the first and second chloro ligands by **tu**, respectively.

In addition, the <sup>195</sup>Pt NMR data show the ultimate final product with a peak at -3884 ppm (**d**). It is known from literature that the  $\delta(^{195}\text{Pt})$  values within the range -3800 to -4000 ppm corresponds to [PtS<sub>4</sub>] usually formed by a complete decoordination of the chelate ligand by **tu** ligands.<sup>49</sup> Thus, the peak at -3884 ppm is for a species for which the N,S chelate is activated to undergo rapid ring-opening at the pyridyl end as soon as the chloride ligand *trans*

to it is substituted by **tu** to form the PtS<sub>4</sub>, **Pt(κ<sub>1</sub>-S<sup>PhF</sup>py)(tu)<sub>3</sub>**. The same labilising does not affect the thioether end of the ligand due to inertness of the thioether towards substitution.<sup>50</sup> Thus, a pendant κ<sub>1</sub>-**SN** monodentate ligand remains coordinated to the metal centre of **Pt(pyS<sup>PhF</sup>)Cl<sub>2</sub>** during the reaction. This is consistent with what was observed by Bellici *et al.*<sup>51</sup> for the slow ring opening of the S,S 1,2-bis(phenylsulfanyl) chelate.



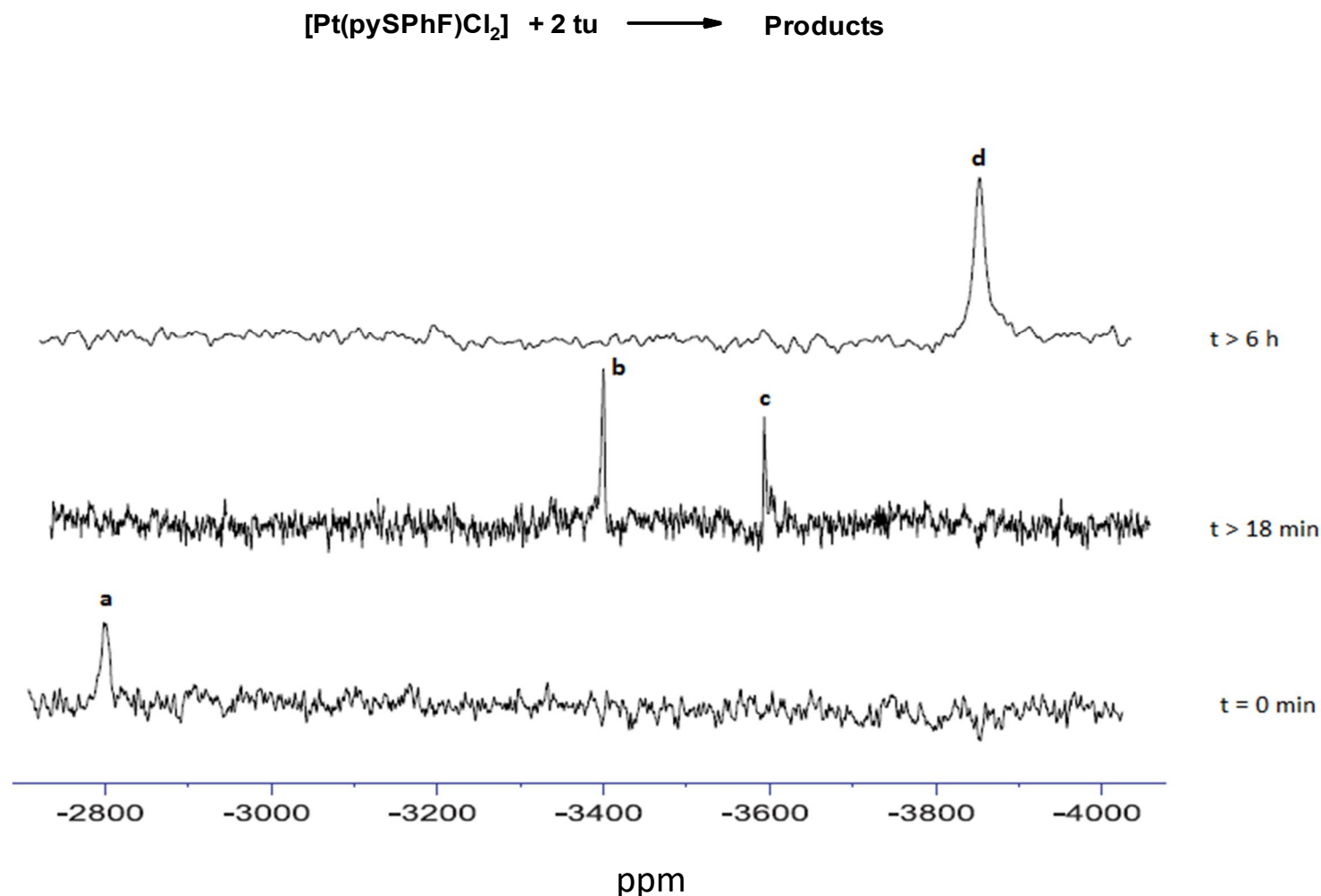


**Figure 4.3**  $^{195}\text{Pt}$  NMR spectra recorded for the reaction of  $\text{Pt}(\text{pyS}^{\text{PhF}})\text{Cl}_2$  and 2 equiv. of **tu**, indicating the unreacted *cis*-Pt(II) complex (**a**,  $\delta = -2796.4$  ppm) before the reaction and the final ring-opened product (**d**,  $\delta = -3884.7$  ppm) corresponding to  $[\text{Pt}(\kappa_1\text{-S}^{\text{PhF}}\text{N})(\text{tu})_3]^{2+}$ . Intermediate products (**b** and **c** at  $\delta = -3414.5$  and  $-3584.9$  ppm) correspond to  $[\text{Pt}(\text{pyS}^{\text{PhF}})(\text{tu})\text{Cl}]^+$  and  $[\text{Pt}(\text{pyS}^{\text{PhF}})(\text{tu})_2]^{2+}$ , respectively.

### 4.5.3 DFT-calculated optimised structures

The DFT-optimised structures of the *cis*-Pt(II) complexes as well as the calculated energy and molecular geometry optimised parameters are shown in **Figure 4.4** and **Table 4.2**, respectively. The ground-state geometry of all the complexes adopts a distorted square-planar arrangement of the coordinated ligands around the Pt atom. For example, **Pt(pyS<sup>Ph</sup>)** the computed Pt-S; Pt-N<sub>py</sub>; Pt-OH<sub>2(1)</sub> and Pt-OH<sub>2(2)</sub> (distances are 2.41; 2.02; 2.12; 2.11 Å and S-Pt OH<sub>2(1)</sub> bond angles are closer to linearity in the range 177.2-177.2° and N<sub>py</sub>-Pt OH<sub>2(2)</sub> in the range 177.1-178.0°, respectively. The deviation from linearity is probably because of the flexible methylene spacer. What is important to note is that going from **Pt(pyS<sup>Ph</sup>)** to **Pt(pyS<sup>Ph(t-but)</sup>)** strikingly, the introduction of the positive  $\sigma$ -inductive electron-donating *tert*-butyl moiety in **Pt(pyS<sup>Ph(t-but)</sup>)** induces a slight shortening of the S-Pt bond by 0.01 Å when compared to **Pt(pyS<sup>Ph</sup>)**.

The mappings of the frontier molecular orbitals in the ground-state indicate that the HOMOs are concentrated directly above and below the Pt(II) ion. The LUMO is concentrated on the pyridyl and thioether moieties of the ligands. This points to an electron-rich metal centre in which electron density can be back-donated toward the ligand framework. The HOMO mappings show significant electron density is also situated on the thioether as well as the phenyl ring for all three complexes which can further contribute to an electron-rich metal centre. The HOMOs are also found on the *tert*-butyl and fluoride substituents of the phenyl ring for the complexes **Pt(pyS<sup>Ph(t-But)</sup>)** and **Pt(pyS<sup>PhF</sup>)**, respectively. There is entirely no contribution from the pyridine ring and the leaving group ligands.

Importantly, the LUMOs for all the complexes are more delocalised onto the metal centre, the thioether and to a lesser extent on the pyridine ring. The phenomenon that the LUMO orbitals are situated to a greater extent on the thioether compared to the  $\pi$ -acceptor pyridine can be explained by the combined  $\sigma$ -donor and  $\pi$ -acceptor nature of the sulphur atom. The sulphur atom has readily accessible empty  $3d \pi^*$ -orbitals which can readily receive electron density from the HOMO orbitals which have significant metal  $d$ -orbital character.<sup>52-54</sup> Pitteri *et al.*<sup>55</sup> showed for an N-S-N tridentate complex that sulphur is not only capable of substituting the *trans* leaving ligand due to its strong  $\sigma$ -*trans*-influence but can also accept electron density from the metal centre to stabilize the 18-electron five-coordinate transition state. Looking at the LUMO maps it seems the pyridine is a weaker  $\pi$ -acceptor of electron

density for the complexes studied. It utilises the  $\pi^*$ -orbitals for back-bonding which may not be as efficient as the  $d\pi^*$  M.O.s of sulphur. This is because the  $d\pi-d\pi^*$  interactions along Pt-S bond are more favourable on energy grounds compared to the  $d\pi-p\pi^*$  along the Pt-N in pulling away electron charge from the metal ion.

The electrophilicity index ( $\omega$ ) which is a measure of the propensity or capacity of a complex to accept electrons<sup>56</sup> points to a more electrophilic Pt(II) metal centre as increasing in the following order: **Pt(pyS<sup>Ph(t-But)</sup>)** (6.48) < **Pt(pyS<sup>Ph</sup>)** (6.68) < **Pt(pyS<sup>PhF</sup>)** (6.84). The observed higher index value of **Pt(pyS<sup>PhF</sup>)** is due to the  $\pi$ -acceptor properties of the thioether induced by the negative  $\sigma$ -inductive electron-withdrawing fluoro substituent, making the Pt(II) metal centre more reactive. The lower index value of **Pt(pyS<sup>Ph(t-But)</sup>)** can be accounted to the positive  $\sigma$ -inductive electron-donating *tert*-butyl substituent which enhances the strong  $\sigma$ -*trans*-influence of the thioether. This leads to a less electrophilic Pt(II) metal centre due to accumulation of electron density. For the complex **Pt(pyS<sup>Ph</sup>)** has a tendency of accumulating electron density onto the metal centre due to a weak  $\sigma$ -donor character of the phenyl ring. Hence, a slightly higher index value is observed for **Pt(pyS<sup>Ph</sup>)** compare to **Pt(pyS<sup>Ph(t-But)</sup>)**.

The NBO charges which represent the individual atomic charge<sup>57</sup> for the complexes give an indication that the electrophilicity of metal atom increases in the following order: **Pt(pyS<sup>Ph(t-But)</sup>)** (0.676) < **Pt(pyS<sup>Ph</sup>)** (0.686) < **Pt(pyS<sup>PhF</sup>)** (0.692). The NBO charges at the Pt(II) centre are sensitive to changes in the electron-donating and electron-withdrawing properties of the *para*-positioned substituents. This is in accordance with the change in the observed trend in electrophilicity indices which measures the degree of electron deficiency in the entire complex<sup>56,57</sup> showing a clear trend of decreasing as the positive  $\sigma$ -inductive electron-donation increases. The lower NBO charge of **Pt(pyS<sup>PhF</sup>)** compared to **Pt(pyS<sup>Ph(t-But)</sup>)** emanates from the accumulation of electron density at the metal centre. The dipole moment values are also a good indicator of the distribution of electrons within the ligand framework of the complexes. An increase in the calculated dipole moment of **Pt(pyS<sup>Ph(t-But)</sup>)** (14.9 D) compared to **Pt(pyS<sup>PhF</sup>)** (13.2 D) and **Pt(pyS<sup>Ph</sup>)** (9.03 D) indicate that the electrons can be donated back onto the ligand backbone and further away from the metal centre.<sup>58,59</sup>

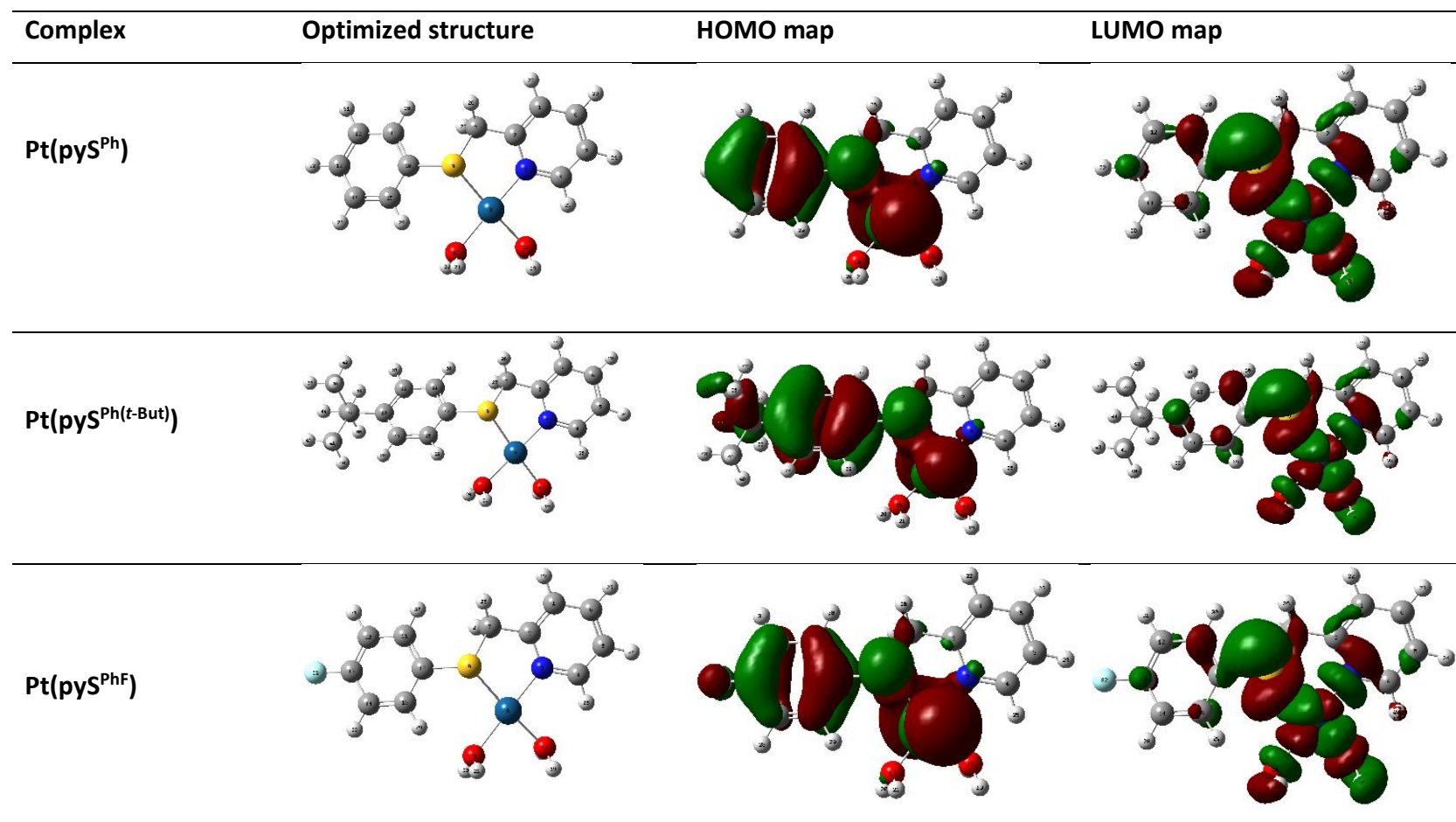
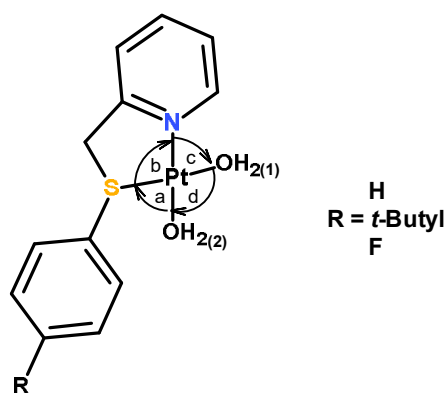


Figure 4.4 Computer-simulated HOMO and LUMO frontier molecular orbitals of Pt(II) complexes.

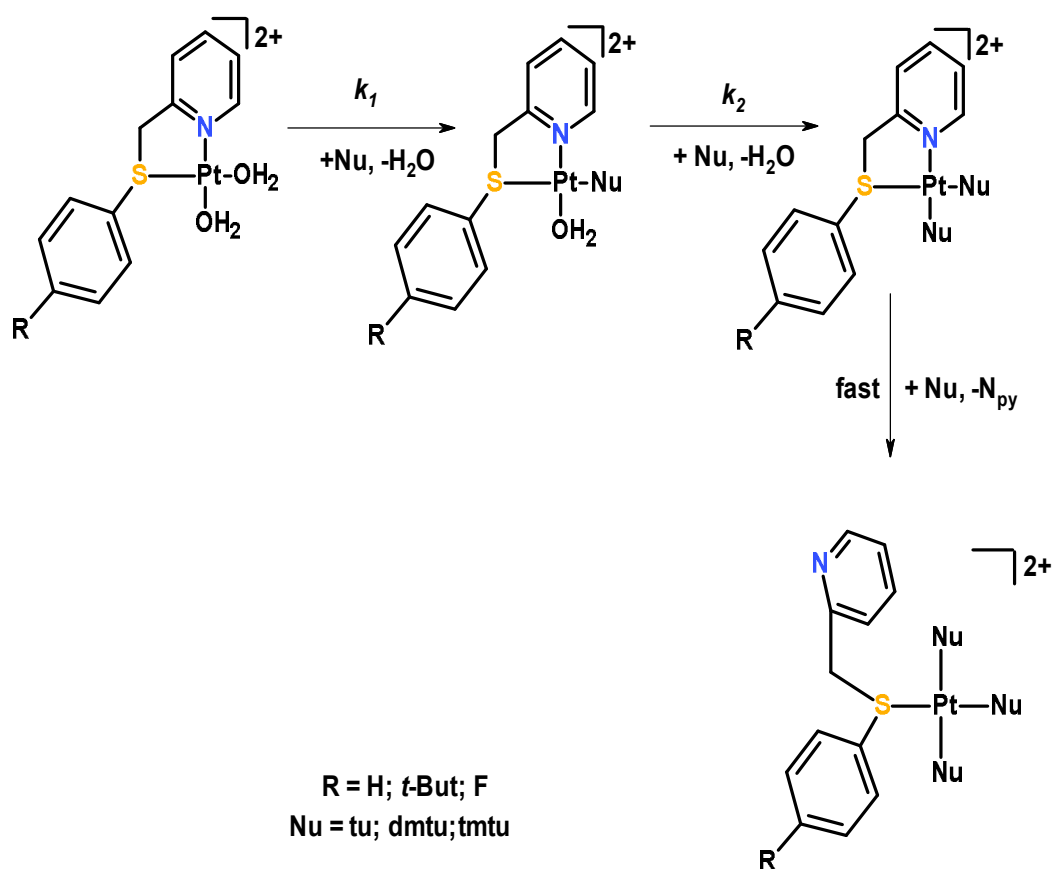
**Table 4.2** Computer simulated data by DFT for *cis*-Pt(II) complexes

Property	Pt(pyS <sup>Ph</sup> )	Pt(pyS <sup>Ph(t-But)</sup> )	Pt(pyS <sup>PhF</sup> )
<b>MO Energy (eV)</b>			
LUMO	-3.18	-3.09	-3.23
HOMO	-7.26	-7.09	7.30
$\Delta E_{L-H}$	4.08	4.00	4.07
<b>NBO Charges</b>			
Pt	0.686	0.676	0.692
Chemical hardness (eV)	2.04	2.00	2.03
Chemical potential (eV)	-5.22	-5.09	-5.27
Electrophilicity index ( $\omega$ )	6.68	6.48	6.84
<b>Bond lengths (Å)</b>			
d Pt-N <sub>py</sub>	2.02	2.02	2.02
d Pt-S	2.41	2.40	2.41
d Pt-OH <sub>2</sub> (1)	2.12	2.12	2.12
d Pt-OH <sub>2</sub> (2)	2.11	2.10	2.11
<b>Bond angle (°)</b>			
<S-Pt-OH <sub>2</sub> (1)	177.2	177.2	176.6
<N <sub>py</sub> -Pt-OH <sub>2</sub> (2)	177.1	178.0	177.9
<b>Dipole moment (D)</b>			
	9.03	14.9	13.2



#### 4.5.4 Kinetic measurements

The summary of the proposed reaction pathway for the substitution reaction of aqua ligands by thiourea nucleophiles (**tu**, **dmtu** and **tmtu**) is shown in **Scheme 4.5**. A typical UV-vis spectrum in **Figure 4.5** shows a preliminary reaction of 0.1 mM **Pt(pyS<sup>Ph</sup>)** with 7 mM **dmtu** for the determination of the wavelengths chosen to monitor the two substitution steps. The first fast substitution step was followed at the wavelength 310 nm and the second slow substitution step at wavelength 290 nm.



**Scheme 4.5** Representation of the sequential aqua ligand substitution of the complexes including a ring-opening step by entering nucleophiles (Nu = **tu**, **dmtu** and **tmtu**).

The initial two steps,  $k_1$  and  $k_2$ , represent the consecutive substitution of the two aqua ligands. Immediately after the first and second substitution of the aqua co-ligands, there is a rapid step corresponding to the ring-opening of the bidentate chelate ligand from the nitrogen end. The stepwise substitution of the two leaving is hypothesised from the unsymmetrical structure of the bidentate ligands coordinated to the Pt(II) complexes. The ligands have a thioether known to have a strong *trans*-labilization effect as well as a  $\pi$ -

withdrawing pyridine ring. Both substitution steps were monitored by the stopped-flow technique.

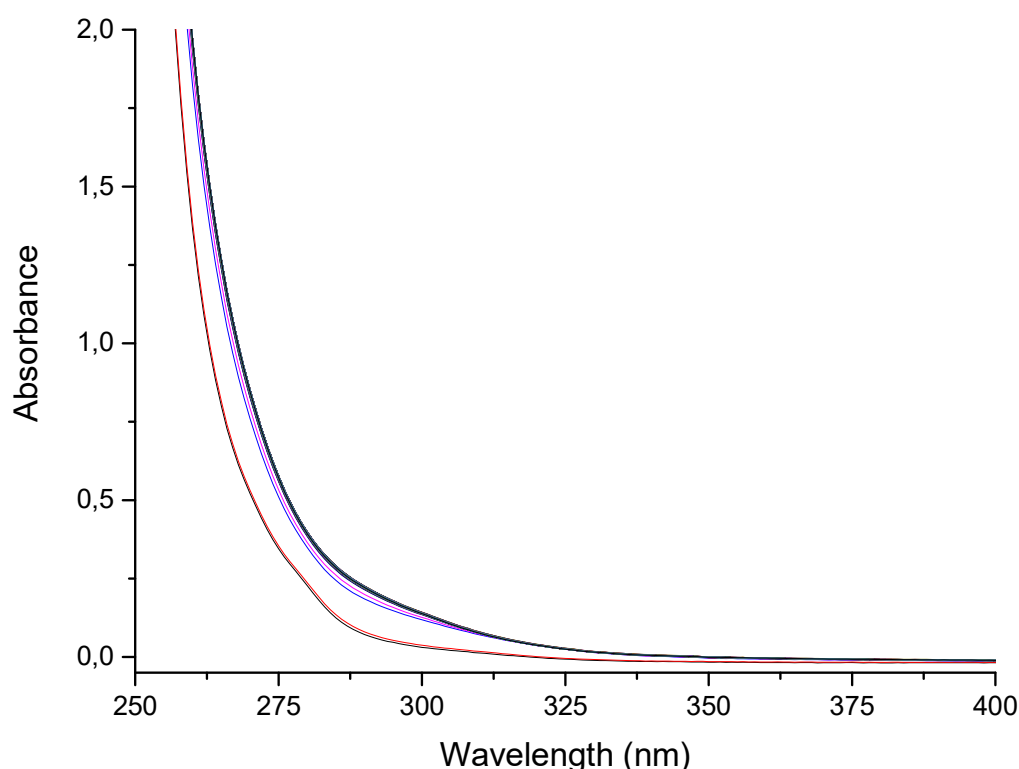


**Figure 4.5** UV-visible spectra recorded for the reaction of 0.1 mM **Pt(pyS<sup>Ph</sup>)** with 7 mM **dmtu** at pH 2 ( $I = 0.1$  M LiOTf/HOTf) and 25 °C.

The kinetic traces fitted well to a single exponential function used to generate the *pseudo*-first order rate constants,  $k_{\text{obs}(1)}$  and  $k_{\text{obs}(2)}$ , at specific nucleophile concentration and temperature, for the first and second substitution steps, respectively. Average  $k_{\text{obs}(1/2)}$  values were calculated from data obtained on 6-8 independent kinetic runs from the stopped-flow analyser. When the observed *pseudo*-first order rate constants,  $k_{\text{obs}(1/2)}$ , were plotted against concentration of the nucleophiles, the second-order rate constants,  $k_1$  and  $k_2$ , which are a measure of the nucleophilic attack on the complex by the nucleophile, were calculated from the slopes of the plots. An exemplary time-resolved kinetic trace for the first substitution step in the two-step reaction between **Pt(pyS<sup>Ph</sup>)** and 20-fold excess of **tu** is shown in **Figure 4.6**.

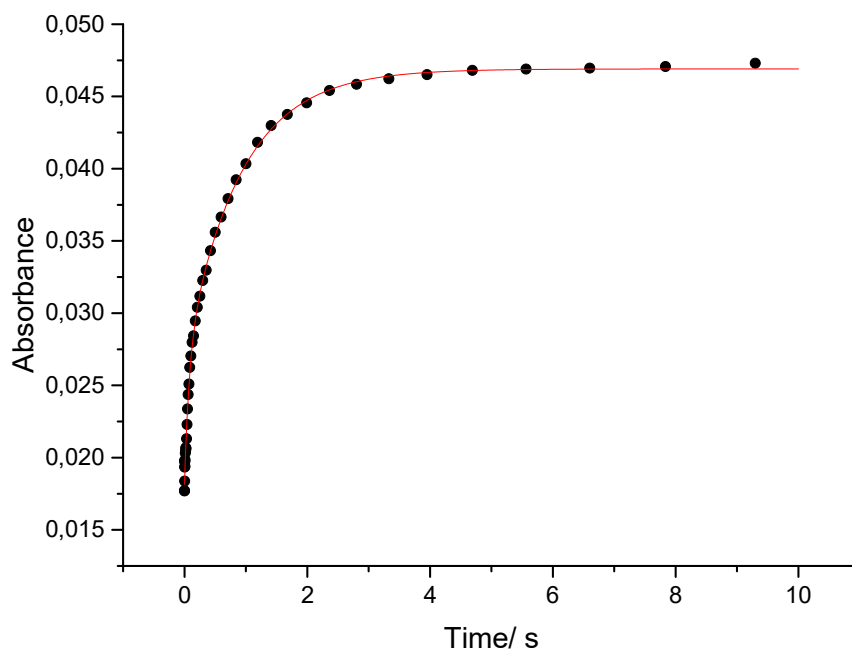


**Figure 4.6** A typical time-resolved kinetic trace for a reaction of 0.1 mM **Pt(pyS<sup>Ph</sup>)** with 2 mM **tu** followed on the stopped-flow at wavelength 321 nm. pH 2 (*I* = 0.1 M LiOTf/HOTf) and 25 °C.

The values of the rate constants ( $k_1$  and  $k_2$ ) are summarised in **Table 4.3**. The substitution of the coordinated aqua ligands by the thiourea nucleophiles followed a mechanism described by equations (4.1 and 4.2).<sup>60, 61</sup>

$$k_{\text{obs}(1)} = k_1[\text{Nu}] + k_{-1} \approx k_1[\text{Nu}] \quad (4.1)$$

$$k_{\text{obs}(2)} = k_2[\text{Nu}] + k_{-2} \approx k_2[\text{Nu}] \quad (4.2)$$

A representative plot of the linear regression passing through the origin is shown in **Figure 4.7**, indicating that the direct nucleophilic pathway for the substitution of the nucleophiles is dominant. The same trend is observed for all the other complexes investigated in this study.



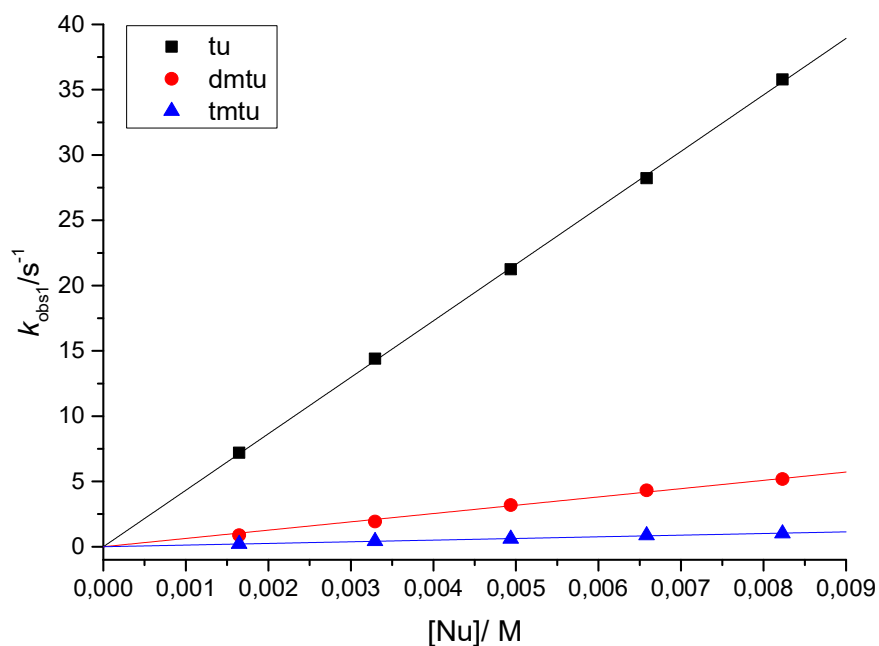


**Figure 4.7** Plots of  $k_{obs1}$  vs  $[Nu]$  for the first substitution step of the reaction of 0.165 mM  $Pt(pyS^{Ph(t-But)})$  at pH 2 ( $I = 0.1$  M LiOTf/HOTf) and 25 °C.

**Table 4.3** Summary of the rate constants for the consecutive substitution steps of the Pt(II) complexes by **tu**, **dmtu** and **tmtu** ( $I = 0.1$  M LiOTf/HOTf).

	Nu	$k_1/M^{-1} s^{-1}$	$k_2/10^{-1} M^{-2} s^{-1}$
<b>Pt(pyS<sup>Ph</sup>)</b>	<b>tu</b>	$303.7 \pm 0.3$	$11.2 \pm 0.8$
	<b>dmtu</b>	$349.7 \pm 6.0$	$4.7 \pm 0.2$
	<b>tmtu</b>	$43.3 \pm 0.60$	$3.4 \pm 0.8$
<b>Pt(pyS<sup>Ph(t-But)</sup>)</b>	<b>tu</b>	$4325.4 \pm 15.7$	$242.6 \pm 11.6$
	<b>dmtu</b>	$635.5 \pm 11.1$	$172.0 \pm 0.5$
	<b>tmtu</b>	$126.7 \pm 2.0$	$65.9 \pm 6.5$
<b>Pt(pyS<sup>PhF</sup>)</b>	<b>tu</b>	$462.8 \pm 1.2$	$3.97 \pm 0.13$
	<b>dmtu</b>	$386.5 \pm 5.5$	$3.76 \pm 0.19$
	<b>tmtu</b>	$61.2 \pm 0.5$	$0.439 \pm 0.015$

#### 4.5.5 Activation parameters

The temperature dependence of the second-order rate constants,  $k_1$  and  $k_2$ , was studied over the temperature range of 15-35 °C at the intervals of 5 °C. A typical Eyring plot is shown for the reaction of **Pt(pyS<sup>Ph(t-But)</sup>)** and thiourea nucleophiles in **Figure 4.8**. The calculated values for  $\Delta H^\ddagger$  and  $\Delta S^\ddagger$  are summarised in **Table 4.4**.

**Table 4.4** Summary of the activation parameters for the consecutive substitution steps of the investigated complexes by **tu**, **dmtu** and **tmtu**, ( $I = 0.1$  M LiOTf/HOTf).

	Nu	$\Delta H^\ddagger_1/\text{kJ mol}^{-1}$	$\Delta S^\ddagger_1/\text{J mol}^{-1}$	$\Delta H^\ddagger_2/\text{kJ mol}^{-1}$	$\Delta S^\ddagger_2/\text{J mol}^{-1}$
<b>Pt(pyS<sup>Ph</sup>)</b>	<b>tu</b>	31 ± 1	-79 ± 4	23 ± 1	-152 ± 5
	<b>dmtu</b>	30 ± 1	-91 ± 3	35 ± 1	-74 ± 3
	<b>tmtu</b>	40 ± 1	-99 ± 2	37 ± 1	-81 ± 4
<b>Pt(pyS<sup>Ph(t-But)</sup>)</b>	<b>tu</b>	28 ± 1	-72 ± 4	36 ± 3	-100 ± 9
	<b>dmtu</b>	45 ± 2	-41 ± 6	47 ± 2	-63 ± 6
	<b>tmtu</b>	36 ± 1	-84 ± 4	17 ± 2	-177 ± 7
<b>Pt(pyS<sup>PhF</sup>)</b>	<b>tu</b>	38 ± 2	-66 ± 7	38 ± 1	-66 ± 5
	<b>dmtu</b>	38 ± 1	-66 ± 5	44 ± 2	-49 ± 7
	<b>tmtu</b>	37 ± 2	-86 ± 7	36 ± 3	-91 ± 10

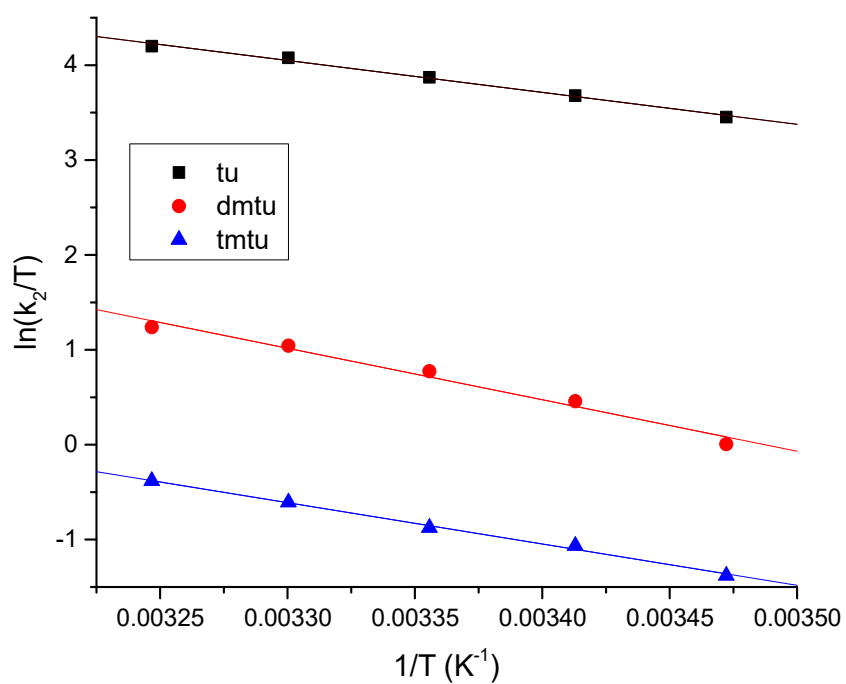


**Figure 4.8** Temperature dependence plots for the reaction of 0.046 mM  $\text{Pt}(\text{pyS}^{\text{Ph}(\text{t-But})})$  with 2.75 mM (Nu = tu, dmtu and tmtu).

#### 4.5.6 Crystal structure of $\text{Pt}(\text{pyS}^{\text{PhF}})\text{Cl}_2$

The crystal structure of  $\text{Pt}(\text{pyS}^{\text{PhF}})\text{Cl}_2$  was shown in **Figure 4.9**.

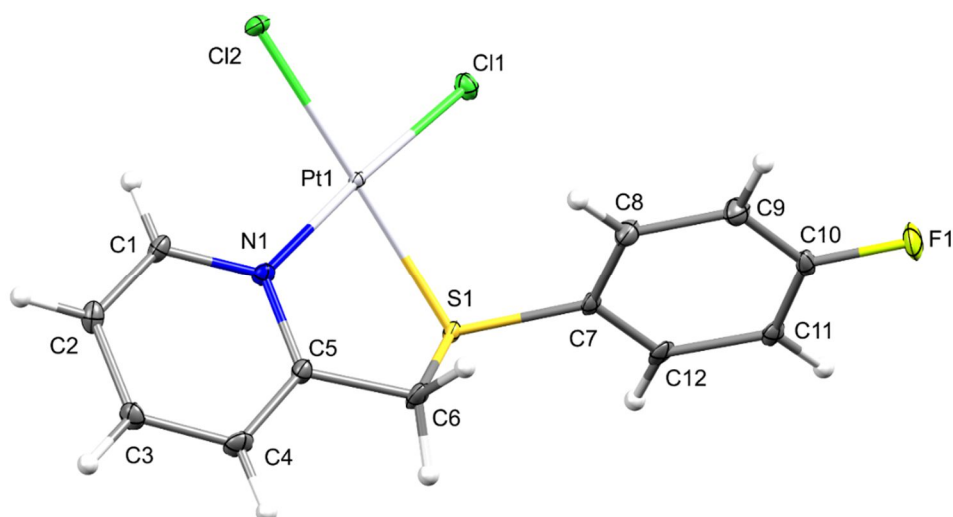


**Figure 4.9:** Thermal ellipsoid diagram (50% probability surfaces) of the molecular structure of  $\text{Pt}(\text{pyS}^{\text{PhF}})\text{Cl}_2$ .

**Figure 4.9** shows that **pyS<sup>PhF</sup>** is coordinated to Pt by N of the pyridyl group and sulphur atom of the thioether. The other two sites are occupied by chlorine atoms coordinated in a *cis* fashion to make up a distorted square-planar geometry. From the data in **Table 4.5** the Cl<sub>(2)</sub>-Pt<sub>(1)</sub> bond length (2.3261 Å) which is *trans* to the thioether is significantly longer than that which is *trans* to the pyridyl nitrogen Cl<sub>(1)</sub>-Pt<sub>(1)</sub> (2.3049). The same discrepancies are also predicted by DFT calculations. This is due to ease of polarisability of the thioether which forms a stronger  $\sigma$ -bond S<sub>(1)</sub>-Pt<sub>(1)</sub> to the Pt atom. This weakens the Pt-Cl/OH<sub>2</sub> bond *trans* to it since both the S and Cl/OH<sub>2</sub> use the same *p*-orbital on the Pt. the strong *trans* influence labilises (elongates the Pt-Cl bond) the Cl ligand *trans* to it. Thus, the substitution of the aqua ligands occurs at distinct rates and thus the process is consecutive, as already proposed. The phenyl ring lies out of plane of the complex (with dihedral angle 78.57 °) and is closer to the Cl atom *trans* to pyridine. This has potential to block the approach of the nucleophile on one side. Thus, the Cl/OH<sub>2</sub> ligand will be substituted even more slowly when compared to the one *trans* to the thioether. The data of the crystal structure is summarised in **Table 4.5**. The metrics (bond lengths and angles) is summarised in **Table 4.6**.

**Table 4.5** Comparison of the experimental and theoretical bond lengths (Å) and bond angles (°) for **Pt(pyS<sup>PhF</sup>)Cl<sub>2</sub>**.

<b>Bond lengths (Å)</b>			
X-ray		DFT	
N <sub>(1)</sub> -Pt <sub>(1)</sub>	2.027 (3)	d Pt-N <sub>py</sub>	2.02
S <sub>(1)</sub> -Pt <sub>(1)</sub>	2.2451 (10)	d Pt-S	2.41
Cl <sub>(1)</sub> -Pt <sub>(1)</sub>	2.3049 (13)	d Pt-OH <sub>2</sub> (1)	2.11
Cl <sub>(2)</sub> -Pt <sub>(1)</sub>	2.3261 (10)	d Pt-OH <sub>2</sub> (2)	2.12
<b>Bond angles (°)</b>			
N <sub>(1)</sub> -Pt <sub>(1)</sub> -Cl <sub>(1)</sub>	175.42(8)	< N <sub>py</sub> -Pt-OH <sub>2</sub> (1)	177.9
S <sub>(1)</sub> -Pt <sub>(1)</sub> -Cl <sub>(2)</sub>	177.68(3)	< S-Pt-OH <sub>2</sub> (2)	176.6

**Table 4.6** Crystal data and structure refinement for **Pt(pyS<sup>PHF</sup>)Cl<sub>2</sub>**.

<b>Parameter</b>	
Empirical formula	C <sub>12</sub> H <sub>10</sub> C <sub>12</sub> FNPtS
Formula weight	485.26
Temperature	100(2) K
Wavelength	0.71073 Å
Crystal system	Monoclinic
Space group	P 21/c
Unit cell dimensions	a = 10.136(5) Å      α = 90° b = 9.345 (4) Å      β = 100.366(5)° c = 14.305(6) Å      γ = 90°
Volume	1332.9(10) Å <sup>3</sup>
Z	4
Density (calculated)	2.418 mg/m <sup>3</sup>
Absorption coefficient	11.075 mm <sup>-1</sup>
F (000)	904
Crystal size	0.220 x 0.190 x 0.140 mm <sup>3</sup>
Theta range for data collection	2.043 to 28.343°
Reflections collected	23313
Independent reflections	3314 [R(int) = 0.0359]
Completeness to theta = 25.242°	99.9 %
Absorption correction	Semi-empirical from equivalents
Max. and min. transmission	0.318 and 0.183
Refinement method	Full-matrix least-squares of F <sup>2</sup>
Data/ restraints/ parameters	3314 / 0 / 163
Goodness-of-fit on F <sup>2</sup>	1.157
Final R indices [I > 2sigma(I)]	R1 = 0.0208, wR2 = 0.0480
R indices (all data)	R1 = 0.0216, wR2 = 0.0483
Largest diff. peak and hole	0.976 and -1.834 e Å <sup>-3</sup>

## 4.6 Discussion

In this study, three square-planar *cis*-Pt(II) complexes comprising 2-(phenylthiomethyl)pyridine chelates with different substituents (**Figure 4.1**) were synthesised, characterized and the substitution reactions of the aqua co-ligands were studied using bio-relevant sulphur-containing thiourea nucleophiles. The non-leaving ligand differs in the substituents on the phenyl ring of the thioether and this may affect the substitution behaviour of the complexes. The unsymmetrical nature of the complexes due to the  $\sigma$ -donor thioether and the  $\pi$ -acceptor pyridine moieties, will affect the lability of the aqua ligands differently leading to a consecutive substitution process. The phenyl ring on the non-leaving ligands bears substituents of different electronic properties on the *para*-position.

In comparing the rate of substitution of the first aqua ligand,  $k_1$ , data in **Table 4.3** shows that the reactivity of *cis*-Pt(II) complexes follows the trend **Pt(pyS<sup>Ph(t-But)</sup>)** > **Pt(pyS<sup>PhF</sup>)** > **Pt(pyS<sup>Ph</sup>)**. If the reactivity of **Pt(pyS<sup>Ph(t-But)</sup>)** with **tu** is taken as a reference, the ratio of reactivity is 12: 1.3: 1, respectively for **Pt(pyS<sup>Ph(t-But)</sup>)**: **Pt(pyS<sup>PhF</sup>)**: **Pt(pyS<sup>Ph</sup>)**. The first substitution occurs at the aqua ligand *trans* to the thioether for all the complexes. This is in accordance with the acquired *pKa* values in **Table 4.1**. The difference in the reactivity between the complexes can be accounted for in terms of the nature of the *para*-substituents on the periphery of the phenyl ring. The results in **Table 4.3** indicate that the positive  $\sigma$ -inductive effect of the *tert*-butyl (-C(CH<sub>3</sub>)<sub>3</sub>) substituent at the *para*-position of the phenyl group increases electron density which is in turn donated onto the thioether. This increases the strength of the strong *trans*-directing ability *via* the ground-state  $\sigma$ -*trans*-influence. Consequently, electron density from the thioether is donated onto the empty 6*p* orbitals of the Pt atom. This leads to the ground state stabilization of the S-Pt bond whilst the Pt-O bond *trans* to itself is labilized and substituted more rapidly by the oncoming thiourea nucleophiles compared to **Pt(pyS<sup>Ph</sup>)**. An unsubstituted phenyl ring is a net  $\sigma$ -donor of electron density but weaker compared to the *tert*-butyl in **Pt(pyS<sup>Ph(t-But)</sup>)**, hence, the slower reactivity of **Pt(pyS<sup>Ph</sup>)**.<sup>62,63</sup>

The negative  $\sigma$ -inductive effect of the *para*-positioned fluoride substituent in **Pt(pyS<sup>PhF</sup>)** deactivates the ring, making it electron deficient. This process activates the  $\pi$ -acceptor capacity of the thioether which pulls away electron charge on the Pt metal ion

making it more electrophilic. Thus, the approach of the entering thiourea nucleophiles to stabilize the transition state is made easier in **Pt(pyS<sup>PhF</sup>)** compared to **Pt(pyS<sup>Ph</sup>)**. Hence, the rate of associative substitution of the aqua ligands is greater for **Pt(pyS<sup>PhF</sup>)** compared to **Pt(pyS<sup>Ph</sup>)**. The reactivity difference between **Pt(pyS<sup>Ph(t-But)</sup>)** and **Pt(pyS<sup>PhF</sup>)** is an indication that the strong *trans*-directing ability *via* the ground-state  $\sigma$ -*trans*-influence of the thioether is greater than its capacity to pull away electron charge *via*  $\pi$ -back bonding in labilizing the aqua ligand *trans* to this moiety.

Density Functional Theory (DFT) calculations were conducted to help support the observed kinetic trends in the reactivity of the complexes (**Table 4.2**). The observed trend can be explained by the fact that the thioether has the capacity to receive electron density from the metal centre *via*  $\pi$ -back bonding. The sulphur atom has synchronous  $\sigma$ -donor/ $\pi$ -acceptor properties and these are based on the substituents on the *para*-position of the phenyl ring. The coordinated thioether has energetically accessible and vacant 3*d*-orbitals which are capable of accepting electron density from the 5*d*-orbitals of the metal centre.<sup>64</sup> Since **Pt(pyS<sup>Ph(t-But)</sup>)** has a greater tendency to donate electron charge onto the metal centre, the capacity for  $\pi$ -back bonding of sulphur (S←Pt) is likewise greater. This then makes the Pt(II) centre more electrophilic and sensitive to the approach of negative charge from the thiourea ligands which stabilizes the 18 electron five-coordinate transition state. The  $\pi$ -back bonding capacity of the thioether in these set of complexes is confirmed by the distribution of electron density in the frontier molecular orbitals (**Figure 4.3**). The ground state LUMO is localized on the thioether specifically on the S-Pt-O axis and to a lesser extent on the pyridine moiety. The same reasoning was used to explain the superior reactivity of a Pt(N-S-N)Cl complex [Pt(bis(2-pyridylmethyl)sulfide)OH<sub>2</sub>](ClO<sub>4</sub>)<sub>2</sub> (**Ptdps**) compared to its N,N,N analogue [Pt(bis(2-pyridylmethyl)amine)OH<sub>2</sub>](ClO<sub>4</sub>)<sub>2</sub> (**Ptdpa**) analogue. The central S-atom of the former complex accepts electron density from the metal *d*-orbitals thereby increasing the electrophilicity of the Pt and the rate of substituting the leaving group.

The slower rate of substitution of the second aqua ligand occurs *trans* to the pyridine moiety. The rate constant, *k*<sub>2</sub>, for the substitution of the second aqua ligand when **tu** is considered decreases in the ratio: 61: 2.8: 1, for **Pt(pyS<sup>Ph(t-But)</sup>)** : **Pt(pyS<sup>Ph</sup>)** : **Pt(pyS<sup>PhF</sup>)**, respectively. The reactivity of the complexes for the second substitution step follows the trend: **Pt(pyS<sup>Ph(t-But)</sup>)** > **Pt(pyS<sup>Ph</sup>)** > **Pt(pyS<sup>PhF</sup>)**. This is consistent with the fact that the

coordination of the first aqua ligand imparts a steric hindrance to the approach of the subsequent entering ligand. Therefore, substitution at the square plane is shielded especially from the approach of these nucleophiles towards the Pt metal centre and the formation of a new bond is thereby made difficult. The shielding by the coordinated **tu** is less, hence, it reacts faster than the other nucleophiles. However, due to the  $\pi$ -acceptor properties of pyridine it is still expected that electron density would be back-donated from the filled *d*-orbitals of the metal centre onto the empty or antibonding orbitals of the pyridine. This would make the metal ion more electropositive. Thus, the approach of the entering ligand would help stabilize the 18-electron five-coordinate transition state.

On coordination, the thiourea nucleophiles labilise the pyridine ligand leading to its immediate substituting by a third thiourea ligand. This step is fast and independent of the concentration of the nucleophiles. This forms the ultimate product **Pt(tu)<sub>3</sub>( $\kappa$ -S<sup>PhR</sup>)**. <sup>195</sup>Pt NMR spectra (**Figure 4.3**) confirms the formation of a pendant  $\kappa$ -SN due to the decoordination of the pyridyl moiety by a peak at -3884 ppm which corresponds to PtS<sub>4</sub>.

#### 4.7 Conclusions

The values of the second-order rate constants,  $k_1$  and  $k_2$ , for the consecutive substitution of the aqua ligands in the *cis*-Pt(II) complexes were sensitive to the nature of substituents on the *para*-position of the thiophenyl. The *trans*-labilizing effect of sulphur was activated or enhanced by the positive  $\sigma$ -inductive donation of density into the phenyl moiety such as *tert*-butyl in the case of **Pt(pyS<sup>Ph(t-But)</sup>)** and the unsubstituted weaker net  $\sigma$ -donor phenyl in **Pt(pyS<sup>Ph</sup>)**. This leads to an increase in the rate of substitution for **Pt(pyS<sup>Ph(t-But)</sup>)** compared to **Pt(pyS<sup>Ph</sup>)**. However, the  $\pi$ -acceptor property of the S-atom (thioether) through its  $\pi^*$  orbitals ensured that the negative  $\sigma$ -inductive effects of substituents such as fluoride (in the case of **Pt(pyS<sup>PhF</sup>)**) increased the electrophilicity of the Pt relative to that of **Pt(pyS<sup>Ph</sup>)**. The low and positive  $\Delta H^\ddagger$  values and the high and negative  $\Delta S^\ddagger$  values confirmed an associative mode of substitution. This study has demonstrated that the reactivity of square-planar *cis*-Pt(II) complexes can be modified through altering the electronic properties of the substituents on the bidentate N,S non-leaving ligand.



## 4.8 References

1. B. Rosenberg and L. Vancamp, *Nature*, 1969, **222**, 385-386.
2. T. C. Johnstone, K. Suntharalingam and S. J. Lippard, *Chemical Reviews*, 2016, **116**, 3436-3486.
3. J. Reedijk, *Chemical Communications*, 1996, 801-806.
4. E. R. Jamieson and S. J. Lippard, *Chemical Reviews*, 1999, **99**, 2467-2498.
5. C. X. Zhang and S. J. Lippard, *Current Opinion in Chemical Biology*, 2003, **7**, 481-489.
6. M. Galanski, M. A. Jakupec and B. K. Keppler, *Current Medicinal Chemistry*, 2005, **12**, 2075-2094.
7. M. Georgi, B. Adriana and K. Margarita, *Current Medicinal Chemistry*, 2005, **12**, 2177-2191.
8. K. R. Harrap, *Cancer Treatment Reviews*, 1985, **12**, 21-33.
9. L. Kelland, *Nat Rev Cancer*, 2007, **7**, 573-584.
10. J. Pracharova, T. Saltarella, T. Radosova Muchova, S. Scintilla, V. Novohradsky, O. Novakova, F. P. Intini, C. Pacifico, G. Natile, P. Ilik, V. Brabec and J. Kasparkova, *Journal of Medicinal Chemistry*, 2015, **58**, 847-859.
11. T. V. Segapelo, I. A. Guzei, L. C. Spencer, W. E. V. Zyl and J. Darkwa, *Inorganica Chimica Acta*, 2009, **362**, 3314-3324.
12. A. Samanta, G. K. Ghosh, I. Mitra, S. Mukherjee, J. C. Bose, S. Mukhopadhyay, W. Linert and S. C. Moi, *RSC Adv.*, 2014, **4**, 43516-43524.
13. B. Desoize and C. Madoulet, *Critical Reviews in Oncology/Hematology*, 2002, **42**, 317-325.
14. M. Fanelli, M. Formica, V. Fusi, L. Giorgi, M. Micheloni and P. Paoli, *Coordination Chemistry Reviews*, 2016, **310**, 41-79.
15. M. R. Shehata, M. M. Shoukry, M. A. Mabrouk and R. Van Eldik, *Journal of Coordination Chemistry*, 2016, **69**, 522-540.
16. N. Shahabadi, S. Kashanian and A. Fatahi, *Bioinorganic Chemistry and Applications*, 2011, **2011**, 687571.
17. S. Grabner, B. Modec, N. Bukovec, P. Bukovec, M. Čemažar, S. Kranjc, G. Serša and J. Sčančar, *Journal of Inorganic Biochemistry*, 2016, **161**, 40-51.

18. G. Berger, L. Fusaro, M. Luhmer, J. Czapla-Masztafiak, E. Lipiec, J. Szlachetko, Y. Kayser, D. L. A. Fernandes, J. Sa, F. Dufrasne and S. Bombard, *Journal of Biological Inorganic Chemistry*, 2015, **20**, 841-853.
19. M. N. Noolvi, H. M. Patel and M. Kaur, *European Journal of Medicinal Chemistry*, 2012, **54**, 447-462.
20. J. Reedijk, *Proceedings of the National Academy of Sciences*, 2003, **100**, 3611-3616.
21. J. Reedijk, *Platinum Metals Review*, 2008, **52**, 2-11.
22. S. Hochreuther, R. Puchta and R. van Eldik, *Inorganic Chemistry*, 2011, **50**, 8984-8996.
23. S. Hochreuther, R. Puchta and R. van Eldik, *Inorganic Chemistry*, 2011, **50**, 12747-12761.
24. Ž. D. Bugarčić, J. Bogojeski, B. Petrović, S. Hochreuther and R. van Eldik, *Dalton Transactions*, 2012, **41**, 12329-12345.
25. S. Hochreuther, S. T. Nandibewoor, R. Puchta and R. van Eldik, *Dalton Transactions*, 2012, **41**, 512-522.
26. B. B. Khusi, A. Mambanda and D. Jaganyi, *Transition Metal Chemistry*, 2016, **41**, 191-203.
27. S. Ray, P. Karmakar, A. Chattopadhyay, D. Nandi, R. Sarkar and A. K. Ghosh, *International Journal of Chemical Kinetics*, 2016, **48**, 347-357.
28. U. Fekl and R. van Eldik, *European Journal of Inorganic Chemistry*, 1998, **1998**, 389-396.
29. N. Summa, W. Schiessl, R. Puchta, N. van Eikema Hommes and R. van Eldik, *Inorganic Chemistry*, 2006, **45**, 2948-2959.
30. P. K. Ghosh, S. Saha and A. Mahapatra, *Chemistry Central Journal*, 2007, **1**, 23-23.
31. D. Gibson, *Dalton Transactions*, 2009, DOI: 10.1039/B918871C, 10681-10689.
32. Ž. D. Bugarčić, J. Bogojeski and R. van Eldik, *Coordination Chemistry Reviews*, 2015, **292**, 91-106.
33. M. R. Malachowski, M. Adams, N. Elia, A. L. Rheingold and R. S. Kelly, *Journal of the Chemical Society, Dalton Transactions*, 1999, DOI: 10.1039/A900223E, 2177-2182.
34. M. R. Malachowski, M. E. Adams, D. Murray, R. White, N. Elia, A. L. Rheingold, L. N. Zakharov and R. S. Kelly, *Inorganica Chimica Acta*, 2009, **362**, 1247-1252.

35. M. J. Rauterkus, S. Fakih, C. Mock, I. Puscasu and B. Krebs, *Inorganica Chimica Acta*, 2003, **350**, 355-365.
36. Ž. D. Bugarčić, B. V. Petrović and R. Jelić, *Transition Metal Chemistry*, 2001, **26**, 668-671.
37. v. B. Origin 7.5TM SRO, Origin Lab Corporation, Northampton, One, Northampton, MA, 01060, USA, 2003.
38. A. D. Becke, *The Journal of Chemical Physics*, 1993, **98**, 5648-5652.
39. C. Lee, W. Yang and R. G. Parr, *Physical review B*, 1988, **37**, 785.
40. P. J. Hay and W. R. Wadt, *The Journal of Chemical Physics*, 1985, **82**, 299-310.
41. R. A. I. Gaussian 09, M. J. Frisch, G. W. Trucks, H. B. Schlegel, G. E. Scuseria, M. A. Robb, J. R. Cheeseman, G. Scalmani, V. Barone, B. Mennucci, G. A. Petersson, H. Nakatsuji, M. Caricato, X. Li, H. P. Hratchian, A. F. Izmaylov, J. Bloino, G. zheng, J. L. Sonnenberg, M. Ehara, K. Toyota, R. Fukuda, J. Hasegawa, M. Ishida, T. Nakajima, Y. Honda, O. Kitao, H. Nakai, T. Vreven, J. A. Montgomery, Jr., J. E. Peralta, F. Ogliaro, M. Bearpark, J. J. Heyd, E. Brothers, K. N. Kudin, V. N. Staroverov, R. Kobayashi, J. Normand, K. Raghavachari, A. Rendell, J. C. Burant, S. S. Iyengar, J. Tomasi, M. Cossi, N. Rega, J. M. Millam, M. Klene, J. E. Knox, J. B. Cross, V. Bakken, C. Adamo, J. Jaramillo, R. Gomperts, R. E. Stratmann, O. Yazyjev, A. J. Austin, R. Cammi, C. Pomelli, J. W. Ochterski, R. L. Martin, K. Morokuma, V. G. Zakrzewski, G. A. Voth, P. Salvador, J. J. Dannenberg, S. Dapprich, A. D. Daniels, O. Farkas, J. B. Foresman, J. V. Ortiz, J. Cioslowski and D. J. Fox, Gaussian, Inc., Wallingford CT, 2009.
42. S. a. S. B. A. I. Bruker APEX2, 2010, Madison, Wisconsin, USA.
43. G. Sheldrick, *Acta Crystallographica Section A*, 2008, **64**, 112-122.
44. D. Jaganyi, F. Tiba, O. Q. Munro, B. Petrović and Ž. D. Bugarčić, *Dalton Transactions*, 2006, DOI: 10.1039/B602950G, 2943-2949.
45. A. Mambanda and D. Jaganyi, *Dalton Transactions*, 2012, **41**, 908-920.
46. A. Mambanda and D. Jaganyi, *Dalton Transactions*, 2011, **40**, 79-91.
47. Z. D. Bugarčić, T. Soldatovic, R. Jelic, B. Alguero and A. Grandas, *Dalton Transactions*, 2004, 3869-3877.
48. H. Erturk, A. Hofmann, R. Puchta and R. van Eldik, *Dalton Transactions*, 2007, DOI: 10.1039/B700770C, 2295-2301.

49. J. R. L. Priqueler, I. S. Butler and F. D. Rochon, *Applied Spectroscopy Reviews*, 2006, **41**, 185-226.
50. K. Lemma, S. K. C. Elmroth and L. I. Elding, *Journal of the Chemical Society, Dalton Transactions*, 2002, 1281-1286.
51. M. Bellicini, L. Cattalini, G. Marangoni and B. Pitteri, *Journal of the Chemical Society, Dalton Transactions*, 1994, DOI: 10.1039/DT9940001805, 1805-1811.
52. J. C. Bailar and A. F. Trotman-Dickenson, *Comprehensive inorganic chemistry*, Pergamon Press; distributed by Compendium Publishers [Elmsford, N.Y.], [Oxford, 1973.
53. F. Basolo and R. G. Pearson, *Mechanisms of inorganic reactions: a study of metal complexes in solution*, Wiley, 1967, 351-404.
54. M. L. Tobe and J. Burgess, *Inorganic reaction mechanisms*, Longman, Harlow, Essex, England; New York, 1999, 30-43, 70-112.
55. B. Pitteri, G. Marangoni and L. Cattalini, *Polyhedron*, 1995, **14**, 2331-2338.
56. C. A. Mebi, *Journal of Chemical Sciences*, 2011, **123**, 727-731.
57. I. M. Wekesa and D. Jaganyi, *Dalton Transactions*, 2014, **43**, 2549-2558.
58. D. P. Rillema, A. J. Cruz, C. Moore, K. Siam, A. Jehan, D. Base, T. Nguyen and W. Huang, *Inorganic Chemistry*, 2013, **52**, 596-607.
59. M. Das and S. E. Livingstone, *Journal of the Chemical Society, Dalton Transactions*, 1975, DOI: 10.1039/DT9750000452, 452-455.
60. R. B. Jordan, *Reaction mechanisms of inorganic and organometallic systems*, Oxford University Press, New York, 1991, 29-40.
61. S. Asperger, *Chemical kinetics and inorganic reaction mechanisms*, Kluwer Academic/Plenum Publishers, New York, 2003, 34-40, 105-106.
62. D. Jaganyi, D. Reddy, J. A. Gertenbach, A. Hofmann and R. van Eldik, *Dalton Transactions*, 2004, DOI: 10.1039/B311595J, 299-304.
63. D. Jaganyi, K.-L. D. Boer, J. Gertenbach and J. Perils, *International Journal of Chemical Kinetics*, 2008, **40**, 808-818.
64. F. A. Cotton and G. Wilkinson, *Advanced inorganic chemistry*, Wiley, New York, 1988.

## 4.9 Supplementary Information

**Table SI 4.1** Selected wavelengths for the **first** substitution reactions of all three nucleophiles at pH 2.

Complex	Nu	Wavelength (nm)
<b>Pt(pyS<sup>Ph</sup>)</b>	tu	321
	dmtu	310
	tmtu	351
<b>Pt(pyS<sup>Ph(t-But)</sup>)</b>	tu	280
	dmtu	280
	tmtu	335
<b>Pt(pyS<sup>PhF</sup>)</b>	tu	310
	dmtu	310
	tmtu	310

**Table SI 4.2** Selected wavelengths for the **second** substitution reactions of all three nucleophiles at pH 2.

Complex	Nu	Wavelength (nm)
<b>Pt(pyS<sup>Ph</sup>)</b>	tu	290
	dmtu	290
	tmtu	320
<b>Pt(pyS<sup>Ph(t-Butyl)</sup>)</b>	tu	268
	dmtu	268
	tmtu	325
<b>Pt(pyS<sup>PhF</sup>)</b>	tu	290
	dmtu	290
	tmtu	320

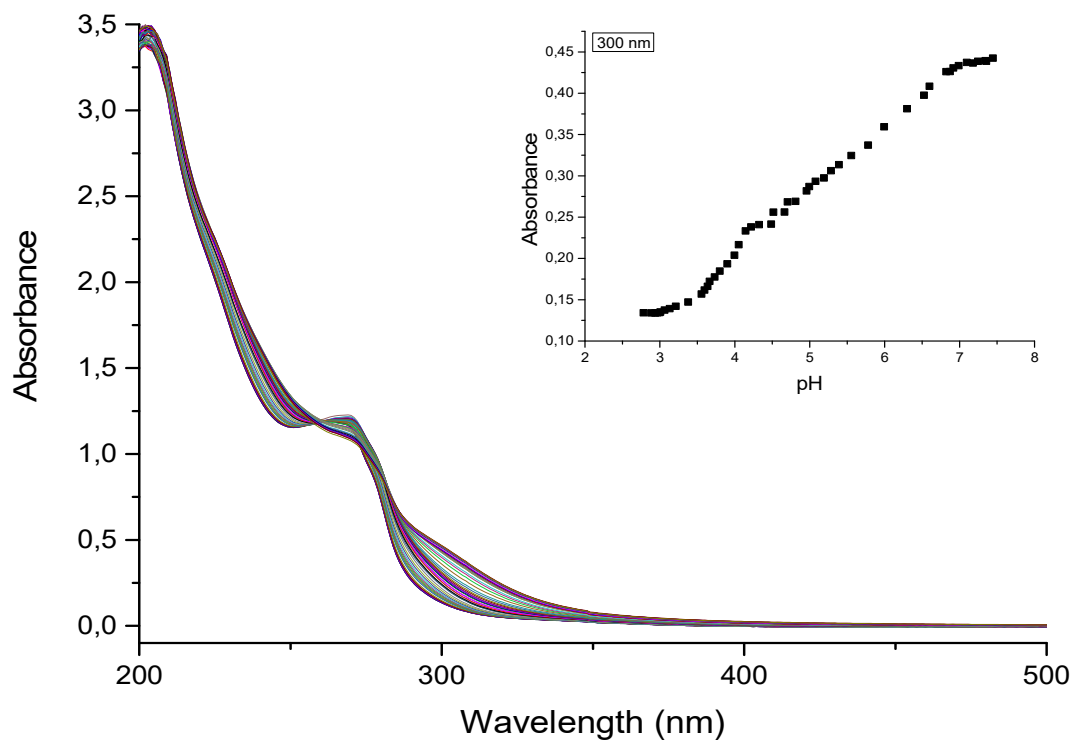


**Figure SI 4.1** UV-visible spectra for the titration of 0.22 mM **Pt(pyS<sup>Ph</sup>)** with NaOH in the pH range 2-8 at  $T = 298$  K. *Inset:* Absorbance versus pH data at 300 nm.

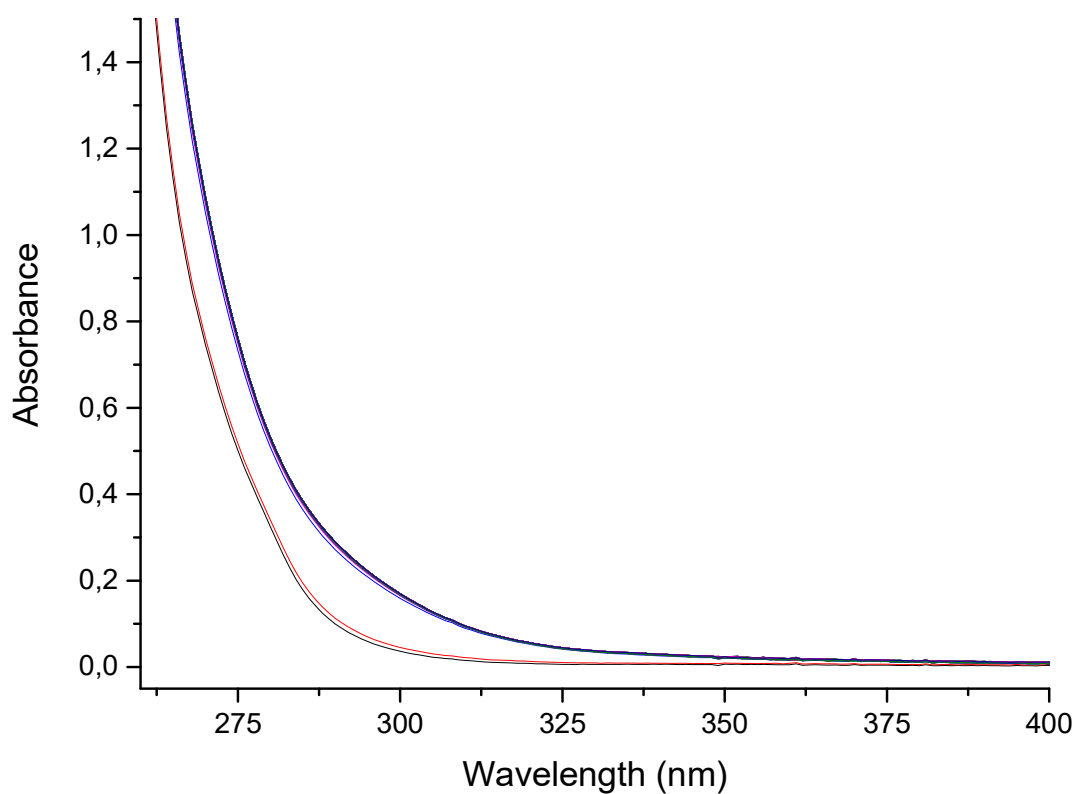


**Figure SI 4.2** UV-visible spectra recorded for the reaction of 0.115 mM **Pt(pyS<sup>Ph</sup>)** with 6.9 mM **tu** at pH 2 ( $I = 0.1$  M LiOTf/HOTf) and 25 °C.

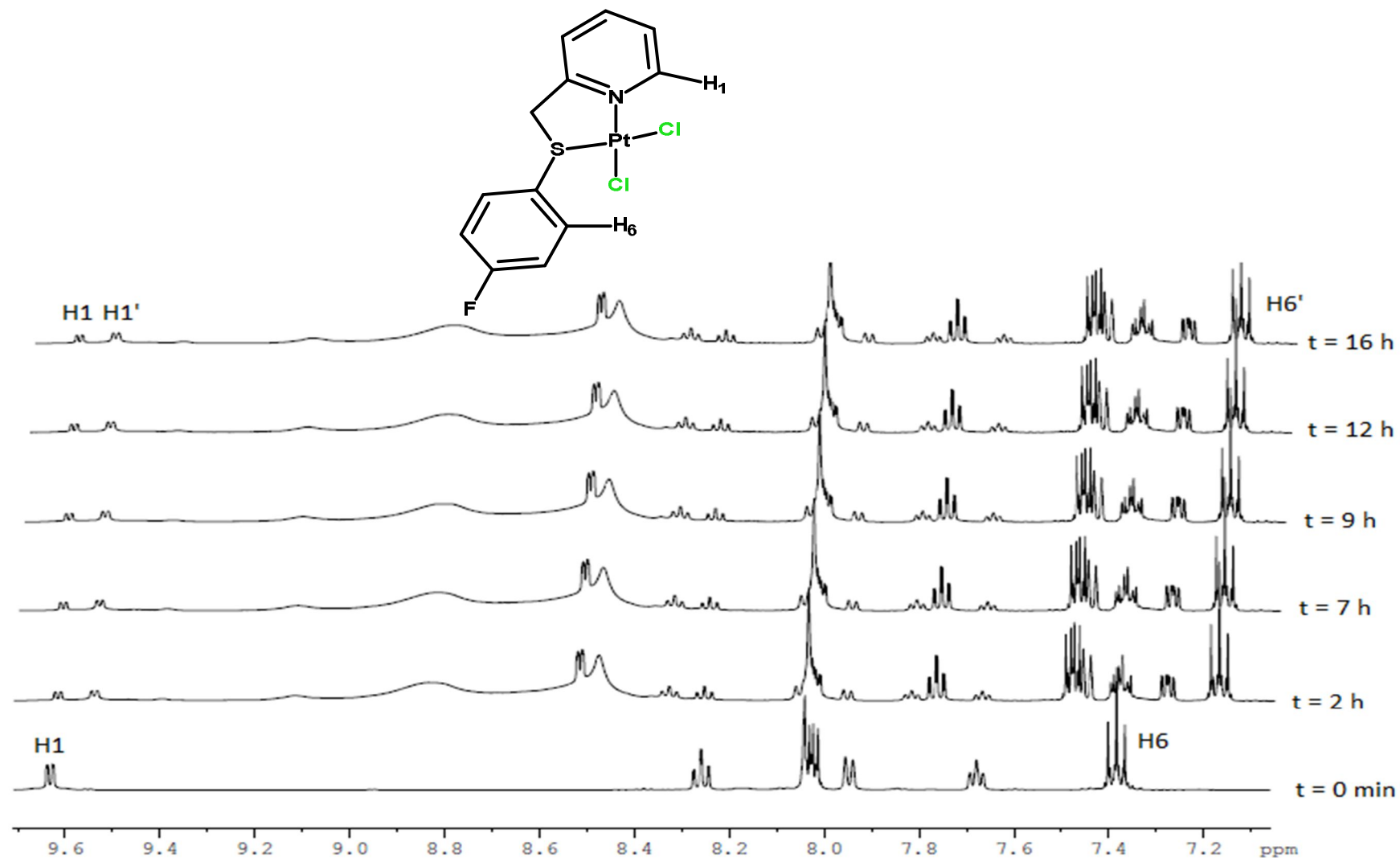


**Figure SI 4.3**  $^1\text{H}$  NMR spectral array (aromatic region) for the reaction of  $[\text{Pt}(\text{pyS}^{\text{PhF}})\text{Cl}_2]$  with two equivalents of thiourea (tu) in  $\text{DMF-d}_7$  at 298 K. The doublet indicated by  $\text{H}_1'$  at  $\delta = 9.54$  ppm corresponds to the substituted product.

## Single Mass Analysis

Tolerance = 5.0 PPM / DBE: min = -1.5, max = 100.0

Element prediction: Off

Number of isotope peaks used for i-FIT = 3

Monoisotopic Mass, Odd and Even Electron Ions

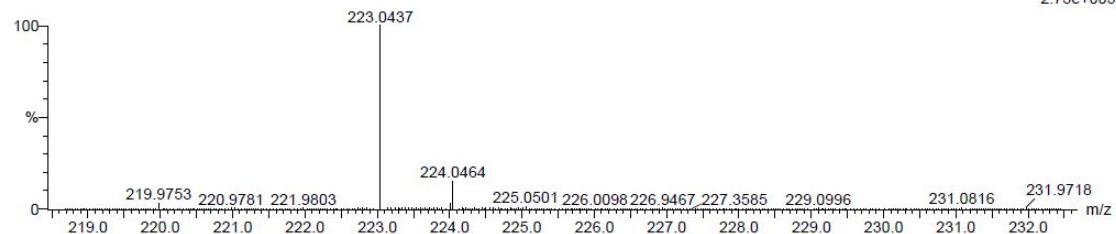
20 formula(e) evaluated with 1 results within limits (up to 20 closest results for each mass)

Elements Used:

C: 5-15 H: 5-15 N: 0-5 Na: 0-1 S: 0-1

Hpy 57 (1.892) Cm (1:61)

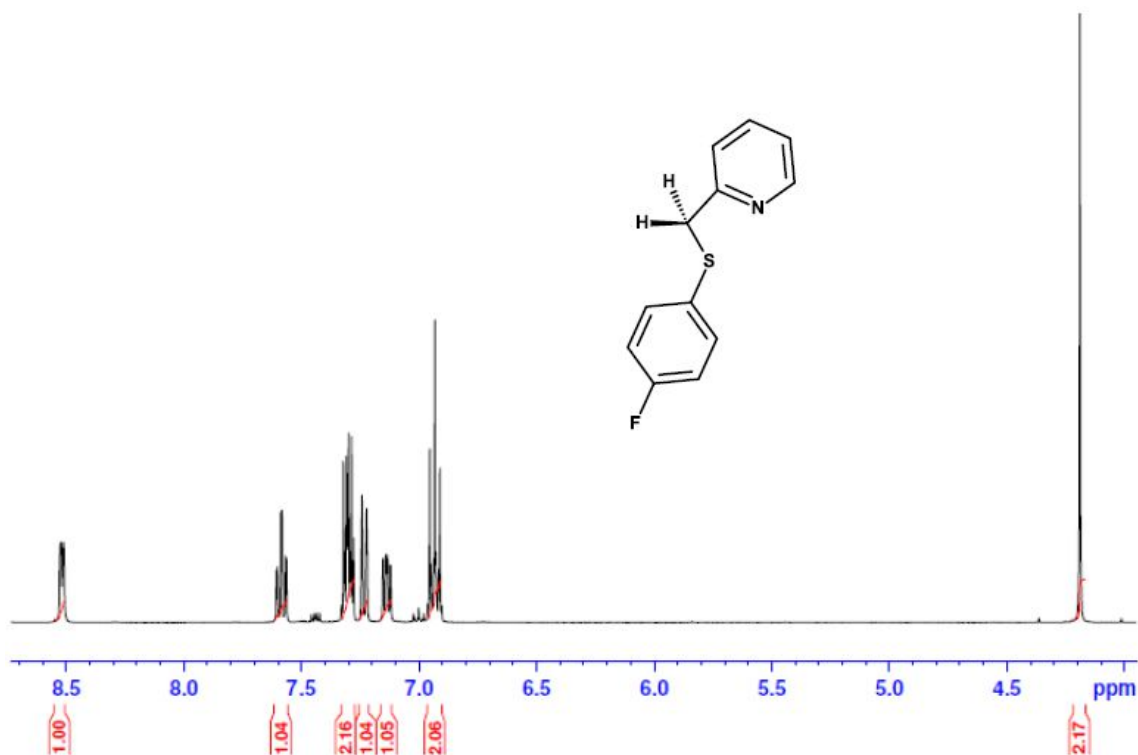
TOF MS ES+



Minimum:

Maximum:

Mass	Calc. Mass	mDa	PPM	DBE	i-FIT	i-FIT (Norm)	Formula
223.0437	223.0432	0.5	2.2	8.0	746.8	0.0	C12 H10 N Na S

Figure SI 4.4 Low resolution ESI mass spectrum of 2-(phenylthiomethyl)pyridine} ( $\text{pyS}^{\text{Ph}}$ ).Figure SI 4.5  $^1\text{H}$  NMR spectrum of 2-(4-fluoro phenylthiomethyl)pyridine} ( $\text{pyS}^{\text{PhF}}$ ).



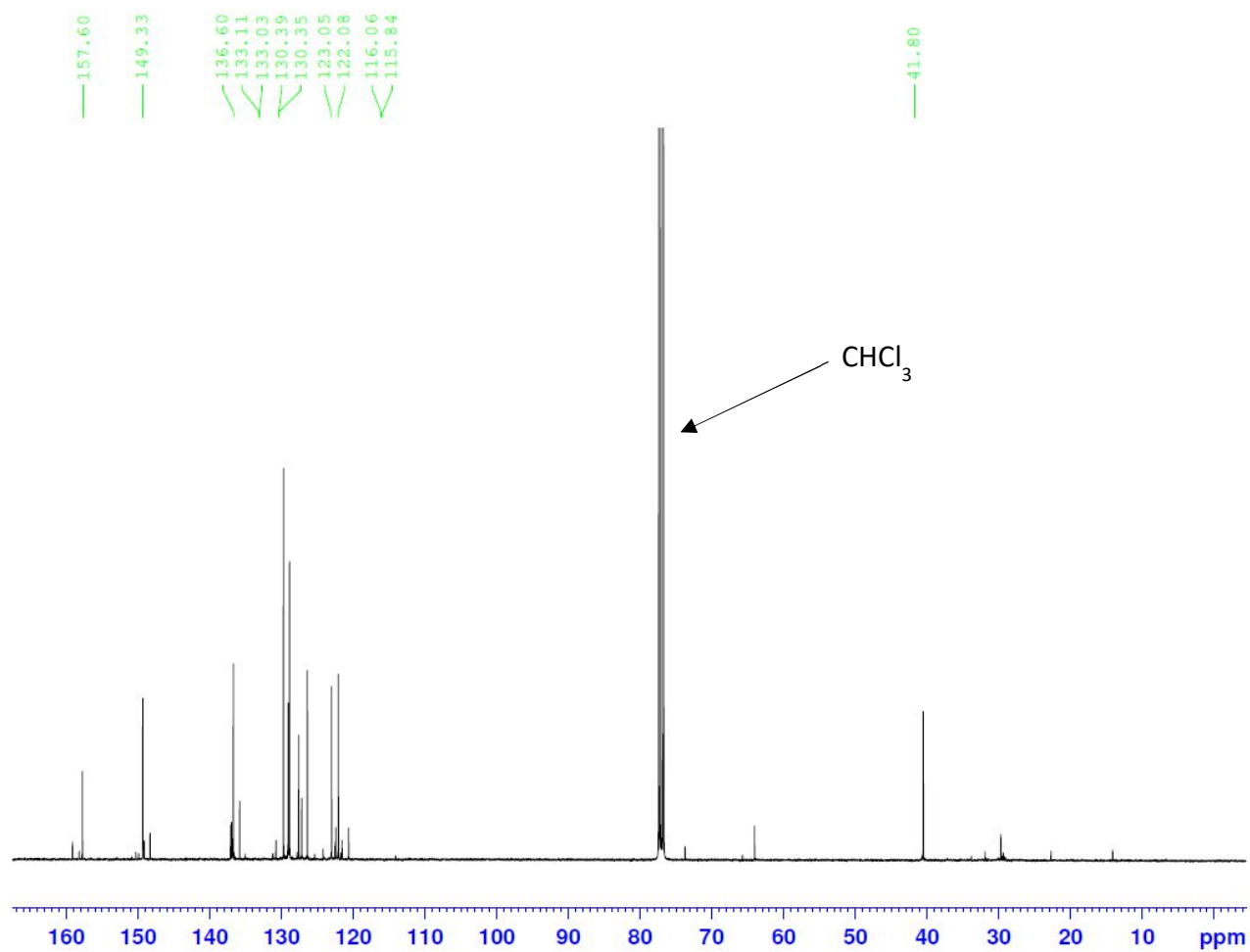


Figure SI 4.6  $^{13}\text{C}$  NMR spectrum of 2-(4-fluorophenylthiomethyl)pyridine ( $\text{pyS}^{\text{PhF}}$ ).

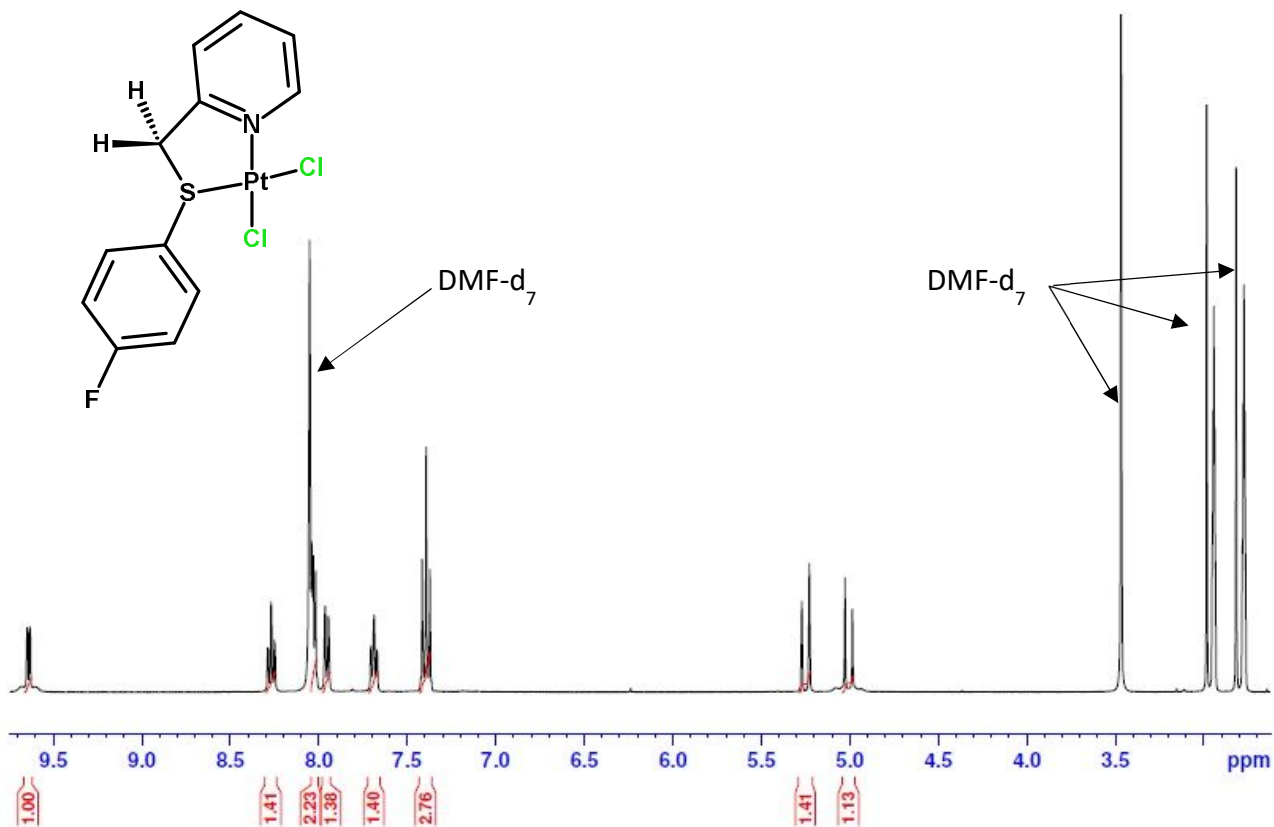


Figure SI 4.7  $^1\text{H}$  NMR spectrum of  $[\text{Pt}\{2\text{-}(4\text{-fluorophenylthiomethyl)pyridine}\}\text{Cl}_2]$   $\text{Pt}(\text{pyS}^{\text{PhF}})$ .

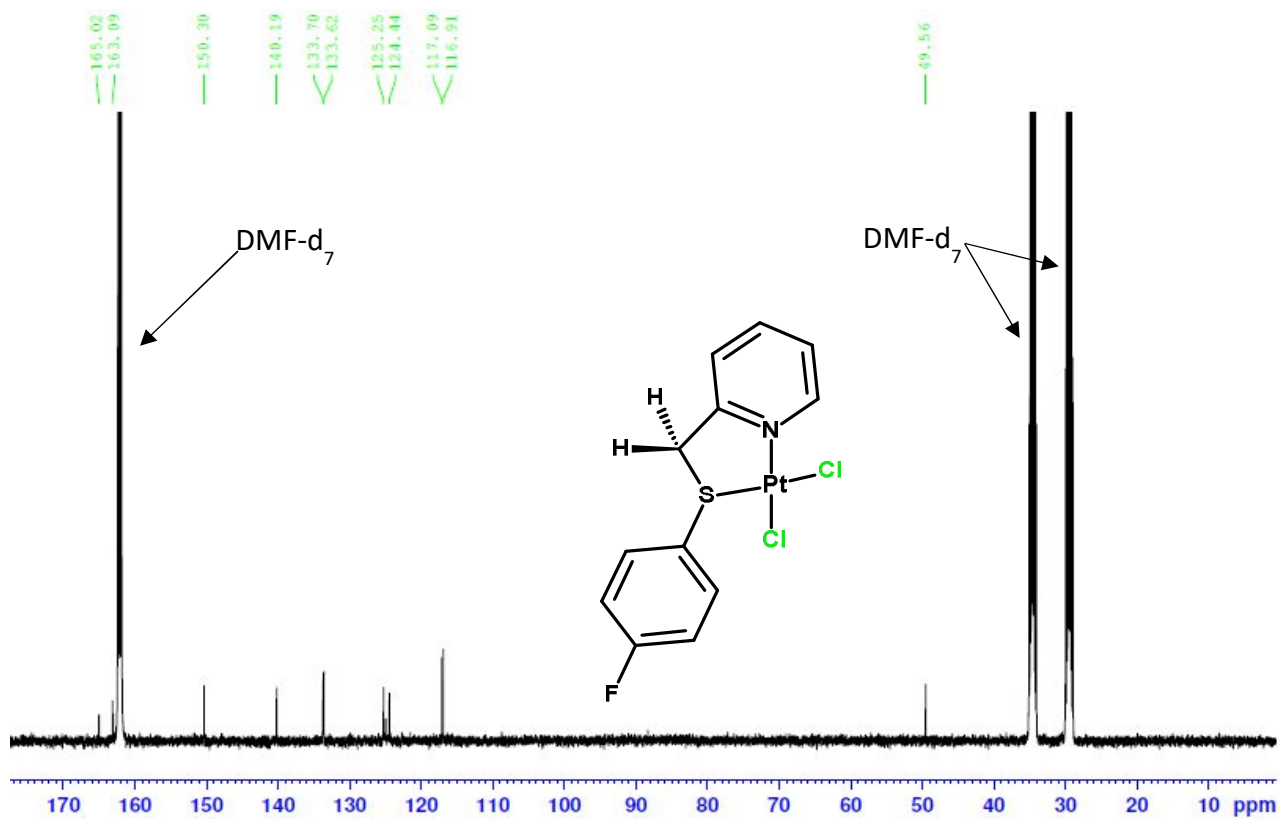
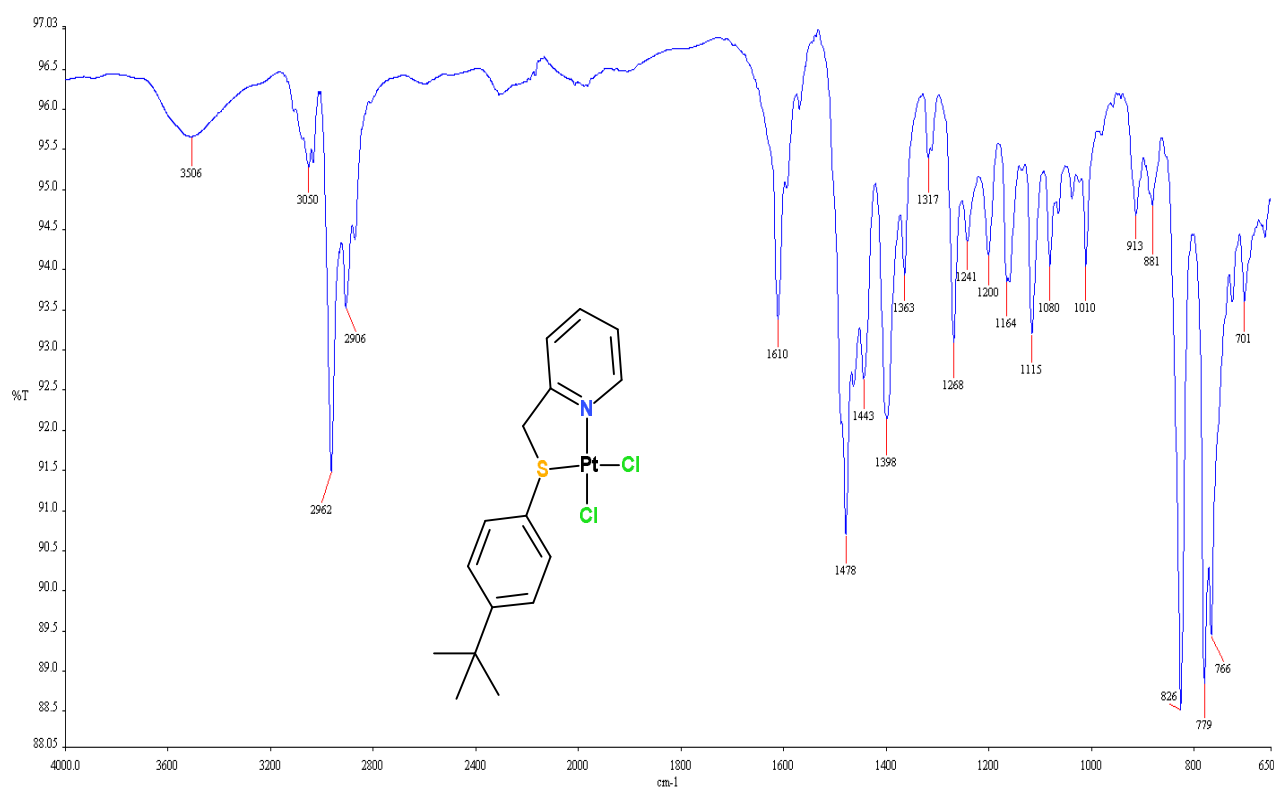


Figure SI 4.8  $^{13}\text{C}$  NMR spectrum of  $[\text{Pt}\{2\text{-}(4\text{-fluorophenylthiomethyl)pyridine}\}\text{Cl}_2]$   $\text{Pt}(\text{pyS}^{\text{PhF}})$ .



**Figure SI 4.9** IR spectrum of [Pt{2-(4-*tert*-butylthiomethyl)pyridine}Cl<sub>2</sub>] Pt(pyS<sup>Ph</sup>(*t*-but)).

**Table SI 4.3** Averaged observed rate constants,  $k_{\text{obs}1}$ , for the reaction of 0.1147 mM Pt(pyS<sup>Ph</sup>) with different nucleophiles at pH 2 ( $I = 0.1$  M LiOTf/HOTf) and 25 °C.

Nucleophile	tu	dmtu	tmtu
[Nu] in mM	$k_{\text{obs}1}$ in s <sup>-1</sup>		
2.294	1,115	1,606	0.1747
4.588	1,814	2,418	0.2759
6.882	2,505	3,202	0.3684
9.176	3,204	3,947	0.4777
11.47	3,903	4,852	0.5702

**Table SI 4.4** Averaged observed rate constants,  $k_{obs2}$ , for the reaction of 0.1147 mM **Pt(pyS<sup>Ph</sup>)** with different nucleophiles at pH 2 ( $I = 0.1$  M LiOTf/HOTf) and 25 °C.

Nucleophile	<b>tu</b>	<b>dmtu</b>	<b>tmtu</b>
[Nu] in mM	$k_{obs1}$ in s <sup>-1</sup>		
2.294	0,00403	0,00772	0,00531
4.588	0,00481	0,0082	0,00568
6.882	0,00594	0,00881	0,00607
9.176	0,00769	0,00943	0,00644
11.47	0,00899	0,00981	0,0069

**Table SI 4.5** Averaged observed rate constants,  $k_{obs1}$ , for the reaction of 0.1646 mM **Pt(pyS<sup>Ph(t-But)</sup>)** with different nucleophiles at pH 2 ( $I = 0.1$  M LiOTf/HOTf) and 25 °C.

Nucleophile	<b>tu</b>	<b>dmtu</b>	<b>tmtu</b>
[Nu] in mM	$k_{obs1}$ in s <sup>-1</sup>		
1.646	7.2	1.776	0.4277
3.292	14.4	3.869	0.8636
4.938	21.25	6.385	1.227
6.584	28.22	8.636	1.738
8.230	35.79	10.37	2.029

**Table SI 4.6** Averaged observed rate constants,  $k_{\text{obs}2}$ , for the reaction of 0.1646 mM **Pt(pyS<sup>Ph(t-But)</sup>)** with different nucleophiles at pH 2 ( $I = 0.1$  M LiOTf/HOTf) and 25 °C.

Nucleophile	<b>tu</b>	<b>dmtu</b>	<b>tmtu</b>
[Nu] in mM	$k_{\text{obs}2}$ in $\text{s}^{-1}$		
3.293	0.4053	0.03305	0,00661
6.584	0.7176	0.07687	0,01537
9.876	0.958	0.2033	0,04066
13.17	1.29	0.3607	0,07214
16.46	1.535	0.4332	0,08664

**Table SI 4.7** Averaged observed rate constants,  $k_{\text{obs}1}$ , for the reaction of 0.04946 mM **Pt(pyS<sup>PhF</sup>)** with different nucleophiles at pH 2 ( $I = 0.1$  M LiOTf/HOTf) and 25 °C.

Nucleophile	<b>tu</b>	<b>dmtu</b>	<b>tmtu</b>
[Nu] in mM	$k_{\text{obs}1}$ in $\text{s}^{-1}$		
0.4946	0.2594	0.2665	0.02513
0.9892	0.5565	0.5369	0.05632
1.484	0.8501	0.8377	0.08496
1.978	1.238	1.111	0.1157
2.473	1.540	1.443	0.1467

**Table SI 4.8** Averaged observed rate constants,  $k_{\text{obs}2}$ , for the reaction of 0.04946 mM **Pt(pyS<sup>Ph</sup>F)** with different nucleophiles at pH 2 ( $I = 0.1$  M LiOTf/HOTf) and 25 °C.

Nucleophile	<b>tu</b>	<b>dmtu</b>	<b>tmtu</b>
[Nu] in mM	$k_{\text{obs}2}$ in $\text{s}^{-1}$		
0.9892	0.4626	0.5492	0.04608
1.978	0.8459	1.044	0.09601
2.968	1.321	1.403	0.1357
3.957	1.634	1.701	0.1726
4.946	2.032	2.079	0.2251

**Table SI 4.9** Temperature dependence of the second-order rate constants,  $k_1/\text{M}^{-1} \text{s}^{-1}$ , for the substitution of the **first** aqua group in **Pt(pyS<sup>Ph</sup>)** by with different nucleophiles at pH 2 ( $I = 0.1$  M LiOTf/HOTf) and 25 °C.

<b>tu</b>		<b>dmtu</b>		<b>tmtu</b>	
$1/T/\text{K}^{-1}$	$\ln(k_2/T)$	$1/T/\text{K}^{-1}$	$\ln(k_2/T)$	$1/T/\text{K}^{-1}$	$\ln(k_2/T)$
0,00347	-2,10773	0,00347	-2,55019	0,00347	-3,44072
0,00341	-1,73985	0,00341	-2,1579	0,00341	-3,08275
0,00336	-1,3843	0,00336	-1,8412	0,00336	-2,87454
0,0033	-1,14353	0,0033	-1,53686	0,0033	-2,63855
0,00325	-0,88758	0,00325	-1,34069	0,00325	-2,405

**Table SI 4.10** Temperature dependence of the second-order rate constants,  $k_1/\text{M}^{-1} \text{s}^{-1}$ , for the substitution of the **first** aqua group in **Pt(pyS<sup>Ph(t-But)</sup>)** by with different nucleophiles at pH 2 ( $I = 0.1 \text{ M LiOTf/HOTf}$ ) and 25 °C.

<b>tu</b>		<b>dmtu</b>		<b>tmtu</b>	
$1/T/\text{K}^{-1}$	$\ln(k_2/T)$	$1/T/\text{K}^{-1}$	$\ln(k_2/T)$	$1/T/\text{K}^{-1}$	$\ln(k_2/T)$
0,00347	3,452	0,00347	0,00551	0,00347	-1,37939
0,00341	3,67833	0,00341	0,45874	0,00341	-1,06533
0,00336	3,87228	0,00336	0,77466	0,00336	-0,87487
0,0033	4,07643	0,0033	1,04257	0,0033	-0,60812
0,00325	4,19966	0,00325	1,23892	0,00325	-0,38105

**Table SI 4.11** Temperature dependence of the second-order rate constants,  $k_1/\text{M}^{-1} \text{s}^{-1}$ , for the substitution of the **first** aqua group in **Pt(pyS<sup>PhF</sup>)** by with different nucleophiles at pH 2 ( $I = 0.1 \text{ M LiOTf/HOTf}$ ) and 25 °C.

<b>tu</b>		<b>dmtu</b>		<b>tmtu</b>	
$1/T/\text{K}^{-1}$	$\ln(k_2/T)$	$1/T/\text{K}^{-1}$	$\ln(k_2/T)$	$1/T/\text{K}^{-1}$	$\ln(k_2/T)$
0,00347	0,03745	0,00347	-0,1442	0,00347	-2,19781
0,00341	0,37429	0,00341	0,18944	0,00341	-1,86308
0,00336	0,65352	0,00336	0,40116	0,00336	-1,64965
0,0033	0,85849	0,0033	0,64788	0,0033	-1,45166
0,00325	1,07558	0,00325	0,91963	0,00325	-1,13509

**Table SI 4.12** Temperature dependence of the second-order rate constants,  $k_2/\text{M}^{-1} \text{s}^{-1}$ , for the substitution of the **second** aqua group in **Pt(pyS<sup>Ph</sup>)** by with different nucleophiles at pH 2 ( $I = 0.1 \text{ M LiOTf/HOTf}$ ) and 25 °C.

<b>tu</b>		<b>dmtu</b>		<b>tmtu</b>	
$1/T/\text{K}^{-1}$	$\ln(k_2/T)$	$1/T/\text{K}^{-1}$	$\ln(k_2/T)$	$1/T/\text{K}^{-1}$	$\ln(k_2/T)$
0,00347	-0,25642	0,00347	-0,45618	0,00347	-3,44072
0,00341	0,30694	0,00341	0,0959	0,00341	-3,02749
0,00336	0,61862	0,00336	0,4656	0,00336	-2,87454
0,0033	1,26377	0,0033	0,75832	0,0033	-2,63855
0,00325	1,59817	0,00325	0,94631	0,00325	-2,405

**Table SI 4.13** Temperature dependence of the second-order rate constants,  $k_2/\text{M}^{-1} \text{s}^{-1}$ , for the substitution of the **second** aqua group in **Pt(pyS<sup>Ph(t-But)</sup>)** by with different nucleophiles at pH 2 ( $I = 0.1 \text{ M LiOTf/HOTf}$ ) and 25 °C.

<b>tu</b>		<b>dmtu</b>		<b>tmtu</b>	
$1/T/\text{K}^{-1}$	$\ln(k_2/T)$	$1/T/\text{K}^{-1}$	$\ln(k_2/T)$	$1/T/\text{K}^{-1}$	$\ln(k_2/T)$
0,00347	-3,51136	0,00347	-4,59617	0,00347	-3,57129
0,00341	-3,15647	0,00341	-4,48904	0,00341	-3,13877
0,00336	-2,92145	0,00336	-4,31196	0,00336	-2,78179
0,0033	-2,66823	0,0033	-4,25058	0,0033	-2,47998
0,00325	-2,5255	0,00325	-4,15611	0,00325	-2,30978



**Table SI 4.14** Temperature dependence of the second-order rate constants,  $k_2/\text{M}^{-1} \text{s}^{-1}$ , for the substitution of the **second** aqua group in **Pt(pyS<sup>PhF</sup>)** by with different nucleophiles at pH 2 ( $I = 0.1 \text{ M LiOTf/HOTf}$ ) and 25 °C.

tu		dmtu		tmtu	
1/T/ K <sup>-1</sup>	ln( $k_2/T$ )	1/T/K <sup>-1</sup>	ln( $k_2/T$ )	1/T/K <sup>-1</sup>	ln( $k_2/T$ )
0,00347	-0,1442	0,00347	-0,24178	0,00347	-2,44072
0,00341	0,18944	0,00341	0,09918	0,00341	-2,02749
0,00336	0,40116	0,00336	0,46139	0,00336	-1,87454
0,0033	0,64788	0,0033	0,66689	0,0033	-1,63855
0,00325	0,91963	0,00325	0,94631	0,00325	-1,405

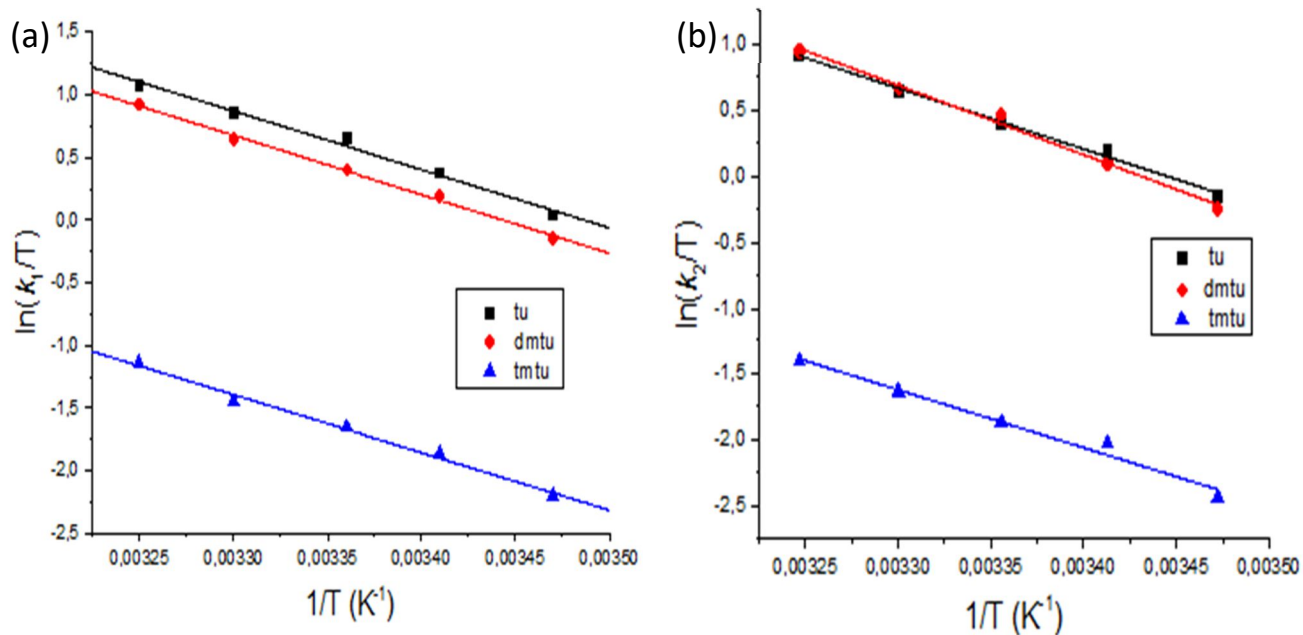


**Figure SI 4.15** Eyring plots for (a) first and (b) second substitution steps for the reactions of 0.1 mM **Pt(pyS<sup>PhF</sup>)** and thiourea nucleophiles, pH 2 ( $I = 0.1 \text{ M LiOTf/HOTf}$ ) and 25 °C.

# Chapter 5

**Role of extended  $\pi$ -conjugation on the rate of substitution of aqua ligands in *cis*-Pt(II) complexes with 2-((4-substituted)phenylthiomethyl)quinoline non-leaving ligands.**

## 5.0 Abstract

The sequential substitution of aqua ligands from [Pt{2-(phenylthiomethyl)quinoline}(H<sub>2</sub>O)<sub>2</sub>]<sup>2+</sup> **Pt(QnS<sup>Ph</sup>)**, [Pt{2-(4-*tert*-butylphenylthiomethyl)quinoline}(H<sub>2</sub>O)<sub>2</sub>]<sup>2+</sup> **Pt(QnS<sup>Ph(t-But)</sup>)**, [Pt{2-(4-fluorophenylthiomethyl)quinoline}(H<sub>2</sub>O)<sub>2</sub>]<sup>2+</sup> **Pt(QnS<sup>PhF</sup>)** and [Pt{2-(4-*tert*-butylphenylthiomethyl)pyridine}(H<sub>2</sub>O)<sub>2</sub>]<sup>2+</sup> **Pt(pyS<sup>Ph(t-But)</sup>)** by three neutral S-containing nucleophiles (Nu) with different steric sizes, thiourea (**tu**), N,N'-dimethylthiourea (**dmtu**) and N,N,N',N'-tetramethylthiourea (**tmtu**), was studied under *pseudo*-first-order conditions as a function of concentration and temperature using stopped-flow and UV-visible spectrophotometric techniques.

The observed *pseudo*-first-order rate constants for the substitutions can be described by the rate law:  $k_{\text{obs}(1/2)} = k_{2(1/2)}[\text{Nu}]$ . The first aqua ligand was substituted opposite to the strong  $\sigma$ -*trans*-directing thioether followed by the aqua ligand opposite to the quinoline or pyridine moieties. The rate of substituting the aqua ligand from the complexes was influenced by the  $\sigma$ -donating *tert*-butyl of **Pt(QnS<sup>Ph(t-But)</sup>)** and  $\sigma$ -withdrawing fluoro of **Pt(QnS<sup>PhF</sup>)** on the *para*-position of the phenyl ring. In both complexes, the substituents on the phenyl ring of the thioether accelerated the rate of substitution when compared to the unsubstituted analogue **Pt(QnS<sup>Ph</sup>)**. When the reactivity for **Pt(pyS<sup>Ph(t-But)</sup>)** is compared to **Pt(QnS<sup>Ph(t-But)</sup>)**, the latter is found to be less reactive by a factor of 13 due to the poor  $\pi$ -acceptor properties of the quinoline ring. Second-order rate constants,  $k_{2(1\text{st})}$ , for the substitution of the first aqua ligand ranged between 9.1 - 21.2 M<sup>-1</sup> s<sup>-1</sup> for **Pt(QnS<sup>Ph</sup>)**, 86.4 - 325.4 M<sup>-1</sup> s<sup>-1</sup> for **Pt(QnS<sup>Ph(t-But)</sup>)**, 58.9 - 287.4 M<sup>-1</sup> s<sup>-1</sup> for **Pt(QnS<sup>PhF</sup>)** and 126.7 - 4325.4 M<sup>-1</sup> s<sup>-1</sup> **Pt(pyS<sup>Ph(t-But)</sup>)**. The ranges of the second-order rate constants,  $k_{2(2\text{nd})}$ , are always lower than the  $k_{2(1\text{st})}$ 's and are 0.35 - 8.9 M<sup>-1</sup> s<sup>-1</sup> for **Pt(QnS<sup>Ph</sup>)**, 2.3 - 19.6 M<sup>-1</sup> s<sup>-1</sup> for **Pt(QnS<sup>Ph(t-But)</sup>)** and 0.29 - 4.8 M<sup>-1</sup> s<sup>-1</sup> for **Pt(QnS<sup>PhF</sup>)** and

6.6 - 24.4 M<sup>-1</sup> s<sup>-1</sup> Pt(pyS<sup>Ph(t-But)</sup>). The second-order rate constants were sensitive to the steric bulk of the entering nucleophiles. The high and negative activation entropy and low and positive activation enthalpy values (Table 5.4) support an associative mechanism of activation, characteristic of substitution reactions occurring in square-planar complexes.

## 5.1 Introduction

Transition metals of low-spin  $d^8$  square-planar Pt(II) complexes have been a subject of medicinal interest for years.<sup>1-4</sup> It is now known that their reactions with DNA nucleic bases is the main mechanistic pathway for anticancer activity against cancerous cells.<sup>5,6</sup> Modification of both steric and electronic attributes of the non-leaving ligand is key to adjusting the reactivity of Pt(II) complexes required to optimise their antitumour potency.<sup>7,8</sup> This argument is demonstrated by the high reactivity factors of between 10<sup>3</sup> - 10<sup>5</sup> of the analogous Pd(II) complexes over the Pt(II) analogues, yet the majority are inactive anticancer agents.<sup>9</sup> The high reactivity of Pd(II) complexes renders them inactive anticancer agents due to rapid deactivation by non-targeted substrates in the plasmic fluids.<sup>10</sup> Additionally, this also leads to high toxicity and development of resistance.<sup>11,12</sup> However, the reactivity of Pd(II) compounds can be slowed down to levels commonly reported for Pt(II) complexes by introducing sterically bulky non-leaving ligands which retards facile approach of plasmic nucleophiles.<sup>13,14</sup>

The reactivity of Pt(II) complexes that possess two sites for substitution can be affected by both steric and electronic factors in the structure of the non-leaving ligand. Pt(II) complexes which have N,N-<sup>13,15-25</sup> or N,S-<sup>26-28</sup> bidentate non-leaving ligands usually display a two-step consecutive substitution of the labile leaving groups, at rates that are dependent on the electronic ( $\sigma$ -donor/ $\pi$ -acceptor) and steric demands of the resident ligand as well as the co-ordinated nucleophile after the first substitution step. Even in complexes where the coordinated bidentate ligand is symmetrical, a consecutive substitution usually occur.<sup>29</sup> In one such set of complexes, substitution of the first leaving group was followed by ring-opening of the S,S bidentate (where S,S = 1,2-bis(phenylsulfanyl)ethane) when neutral pyridine was used as a substituting ligand.<sup>30</sup>

When the non-leaving ligand has fused aromatic rings, the rate of substitution is increased due to the strong  $\pi$ -acceptor property of the ligand. Theoretically, extending the  $\pi$ -surface of a strong  $\pi$ -acceptor ring such as pyridine to a quinoline moiety is expected to

accelerate the rate of substitution due to an increased propensity of the latter moiety to receive electron density into its low-energy, extended molecular orbitals through back bonding. However, recent reports<sup>31-33</sup> have demonstrated an antithesis of this observation for which a dominant  $\sigma$ -*cis*-effect of an isoquinoline and quinoline moieties for tridentate N,N,N terpy-analogues retard the rate of substitution of the labile leaving group relative to Pt(terpy). This has been consistently observed due to accumulation of electron density on the Pt(II) metal centre of the iso/quinolyl complexes.<sup>31-33</sup> This leads to the destabilization of the transition state.<sup>34,35</sup> A similar trend in reactivity was observed by Khusi *et al.*<sup>36</sup> for N,N bidentate coordinated Pt(II) complexes for which replacing the pyridyl moiety of the bidentate with a quinolyl moiety retarded the rate of stepwise substitution of the aqua leaving groups positioned *trans* to the moiety. This study serves to extend the knowledge on the role of extended  $\pi$ -conjugation of a non-leaving ligand on the rate of aqua ligand substitution in *cis*-Pt(II) complexes bearing 2-((4-substituted)phenylthiomethyl)quinoline N,S bidentate ligands (see **Figure 5.1**). The entering thiourea nucleophiles were chosen due to their neutral character, good aqueous solubility and nucleophilicity.<sup>37</sup>

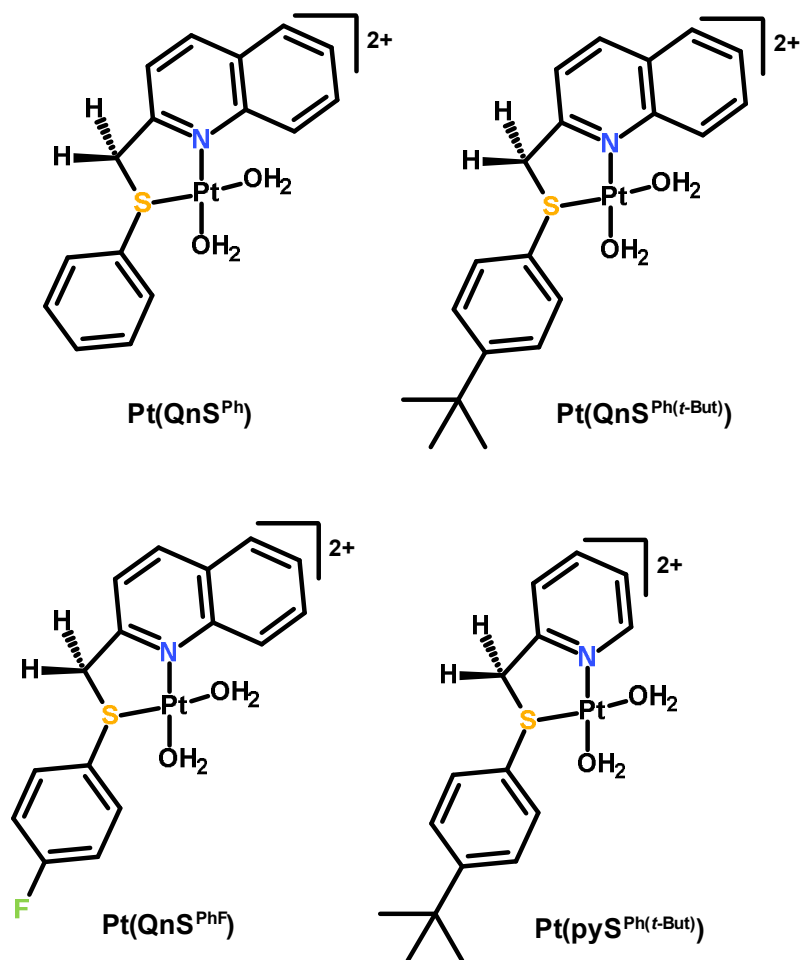


**Figure 5.1** Structures of the *cis*-Pt(II) complexes with 2-(phenylthiomethyl)quinolone moieties.

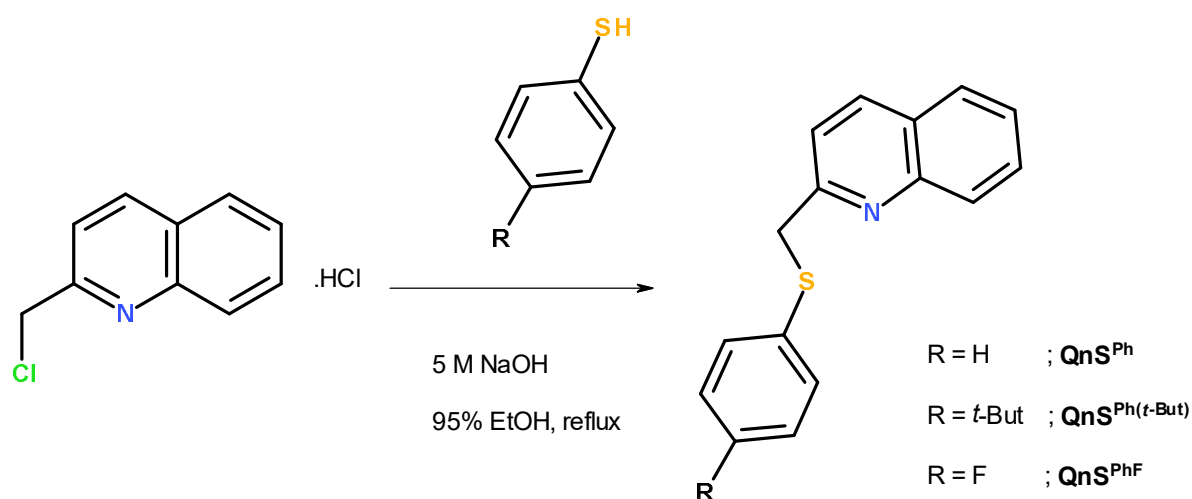
## 5.2 Experimental

### 5.2.1 Materials

Synthesis of the ligands was carried out under inert nitrogen conditions using standard Schlenk techniques. Ligand and complex precursors were obtained from Aldrich and used without further purification. Silver trifluoromethanesulfonate ( $\text{CF}_3\text{SO}_3\text{Ag}$ , 99 %, Aldrich) was stored under nitrogen as per specifications and used as received. The nucleophiles *viz.*, thiourea (**tu**, 99 %), *N,N*-dimethylthiourea (**dmtu**, 99 %), *N,N,N',N'*-tetramethylthiourea and (**tmtu**, 99 %) were also purchased from Aldrich and used without further purification. Ultrapure water (MODULAB purification system) was used for all aqueous reactions. All other chemicals and solvents were of reagent grade and used as received.

## 5.2.2 Synthesis of the N,S ligands

Bidentate N,S ligands, namely 2-(phenylthiomethyl)quinoline **QnS<sup>Ph</sup>**, 2-(4-*tert*-butylphenylthiomethyl)quinoline **QnS<sup>Ph(t-But)</sup>** and 2-(4-fluorophenylthiomethyl)quinoline **QnS<sup>PhF</sup>** were prepared *via* a nucleophilic S-alkylation reaction of either thiophenol, 4-*tert*-butylthiophenol, or 4-fluorothiophenol with 2-(chloromethyl)quinoline hydrochloride (**Scheme 5.1**).<sup>38,39</sup> The pyridyl ligand 2-(4-*tert*-butylphenylthiomethyl)pyridine **pyS<sup>Ph(t-But)</sup>** was synthesised as described in Chapter 4, Section 4.2.2 and was included herein for comparison purpose. All ligands were obtained in moderate to satisfactory yields (58-64 %) and as yellow or brown oils of adequate purity for further use for platinum coordination. The purity of the ligands was confirmed by <sup>1</sup>H and <sup>13</sup>C NMR, TOF-MS-ESI<sup>+</sup> and CHN elemental analysis techniques. The IR spectra of the ligands gave the following peak frequencies cm<sup>-1</sup>: 3100-3000 (broad, medium, C<sub>sp</sub><sup>3</sup>-H stretch); 1583 (sharp and strong, C<sub>sp</sub><sup>2</sup>=N stretch, quinolyl rings)



**Scheme 5.1** Synthesis of the 2-(phenylthiomethyl)quinoline ligands.

### 2-(phenylthiomethyl)quinoline (**QnS<sup>Ph</sup>**)

The yield of 1.073 g (63 %, brown) for **QnS<sup>Ph</sup>** was obtained. Proton-1 NMR (400 MHz: CDCl<sub>3</sub>):  $\delta_{\text{H}}$  (ppm) referenced to TMS; 4.47 (s, 2H, -CH<sub>2</sub>-), 7.16-7.20 (t, 1H, Ph), 7.24-7.27 (t, 2H, Ph), 7.40-7.42 (d, 2H, Ph), 7.52-7.56 (d, 1H, Qn), 7.52-7.56 (t, 1H, Qn), 7.71-7.75 (t, 1H, Qn), 7.80-7.82 (d, 1H, Qn), 8.07 (d, 1H, Qn), 8.13 (d, 1H, Qn). Carbon-13 NMR (100 MHz: CDCl<sub>3</sub>):  $\delta_{\text{C}}$  (ppm); 41.1; 120.9; 126.4; 127.1; 127.5; 128.9; 129.1; 129.7; 136.9; 158.1. Infrared (KBr, 4000-650 cm<sup>-1</sup>)  $\bar{\nu}$ : 3056 (C=C-H asymmetric stretch), 1596 (C=N, quinolyl). Time-of-flight MS-ESI<sup>+</sup>

$m/z$ : 252.0961, 100 (M)<sup>+</sup>. *Anal. Calc. for* C<sub>16</sub>H<sub>13</sub>NS: C: 76.46, H: 5.21, N: 5.57, S: 12.76 %. *Found*: C: 76.31, H: 5.25, N: 5.21, S: 12.51 %.

### 2-(4-*tert*-butylthiophenol)quinoline (QnS<sup>Ph(t-But)</sup>)

The yield of 1.241 g (58 %, yellow) for QnS<sup>Ph(t-But)</sup> was obtained. Proton-1 NMR (400 MHz: CDCl<sub>3</sub>):  $\delta_{\text{H}}$  (ppm) referenced to TMS; 1.30 (s, 9H, -C(CH<sub>3</sub>)<sub>3</sub>), 4.45 (s, 2H, -CH<sub>2</sub>-), 7.27 (d, 2H, Ph), 7.35 (d, 2H, Ph), 7.51 (t, 1H, Qn), 7.56 (d, 1H, Qn), 7.70-7.74 (t, 1H, Qn), 7.79-7.81 (d, 1H, Qn), 8.08 (d, 1H, Qn), 8.10-8.12 (d, 1H, Qn). Carbon-13 NMR (100 MHz: CDCl<sub>3</sub>):  $\delta_{\text{C}}$  (ppm); 41.8; 115.8; 116.1; 122.1; 123.1; 130.3854; 133.1091; 136.6; 149.3; 157.6. Infrared (KBr, 4000-650 cm<sup>-1</sup>)  $\bar{\nu}$ : 3059 (C=C-H Asymmetric stretch), 1598 (C=N, quinolyl). *Anal. Calc. for* C<sub>20</sub>H<sub>21</sub>NS: C: 78.13, H: 6.88, N: 4.56, S: 10.43 %. *Found*: C: 78.01, H: 6.12, N: 4.53, S: 10.84 %.

### 2-(4-fluorothiophenol)quinoline (QnS<sup>PhF</sup>)

The yield of 1.139 g (64 %, orange) for QnS<sup>PhF</sup> was obtained. Proton-1 NMR (400 MHz: CDCl<sub>3</sub>):  $\delta_{\text{H}}$  (ppm) referenced to TMS; 4.40 (s, 2H, -CH<sub>2</sub>-), 6.92-6.96 (d, 2H, Ph), 7.34-7.38 (d, 2H, Ph), 7.47-7.49 (d, 1H, Qn), 7.52-7.56 (t, 1H, Qn), 7.70-7.74 (t, 1H, Qn), 7.79-7.81 (d, 1H, Qn), 8.05 (d, 1H, Qn), 8.11 (d, 1H, Qn). Carbon-13 NMR (100 MHz: CDCl<sub>3</sub>):  $\delta_{\text{C}}$  (ppm); 42.3; 115.9; 116.1; 111.0; 126.5; 127.5; 129.8; 131.3; 133.1; 158.0. Infrared (KBr, 4000-650 cm<sup>-1</sup>)  $\bar{\nu}$ : 3057 (C=C-H asymmetric stretch), 1592 (C=N, quinolyl). Time-of-flight MS-ESI<sup>+</sup>  $m/z$ : 268, 100 (M-1). *Anal. Calc. for* C<sub>16</sub>H<sub>12</sub>FNS: C: 71.35, H: 4.49, N: 5.20, S: 11.91 %. *Found*: C: 71.29, H: 4.31, N: 5.15, S: 11.43 %.

### 2-(4-*tert*-butylthiophenol)pyridine (pys<sup>Ph(t-But)</sup>) (see also Chapter 4 Section 4.2.2)

The yield of 1.457 g (57 %, light-brown) for pys<sup>Ph(t-But)</sup> was obtained. Proton-1 NMR (400 MHz: CDCl<sub>3</sub>):  $\delta_{\text{H}}$  (ppm) referenced to TMS; 1.30 (s, 9H, -C(CH<sub>3</sub>)<sub>3</sub>), 4.27 (s, 2H, -CH<sub>2</sub>-), 7.17-7.18 (t, 1H, py), 7.28 (d, 4H, Ph), 7.36 (d, 1H, py), 7.62-7.65 (t, 1H, py), 8.55 (d, 1H, py). Infrared (KBr, 4000-650 cm<sup>-1</sup>)  $\bar{\nu}$ : 3059 (C=C-H asymmetric stretch), 1598 (C=N, pyridyl). Time-of-flight MS-ESI<sup>+</sup>  $m/z$ : 258.1181, 100 (M+1). *Anal. Calc. for* C<sub>16</sub>H<sub>19</sub>NS: C: 74.66, H: 7.44, N: 5.44, S: 12.46 %. *Found*: C: 74.47, H: 7.50, N: 5.58, S: 12.28 %.

## 5.2.3 Synthesis of Pt(II) complexes

Three mononuclear *cis*-Pt(II) complexes *viz.*, [Pt{2-(phenylthiomethyl)quinoline}Cl<sub>2</sub>], Pt(Qn<sup>SPh</sup>)Cl<sub>2</sub>, [Pt{2-(4-*tert*-butylthiophenol)quinoline}Cl<sub>2</sub>], Pt(QnS<sup>Ph(t-But)</sup>)Cl<sub>2</sub>, and [Pt{2-(4-

fluorothiophenol)quinoline}Cl<sub>2</sub>], **Pt(QnS<sup>PhF</sup>)Cl<sub>2</sub>**, were synthesised from their respective ligands according to a method outlined in Chapter 4, Section 4.2.3. The purity of the complexes was confirmed by NMR (<sup>1</sup>H, <sup>13</sup>C, and <sup>195</sup>Pt), CHN elemental analyser, TOF MS-ESI<sup>+</sup> and IR spectroscopy.

The yield of 0.3576 g (77 %) for **Pt(QnS<sup>Ph</sup>)Cl<sub>2</sub>** was obtained. Proton-1 NMR (400 MHz: DMF-d<sub>7</sub>): δ<sub>H</sub> (ppm) referenced to TMS; 4.30 (d, 2H, -CH<sub>2</sub>-, AB-spin system), 7.16 (t, 1H, Ph), 7.27 (t, 2H, Ph), 7.37 (d, 2H, Ph), 7.33 (t, 1H, Qn), 7.52-7.54 (d, 1H, Qn), 7.60-7.64 (t, 1H, Qn), 8.56 (d, 1H, Qn). Platinum-195 NMR (400 MHz: DMF-d<sub>7</sub>): δ<sub>Pt</sub> (ppm); -2717. Infrared (KBr, 4000-650 cm<sup>-1</sup>)  $\bar{\nu}$ : 3055 (C=C-H asymmetric stretch), 1583 (C=N, quinolyl). *Anal. Calc. for C<sub>16</sub>H<sub>13</sub>Cl<sub>2</sub>NPtS*: C: 37.15, H: 2.53, N: 2.71, S: 6.20 %. *Found*: C: 36.98, H: 2.42, N: 2.57, S: 6.02 %.

The yield of 0.2048 g (60 %, yellow) for **Pt(QnS<sup>Ph(t-But)</sup>)Cl<sub>2</sub>** was obtained. Proton-1 NMR (400 MHz: CDCl<sub>3</sub>): δ<sub>H</sub> (ppm) referenced to TMS; 1.30 (s, 9H, -C(CH<sub>3</sub>)<sub>3</sub>), 4.27 (d, 2H, -CH<sub>2</sub>-, AB-spin system), 7.17-7.18 (t, 1H, Qn), 7.28 (d, 4H, Ph), 7.36 (d, 1H, Qn), 7.62-7.65 (t, 1H, Qn), 8.55 (d, 1H, Qn). Platinum-195 Pt NMR (400 MHz: DMF-d<sub>7</sub>): δ<sub>Pt</sub> (ppm); -2711. Infrared (KBr, 4000-650 cm<sup>-1</sup>)  $\bar{\nu}$ : 3059 (C=C-H asymmetric stretch), 1598 (C=N, quinolyl). *Anal. Calc. for C<sub>20</sub>H<sub>21</sub>Cl<sub>2</sub>NPtS*: C: 41.89, H: 3.69, N: 2.44, S: 5.59 %. *Found*: C: 41.35, H: 3.30, N: 2.69, S: 6.57 %.

The yield of 0.1986 g (44 %, yellow) for **Pt(QnS<sup>PhF</sup>)Cl<sub>2</sub>** was obtained. Proton-1 NMR (400 MHz: CDCl<sub>3</sub>): δ<sub>H</sub> (ppm) referenced to TMS; 4.19 (d, 2H, -CH<sub>2</sub>-, AB-spin system), 6.91-7.00 (d, 2H, Ph), 7.12-7.15 (t, 1H, Qn), 7.23 (d, 1H, Qn), 7.32 (d, 2H, Ph), 7.57-7.60 (t, 1H, Qn), 8.51-8.52 (d, 1H, Qn). Platinum-195 NMR (400 MHz: DMF-d<sub>7</sub>): δ<sub>Pt</sub> (ppm); -2718. Infrared (KBr, 4000-650 cm<sup>-1</sup>)  $\bar{\nu}$ : 3066 (C=C-H asymmetric stretch), 1588 (C=N, quinolyl). *Anal. Calc. for C<sub>16</sub>H<sub>12</sub>Cl<sub>2</sub>FNPtS*: C: 35.90, H: 2.26, N: 2.62, S: 5.98 %. *Found*: C: 35.14, H: 2.05, N: 2.52, S: 6.06 %.

The yield of 0.3257 g (57 %, light-brown) for **Pt(pyS<sup>Ph(t-But)</sup>)Cl<sub>2</sub>** was obtained. Proton-1 NMR (400 MHz: CDCl<sub>3</sub>): δ<sub>H</sub> (ppm) referenced to TMS; 1.30 (s, 9H, -C(CH<sub>3</sub>)<sub>3</sub>), 4.27 (d, 2H, -CH<sub>2</sub>-, AB-spin system), 7.17-7.18 (t, 1H, py), 7.28 (d, 4H, Ph), 7.36 (d, 1H, py), 7.62-7.65 (t, 1H, py), 8.55 (d, 1H, py). Platinum-195 NMR (400 MHz: DMF-d<sub>7</sub>): δ<sub>Pt</sub> (ppm); -2786. Infrared (KBr, 4000-650 cm<sup>-1</sup>)  $\bar{\nu}$ : 3059 (C=C-H asymmetric stretch), 1598 (C=N, pyridyl). *Anal. Calc. for C<sub>16</sub>H<sub>19</sub>Cl<sub>2</sub>NPtS*: C: 36.72, H: 3.66, N: 2.68, S: 6.13 %. *Found*: C: 36.85, H: 3.53, N: 2.53, S: 7.06 %.



### 5.3 Preparation of the diaqua Pt(II) complexes

Solutions of the diaqua Pt(II) complexes of **Pt(QnS<sup>Ph</sup>)Cl<sub>2</sub>**, **Pt(QnS<sup>Ph(t-But)</sup>)Cl<sub>2</sub>**, and **Pt(QnS<sup>PhF</sup>)Cl<sub>2</sub>** were prepared following a method described in literature<sup>40</sup> and elaborated in Chapter 4 section 4.2.4. Solutions of the thiourea nucleophiles *viz.*, **tu**, **dmTu** and **tmtu** were prepared by dissolving a known amount of the nucleophile in 0.1 M LiOTf/HOTf solution. The adjustment of  $I = 0.10$  M with CF<sub>3</sub>SO<sub>3</sub>Li was undertaken to ensure a constant ionic strength throughout the kinetic measurements.

### 5.4 Instrumentation and physical measurements

NMR spectrometers (Bruker Avance DRX 400 or DRX 500) and a FLASH 2000 CHN analyser were used for the characterization and chemical analysis of the synthesized ligands and complexes. Low-resolution electron-spray ionization (ESI<sup>+</sup>) mass spectra of the ligands and complexes were analysed on a time-of-flight (TOF) micromass spectrometer. A Perkin Elmer Spectrum One FTIR spectrometer using KBr discs was used to obtain Infrared (IR) spectra of the ligands and complexes. Rapid kinetic measurements were followed using an Applied Photophysics SX 18MV stopped-flow spectrophotometer coupled to an online data acquisition system. The temperature of the instrument was controlled to within  $\pm 0.1$  °C for all measurements. A Cary 100 BIO UV-visible spectrophotometer equipped with a Varian Peltier temperature controller with an accuracy of  $\pm 0.05$  °C was used for the determination of the *pKa* values of the diaqua complexes. The pH measurements were determined on a Jenway 4330 pH meter equipped with a 4.5  $\mu$ m glass electrode. The micro-electrode was calibrated at 25 °C using standard buffer solutions (Merck) at pH 4.0, 7.0, and 10.0. *pKa* titration curves and time-resolved kinetic traces were graphically analysed using Origin 7.5® software package.<sup>41</sup>

#### 5.4.1 *pKa* determination for the diaqua complexes

Spectrophotometric acid-base titrations were undertaken for the determination of *pKa* values of the diaqua complexes. Changes in absorbance of the diaqua complex after addition of aliquots of NaOH were plotted as a function of pH within the range 2-9. In the low pH range (2-3),  $\Delta$ pH for the titrated solution was small and thus required crushed NaOH pellets. For the subsequent increase in pH, dilute NaOH solutions of varying concentrations were used for the titrations. After each addition of a portion of NaOH, approximately 1 mL

samples were taken from the titration vessel for pH measurement. The samples were discarded to avoid probable contamination from leaching chloride ions from the pH electrode. The spectral data were analysed with Origin7.5® software suite for which the  $pK_a$  values were obtained from a plot of the sigmoidal curve fitting of absorbance vs pH.

#### 5.4.2 Kinetics measurements

The rate of substitution of the coordinated aqua ligands from the Pt(II) complexes were undertaken under *pseudo*-first-order conditions for which the concentration of nucleophiles was at least 10-fold in excess of the Pt(II) complex. At all times, the solutions were kept at pH 2 to ensure the presence of only the diaqua form of the complexes in solution. The rate of slow reactions was followed on the UV-visible spectrophotometer following a manual mixing of the complex and the nucleophile in a tandem Suprasil cuvette. For rapid reactions, an automated stopped-flow analyser equipped with a pressure-driven cross-plunger for an instant mixing of the complex and nucleophile solutions was used. Prior to kinetics measurements on the stopped-flow, trial kinetic reactions of the Pt(II) metal complexes with the nucleophiles were briefly undertaken spectrophotometrically. This was done to determine suitable wavelengths at which kinetic traces could be followed. All the reported rate constants from the stopped-flow analyser are averages of six to eight independent kinetic runs. The temperature dependence of the rate of substitution was studied within the range of 15-35 °C.

#### 5.4.3 Computer simulation studies

The geometry-optimized molecular structures of the complexes **Pt(QnS<sup>Ph</sup>)**, **Pt(QnS<sup>Ph(t-But)</sup>)** and **Pt(QnS<sup>PhF</sup>)** were computed at the DFT level of theory following the (B3LYP(CPCM)/LANL2DZp//B3LYP/-LAN2DZp) method<sup>42-44</sup> powered by the Gaussian 09 software suite.<sup>45</sup> The geometry optimized structures were conducted in the gaseous phase and the calculated structural parameters are presented in **Table 5.2** and **Figure 5.4**, respectively. A charge of +2 was maintained for the cationic diaqua complexes.

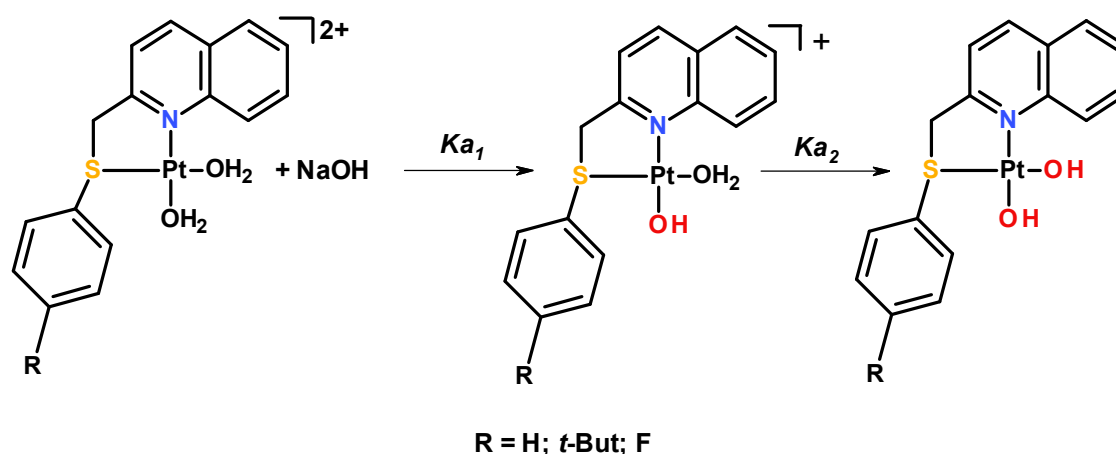
### 5.5 Results

Three square-planar Pt(II) complexes comprising 2-(phenylthiomethyl)quinoline bidentate (N,S) chelates (**Figure 5.1**) were synthesised, characterized and their rates of

reaction with nucleophiles were investigated. The substituents on the phenyl ring of the N,S carrier ligand backbone confers different electronic and steric effects on the structure of the complexes, which in turn influence the rate of substitution from the complexes.

### 5.5.1 Acidity of the diaqua Pt(II) complexes

The **Figure 5.2** shows an example of the spectral changes observed during the  $pK_a$  titration of **Pt(QnS<sup>Ph</sup>)** with NaOH. The  $pK_a$  values were calculated from separate single sigmoidal curve fittings of changes in absorbance data using the Boltzmann distribution parameters as shown from the inset in **Figure 5.2** for the complex **Pt(QnS<sup>Ph</sup>)**. Origin 7.5 software suite was used to acquire the  $pK_a$  values for the consecutive deprotonation of the aqua co-ligands. The values are summarised in **Table 5.1**. The acid-base neutralisation reaction is a consecutive two-step reaction process and is summarised in **Scheme 5.2** where the [Pt(N,S) (H<sub>2</sub>O)(OH)] species is an intermediate. The pyridyl complex **Pt(pyS<sup>Ph(t-But)</sup>)** was included to compare the  $pK_a$  values.



**Scheme 5.2** Deprotonation of the diaqua Pt(II) complexes

**Table 5.1** Summary of  $pK_a$  values obtained for the consecutive deprotonation of aqua ligands coordinated to the Pt(II) complexes

	Pt(QnS <sup>Ph</sup> )	Pt(QnS <sup>Ph(t-But)</sup> )	Pt(QnS <sup>PhF</sup> )	Pt(pyS <sup>Ph(t-But)</sup> )
$pK_{a1}$	$3.95 \pm 0.04$	$4.12 \pm 0.01$	$4.00 \pm 0.02$	<sup>a</sup> 3.87
$pK_{a2}$	$5.85 \pm 0.02$	$6.10 \pm 0.05$	$5.67 \pm 0.03$	<sup>a</sup> 5.60

<sup>a</sup> $pK_a$  values reproduced from Chapter 4, Table 4.1.

The results in **Table 5.1** clearly show the sensitivity of the  $pK_a$  values on the electronic effects of the substituents on the phenyl *para*-position. The  $pK_{a1}$  values for the deprotonation of the first coordinated aqua ligand increase in the order: **Pt(pyS<sup>Ph(t-But)</sup>)** < **Pt(QnS<sup>PhF</sup>)** < **Pt(QnS<sup>Ph</sup>)** < **Pt(QnS<sup>Ph(t-But)</sup>)**, respectively. The positive  $\sigma$ -inductive effect of the *tert*-butyl group causes accumulation of electron density on the Pt(II) metal centre for the complex **Pt(QnS<sup>Ph(t-But)</sup>)**. This makes the Pt(II) ion less electrophilic and the formation of the aqua-hydroxo species from the diaqua kinetically unfavourable due to a weaker Pt-OH<sub>2</sub> bond which makes deprotonation of the aqua ligand more difficult. Consequently, a higher  $pK_{a1}$  value is observed for **Pt(QnS<sup>Ph(t-But)</sup>)** when compared to **Pt(QnS<sup>Ph</sup>)** which only has a weak  $\sigma$ -donor phenyl ring.

Due to the negative  $\sigma$ -inductive effect of the fluoro substituent, it withdraws electron density from the phenyl group, making the metal centre more electrophilic in **Pt(QnS<sup>PhF</sup>)**. Hence, it can stabilize the hydroxo species formed during the neutralization process. This trend in the  $pK_a$  results from this study is the same as that reported by Khusi *et al.*<sup>36</sup> for the bidentate N,N quinoline-bearing Pt(II) complexes. The complex bearing electron-withdrawing groups, (-CF<sub>3</sub>), on the 3,5-positions of the pyrazole ring had a higher NBO charge on the Pt(II) ion. Thus, a lower  $pK_a$  of 4.07 was reported when compared to a  $pK_a$  of 4.88 for the analogous complex with electro-donating methyl substituents, (-CH<sub>3</sub>), at the 3,5-positions of pyrazole.

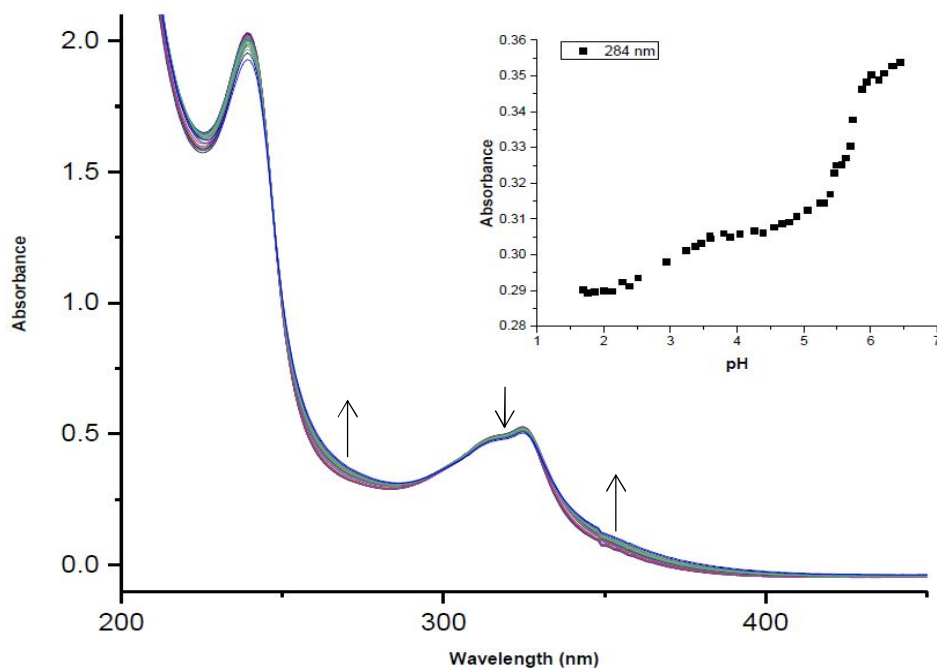


**Figure 5.2** UV-visible spectra for the titration of 0.2 mM **Pt(QnS<sup>Ph</sup>)** with NaOH in the pH range 2-7 at  $T = 298$  K. *Inset:* Absorbance versus pH data at 284 nm.

The lower  $pK_a$  values for the complex **Pt(pyS<sup>Ph(t-But)</sup>)** when compared to its quinolyl analogue can be explained by the  $\pi$ -acceptor properties of the pyridine. Relative to the quinolyl group of **Pt(QnS<sup>Ph(t-But)</sup>)**, the pyridyl group of **Pt(pyS<sup>Ph(t-But)</sup>)** stabilizes the hydroxo species due to its superior withdrawal of electron density from the Pt(II) metal centre.<sup>26</sup> As a result, deprotonation of the first aqua ligand occurs at lower  $pK_{a1}$  values for **Pt(pyS<sup>Ph(t-But)</sup>)** when compared to the quinolyl derivative.

### 5.5.2 DFT-calculated optimised structures

The three Pt(II) complexes all have a common quinolyl moiety in the bidentate N,S non-leaving ligand and only differ in the substituents in the phenyl ring of the thioether group. Density Functional Theory (DFT) calculations were performed to compare the structural parameters due to differences on the substituents on the thioether group. The coordination of the N,S-bidentate ligands to Pt is similar to that of Pt(II) complexes previously reported.<sup>32,33,36</sup> Geometry-optimized structures and the HOMO and LUMO frontier molecular orbitals are depicted in **Table 5.2**, while the molecular geometry optimized parameters are summarized in **Figure 5.3**. Bond angles indicate a slightly distorted square-planar around the Pt(II) metal centre.

For all the complexes, a significant isodensity of the HOMOs lies on the quinoline moiety. The HOMOs are also located on the Pt(II) metal centre but at a much lower density. The mapping of the electronic charge distribution of the HOMOs of the quinolyl complexes implies a less electrophilic Pt(II) ion when compared to their pyridyl analogues reported in Chapter 5 Section 5.3.2. Therefore, it would be expected that the quinolyl complexes have a lower rate of substitution when compared to the pyridyl complex. The LUMOs are concentrated on the thioether and to a lesser extent on the quinoline moiety. Electron density on the thioether indicates the  $\pi$ -acceptor capacity of this moiety and its propensity to pull away electronic charge from the metal centre, making it more electropositive. There is no significant difference in the energy gaps,  $\Delta E$  (HOMO-LUMO) of the frontier orbitals, although the strong electron-donating *tert*-butyl moiety for **Pt(QnS<sup>Ph(t-But)</sup>)** increases the gap slightly when compared to the weak  $\sigma$ -donor phenyl for **Pt(QnS<sup>Ph</sup>)** and electron-withdrawing fluoro for **Pt(QnS<sup>PhF</sup>)** substituents. The NBO charges increase in the following order: **Pt(QnS<sup>Ph(t-But)</sup>)** (0.641) < **Pt(QnS<sup>Ph</sup>)** (0.645) < **Pt(QnS<sup>PhF</sup>)** (0.648) < **Pt(pyS<sup>Ph(t-But)</sup>)** (0.676) and reflects the  $\pi$ -back-bonding capacity of the pyridine ring. This makes its Pt ion more electrophilic.<sup>46-48</sup>

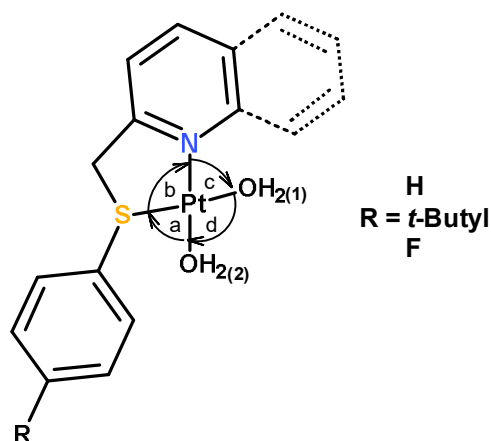


**Table 5.2** DFT calculated parameters for the *cis*-Pt(II).

Property	Pt(QnS <sup>Ph</sup> )	Pt(QnS <sup>Ph(t-But)</sup> )	Pt(QnS <sup>PhF</sup> )	Pt(pyS <sup>Ph(t-But)</sup> ) <sup>b</sup>
<b>MO Energy (eV)</b>				
LUMO	-3.27	-3.23	-3.30	-3.09
HOMO	-7.20	-7.19	-7.22	-7.09
$\Delta E_{L-H}$	3.93	3.96	3.92	4.00
<b>NBO charges</b>				
Pt	0.645	0.641	0.648	0.676
<b>Bond lengths (Å)</b>				
d Pt- <sup>a</sup> N <sub>qn/py</sub>	2.04	2.04	2.04	2.02
d Pt-S	2.40	2.39	2.40	2.41
d Pt-OH <sub>2</sub> (1)	2.13	2.13	2.13	2.12
d Pt-OH <sub>2</sub> (2)	2.11	2.10	2.10	2.11
<b>Bond angle (°)</b>				
S-Pt-OH <sub>2</sub> (1)	174.8	172.9	175.1	176.6
N <sub>qn/py</sub> -Pt-OH <sub>2</sub> (2)	178.5	178.1	178.5	177.9
A	98.7	97.9	98.9	96.4
B	82.5	83.0	82.5	83.9
C	99.3	98.7	99.3	92.8
D	79.5	80.7	79.3	86.9

<sup>a</sup>N<sub>qn/py</sub> = coordinated N-donor atom in the quinoline or pyridine ring.

<sup>b</sup>DFT-simulated calculations reproduced from Chapter 4, Table 4.2.

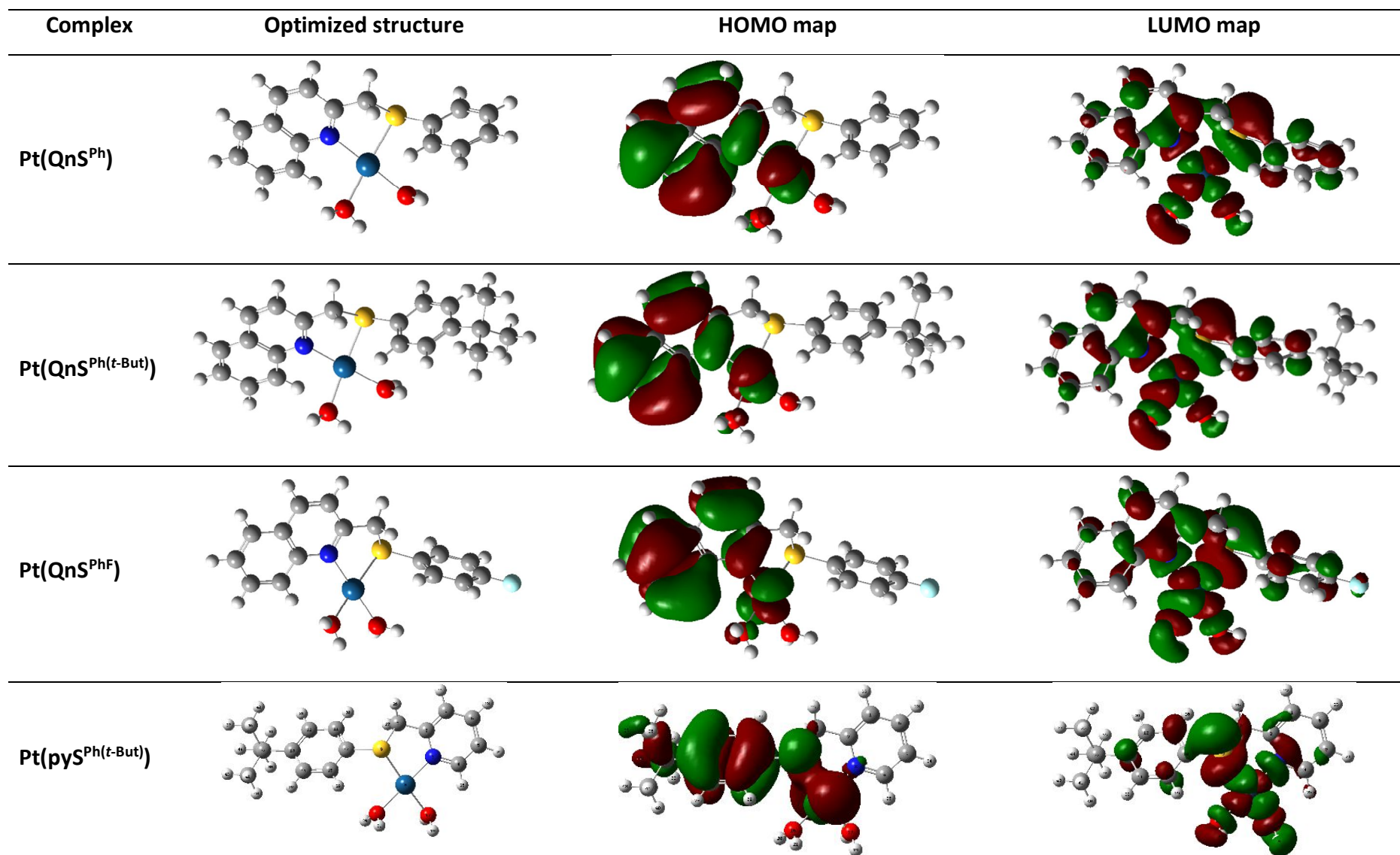
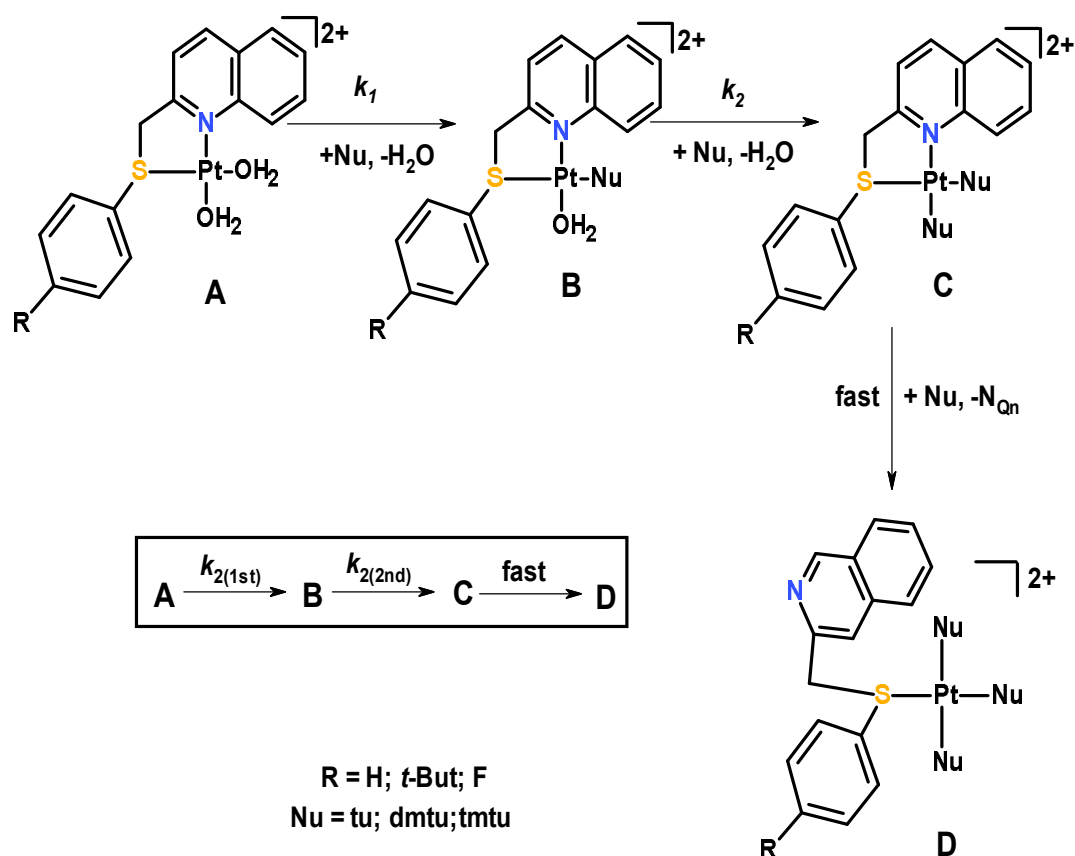


Figure 5.3 DFT geometry-optimized structures of the Pt(II) complexes.



### 5.5.3 Kinetic Measurements

Substitution of the aqua co-ligands from the Pt(II) complexes by thiourea nucleophiles proceeds by a two-step sequential process represented by  $k_{2(1st)}$  and  $k_{2(2nd)}$  as depicted in **Scheme 5.3**. The mechanism of substitution is based on  $^{195}\text{Pt}$  NMR data for the pyridyl derivatives already described in Chapter 4, Section 4.3.2. The first substitution forms **B** which reacts with a second nucleophile to form **C** whose N-end of the N,S non-leaving ligand is simultaneously labilised by the trans coordinated thiourea nucleophile, facilitating the rapid coordination a third thiourea nucleophile to produce **D**, for which four S atoms are coordinated to Pt(II) ion.



**Scheme 5.3** Schematic representation of the two-step substitution of the aqua ligands and the simultaneous decooordination of the N-end of the N,S ligand by entering thiourea nucleophiles (Nu = **tu**, **dmTu** and **tmtu**).

Substitution of the aqua ligand *trans* to the thioether by thiourea nucleophiles, represented as the first step (**A** → **B**) was monitored on the stopped-flow reaction analyser. **Figure 5.4** shows recorded UV-visible spectral changes for the reaction of **Pt(QnS<sup>Ph</sup>)** and **dmTu** used to

choose the appropriate wavelength for monitoring the reaction on the stopped-flow instrument.

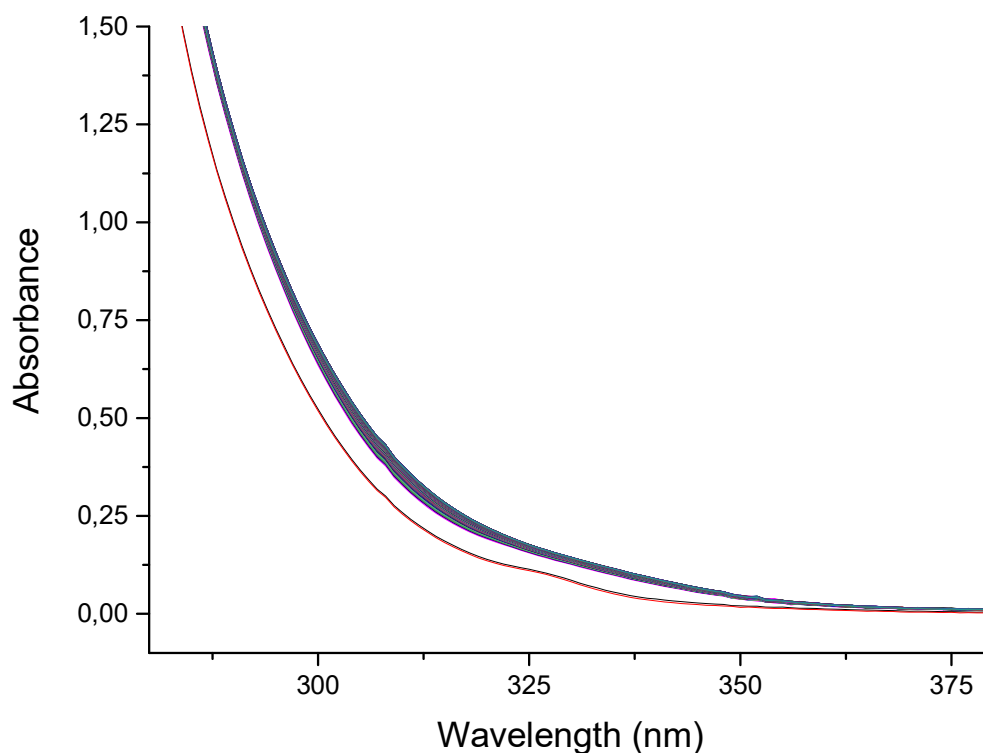


**Figure 5.4** Preliminary UV-visible spectra prior to kinetic measurements on the stopped-flow recorded for the reaction of 0.05 mM **Pt(QnS<sup>Ph</sup>)** with 3 mM **dm<sub>tu</sub>** at pH 2.

The plots of  $k_{\text{obs}(1\text{st})}$  vs [Nu] gave linear regressions lines as shown in **Figure 5.5** for the reaction of **Pt(QnS<sup>Ph</sup>)** and **dm<sub>tu</sub>**.

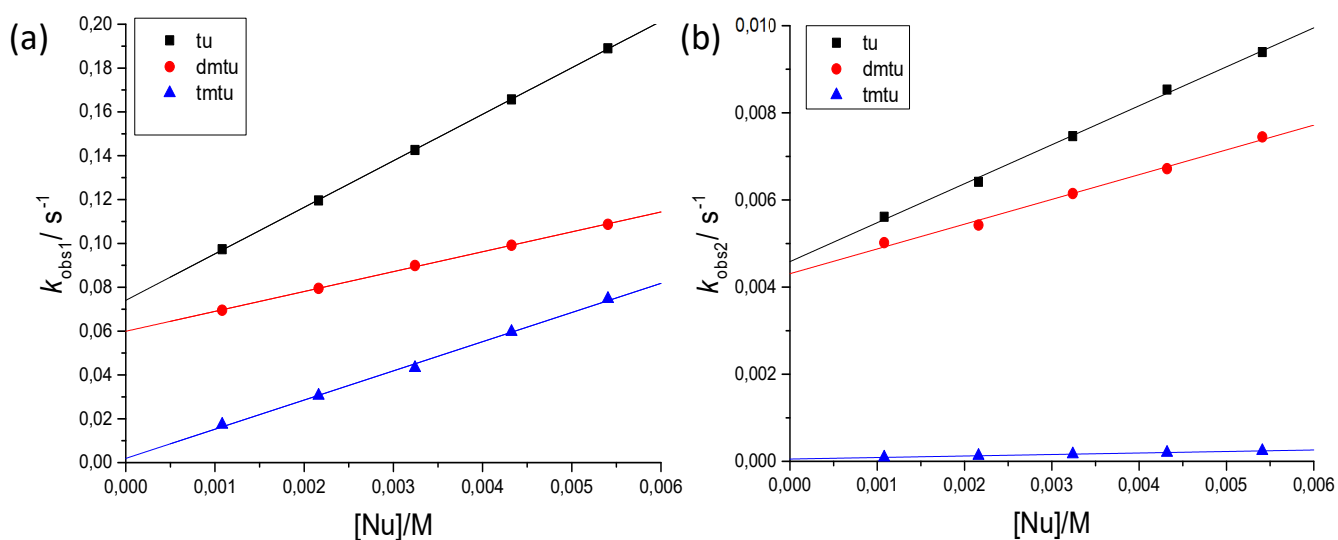


**Figure 5.5** Plots of  $k_{obs1}$  vs  $[Nu]$  for the (a) first and (b) second substitution steps of the reaction of 0.1 mM  $Pt(QnS^{Ph})$  at pH 2 ( $I = 0.1$  M LiOTf/HOTf) and 25 °C.

The rate law for the substitution process can be expressed by *Equation 5.1*.<sup>49,50</sup>

$$k_{obs(1/2)} = k_{2(1st/2nd)}[Nu] + k_{-1(1st/2nd)} \approx k_{2(1st/2nd)}[Nu] \quad (5.1)$$

where  $[Nu] = tu, dmtu$  and  $tmtu$ .

The second-order rate constants  $k_{2(1st)}$  was determined from the slopes of the plots of  $k_{obs(1st)}$  vs  $[Nu]$ . The intercepts of  $k_{2(1st)}$  represent either a solvolysis pathway for which a solvent molecule substitutes the aqua ligand prior to being subsequently substituted by the entering nucleophiles or the reverse substitution of the thiourea nucleophiles by water molecules. The first-order rate constants,  $k_{-1(1st)}$ , were neglected due to their small magnitudes when compared to those of  $k_{2(1st)}$  which represent the direct substitution of the aqua ligand by the thiourea nucleophiles. The dependence of the  $k_{2(1st)}$  rate constants on concentration and temperature for the different nucleophiles are given in **Tables 5.3** and **5.4**.

**Table 5.3** Summary of the rate constants for the consecutive substitution steps.

	Nu	$k_{2(1st)}/M^{-1} s^{-1}$	$k_{2(2nd)}/10^{-1} M^{-1} s^{-1}$
<b>Pt(QnS<sup>Ph</sup>)</b>	<b>tu</b>	$21.2 \pm 0.1$	$89.4 \pm 2.8$
	<b>dmtu</b>	$13.3 \pm 0.1$	$56.8 \pm 2.6$
	<b>tmtu</b>	$9.1 \pm 0.4$	$3.5 \pm 0.1$
<b>Pt(QnS<sup>Ph(t-But)</sup>)</b>	<b>tu</b>	$335.4 \pm 2.3$	$196.0 \pm 1.0$
	<b>dmtu</b>	$253.6 \pm 1.6$	$115.1 \pm 1.7$
	<b>tmtu</b>	$86.4 \pm 0.4$	$23.5 \pm 0.8$
<b>Pt(QnS<sup>PhF</sup>)</b>	<b>tu</b>	$287.4 \pm 3.9$	$48.1 \pm 1.1$
	<b>dmtu</b>	$154.5 \pm 4.2$	$26.4 \pm 0.7$
	<b>tmtu</b>	$58.9 \pm 1.3$	$2.9 \pm 0.6$
<b>Pt(pyS<sup>Ph(t-But)</sup>)<sup>a</sup></b>	<b>tu</b>	$4325.4 \pm 15.7$	$242.6 \pm 11.6$
	<b>dmtu</b>	$635.5 \pm 11.1$	$172.0 \pm 0.5$
	<b>tmtu</b>	$126.7 \pm 2.0$	$65.9 \pm 6.5$

<sup>a</sup>Kinetic data reproduced from Chapter 4, Table 4.3.

A typical time-resolved kinetic trace for the substitution of the first aqua ligand for the reaction of **Pt(QnS<sup>Ph</sup>)** and 40-fold **tu** is depicted in **Figure 5.6**.

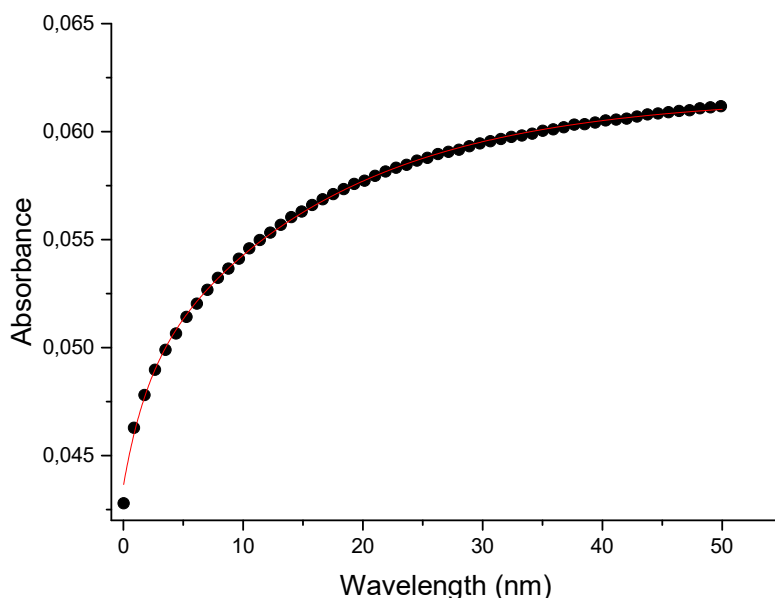


**Figure 5.6** A typical time-resolved kinetic trace at 293 nm for the first substitution step for the reaction of 0.115 mM **Pt(QnS<sup>Ph</sup>)** and 2.29 mM **tu** followed on the stopped-flow analyser.

The second substitution step (**B** → **C**) is ascribed to the substitution of the second aqua ligand *trans* to the quinoline or pyridine moieties. This step is represented by the rate constant  $k_{2(2nd)}$  which is determined from the plot of  $k_{obs2}$  vs [Nu]. The slower rate of substitution of the second aqua ligand is due to crowding of the square-plane by the coordinated thiourea nucleophiles. The  $\sigma$ -inductive donation of the coordinated thiourea nucleophile further increases the electron density onto the metal centre making it less electrophilic. Combined, these factors result in the slower rate of substitution of the second aqua ligand.

As described for the pyridyl analogues, the substitution of the second aqua ligand to form **C** triggers a rapid and simultaneous *trans* labilisation of the N-end of the N,S non-leaving ligand by a third thiourea nucleophile resulting in a PtS<sub>4</sub> species, **D**. This mechanism is similar to that already reported in Chapter 4, Section 4.3.2 for the Pt(II) complexes with pyridyl moieties. The temperature dependence of the second-order rate constants was regressed according to the Eyring Equation 5.2.<sup>51</sup>

$$\ln[k_{2(1st/2nd)}/T] = -(\Delta H^\ddagger_{1/2}/R) \cdot 1/T + [23.8 + (\Delta S^\ddagger_{1/2}/R)] \quad (5.2)$$

where  $T$  and  $R$  represent the Kelvin temperature and ideal gas constant ( $8.315 \text{ J K}^{-1} \text{ mol}^{-1}$ ), respectively. Exemplary Eyring plots are shown below in **Figure 5.7**.

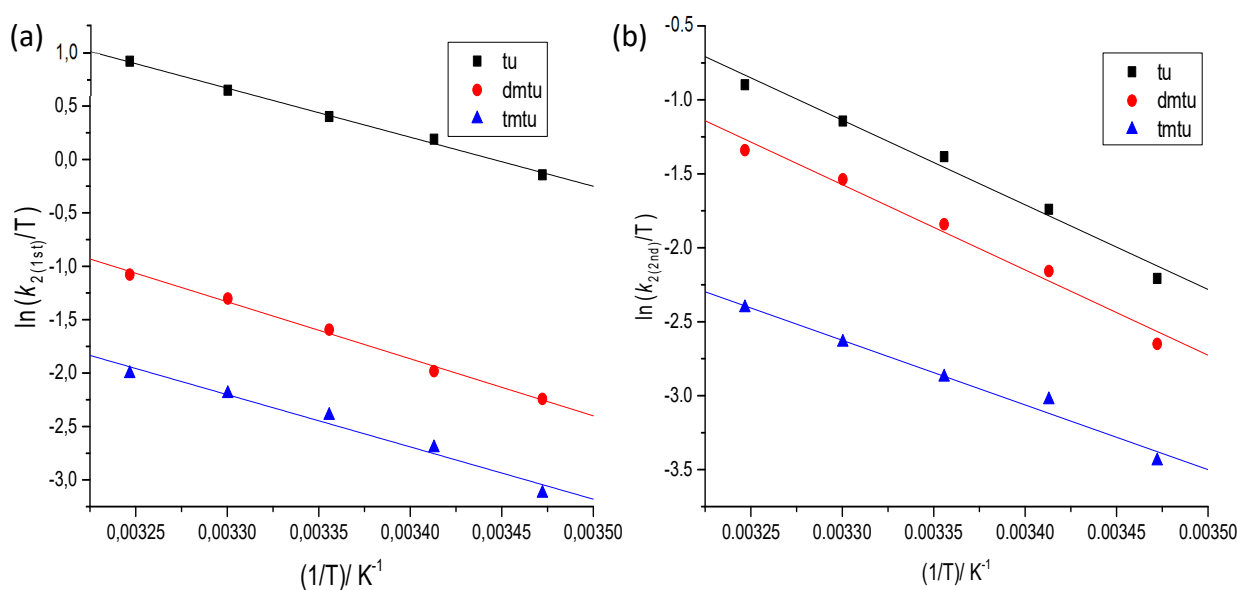


**Figure 5.7** Eyring plots for (a) first and (b) second substitution steps for the reactions of 0.1 mM Pt(QnS<sup>Ph</sup>) and thiourea nucleophiles, pH 2 ( $I = 0.1 \text{ M LiOTf/HOTf}$ ) and 25 °C.

The activation enthalpy ( $\Delta H^\ddagger_{1/2}$ ) and activation entropy ( $\Delta S^\ddagger_{1/2}$ ) were calculated from the slope and y-intercepts of the plots, respectively. The data is summarized in **Table 5.4**.

**Table 5.4** Summary of the activation parameters for the consecutive substitution steps.

	Nu	$\Delta H^\ddagger_{(1st)}/\text{kJ mol}^{-1}$	$\Delta S^\ddagger_{(1st)}/\text{J mol}^{-1} \text{K}^{-1}$	$\Delta H^\ddagger_{(2nd)}/\text{kJ mol}^{-1}$	$\Delta S^\ddagger_{(2nd)}/\text{J mol}^{-1} \text{K}^{-1}$
	<b>tu</b>	44 ± 2	-63 ± 7	39 ± 1	-87 ± 3
<b>Pt(QnS<sup>Ph</sup>)</b>	<b>dmtu</b>	38 ± 1	-66 ± 5	56 ± 2	-79 ± 5
	<b>tmtu</b>	41 ± 3	-86 ± 9	38 ± 4	-81 ± 11
	<b>tu</b>	69 ± 3	-93 ± 8	56 ± 1	-89 ± 3
<b>Pt(QnS<sup>Ph(t-But)</sup>)</b>	<b>dmtu</b>	57 ± 2	-106 ± 6	49 ± 1	-96 ± 3
	<b>tmtu</b>	43 ± 2	-86 ± 7	38 ± 3	-81 ± 8
	<b>tu</b>	53 ± 3	-28 ± 9	43 ± 2	-78 ± 6
<b>Pt(QnS<sup>PhF</sup>)</b>	<b>dmtu</b>	53 ± 2	-28 ± 6	69 ± 3	-73 ± 8
	<b>tmtu</b>	40 ± 3	-79 ± 8	34 ± 2	-93 ± 6
	<b>tu</b>	28 ± 1	-72 ± 4	36 ± 3	-100 ± 9
<b>Pt(pyS<sup>Ph(t-But)</sup>)</b>	<b>dmtu</b>	45 ± 2	-41 ± 6	47 ± 2	-63 ± 6
	<b>tmtu</b>	36 ± 1	-84 ± 4	37 ± 2	-177 ± 7

## 5.6 Discussion

The results in **Table 5.3** indicate that the rate of substitution of the aqua leaving groups is sensitive to the nature of the substituents on the phenyl group of the coordinated thioether. The aqua ligand which is *trans* to the thioether group is substituted first. This is due to the strong  $\sigma$ -*trans*-directing ability of this moiety which labilizes the Pt-OH<sub>2(1)</sub> bond *trans* to its position. The substitution of the first aqua ligand by thiourea as the entering nucleophile

decreases in the following order: **Pt(pyS<sup>Ph(t-But)</sup>)** < **Pt(QnS<sup>Ph(t-But)</sup>)** < **Pt(QnS<sup>PhF</sup>)** < **Pt(QnS<sup>Ph</sup>)** and by factors of 204: 15: 14: and 1, respectively.

The strong positive  $\sigma$ -inductive donation of the *tert*-butyl substituent of **Pt(QnS<sup>Ph(t-But)</sup>)** enhances the *trans*-directing ability of the thioether. This leads to an increased rate of substitution *via* the ground-state *trans*-influence when compared to the weaker  $\sigma$ -donor phenyl group for **Pt(QnS<sup>Ph</sup>)**. Due to the biphilic nature of the thioether, its  $\pi$ -acceptor capacity is boosted by the negative  $\sigma$ -inductive withdrawal of the fluoro substituent for **Pt(QnS<sup>PhF</sup>)** and leads to an increase in the rate of substitution when compared to **Pt(QnS<sup>Ph</sup>)**. As a result, electron density is back-donated from the filled 5*d*-orbitals of the Pt(II) ion of **Pt(QnS<sup>PhF</sup>)** onto the empty 3*d*-orbitals of its thioether, resulting in a more electropositive metal centre. Consequently, the formation of the bond with the entering thiourea nucleophiles stabilizes the transition states of the reactions of **Pt(QnS<sup>PhF</sup>)** relative to that of **Pt(QnS<sup>Ph</sup>)**.

Replacing the pyridine group with quinoline results in a decrease in the rate of substitution of the aqua leaving groups. A comparison of the rate constants for **Pt(pyS<sup>Ph(t-But)</sup>)** and **Pt(QnS<sup>Ph(t-But)</sup>)** demonstrate this fact. The decreased reactivity for **Pt(QnS<sup>Ph(t-But)</sup>)** when compared to **Pt(pyS<sup>Ph(t-But)</sup>)** is due to the poor  $\pi$ -back-donation of the quinolyl group which increases electron density on the Pt(II) metal centre. Similar trends have been reported by Khusi *et al*<sup>36</sup>, Ongoma and Jaganyi<sup>31</sup>, Kinunda and Jaganyi<sup>32</sup> and Wekesa and Jaganyi.<sup>33</sup>

The second substitution of the aqua leaving group occurs *trans* to the quinoline moiety. Coordination of the first thiourea nucleophile imparts a steric hindrance upon the axial approach of the subsequent ligands. The steric hindrance of the coordinated thiourea on square-plane accounts for the slower substitution of the second aqua ligand. The reactivity factors for the substitution of the second aqua when thiourea is used as the entering nucleophile are 6: 5: 2: 1 for and order of reactivity of the complexes is **Pt(pyS<sup>Ph(t-But)</sup>)** < **Pt(QnS<sup>Ph(t-But)</sup>)** < **Pt(QnS<sup>PhF</sup>)** < **Pt(QnS<sup>Ph</sup>)**.

The substituting thiourea nucleophiles have a biphilic character in that they can act as thiols ( $\sigma$ -donors) as well as thioethers ( $\sigma$ -donors/ $\pi$ -acceptors).<sup>52</sup> Consequently, the thiourea ligand *trans* to the coordinated quinoline or pyridine can potentially labilise the Pt-N bond to these moieties *via* its strong  $\sigma$ -donor character.<sup>34</sup> The labilization of the Pt-N bonds leads to the facile substitution of these moieties from the coordination sphere by a third thiourea

nucleophile as outlined in **Scheme 5.3** as well as in Chapter 4, Section 4.3.2. However, the N,S bidentate of the ligand remains coordinated to the Pt(II) metal centre through the S atom of the thioether. The labilization effect of the thioether by *trans*-coordinated thiourea is levelled off by its strong  $\sigma$ -donor capacity.

## 5.7 Conclusions

Substitution of aqua ligands in three complexes bearing 2-(phenylthiomethyl)quinoline chelates were studied spectrophotometrically under *pseudo*-first-order conditions. The substitution of the first aqua ligand is dependent upon the nature of the substituents and decreases in the order: **Pt(pyS<sup>Ph(t-But)</sup>)** > **Pt(QnS<sup>Ph(t-But)</sup>)** > **Pt(QnS<sup>PhF</sup>)** > **Pt(QnS<sup>Ph</sup>)**. Both electron-donating **{Pt(QnS<sup>Ph(t-But)</sup>)}** and **{Pt(pyS<sup>Ph(t-But)</sup>)}** and electron-withdrawing groups **{Pt(QnS<sup>PhF</sup>)}** increase the rate of substitution when compared to **Pt(QnS<sup>Ph</sup>)**. Replacing the  $\pi$ -acceptor pyridine with a poor  $\pi$ -acceptor and better groups such as the quinolyl moiety retards the rate of substitution. The reactivity of the nucleophiles towards all the complexes decreases in the order: **tu** > **dm<sub>2</sub>tu** > **tmtu**, which reflects the influence of their steric bulkiness. Low enthalpies of activation, negative entropies of activation and dependence of rate on the concentration of the nucleophiles all support an associative mode of substitution of the labile ligands from the complexes.



## 5.8 References

1. A. J. Thomson, R. J. P. Williams and S. Reslova, in *Structure and Bonding, Volume 11*, Springer Berlin Heidelberg, Berlin, Heidelberg, 1972, DOI: 10.1007/BFb0002459, pp. 1-46.
2. B. Rosenberg, *Naturwissenschaften*, 1973, **60**, 399-406.
3. F. Haviv, R. W. DeNet, R. J. Michaels, J. D. Ratajczyk, G. W. Carter and P. R. Young, *Journal of Medicinal Chemistry*, 1983, **26**, 218-222.
4. P. J. Sadler and Z. Guo, *Pure and Applied Chemistry*, 1998, **70**, 863-871.
5. F. Muggia, A. Bonetti, J. Hoeschele, M. Rozenzweig and S. Howell, *Journal of clinical oncology: official journal of the American Society of Clinical Oncology*, 2015, **33**, 4219-4226.
6. T. C. Johnstone, K. Suntharalingam and S. J. Lippard, *Chemical Reviews*, 2016, **116**, 3436-3486.
7. T. Soldatović, S. Jovanović, Ž. D. Bugarčić and R. van Eldik, *Dalton Transactions*, 2012, **41**, 876-884.
8. Ž. D. Bugarčić, J. Bogojeski and R. van Eldik, *Coordination Chemistry Reviews*, 2015, **292**, 91-106.
9. M. Kosović, Ž. Jaćimović, Ž. D. Bugarčić and B. Petrović, *Journal of Coordination Chemistry*, 2015, **68**, 3003-3012.
10. D. Wang and S. J. Lippard, *Nat Rev Drug Discov*, 2005, **4**, 307-320.
11. J. Reedijk, *Chemical Communications*, 1996, 801-806.
12. L. Kelland, *Nat Rev Cancer*, 2007, **7**, 573-584.
13. J. Bogojeski, J. Volbeda, Ž. D. Bugarčić, M. Freytag and M. Tamm, *New Journal of Chemistry*, 2016, **40**, 4818-4825.
14. J. Bogojeski, J. Volbeda, M. Freytag, M. Tamm and Ž. D. Bugarčić, *Dalton Transactions*, 2015, **44**, 17346-17359.
15. N. Summa, W. Schiessl, R. Puchta, N. van Eikema Hommes and R. van Eldik, *Inorganic Chemistry*, 2006, **45**, 2948-2959.
16. N. Summa, T. Soldatović, L. Dahlenburg, Ž. D. Bugarčić and R. van Eldik, *JBIC Journal of Biological Inorganic Chemistry*, 2007, **12**, 461-475.

17. B. B. Khusi, A. Mambanda and D. Jaganyi, *Transition Metal Chemistry*, 2016, **41**, 191-203.
18. U. Fekl and R. van Eldik, *European Journal of Inorganic Chemistry*, 1998, **1998**, 389-396.
19. S. Hochreuther, R. Puchta and R. van Eldik, *Inorganic Chemistry*, 2011, **50**, 8984-8996.
20. A. Shoukry, T. Rau, M. Shoukry and R. van Eldik, *Journal of the Chemical Society, Dalton Transactions*, 1998, DOI: 10.1039/A804141E, 3105-3112.
21. P. Karmakar, *Transition Metal Chemistry*, 2014, **39**, 727-733.
22. S. Ray, P. Karmakar, A. Chattopadhyay, D. Nandi, R. Sarkar and A. K. Ghosh, *International Journal of Chemical Kinetics*, 2016, **48**, 347-357.
23. S. Ray, P. Karmakar, A. Chattopadhyay, D. Nandi, S. Ukil, R. Sarkar and A. K. Ghosh, *Journal of Chemical Sciences*, 2016, **128**, 1327-1335.
24. P. Jarzynka, A. Topolski, M. Uzarska and R. Czajkowski, *Inorganica Chimica Acta*, 2014, **413**, 60-67.
25. S. K. Bera, S. K. Chandra and G. S. De, *International Journal of Chemical Kinetics*, 2005, **37**, 489-495.
26. S. Hochreuther, S. T. Nandibewoor, R. Puchta and R. van Eldik, *Dalton Transactions*, 2012, **41**, 512-522.
27. A. Samanta, G. K. Ghosh, I. Mitra, S. Mukherjee, J. C. Bose, S. Mukhopadhyay, W. Linert and S. C. Moi, *RSC Adv.*, 2014, **4**, 43516-43524.
28. S. Hochreuther, R. Puchta and R. van Eldik, *Inorganic Chemistry*, 2011, **50**, 12747-12761.
29. M. Kosović, S. Jovanović, G. A. Bogdanović, G. Giester, Ž. Jaćimović, Ž. D. Bugarčić and B. Petrović, *Journal of Coordination Chemistry*, 2016, DOI: 10.1080/00958972.2016.1224336, 1-13.
30. M. Bellicini, L. Cattalini, G. Marangoni and B. Pitteri, *Journal of the Chemical Society, Dalton Transactions*, 1994, DOI: 10.1039/DT9940001805, 1805-1811.
31. P. Ongoma and D. Jaganyi, *Dalton Transactions*, 2012, **41**, 10724-10730.
32. G. Kinunda and D. Jaganyi, *Transition Metal Chemistry*, 2014, **39**, 451-459.
33. I. M. Wekesa and D. Jaganyi, *Journal of Coordination Chemistry*, 2016, **69**, 389-403.

34. F. Basolo and R. G. Pearson, *Mechanisms of inorganic reactions: a study of metal complexes in solution*, Wiley, 1967, 351-404.
35. M. L. Tobe and J. Burgess, *Inorganic reaction mechanisms*, Longman, Harlow, Essex, England; New York, 1999, 30-43, 70-112.
36. B. B. Khusi, A. Mambanda and D. Jaganyi, *Journal of Coordination Chemistry*, 2016, **69**, 2121-2135.
37. W. C. Schiessl, N. K. Summa, C. F. Weber, S. Gubo, C. Dücker-Benfer, R. Puchta, N. J. R. van Eikema Hommes and R. van Eldik, *Zeitschrift für anorganische und allgemeine Chemie*, 2005, **631**, 2812-2819.
38. M. A. M. R. Malachowski, D. Murray, R. White, N. Elia, A. L. Rheingold, L. V. Zakharov R. S. Kelly, *Inorg. Chim. Acta.*, 2009, **362**, 1247.
39. M. R. Malachowski, M. Adams, N. Elia, A. L. Rheingold and R. S. Kelly, *Journal of the Chemical Society, Dalton Transactions*, 1999, DOI: 10.1039/A900223E, 2177-2182.
40. Ž. D. Bugarčić, B. V. Petrović and R. Jelić, *Transition Metal Chemistry*, 2001, **26**, 668-671.
41. v. B. Origin 7.5TM SRO, Origin Lab Corporation, Northampton, One, Northampton, MA, 01060, USA, 2003.
42. A. D. Becke, *The Journal of Chemical Physics*, 1993, **98**, 5648-5652.
43. C. Lee, W. Yang and R. G. Parr, *Physical review B*, 1988, **37**, 785.
44. P. J. Hay and W. R. Wadt, *The Journal of Chemical Physics*, 1985, **82**, 299-310.
45. R. A. I. Gaussian 09, M. J. Frisch, G. W. Trucks, H. B. Schlegel, G. E. Scuseria, M. A. Robb, J. R. Cheeseman, G. Scalmani, V. Barone, B. Mennucci, G. A. Petersson, H. Nakatsuji, M. Caricato, X. Li, H. P. Hratchian, A. F. Izmaylov, J. Bloino, G. zheng, J. L. Sonnenberg, M. Ehara, K. Toyota, R. Fukuda, J. Hasegawa, M. Ishida, T. Nakajima, Y. Honda, O. Kitao, H. Nakai, T. Vreven, J. A. Montgomery, Jr., J. E. Peralta, F. Ogliaro, M. Bearpark, J. J. Heyd, E. Brothers, K. N. Kudin, V. N. Staroverov, R. Kobayashi, J. Normand, K. Raghavachari, A. Rendell, J. C. Burant, S. S. Iyengar, J. Tomasi, M. Cossi, N. Rega, J. M. Millam, M. Klene, J. E. Knox, J. B. Cross, V. Bakken, C. Adamo, J. Jaramillo, R. Gomperts, R. E. Stratmann, O. Yazyjev, A. J. Austin, R. Cammi, C. Pomelli, J. W. Ochterski, R. L. Martin, K. Morokuma, V. G. Zakrzewski, G. A. Voth, P. Salvador, J. J. Dannenberg, S. Dapprich, A. D. Daniels, O. Farkas, J. B. Foresman, J. V. Ortiz, J. Cioslowski and D. J. Fox, Gaussian, Inc., Wallingford CT, 2009.

46. A. Mambanda, D. Jaganyi, S. Hochreuther and R. van Eldik, *Dalton Transactions*, 2010, **39**, 3595-3608.
47. A. Mambanda and D. Jaganyi, *Dalton Transactions*, 2012, **41**, 908-920.
48. A. Shaira, D. Reddy and D. Jaganyi, *Dalton Transactions*, 2013, **42**, 8426-8436.
49. J. D. Atwood, *Inorganic and organometallic reaction mechanisms*, Wiley-VCH, New York, 1997.
50. S. Asperger, *Chemical kinetics and inorganic reaction mechanisms*, Kluwer Academic/Plenum Publishers, New York, 2003, 34-40, 105-106.
51. R. B. Jordan, *Reaction mechanisms of inorganic and organometallic systems*, Oxford University Press, New York, 1991, 29-40.
52. L. Cattalini, A. Orio and A. Doni, *Inorganic Chemistry*, 1966, **5**, 1517-1519.

## 5.7 Supplementary Information

**Table SI 5.1** Selected wavelengths for the **first** substitution reactions of all three nucleophiles at pH 2.

Complex	Nu	Wavelength (nm)
<b>Pt(QnS<sup>Ph</sup>)</b>	tu	293
	dmtu	293
	tmtu	353
<b>Pt(QnS<sup>Ph(t-But)</sup>)</b>	tu	305
	dmtu	305
	tmtu	329
<b>Pt(QnS<sup>PhF</sup>)</b>	tu	283
	dmtu	283
	tmtu	340

**Table SI 5.2** Selected wavelengths for the **second** substitution reactions of all three nucleophiles at pH 2.

Complex	Nu	Wavelength (nm)
<b>Pt(QnS<sup>Ph</sup>)</b>	tu	276
	dmtu	276
	tmtu	324
<b>Pt(QnS<sup>Ph(t-Butyl)</sup>)</b>	tu	285
	dmtu	285
	tmtu	295
<b>Pt(QnS<sup>PhF</sup>)</b>	tu	270
	dmtu	270
	tmtu	315

## Single Mass Analysis

Tolerance = 5.0 PPM / DBE: min = -1.5, max = 100.0

Element prediction: Off

Number of isotope peaks used for i-FIT = 3

Monoisotopic Mass, Even Electron Ions

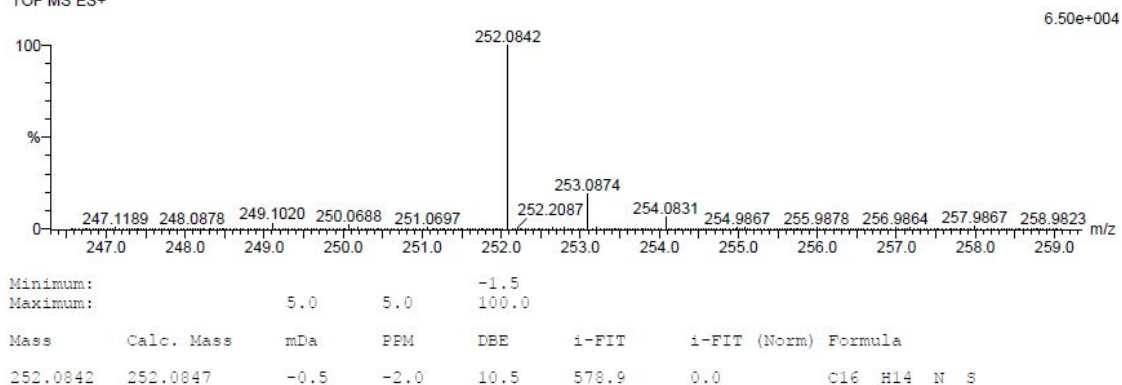
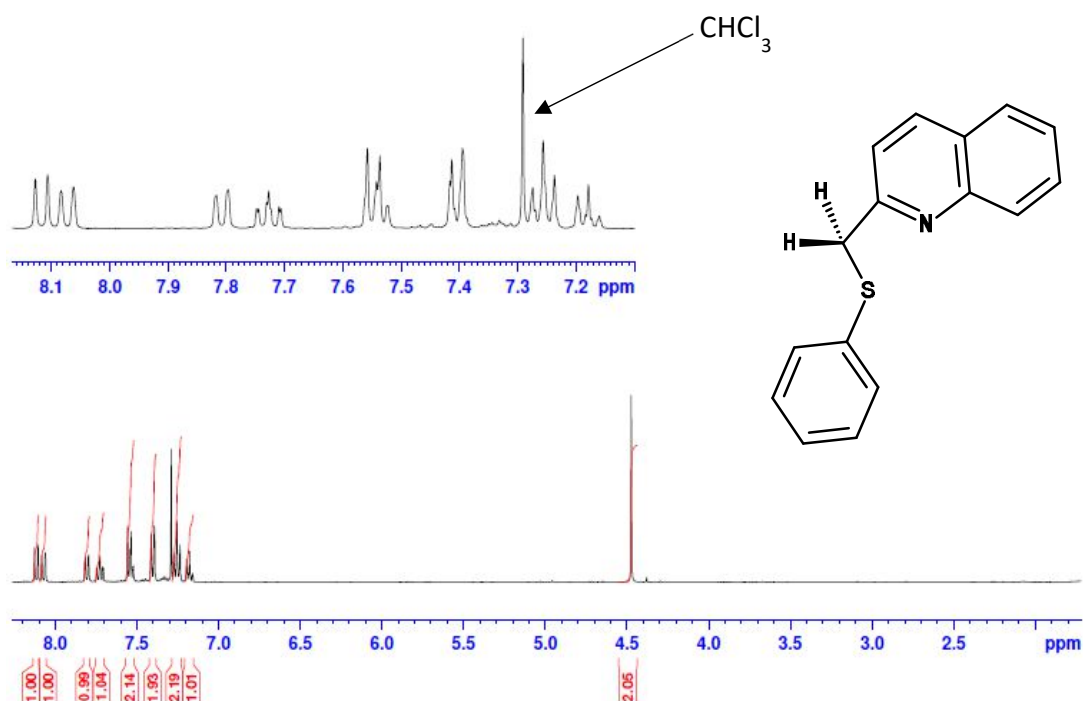
10 formula(e) evaluated with 1 results within limits (up to 20 closest results for each mass)

Elements Used:

C: 15-20 H: 10-15 N: 0-5 S: 0-2

HQn 56 (1.858) Cm (1.61)

TOF MS ES+

Figure SI 5.1 Low resolution ESI mass spectrum of 2-(phenylthiomethyl)quinoline} (QnS<sup>Ph</sup>).Figure SI 5.2 <sup>1</sup>H NMR spectrum of 2-(phenylthiomethyl)quinoline} (QnS<sup>Ph</sup>).

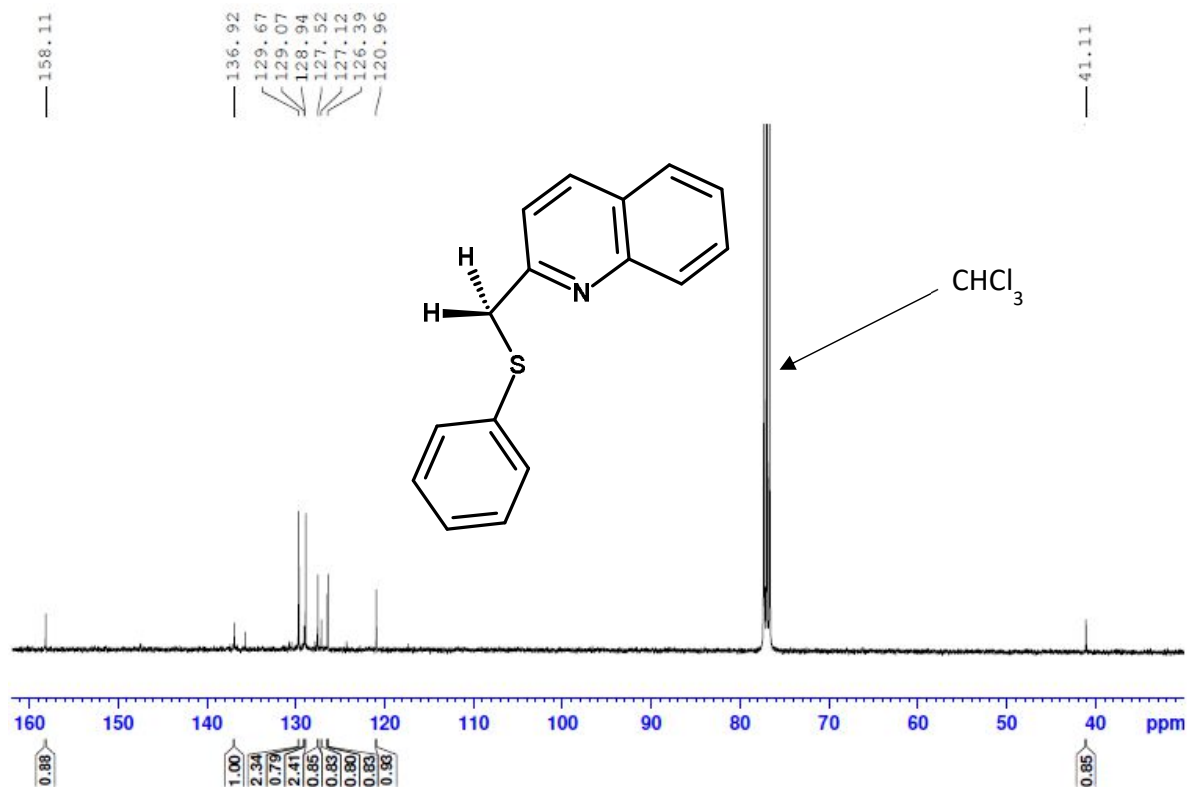


Figure SI 5.3 <sup>13</sup>C NMR spectrum of 2-(phenylthiomethyl)quinoline} (QnS<sup>Ph</sup>).

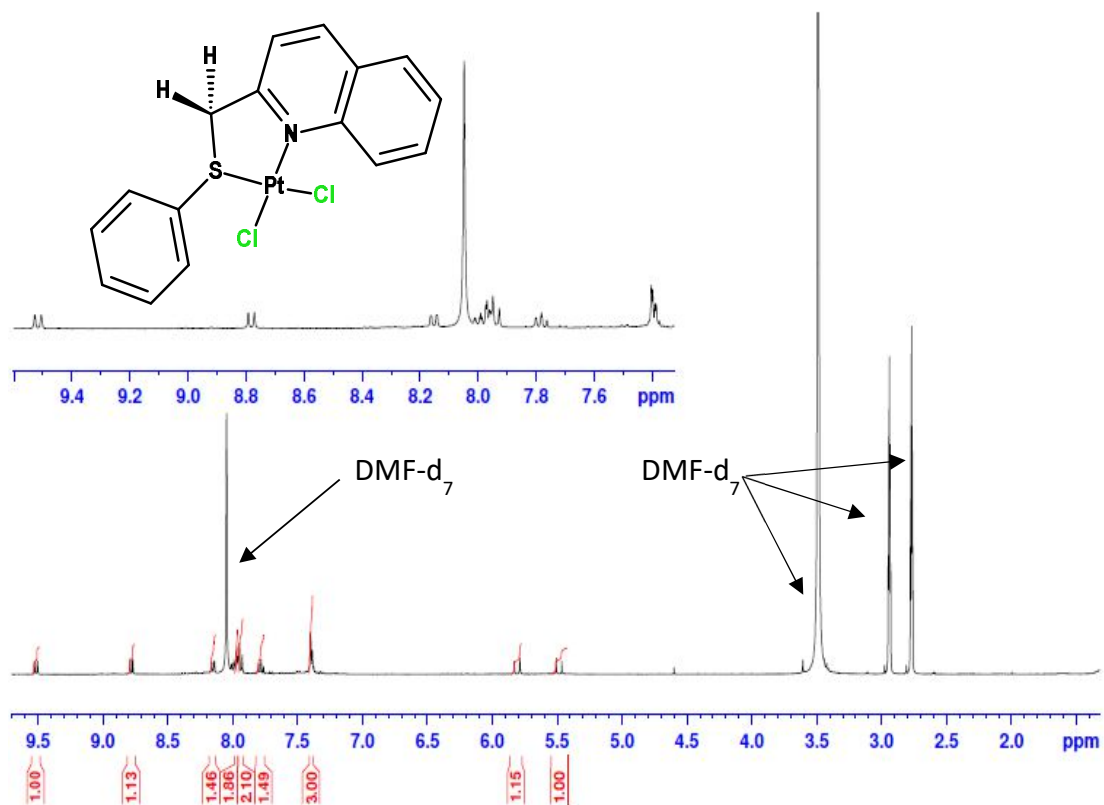


Figure SI 5.4 <sup>1</sup>H NMR spectrum of [Pt{2-(phenylthiomethyl)quinoline}Cl<sub>2</sub>] (Pt(QnS<sup>Ph</sup>)).

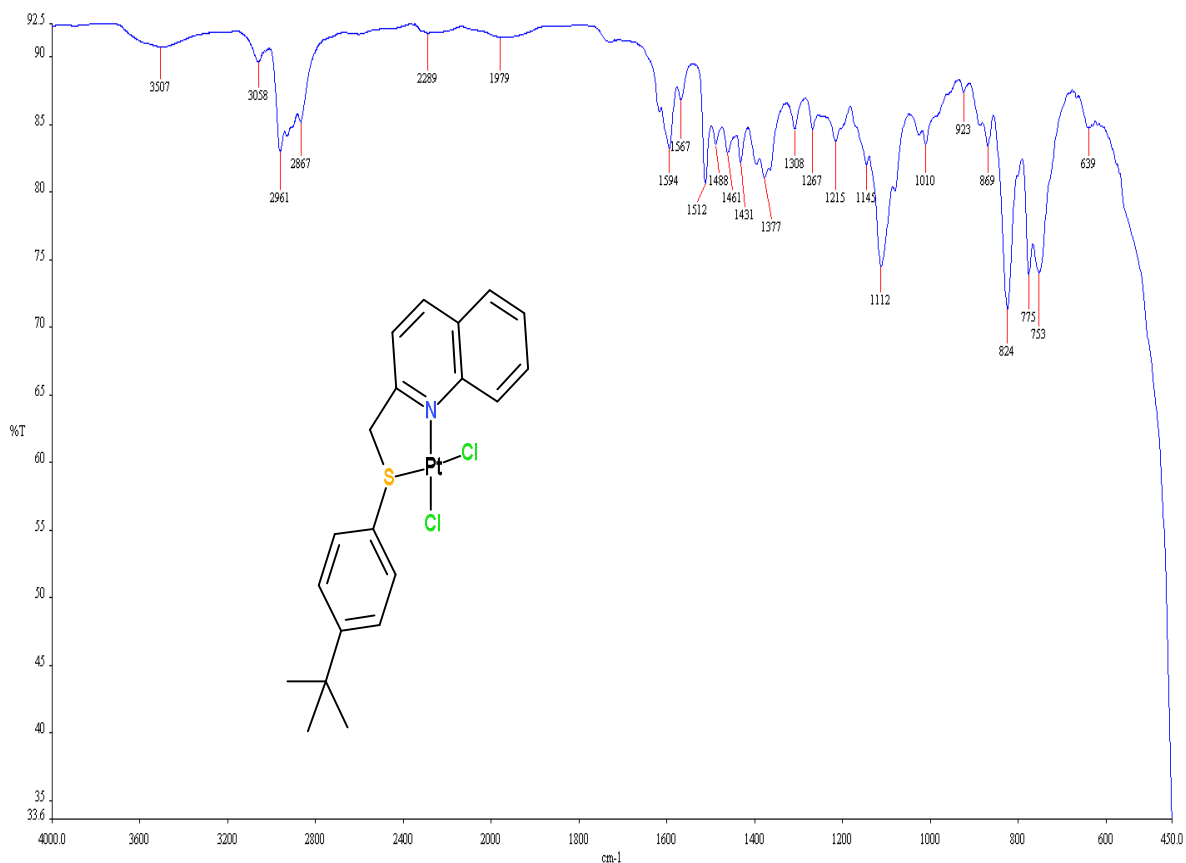


Figure SI 5.5 IR spectrum of  $[Pt\{2-(4\text{-}tert\text{-butylphenylthiomethyl)quinoline}\}Cl_2] Pt(QnS^{Ph(t-But)})$ .

Elemental Composition Report

Single Mass Analysis

Tolerance = 5.0 PPM / DBE: min = -1.5, max = 100.0

Element prediction: Off

Number of isotope peaks used for i-FIT = 3

Monoisotopic Mass, Even Electron Ions

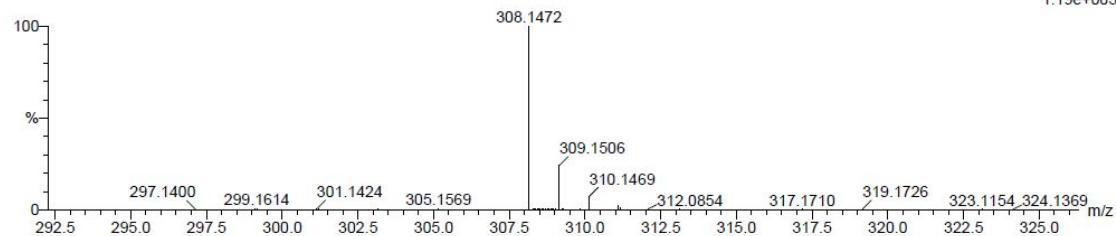
5 formula(e) evaluated with 1 results within limits (up to 20 closest results for each mass)

Elements Used:

C: 15-20 H: 20-25 N: 0-5 S: 0-1

t-ButylQn 2 (0.034) Cm (1:61)

TOF MS ES+



Minimum:  
Maximum:

5.0 5.0 -1.5 100.0

Mass	Calc. Mass	mDa	PPM	DBE	i-FIT	i-FIT (Norm)	Formula
308.1472	308.1473	-0.1	-0.3	10.5	561.3	0.0	C20 H22 N S

Figure SI 5.6 Low resolution ESI mass spectrum of 2-(4-tert-butylphenylthiomethyl)quinoline  $QnS^{Ph(t-But)}$ .



**Table SI 5.3** Averaged observed rate constants,  $k_{\text{obs1}}$ , for the reaction of 0.05405 mM **Pt(QnS<sup>Ph</sup>)** with different nucleophiles at pH 2 ( $I = 0.1$  M LiOTf/HOTf) and 25 °C.

Nucleophile	<b>tu</b>	<b>dmtu</b>	<b>tmtu</b>
[Nu] in mM	$k_{\text{obs1}}$ in s <sup>-1</sup>		
0,00108	0,09735	0,06952	0,01732
0,00216	0,1196	0,07946	0,03057
0,00324	0,1426	0,08987	0,0432
0,00432	0,1657	0,09915	0,05968
0,00541	0,189	0,1087	0,0747

**Table SI 5.4** Averaged observed rate constants,  $k_{\text{obs2}}$ , for the reaction of 0.05405 mM **Pt(QnS<sup>Ph</sup>)** with different nucleophiles at pH 2 ( $I = 0.1$  M LiOTf/HOTf) and 25 °C.

Nucleophile	<b>tu</b>	<b>dmtu</b>	<b>tmtu</b>
[Nu] in mM	$k_{\text{obs2}}$ in s <sup>-1</sup>		
0,00108	0,00561	0,00502	8,93717E-5
0,00216	0,00642	0,00542	1,3011E-4
0,00324	0,00746	0,00615	1,65183E-4
0,00432	0,00853	0,00672	1,99758E-4
0,00541	0,00939	0,00745	2,4157E-4

**Table SI 5.5** Averaged observed rate constants,  $k_{obs1}$ , for the reaction of 0.0783 mM **Pt(QnS<sup>Ph(t-But)</sup>)** with different nucleophiles at pH 2 ( $I = 0.1$  M LiOTf/HOTf) and 25 °C.

Nucleophile	<b>tu</b>	<b>dmtu</b>	<b>tmtu</b>
[Nu] in mM	$k_{obs1}$ in s <sup>-1</sup>		
1.566	0,061	0,021	0,0888
3.132	0,78	0,38	0,2735
4.698	1,295	0,75	0,4193
6.264	1,8212	1,1502	0,5318
7.830	2,4279	1,6079	0,6185

**Table SI 5.6** Averaged observed rate constants,  $k_{obs2}$ , for the reaction of 0.0783 mM **Pt(QnS<sup>Ph(t-But)</sup>)** with different nucleophiles at pH 2 ( $I = 0.1$  M LiOTf/HOTf) and 25 °C.

Nucleophile	<b>tu</b>	<b>dmtu</b>	<b>tmtu</b>
[Nu] in mM	$k_{obs2}$ in s <sup>-1</sup>		
1.566	0,04106	0,03586	0,00421
3.132	0,0735	0,05826	0,00904
4.698	0,1016	0,08085	0,01266
6.264	0,128	0,1022	0,01814
7.830	0,157	0,1204	0,02464

**Table SI 5.7** Averaged observed rate constants,  $k_{\text{obs1}}$ , for the reaction of 0.04483 mM **Pt(QnS<sup>PhF</sup>)** with different nucleophiles at pH 2 ( $I = 0.1$  M LiOTf/HOTf) and 25 °C.

Nucleophile	<b>tu</b>	<b>dmtu</b>	<b>tmtu</b>
[Nu] in mM	$k_{\text{obs1}}$ in s <sup>-1</sup>		
8,966E-4	0,225	0,2457	0,1268
0,00179	0,5033	0,4047	0,1741
0,00269	0,7529	0,5453	0,2357
0,00359	1,016	0,6761	0,2852
0,00448	1,257	0,8026	0,3353

**Table SI 5.8** Averaged observed rate constants,  $k_{\text{obs2}}$ , for the reaction of 0.04483 mM **Pt(QnS<sup>PhF</sup>)** with different nucleophiles at pH 2 ( $I = 0.1$  M LiOTf/HOTf) and 25 °C.

Nucleophile	<b>tu</b>	<b>dmtu</b>	<b>tmtu</b>
[Nu] in mM	$k_{\text{obs2}}$ in s <sup>-1</sup>		
4,483E-4	0,00546	0,00572	5,46427E-4
8,966E-4	0,00681	0,00791	6,80592E-4
0,00134	0,00769	0,01005	7,69024E-4
0,00179	0,00921	0,01235	9,20846E-4
0,00224	0,01019	0,01427	0,0012

**Table SI 5.9** Temperature dependence of the second-order rate constants,  $k_2/\text{M}^{-1} \text{s}^{-1}$ , for the substitution of the **first** aqua group in **Pt(QnS<sup>Ph</sup>)** by with different nucleophiles at pH 2 ( $I = 0.1 \text{ M LiOTf/HOTf}$ ) and 25 °C.

<b>tu</b>		<b>dmtu</b>		<b>tmtu</b>	
$1/T/\text{K}^{-1}$	$\ln(k_2/T)$	$1/T/\text{K}^{-1}$	$\ln(k_2/T)$	$1/T/\text{K}^{-1}$	$\ln(k_2/T)$
0,00347	-0,1442	0,00347	-2,24241	0,00347	-3,12544
0,00341	0,18944	0,00341	-1,98224	0,00341	-2,69938
0,00336	0,40116	0,00336	-1,59347	0,00336	-2,39599
0,0033	0,64788	0,0033	-1,302	0,0033	-2,19206
0,00325	0,91963	0,00325	-1,07884	0,00325	-2,0045

**Table SI 5.10** Temperature dependence of the second-order rate constants,  $k_1/\text{M}^{-1} \text{s}^{-1}$ , for the substitution of the **first** aqua group in **Pt(QnS<sup>Ph(t-But)</sup>)** by with different nucleophiles at pH 2 ( $I = 0.1 \text{ M LiOTf/HOTf}$ ) and 25 °C.

<b>tu</b>		<b>dmtu</b>		<b>tmtu</b>	
$1/T/\text{K}^{-1}$	$\ln(k_2/T)$	$1/T/\text{K}^{-1}$	$\ln(k_2/T)$	$1/T/\text{K}^{-1}$	$\ln(k_2/T)$
0,00347	2,09996	0,00347	-0,32261	0,00347	-3,68197
0,00341	2,80831	0,00341	0,26667	0,00341	-3,36791
0,00336	3,23629	0,00336	0,70998	0,00336	-3,17746
0,0033	3,60264	0,0033	0,9943	0,0033	-2,9107
0,00325	3,80187	0,00325	1,20008	0,00325	-2,68363

**Table SI 5.11** Temperature dependence of the second-order rate constants,  $k_1/\text{M}^{-1} \text{s}^{-1}$ , for the substitution of the **first** aqua group in **Pt(QnS<sup>PhF</sup>)** by with different nucleophiles at pH 2 ( $I = 0.1 \text{ M LiOTf/HOTf}$ ) and 25 °C.

<b>tu</b>		<b>dmtu</b>		<b>tmtu</b>	
$1/T/\text{K}^{-1}$	$\ln(k_2/T)$	$1/T/\text{K}^{-1}$	$\ln(k_2/T)$	$1/T/\text{K}^{-1}$	$\ln(k_2/T)$
0,00347	-0,35392	0,00347	-1,82184	0,00347	-2,545
0,00341	0,12255	0,00341	-1,40305	0,00341	-2,11578
0,00336	0,5321	0,00336	-0,99272	0,00336	-1,83149
0,0033	0,80128	0,0033	-0,70567	0,0033	-1,62541
0,00325	1,08302	0,00325	-0,36766	0,00325	-1,43101

**Table SI 5.12** Temperature dependence of the second-order rate constants,  $k_2/\text{M}^{-1} \text{s}^{-1}$ , for the substitution of the **second** aqua group in **Pt(QnS<sup>Ph</sup>)** by with different nucleophiles at pH 2 ( $I = 0.1 \text{ M LiOTf/HOTf}$ ) and 25 °C.

<b>tu</b>		<b>dmtu</b>		<b>tmtu</b>	
$1/T/\text{K}^{-1}$	$\ln(k_2/T)$	$1/T/\text{K}^{-1}$	$\ln(k_2/T)$	$1/T/\text{K}^{-1}$	$\ln(k_2/T)$
0,00347	-2,20773	0,00347	-2,65019	0,00347	-3,44072
0,00341	-1,73985	0,00341	-2,1579	0,00341	-3,02749
0,00336	-1,3843	0,00336	-1,8412	0,00336	-2,87454
0,0033	-1,14353	0,0033	-1,53686	0,0033	-2,63855
0,00325	-0,89802	0,00325	-1,34069	0,00325	-2,405

**Table SI 5.13** Temperature dependence of the second-order rate constants,  $k_2/\text{M}^{-1} \text{s}^{-1}$ , for the substitution of the **second** aqua group in **Pt(QnS<sup>Ph(t-But)</sup>)** by with different nucleophiles at pH 2 ( $I = 0.1 \text{ M LiOTf/HOTf}$ ) and 25 °C.

<b>tu</b>		<b>dmtu</b>		<b>tmtu</b>	
$1/T/\text{K}^{-1}$	$\ln(k_2/T)$	$1/T/\text{K}^{-1}$	$\ln(k_2/T)$	$1/T/\text{K}^{-1}$	$\ln(k_2/T)$
0,00347	-4,7374	0,00347	-5,02454	0,00347	-4,95834
0,00341	-3,82398	0,00341	-4,85676	0,00341	-3,9557
0,00336	-3,38353	0,00336	-4,56424	0,00336	-3,18646
0,0033	-3,00933	0,0033	-4,51769	0,0033	-2,80756
0,00325	-2,80854	0,00325	-4,39161	0,00325	-2,57347

**Table SI 5.14** Temperature dependence of the second-order rate constants,  $k_2/\text{M}^{-1} \text{s}^{-1}$ , for the substitution of the **second** aqua group in **Pt(QnS<sup>PhF</sup>)** by with different nucleophiles at pH 2 ( $I = 0.1 \text{ M LiOTf/HOTf}$ ) and 25 °C.

<b>tu</b>		<b>dmtu</b>		<b>tmtu</b>	
$1/T/\text{K}^{-1}$	$\ln(k_2/T)$	$1/T/\text{K}^{-1}$	$\ln(k_2/T)$	$1/T/\text{K}^{-1}$	$\ln(k_2/T)$
0,00347	-1,10773	0,00347	-1,55019	0,00347	-2,44072
0,00341	-0,73985	0,00341	-1,1579	0,00341	-2,08275
0,00336	-0,3843	0,00336	-0,8412	0,00336	-1,87454
0,0033	-0,14353	0,0033	-0,53686	0,0033	-1,63855
0,00325	-1,62876E-5	0,00325	-0,34069	0,00325	-1,405

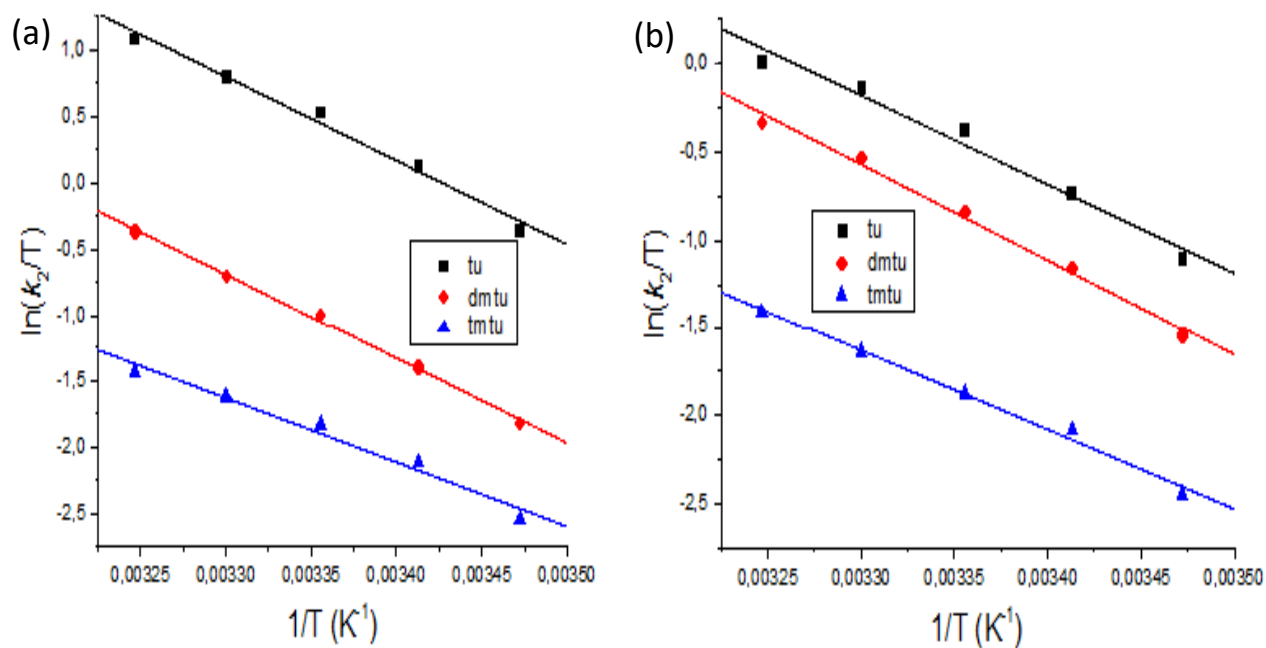


**Figure SI 5.7** Eyring plots for (a) first and (b) second substitution steps for the reactions of 0.1 mM  $Pt(QnS^{PhF})$  and thiourea nucleophiles, pH 2 ( $I = 0.1$  M LiOTf/HOTf) and 25 °C.